EFFECT OF FIBER/MATRIX INTERPHASE ON THE LONG TERM BEHAVIOR OF CROSS-PLY LAMINATES

by

Suresh Subramanian

Dissertation submitted to the Faculty of the

Virginia Polytechnic Institute and State University

in partial fulfillment of the requirements for the degree of

Doctor of Philosophy

in

Engineering Mechanics

APPROVED :

W. W. Stinchcomb, Chairman

K. L. Reifsnider

R. D. Kriz

A. C. Loos

R. G. Kander

May, 1994

Blacksburg, Virginia

EFFECT OF FIBER/MATRIX INTERPHASE ON THE LONG TERM BEHAVIOR OF CROSS-PLY LAMINATES

by Suresh Subramanian

Dr. Wayne W. Stinchcomb, Chairman

Engineering Science and Mechanics Department

ABSTRACT

A systematic study was conducted to examine the influence of fiber surface treatment and sizing on the formation of fiber-matrix interphase and its effects on the mechanical properties of composite laminates. Three material systems having the same Apollo graphite fibers and HC 9106-3 toughened epoxy matrix, but with different fiber surface treatments and sizings were used in this study. The fibers used in the 810 A and 820 A systems received 100 % and 200 % industry standard surface treatments respectively, and were sized with Bisphenol-A unreacted epoxy material. The 810 O system was manufactured with 100 % surface treated fiber that were sized with pvp (polyvinylpyrrolidone), a thermoplastic material.

The presence of different interphase in these materials was confirmed using a permanganic etching technique. Results indicate that the interphase is discontinuous and made of linear chain polymeric material in the 810 A system. The interphase in the 810 O system has a gradient morphology while the 820 A system does not possess a well defined interphase.

Mechanical test results indicate that the 810 O system significantly greater longitudinal tensile strength and failure strain compared to the 810 A system. The 810 A and 820 A systems have similar longitudinal tensile properties. Transverse tensile test results indicate that the 820 A system has the highest strength while the 810 O system has the lowest strength. The $(0,90_3)_s$ cross-ply laminates from the three material systems exhibit different damage mechanisms and failure modes under monotonic tensile loading.

Fatigue test results indicate that the 810 O laminates have longer fatigue lives at higher load levels and shorter fatigue lives at lower load levels compared to the 810 A laminates. The 820 A laminates have

longer life compared to the other two materials systems, at all three load levels. The 810 O material exhibits greater damage and stiffness reduction than the other two materials. The 810 A and 820 A systems exhibit a brittle stress concentration controlled failure, while the pvp sized 810 O system exhibits a global strain controlled failure.

A micromechanics model was developed to investigate the role of the interphase on the tensile strength of unidirectional laminates. A new parameter called the 'efficiency of the interface', is introduced in the model. A simple scheme that uses the experimentally determined tensile modulus of unidirectional laminates in a concentric cylinders model, is described to estimate the interfacial efficiency. The tensile fatigue performance of cross-ply laminates is predicted using this micromechanics model in a cumulative damage scheme. The predicted fatigue lives and failure modes agree well with experimental results.

ACKNOWLEDGEMENTS

The author would like to greatfully acknowledge the support and contributions of the following people :

- Thangam and Subramanian, the author's parents, for showering unlimited love and affection and helping him understand the true meaning of life.

- Dr. Wayne Stinchcomb, the chairman of the committee, for extending the author complete freedom to conduct this investigation, and yet maintain focus on the main goals. Other than his support in technical matters, his loving nature and patience with the author made his stay at Virginia Tech. a very pleasant and memorable experience. His unfortunate demise, two months prior to the author's defence, is a personal blow to the author and a big setback to all the members of the Materials Response Group.

- Dr. K. L. Reifsnider, for his encouragement and support throughout the author's stay here. Other than helping gain a clear understanding of the mechanics of composite materials, he has helped the author learn the real meaning of professionalism and humility. As the head of Materials Response Group, he has provided a working environment that the author has been very fortunate to have been a part of.

- Dr. R. G. Kander, for taking time from his busy schedule and reading through the dissertation manuscript carefully, and making very useful and helpful suggestions.

- Dr. Kriz and Dr. Loos for serving on the author's advisory committee.

- Dexter Hysol, Pittsburg, California, for donating material used in the study.

- Edwards Air Force Base (Phillips Laboratory) and NASA LRC for financial support.

- Jack Lesko, for his friendship and all the long hours of discussion, trying to better understand the 'PVP mystery'. Jack is one of the finest experimentalist that the author has seen and the author would like to thank him for sharing his knowledge and experience with him.

- The author would like to thank Nagendra Somanath, Naganand Doraiswamy, Wilfred Mascarenhas, Anand Rau, Nirmal Iyengar, Narayana Vure, Jyothikumar, Anil Tiwari, Nachiketa Tiwari, Scott Case, Jennifer

Elmore, Hari Reddy, Krishnan Jayaraman, Yongli Xu, Kami Razvan and Kin Liao for their friendship and support.

- All members of the Materials Response Group family, for making the author's stay a pleasant and enjoyable one.

TABLE OF CONTENTS

LIST OF FIGURES

LIST OF TABLES

1.0 INTRODUCTION AND OBJECTIVE

1.1 Introduction

Although the concept of fiber reinforced composite materials has been around for a long time, there has been an upsurge of interest in this class of materials over the last two decades. This has primarily been due to the demands placed on materials performance by advanced technology in the aerospace industry. In order to satisfy the requirements of the aerospace industry, materials engineers have been actively pursuing the goal of creating new material systems which possess high specific strength and stiffness. In this effort, man has turned to nature to draw on its expertise in creating the most optimized systems for different purposes. Natural wood, the human bone, etc are some common examples of " fibrous composites " created by nature to best meet the requirements placed on these structures. In creating newer material systems, materials engineers have combined high strength and stiffness fibers with softer, less strong matrix materials to form composite materials with high specific strength and stiffness. During the last decade, a great deal of attention has been focussed on improving the performance of the two basic constituents of the composite material, namely, the fiber and matrix. Stronger, stiffer and lighter fibers are being developed towards this end. The performance of the matrix is being improved by developing tougher, damage tolerant matrices. However, in the last few years, the role of the third constituent of the composite called the "Interphase/Interface", has also received a great deal of attention in the composites community. The role of the interphase/interface in the performance of the composite system has been actively pursued by a number of researchers. Composites engineers are currently seeking to answer the following question: ***" Can the performance of the composite system be improved by tailoring the interphase/interface region? "*** It must be admitted that the composites community is far from having a simple answer to this question, but numerous investigations are being carried out to better understand the role of fiber-matrix interface/interphase in the performance of advanced composites.

The objective of the present study is to investigate the influence of the fiber-matrix interphase on

the damage characteristics and performance of cross-ply laminates under monotonic and long-term (fatigue and creep) loading. Three material systems having the same Apollo graphite fibers and HC9106-3 toughened epoxy matrix, but with different fiber surface treatments (100 % and 200 %) and sizing (Bisphenol-A (unreacted epoxy) and Polyvinylpyrrolidone (thermoplastic)) were used in this study. A $(0,90_3)_s$ cross-ply laminate configuration was used to study the performance of these material systems. Some of the specific goals of this investigation are discussed in the next section.

A comprehensive review of the literature on the techniques available for the characterization of the fiber-matrix interphase and the influence of interphase on the mechanical properties of composite materials is presented in section 2.1. Since the goal of this work is to investigate the role of the fiber-matrix interphase on the long term performance of composites, some studies on the analytical and experimental characterization of damage in composite materials under fatigue and creep loading are discussed in sections 2.2 and 2.3 respectively.

A detailed description of the material system used in this study, and of the testing procedure used for characterizing static and long-term behavior are provided in chapter 3.

The results from the various tests on unidirectional and cross-ply laminates subjected to monotonic, fatigue and creep loading are discussed in chapters 4 through 8. The results from the interphase characterization tests are discussed in chapter 4. This includes both qualitative assessment of the interphase characteristics and quantitative interfacial shear strength results. The unidirectional laminate test results (longitudinal tensile and transverse tensile tests) for the three material systems used in this study are detailed in chapter 5. In chapter 6, the damage analysis and strength results from quasi-static tests on $(0,90_3)_s$ laminates are discussed. The damage characteristics and lives of cross-ply laminates subjected to tension-tension fatigue loading are presented in chapter 7. The role of the interphase in the damage progression in cross-ply laminates under monotonic and fatigue loading is contrasted in that chapter. The room temperature creep response of the $(90)_{12}$ and $(0,90_3)_s$ cross-ply laminates and the elevated temperature short-term creep response of $(90)_{12}$ laminates are discussed in chapter 8.

Some analytical models used to predict the influence of the interphase on the damage and life of composite laminates under monotonic and long-term (fatigue and creep) loading are detailed in chapter 9. The salient features of the cumulative damage scheme used to predict the fatigue life of cross-ply laminates (including the effect of interphase) are also highlighted in that chapter.

Some conclusions on the role of the fiber-matrix interphase in the damage characteristics and strength and life of composites are listed in chapter 10.

1.2 Objectives

The objective of this work is to study the influence of fiber-matrix interphase on the damage and performance characteristics of graphite/toughened epoxy laminates under monotonic and fatigue and creep long term loading. Some of the specific objectives of this study are highlighted below

- To establish the formation of different fiber-matrix interphases by varying the fiber surface treatments and sizing using qualitative and quantitative interphase characterization techniques.
- To evaluate the effect of the interphase on the unidirectional properties such as longitudinal and transverse stiffness and strength.
- To investigate the influence of the interphase on the damage characteristics and strength of $(0,90_3)_s$ laminates under monotonic loading. Various non-destructive techniques such as edge replication, x-ray radiography, acoustic emission etc are used to document the progression of damage in the cross-ply laminate.
- To evaluate the role of fiber-matrix interphase on the damage progression and life of cross-ply laminates subjected to tension-tension fatigue loading.
- To experimentally determine the creep response of unidirectional and cross-ply laminates with different fiber-matrix interphases.
- To construct analytical models including the effect of interphase, to predict the various damage mechanisms such as matrix cracking, fiber-matrix debonding, fiber fracture and creep deformation.

- To develop a cumulative damage scheme (that uses the models developed to predict the various damage mechanisms) and estimate the fatigue life of cross-ply laminates.

2.0 LITERATURE REVIEW

Since the scope of this study is broad, the literature review will be presented in three sections. The recent efforts in the area of characterization and evaluation of the influence of interphase on the performance of composites will be reviewed in section 2.1. A general discussion on the various analytical and experimental techniques available to characterize damage under fatigue loading in composite materials will be presented in section 2.2. In section 2.3, some of the recent literature on the time dependent response of carbon fiber reinforced composites will be reviewed.

2.1 The Interphase Concept

Numerous studies have been carried out in the last few years to characterize and evaluate the properties of the interface/interphase region. Before delving into this topic, it is only appropriate that the terms interphase and interface be defined. Jayaraman et al. [1] have pointed out that the terms interface and interphase are being used loosely in the literature often to refer to the same entity. In an effort to distinguish these terms, they have defined "Interphase" as the region formed due to the bonding between the fiber and matrix, having a morphology and/or chemical composition different from the bulk matrix and fiber. They also conclude that the interphase may possess characteristics such as a finite thickness, degree of anisotropy, tensorial bond strength, tensorial properties such as stiffness, coefficient of thermal expansion, Poisson's ratio etc. In contrast, they have defined the "Interface" as the two dimensional border separating the bulk phases such as fiber, matrix and interphase. Thus it could be said that the interphase becomes the interface as the thickness dimension of the interphase becomes vanishingly small.

One of the basic questions in connection with the interphase concept that needs to be addressed is : " How does the nature of bonding between the fiber and matrix and the presence of the third constituent (called the "Interphase") between the fiber and the matrix affect the performance of the composite material ? " . The answer to this question is not simple and there is not enough data available in the literature to support any conclusions. However, based on the numerous recent investigations in this area, it can be said

with some degree of confidence that the nature of the interface/interphase does indeed affect the performance of the composite material.

In order to fully understand the influence of the fiber-matrix interface/interphase on the performance of composites, it is necessary to first evaluate the properties (both stiffness and strength) of the interphase. A cursory glace at the current literature indicates that even though a great deal of progress has been made in the area of determination of the fiber-matrix bond strength, there is hardly any standard method available to determine the in-situ elastic moduli of the interphase in the composites. This is primarily due to the myriad of variables involved in the formation of the interphase (material variables, processing variable etc), and the small dimension of the interphase region (of the order of micrometers). This has restricted the analyses of composite properties including the effect of interphase to a great extent. In most analyses, the interphase is reduced to a two-dimensional interface region with the bond strength being the only variable included in the analysis. In order to capture the influence of fiber-matrix interphase, the analytical models have to consider the interphase as a distinct region with properties different from those of the bulk matrix and the fiber. In a recent paper Jayaraman et al. [2,3] have reviewed the progress in the field of experimental and analytical evaluation of the properties of the interphase in composite materials. They have also provided a comprehensive evaluation of the various experimental and analytical techniques currently available, to evaluate the fiber-matrix bond strength in fiber reinforced composites. Since the focus of this investigation is to evaluate the influence of various fiber-matrix interphases on the static and long-term performance of composite laminates, the literature on the determination of the interphase properties will not be reviewed extensively. Only the literature on methods used widely to characterize the interphase, will be examined in section 2.1.1. In section 2.1.2, the results from some of the recent investigations on the effect of the fiber-matrix interphase on the mechanical properties of composite materials will be reviewed.

2.1.1 Characterization of Interphase

The various techniques available to characterize the interphase in fiber reinforced composites can be broadly grouped under two categories - Qualitative and Quantitative assessment of interphase characteristics. Some commonly used interfacial characterization techniques are discussed in this section. It must be added that some of the quantitative interfacial strength characterization techniques have been extended recently to estimate the elastic moduli of the interphase region. A brief discussion of these results are also provided in this section.

a. Qualitative Assessment of Interphase Characteristics

The techniques used to qualitatively assess the nature of the interphase in composites include the Dynamic Mechanical Analysis (DMA) [4-6], Etching and Scanning Electron Microscopy [7-9], X-Ray Photoelectron Spectroscopy (XPS) [10-12], Raman Spectroscopy [13], Inverse Gas Chromatography (IGC) [14], Scanning Electron Microscopy (of fiber surface) [15] etc. The first two tests are performed on the composite specimen, while the other tests are performed on the fibers. Some of the techniques mentioned above are discussed in this section.

Dynamic Mechanical Analysis (DMA)

Since polymeric materials are viscoelastic in nature, the dynamic mechanical analysis technique is used widely to characterize the viscoelastic response of composites in the matrix dominated direction. Some recent investigations have revealed that the dynamic mechanical response of polymeric composites is sensitive to the quality of fiber-matrix bonding. Reed [4] has reported an additional glass transition (T_g) peak above the T_g peak of the matrix, in a glass/epoxy composite. He attributes this peak to the formation of an interphase. Thomason [5] has reported results similar to those reported by Reed. But, he claims that the additional peak is an artifact, formed due to the thermal lag in the different regions of the specimen. He however has reported another minor transition below the T_g of the matrix. He has concluded that this transition is due to presence of the interphase between the glass fibers and the epoxy matrix. Gerard et al.

[6] have investigated the influence of fiber sizing on the T_g of graphite/epoxy composites. They have concluded that the T_g of the composite reduces in the presence of a compliant interphase region. They have attributed this to the increased mobility of polymer chains in the fiber-matrix interphase region. They have also reported a reduction in the storage modulus in composites with a compliant interphase. It is thus seen that the dynamic mechanical properties of composites are sensitive to the small changes in the fiber-matrix interphase. The DMA results provide a qualitative insight into the nature of interphase present in the composite.

Etching and Scanning Electron Microscopy

One of the methods to directly image the microstructural details at the fiber-matrix-interphase level is through the use of scanning electron microscopy. Recently, Peacock et al. [7] have used the permanganic etching technique [8], to study the microstructural details of the region near the fiber, in AS4/PEEK (semi-crystalline) composites. They have reported that by using the etching technique described in [8], the amorphous linear chain PEEK material in the composite can be etched away, revealing the spherulitic crystal growth emanating from the fiber surface, under the scanning electron microscope. Peters and Albertsen [9] have presented the morphology of specimen etched using the permanganic etching technique [8] from a series of graphite/toughened epoxy specimen with fiber surface treatment levels ranging from 0 % to 100 %. They claim that the morphology of the etched specimen with varying levels of surface treatment are different. It is thus possible to obtain qualitative information about the interphase using the etching and scanning electron microscopy technique.

X-Ray Photoelectron Spectroscopy

X-Ray Photoelectron Spectroscopy (XPS) is one of the most commonly used techniques to analyze the surface chemistry of the carbon fibers. This technique reveals the amounts of nitrogen, oxygen, and carbon on the surface of the fiber. It is well recognized that the fiber surface treatment process removes surface layers from the fiber and adds some chemically active groups on the fiber surface. The changes in the amounts of chemically active groups on the fiber surface can be detected using the XPS technique.

Hodges et al. [10] and Bascom et al. [11] have reported that as the oxygen content on the surface of the fiber increases, the bond strength of the interface also increases. Recently, Chang [12] in his work with AU4, AS4, and AS4CGP fibers in J2 (Thermoplastic) matrix, has observed trends similar to that reported in [10] and [11]. It is thus possible to estimate the quality of bonding based on the XPS results.

Scanning Electron Microscopy (on fiber surface)

It is well recognized that the degree of surface roughness affects the bonding characteristics of the fibers. As the surface roughness increases, the mechanical interlocking capacity increases, yielding a better bond. The observation of fibers under the SEM at high magnifications yields valuable information about the fiber diameter, surface roughness of the fiber, and the presence/uniformity of coating material on the fiber surface. Yip and Lin [15] have recently correlated increase in fiber-matrix adhesion in a carbon/epoxy system with the increase in surface roughness. However, Chang [12] has reported that the adhesion in the untreated AU4/J2 system is lower than the surface treated AS4/J2 and AS4CGP/J2 systems, even though the AU4 fibers have greater surface roughness. He has attributed this to the presence of weak layers, and the absence of chemically active groups on the fiber surface in the untreated AU4 fibers.

b. Quantitative Assessment of Interphase Characteristics

Many recent efforts have focussed on development of techniques to determine the strength of the fiber-matrix bond. Most methods available currently to determine the interfacial bond strength use model composite specimens, and do not account for the irregular fiber packing, fiber-fiber interaction etc. Some commonly used techniques include the Single Fiber Pull-Out test [16], Single Fiber Fragmentation Test [17,18], Single Fiber Micro-Indentation test [19,20], and Meso-Indentation test (Continuous Ball Indentation Technique)[21]. The first two techniques use model composites, with a single fiber embedded in an infinite matrix material. The results from these tests do not include the fiber-fiber interaction effects. In the single fiber micro-indentation test, a single fiber in the laminated composite cross-section is indented and the results are used in a finite element analysis code,to estimate the interfacial strength. In the meso-

indentation test, a group of fibers are indented and the average failure strength of the fiber-matrix interface is calculated using a cellular analysis developed by Carman et al. [22]. Some of these techniques are discussed in this section. A critical review of the various micromechanical tests for ISS measurement in composite materials is presented in reference [23].

Single Fiber Fragmentation Test (SFFT)

This test was first used by Kelly and Tyson [17] to measure the adhesion of glass fibers to polymer matrices. Drzal et al. [18] have recently used this technique to evaluate the interfacial strength of carbon fiber-epoxy matrix composites. A tensile dogbone test specimen is used in this test. The test coupon consists of a single fiber embedded in the selected matrix material. The specimen is loaded in the stage of a polarized transmitted light microscope. The fiber breaks into progressively smaller fragments under increasing loads until a "critical length" is reached. Beyond this, the fiber does not fragment into smaller pieces under increasing loads. The experimentally measured "critical length" is used in a shear lag analysis model [17] to estimate the interfacial shear strength (ISS). It has been observed [18] that the strain to failure of the matrix must exceed three times the fiber failure strain in order for the fiber to achieve the "critical length" before catastrophic specimen failure occurs. This limits the use of this technique, especially in systems with high strain fibers. It is also noted in passing that this technique uses a model composite and hence, the effects of fiber-fiber interactions are not included. In this method, the interfacial debonding is precipitated by the fiber fracture. This means that the statistics of the distribution of strength of the fiber must be considered in the ISS calculation. One important advantage of using this technique is that the stress state in the interface region is relatively simple and better understood comared to the other interfacial strength determination techniques. This makes the estimation of ISS from this test simple and reliable. It must be mentioned that in order to obtain better estimates of the ISS using this technique, the effect of local matrix yielding must be considered in the analysis. Another added advantage of this technique is that the stress birefringence patterns at fiber breaks can be used to make qualitative estimates of the nature of bonding. It has been reported [11] that in the case of a weak interfacial bond, stress

birefringence appears at fiber breaks and with the slightest increase in load, the birefringent nodes recedes from the fiber break as if the matrix is "unzipping" from the fiber. In the case of a strong bond, the nodes remain close to the fiber break. Also, relaxation of tension on the specimen causes all of the birefingence to dissipate in the case of weak bonding. In the material with strong interfacial bonding, the lip of birefringence remains indicating shear yielding. Due to the nature of loading and the failure process involved in this method, it is the author's opinion that the ISS estimated using this technique is probably most representative of the interfacial debonding observed in 0° plies in composite laminates under axial tensile loading.

Meso-Indentation Technique (Continuous Ball Indentation Test)

The Continuous ball Indentation Test has been used by Lesko [21] to estimate the interfacial shear strength of composites. The details of the experimental setup are described in [21]. In this technique, a region of the composite material is indented with a 0.06" diameter hardened steel ball indenter. Since the indentation is made over a large area, the influence of fiber-fiber interactions and irregular fiber distribution are accounted for in an average sense in this techniques. However, since the failure occurs over an area that spans more than one fiber, and since the applied loading results in a complex stress state, the absolute values of interfacial strength obtained from this analysis must be treated with some degree of caution. In the author's opinion, this technique does provide a good insight into the nature of fiber-matrix bonding present in the composite.

c. Estimation of Elastic Properties of the Interphase

As mentioned earlier, most efforts in recent years have been directed towards the determination of the interfacial strength in composite materials. In all these techniques, the interphase is assumed to be a two dimensional interface region. In the authors opinion, this may not represent the physics of the problem accurately. In order to obtain better estimates of the interfacial strength, the interphase must be represented by a distinct region with properties different from those of the fiber and the matrix. However,

due to limitations mentioned earlier, the determination of the properties of the interphase is currently the biggest challenge facing the micromechanics community.

Some recent efforts have been directed towards backing out the interphase properties from the micro-level tests described in the previous section. The discussion on the various techniques available currently will be restricted in this section. A detailed discussion of these techniques can be found in [2]. Tsai et al. [24] have used the results from the micro-indentation tests obtained by Mandell et al. [20], in conjunction with a shear lag model to back out the shear modulus of the interphase. They have concluded that the shear modulus of the interphase is several hundred times smaller than that of the matrix material for the graphite/epoxy system used in the study. Asloun et al. [25] have used the results from the single fiber fragmentation tests for a carbon/epoxy system with a shear lag analysis to estimate the Young's modulus of the interphase. They have concluded that the Young's modulus of the interphase is greater than that of the matrix material. Recently Sottos et al. [26] have used a Laser micro-interferometric technique to estimate the properties of the interphase in graphite/epoxy composites. They have backed out the Young's modulus of the interphase by matching the experimental and theoretical displacement profiles of the composite. They have concluded that the Young's modulus of the interphase calculated using this technique is almost an order of magnitude lower than that of the bulk matrix.

It may thus be concluded that the science of estimation of interphasial properties such as Young's modulus, Shear modulus etc. is at best in its infancy. More work needs to be done to develop better techniques to estimate the properties of the interphase. Due to the limited information available on the properties of the interphase, most techniques used to estimate the strength of the interphase are restricted to considering the interphase as a two dimensional region. The techniques used to calculate the interfacial shear strength (ISS) values use some analytical tools (shear lag analysis, finite element analysis) to estimate the stress state in the interface region. These stresses are used in conjunction with the experimentally obtain loads to interfacial failures, to calculate the ISS. In the authors opinion, in order to estimate the local stress state at the fiber-matrix interface accurately, the interphase should be modeled as a region with finite

thickness, and having properties distinctly different from that of the matrix material. This is currently one of the biggest challenges facing the composites micromechanics community.

Before leaving this section, some aspects of the interphase concept that have not received much attention, but could prove to be important in understanding the role of interphase in the performance of composites, will be highlighted. The issue of toughness of the interphase has not been discussed widely in the composites literature. In the authors opinion, in order to understand the influence of interphase on the composite properties, the issue of the fracture toughness of the interphase/interface must be addressed. Since the failure of the interphase could be due to combined normal and shear stresses in composite laminates, the use of energy based failure criterion could be more advantageous. In this regard, it may be advantageous to define the work of fracture of the interphase. Since most recent results indicate that the elastic modulus of the interphase region could be significantly different from that of the bulk matrix material, the use of a work of fracture term could be more meaningful than the strength or strain to failure of the interphase. Another issue that has received little attention is the failure mode of the interphase. As discussed earlier, all the quantitative interphase strength measurement techniques provide an estimate of the interfacial shear strength. Care must be exercised while using this interfacial strength to situations where the failure of the interface is dominated by normal stresses (eg. failure of interface in 90° ply under uniaxial tensile loading). In the authors opinion, the term interfacial strength is very general, and must be used with caution. It would be advantageous to use two different quantities to characterize the interface; interfacial normal strength and interfacial shear strength. Yet another subtle but important factor that needs to be addressed is the issue of loading mode in the interfacial characterization test. It has been reported in the literature, that the interfacial shear strengths obtained from the single fiber fragmentation test and the micro-indentation test are significantly different. In the SFFT, the loading mode is tensile, and the interfacial failure is precipitated by fiber breakage. In the SFIT, the fiber is loaded in compression, and there is no fiber breakage prior to interfacial failure. Since the loading direction is reversed in these two tests, the effect of Poisson's contraction will also be reversed. All these factors could contribute to the

differences in the ISS values obtained from these two types of test. In the authors opinion, the ISS obtained from the SFFT would best describe the fiber-matrix debonding near fiber fractures in 0° plies under tensile loading. The ISS obtained from SFIT would better describe the interfacial failure observed in unidirectional composites under compressive loading.

It must also be mentioned here that there has been no systematic study to evaluate the interfacial strength under fatigue and creep loading. The higher interfacial strength obtained from conventional tests may not necessarily translate into good interfacial bonding under long-term loading conditions. For example, a material system could have high interfacial strength under static loading conditions, but may undergo early interfacial debonding under long-term loading conditions. Some effort must be directed towards understanding how the integrity of the interface is affected under long-term loading conditions. These studies must investigate the influence of rate and time dependent processes on the interphase characteristics.

2.1.2 Influence of Interphase on the Mechanical Properties of Composite Materials

The fiber-matrix adhesion in graphite fiber reinforced composites is commonly altered by varying the level of surface treatment on the fibers and by changing the sizing material on the fibers. Numerous recent investigations have focussed on the influence of carbon fiber surface treatment and fiber sizing on the fiber-matrix bond strength and the mechanical properties of composite materials. Some of the findings from these studies are discussed in this section.

Recent work by Madhukar and Drzal [27-30] has revealed that the longitudinal tensile, compressive and inplane shear strength depend on the type of interphase present in the composite. They have varied the interphase by altering the surface treatment and the fiber sizing. They used the untreated (AU4) fibers, surface treated AS4 fibers and surface treated and sized (with unreacted epoxy) AS4C fibers in Epon 828 matrix to obtain three systems of composites with different interphases. The authors have reported that the longitudinal tensile, compressive, transverse tensile strength, and mode I and mode II fracture toughness

are in the following order; AS4CGP > AS4 > AU4 system. They have attributed the improvement in mechanical properties to the improved bonding in the AS4 and AS4CGP system.

In their work with Hysol Grafil XA carbon fibers and EA9101 epoxide based resin matrix, Lehmann et al. [31] have observed that both fiber surface treatment and sizing affect the longitudinal tensile strength, longitudinal flexural strength, and short beam shear strength. They have reported that initially, increasing levels of surface treatments result in improved performance of the composite. However, at higher surface treatment levels (beyond 100 % in their investigation), the strength of the composite reduces with increasing surface treatment. They also observed an increase in longitudinal flexural strength (at all surface treatment levels) in laminates with a proprietary sizing based on a silicon containing backbone.

Fitzer et al. [32] have performed a systematic study of the effect of the various surface treatment processes on the adhesion characteristics of carbon/epoxy materials. They have concluded that the amount of reactive surface groups on the fiber surface and the short beam shear strength depend on the surface treatment process used. They have attributed the increase in SBS strength to the increase in the amount of reactive surface groups on the fiber surface.

Albertsen and Peters [33,34] have investigated the influence of fiber surface treatment on the fracture toughness (mode I and II) and strain to interphase failure (obtained from the crack density measurement on cross-ply laminates) in carbon/toughened epoxy composites. They have concluded that the strain to interphase failure, mode I and mode II interlaminar fracture toughness increase with increasing amounts of surface treatment. They have attributed this to the change in the crack path from fiber-matrix debonding in the untreated system to bulk matrix cracking in the 100 % treated system.

Schwartz et al. [35] have reported that the transverse strain to failure and mode I fracture toughness of graphite/epoxy laminates could be significantly altered by using an FM-1000 (adhesive material) sizing in graphite/epoxy composites.

Recently, Ivens et al. [36] have investigated the influence of fiber surface treatment on the matrix cracking behavior and strength of cross ply laminates under monotonic loading. They have concluded that

the strain to onset of transverse matrix cracking can be delayed by increasing the surface treatment level. They have attributed this to improved bonding resulting from surface treatment. They have also reported an increase in tensile strength of the cross-ply laminate with 10 % surface treatment compared to the untreated system. However, further increase in surface treatment resulted in reduction in the strength and strain to failure of the laminates. They have reported that the failure of laminates with higher surface treatments is brittle. It has been concluded that the reduction in strength at higher levels of surface tretment is due to the increased notch sensitivity in laminates.

Lesko et al. [37] have recently studied the influence of fiber surface treatment and sizing on the compressive strength of graphite/toughened epoxy composites. Their data indicates that the compressive strength of the composites can be varied by changing the surface treatment and sizing.

Some recent studies [38-42] have revealed that the interlaminar fracture toughness of carbon fiber reinforced composites could be changed significantly by altering the fiber-matrix bonding. A detailed review of these results are in reference [42]. It must be mentioned here that the mode I and mode II fracture toughness of the material system used in the present study are reported in reference [42]. It was observed that the mode I fracture toughness G_{Ic} of the laminates did not change with incresing surface treatment levels, but there was a significant increase in G_{Ic} in the laminates with a thermoplastic (PVP) sizing. The mode II fracture toughness results however indicated that the G_{IIc} of the 200 % surface treated system was the highest, followed by the PVP sized 100 % surface treated system. The 100 % surface treated Bisphenol-A epoxy sized system possesed the lowest G_{IIc} value. It must be mentioned that these results are at odds with some of the other results reported in the literature [40,41] for similar material system.

As pointed out by Swain [43], surprisingly absent in the literature is a systematic study of the role of the interphase on the long term behaviour (including fatigue and creep) of composites. Shih and Ebert [44] and Vincent [45] have examined the role of interphases on flexural fatigue behaviour of glass/epoxy composites. They have concluded that composites with greater bond strength (as measured by interlaminar

shear strength) had longer flexural fatigue lives.

Alstadt et al. [46] have investigated the effect of surface treatment on the mode I cyclic delamination growth characteristics of G30/EP5 graphite epoxy laminates. They observed that even though the mode I fracture toughness (G_{Ic}) increases with surface treatment, the fatigue delamination onset and growth characteristics remain relatively unchanged.

In a recent work, Swain [43] has investigated the fatigue performance of carbon fiber reinforced toughened epoxy laminates. The affect of the interphase was studied by systematically altering the surface treatment (from 10 % to 200 %) and fiber sizing (designated by the fiber manufacturer as "A" and "O" sizing). The laminate configurations used in this study included $(\pm 45)_{4s}$ and $(0,90)_{8s}$ layups. Laminates with 0.25" center notch were tested under fully reversed loads (R=-1) and 10 Hz frequency. Swain has concluded that both fiber sizing and surface treatment affect the fatigue life of these composites. An attempt was made to correlate the fatigue characteristics with the bond strength. The damage analysis performed in this study revealed significant differences in damage modes in laminates with different interphases. The interfacial strength and damage analysis results were used to explain the varied fatigue performance characteristics of these laminates. The results from this investigation indicated that the extent to which the interphase affected the fatigue life of the composite depended on the stacking sequence and presence of a notch.

To the best of the authors knowledge, there has been no investigation to date to study the affect of interphase on the creep and creep rupture properties of carbon/epoxy composites. However, in a recent work at Virginia Tech by Chang [12], a systematic study was performed to investigate the affect of the interphase on creep and creep rupture characteristics of the AS4/J2 (Thermoplastic) system. The interphase affect was studied by using untreated, treated and sized AS4 fibers in J2 matrix. Chang concluded that the creep response of the system investigated was insensitive to the interfacial shear strength. It was also observed that the degradation rate of the creep rupture strength was not affected by the interphase properties. However, the system with sized fibers (a compliant sizing designated as AS4CGP by the

manufacturer) was found to have higher creep rupture strength compared to the AS4/J2 system in a $(\pm 45,90_2)_s$ layup, even though the static strength of these two systems were nearly equal. Chang has concluded that the affect of the interphase on the static and long term properties are not necessarily similar. It was also noted that the damage modes in the laminates used in this study depended on the type of interphase present.

2.2 Long Term Characterization of Composites

2.2.1 Fatigue Damage in Composites (Experimental Studies)

The fatigue behaviour of composite materials has been a subject of active research in the recent years. The damage process in laminated composites subjected to fatigue loading is significantly different than that observed in conventional materials. The four main damage modes observed in laminated composites under fatigue loading are matrix cracking, fiber-matrix debonding, delamination and fiber fracture [47,48]. The initial stage consists primarily of matrix cracking along the fiber direction in the off-axis plies. The density of cracks increases at a rate proportional to the applied stress and the constraint provided by the adjacent plies. The cracking density increases until an equilibrium or saturation crack spacing called the characteristic damage state (CDS) is reached [48].

As the primary cracks develop, they create a complex 3-d stress state at the interface of the plies. Secondary cracks running perpendicular to the primary cracks initiate in the adjacent plies along these primary cracks. Local ply delaminations also initiate at the locations of the intersections of the primary and secondary cracks.

The next event that occurs is delamination between plies at the free edges. The high interlaminar stresses at the free edges are the driving force behind the formation and growth of the edge delaminations.

The final stage of damage is dominated by the accumulation of fiber fractures in the primary load carrying ply. These fiber fractures have been found to be concentrated in the plies adjacent to the weaker off-axis plies which undergo transverse matrix cracking. The stress concentrations around the primary

cracks result in local accumulation of fiber fractures in the region close to the primary matrix cracks [49].

The individual mechanisms do not occupy distinct regions in the damage growth process. However, each mechanism is dominant in some distinct stage of damage growth. For example, the first stage is dominated by matrix cracks, while delaminations are dominant in the middle stage and fiber fractures are dominant in the final stage.

It has been observed that the stiffness of the laminate reduces during the process of damage accumulation in composites [50-52]. During the matrix cracking stage, the cracked plies undergo local stress relaxation and the adjacent plies carry additional loads. Even though the local stress state is complex, there is an affective increase in strain in the laminate. This results in a reduction of the global stiffness of the laminate. Reifsnider and Stinchcomb [53] have investigated the concept of using stiffness change as a nondestructive fatigue damage parameter. In general, they found that stiffness change can be quantitatively related to the fatigue life and residual strength of composite laminates through various models based on the observed micro-damage.

2.2.2 Fatigue damage in composites (Analytical Studies)

The analytical modeling of damage in composite materials and the prediction of degradation of properties under cyclic loading have received a great deal of attention in the last few years. The discipline underscoring this approach has emerged under the name of "Damage Mechanics" [54]. The focus of this discipline has been on the integration of experimentally observed damage mechanisms with the micromechanical representation of these damage modes using standard elasticity solutions. Two distinct approaches have been used in the literature to model the progressive damage in composite materials. In the first approach called the Representative Volume Element (RVE) approach, a unit cell is constructed, in which the material configuration details and the damage configuration details are incorporated. A boundary value problem is formulated on the RVE and the solution of this problem yields the required stress state in the material.

Numerous models based on the RVE concept have been proposed in the recent years. Aboudi [55] has proposed a micromechanical model based on the method of cells to determine the local stresses in the fiber, matrix and interphase at a micro level. A rectangular area is considered for analysis and this representative area is subdivided in four rectangular subcells. One subcell represents the fiber while the other three represent the matrix material. The volume fraction of the composite is varied by changing the dimensions of the subcells. A concentration matrix B is defined for each subcell and an elasticity approach (linear elastic constitutive relationship, displacement and traction continuity at the subcell interfaces) is used to determine the microlevel stresses.

The second approach to modeling progressive damage consists of characterizing damage by a set of internal variables representing the state of the material. A set of phenomenological relationships between the response and damage state variables are developed using the principles of thermodynamics. Talreja [54] has used vectors to characterize damage, and has used the second law of thermodynamics to obtain a constitutive relationship which involves the components of the damage vector. This approach requires evaluation of some phenomenological constants. Using this approach, Talreja has predicted progressive damage and the associated reduction in various properties such as E_1,E_2,G_{12} etc. under static and fatigue loading. Talreja has pointed out that due to damage, the initially orthotropic lamina becomes more generally anisotropic. Numerous other models based on internal variable have been proposed by Allen et al. [56], Joshi et al. [57] etc.

One of the popular schemes used by researchers in the area of Damage Mechanics is the so called " Cumulative Damage Model". This is a semi-empirical analysis method. In this approach, the different damage modes such as matrix cracks, delaminations etc. are represented by a boundary value problem. A solution to this boundary value problem yields the local stresses in the damaged material. These local stresses are used to estimate the degradation in material properties. The degraded properties along with the modified stresses are used to predict cumulative damage progression. A formalized model based on this approach, called the critical element model, was proposed by Reifsnider and Stinchcomb [58]. In this

approach, the material is assumed to be composed of sub-critical elements and critical elements. The primary load carrying members (eg. the fiber at the fiber/matrix level, the primary load carrying ply at the lamina level) are normally the critical element. The secondary, non-load carrying members (eg. matrix at the fiber/matrix level, off-axis ply at the laminate level) are called the sub-critical element. Non-catastrophic damage such as matrix cracks, fiber/matrix debonding etc. are typically associated with the sub-critical element . The final failure of the material is associated with the failure of the critical element. The cumulative damage model consists of calculating the stress state in the sub-critical element and estimating the values of properties of the damaged material in the subcritical elements after a specified number of cycles or time. Using these stresses and damaged properties, the stresses in the critical element are estimated. The reduction in strength (fatigue/creep rupture) in the critical element is also estimated from basic material characterization data. A suitable failure criterion (Tsai-Hill or Maximum stress) is then used to check for the failure of the critical element. The fatigue or creep life of the laminate is estimated by calculating the cycles or time required for the failure of the critical element.

Numerous semi-empirical models have been proposed to predict the stiffness degradation and life estimation of laminated composite materials. Daniels and Lee [59] have used a semi-empirical approach to predict the property degradation and fatigue life of cross ply laminates. They have developed empirical relationships to correlate the damage with the stiffness degradation in the laminate (measured experimentally). Using this in conjunction with the S-N curves for the 0° and 90° laminates, the fatigue life of the cross ply laminate was predicted. Wang [60] has used a Monte-Carlo simulation method to account for the statistical variation in strength of the transverse ply in cross ply laminates. Using this approach in conjunction with a Paris law representation of damage growth, the damage progression and stiffness degradation in cross ply graphite/epoxy laminates was predicted.

Hashin and Rotem [61] have proposed a macromechanics approach to predict the fatigue life of composite materials. In their approach, it was assumed that failure could be described by a macroscopic failure function in terms of the applied load. The failure function contains unknown parameters which are

determined from simple experiments. The failure functions are dependent on the stress ratio, applied load frequency and cycles.

Recently Reifsnider and Gao [62] have proposed a micromechanics based approach to predict the fatigue life of unidirectional laminates. They have used a modified form of the Mori-Tanaka [63] method to estimate the stresses in the matrix and fiber phases. This was used in conjunction with the failure functions for the matrix/fiber phases in the appropriate failure criterion (Tsai-Hill or maximum stress type) to estimate the fatigue life of unidirectional laminates. This approach is particularly attractive because it allows for the consideration of a third distinct " Interphase" phase in the local stress analysis and hence in the life prediction.

2.3 Creep Damage

Viscoelastic materials such as polymers, subjected to static or cyclic loads exhibit time dependent deformation (creep) and delayed failures (creep rupture). The prediction of creep damage and creep rupture is complex because it involves the knowledge of load, temperature and environmental history. Further, the viscoelastic behaviour can be non-linear at different loads and temperatures, making the analysis complicated.

2.3.1 Experimental Observations

The creep response of composites has been studied by numerous authors. Yeow [64] observed that the transverse compliance and shear compliance (S_{22} and S_{66}) were time dependent while S_{11} was relatively time independent for graphite/epoxy systems. Dillard [65] reported a 10% reduction in transverse compliance S_{22} over four orders of time for graphite/epoxy materials. Gramoll [66] has reported a time dependent behaviour in the fiber direction in the Kevlar/epoxy laminates used in his study. He has attributed this to the viscoelastic nature of the Kevlar fibers. Moore [67] has studied the time dependent damage of graphite/epoxy and kevlar/epoxy cross-plied laminates. He has reported time dependent matrix cracking in both material systems. It was observed that the number of matrix cracks in the transverse plies

increased with time under constant applied loads and achieved a saturation spacing similar to the CDS state observed in the static loading. Damage analysis indicated that the time dependent matrix cracks did not always extend through the width of the laminates as is the case under static loading. Moore observed that these cracks grew across the width of the laminate with time and many of the cracks were arrested before they could grow across the width of the laminate.

The dynamic mechanical analyzer (DMA) has been used by numerous researchers [68,69] to characterize the creep response of laminated composites. Recently Chang [12] has used the DMA to characterize the creep response of graphite/thermoplastic composites. He has generated short-term (10 minute) creep compliance data at various temperatures using (90_{12}) laminates. The creep master curve was then generated using the time-temperature superposition principle [70]. Using this method, long-term creep response was estimated from the short-term creep test data. It must be pointed out here that the creep data obtained using DMA represents the flexural creep response of the material. This could be different from the tensile creep response obtained from conventional creep tests.

2.3.2 Analytical Modeling of Creep Behaviour

Linear viscoelastic behaviour is most commonly represented by mechanical analogs using spring and dashpot systems connected in series or parallel [71]. The two basic models used are the Kelvin model(parallel) and Maxwell model(series). By combining a series of such elements, the accurate representation of the viscoelastic material behaviour is achieved. The time dependent creep compliance for a series of Kelvin elements is given by

$$D(t) = \sum \frac{1}{E_i}[1 - \exp(-E_i t/\mu_i)]$$

where E_i is the stiffness of the i^{th} spring and μ_i is the viscosity of the i^{th} dashpot. By adding a spring in series with the Kelvin model, a viscoelastic solid response can be achieved.

The Boltzman superposition principle is often used to find the response of a linear viscoelastic material for any arbitrary stress history by representing the stress history as a series of small steps in stress

$$\varepsilon(t) = \int D(t-\tau)\frac{d\sigma}{d\tau}d\tau$$

where D(t) is the compliance function of the material, t is the time at the end of each step. The time-temperature superposition principle as reported by Leaderman [70] is often used in creep analysis. In this the creep compliance curves at various temperatures are superimposed using a horizontal shift factor.

Recently numerous non-linear viscoelastic behaviour models have been proposed. The Schapery integral [72] is based on an irreversible thermodynamics principle. Wilshire and Evans [73] have recently proposed the " Theta Projection" model in which the creep strain is represented by

$$\varepsilon_c = \theta_1(1-e^{-\theta_2 t}) + \theta_3(e^{\theta_4 t}-1)$$

where θ_1 and θ_2 act as scaling terms and θ_3 and θ_4 are rate parameters governing the curvature of the creep curve. They proposed a simple linear relationship to represent the stress and time dependence of the theta terms in the form

$$\log\theta_i = a_i + b_i\sigma + c_iT + d_i\sigma T$$

where a_i, b_i, c_i and d_i are experimentally determined constants.

Gramoll [66] has proposed a "quadratic power law" to model the creep behaviour of fiber reinforced laminates in the form

$$S_{ij}(t,T,\sigma) = S_{ij}^{o}(1+g_{ij}\sigma^2) + m_{ij}(1+f_{ij}\sigma^2)t^n$$

where S_{ij}, m_{ij} are linear constants and f_{ij} and g_{ij} are non-linear stress constants.

Hackett and Dozier [74] have used a cumulative damage scheme to include the affect of creep and damage to predict the creep rupture strength of filament wound spherical pressure vessels. In their analysis, they have applied the elastic-viscoelastic correspondence principle in conjunction with the method of collocation to obtain the time dependent stress variations. A cumulative damage scheme consisting of discretizing in the time domain, similar to the ones used for fatigue loading, was used to predict the creep rupture strength.

Dillard et al. [75] have also used a modified form of power law rate equation to predict the creep rupture strength of graphite/epoxy laminates with a limited degree of success. This scheme yielded good results for matrix dominated layups but was not very affective for the fiber dominated layups.

Recently Aboudi [76] has extended the method of cells analysis to predict the creep response of unidirectional composites. In this analysis, the fiber is considered to be elastic, while the matrix is assigned time dependent properties. Using the time dependent properties of the matrix and the micromechanics analysis based on the method of cells, the time dependent response of the composite is predicted. The predicted time dependent response of the composite agrees well with the experimental results.

3.0 MATERIAL SYSTEM AND TEST PROCEDURE

3.1 Material System

Material used in this study was obtained from McDonnell Aircraft Co., through Dexter Hysol. Three material systems having the same high modulus Apollo carbon fibers (manufactured by Courtoulds Research) and HC 9106-3 toughened epoxy matrix, but with different fiber sizing and surface treatment, were used to study the effects of interphase. For convenience, these are designated 810 A, 820 A and 810 O systems. Table I shows the description of the fiber, sizing and matrix used in the three material system. The fibers used in the 810 A and 810 O systems received 100 % industry standard surface treatment, while the fibers used in the 820 A system received 200 % industry standard surface treatment. The details of the process used to obtain the different levels of surface treatment are proprietary information, and are not known to the author at present. However, in general, the surface treatment process consists of passing the tows of graphite fibers through an electrolytic bath. The different levels of surface treatment are achieved by varying the time of exposure in the bath. The function of surface treatment is threefold. The solution in the electrolytic bath removes the weak outer layers in the fibers, deposits chemically active groups on the fiber surface, and generates 'pits'on the fiber surface. All the above mentioned actions influence the bond strength of the fibers. The 'A' and 'O' represent the two different sizing used in the fibers. Lesko et al. [77] have identified these sizings with permission from the manufacturers. The "A" sizing is an unreacted Bisphenol-A epoxy and the "O" sizing is Polyvinylpyrrolidone (PVP), a thermoplastic material. Again, the exact process used to get the sizing material on the fiber surface is not known (proprietary information). In general, after receiving the surface treatment, the fiber tows are passed through a bath containing the sizing material dissolved in some solvent. The fibers are coated with a thin layer of sizing material as they come out of this bath. The solvent is then removed by drying the fibers. It is interesting to note that the individual fibers are not coated with sizing material. Only tows of fiber are coated. The fiber sizing results in improved handleabilty. The sizing material (usually a polymer) also acts as a site

for nucleation of polymer cross-linking, and results in better bonding between fiber and matrix. Reference [78] lists several properties of the neat resin including glass transition temperature, tensile modulus, fracture toughness etc. The Apollo fibers have a circular cross-section, with a 5 micron nominal fiber diameter. The manufacturer reported properties of the fiber and matrix used in this study are listed in Tables II and III (obtained from reference [78]).

3.2 Laminate Configuration and Specimen Geometry

Laminates were manufactured by Dexter Hysol as 6" x 6" panels using an autoclave processing method in the following lay-ups : $(0,90_3)_s$, $(0)_{12}$ and $(0)_8$. All panels were inspected for manufacturing flaws using an ultrasonic C-scan technique. The fiber volume fraction in each panel were determined using the IsoPropyl Alcohol (IPA) technique. A complete description of the IPA technique is given in reference [43]. In this technique, the panels are weighed in air (W_a) and in Isopropyl Alcohol (W_i). Using Archimedes principle, and knowing the density of fiber and matrix and IPA, the density of the composite is estimated using the following relationship

$$\rho_c = \frac{W_a \rho_i}{W_a - W_i}$$

The fiber volume fraction is then estimated using the rule of mixtures as

$$FVF = \frac{\rho_c - \rho_m}{\rho_f - \rho_m}$$

It must be noted that this technique does not measure the void fraction present in the system. The average fiber volume fractions in the $(0)_8$, $(0)_{12}$, and $(0,90_3)_s$ panels are given in Table IV. All panels had fiber volume fractions between 56 % and 59 %. Specimens measuring 6" long and 1" wide were cut from the $(0,90_3)_s$ panels using a diamond saw for static and fatigue test. 6" long and 0.5" wide specimen were cut from the 8 ply and 12 ply unidirectional laminates. The 8 ply panels were cut along the fiber direction for

Table I Description of the three material systems used in this study.

	810 A	820 A	810 O
Fiber	Apollo	Apollo	Apollo
Matrix	HC 9106-3	HC 9106-3	HC 9106-3
Surface Treatment	100 %	200 %	100 %
Sizing	Bisphenol-A	Bisphenol-A	PolyVinylPyrrolidone

Table II Properties of fibers used in the 810 A, 820 A and 810 O material system [78].

Fiber	Tensile Modulus E_f (msi)	Tensile strength X_t (ksi)	Density (lb/in^3)	Diameter (micrometer)
Apollo (810-A)	45.4	765	0.0635	5.0
Apollo (820-A)	46.2	730	0.0632	5.0
Apollo (810-O)	44.0	780	0.0642	5.0

Table III Properties of HC 9106-3 matrix used in the 810 A, 820 A and 810 O material system [78].

Matrix	Tensile modulus E_m (msi)	Tensile strength X_m (ksi)	T_g (° C)
HC 9601-3	0.544	11.6	188

Table IV Fiber volume fractions in the various laminates (estimated using IPA technique).

Laminate	810-A	820-A	810-O
$(0,90_3)_s$	55.90	57.07	57.16
$(0)_8$	56.44	56.83	58.13
$(0)_{12}$	57.46	58.27	57.41

longitudinal tensile test specimen, and the 12 ply panels were cut perpendicular to the fiber direction for transverse tensile test specimen. From all three material systems, small pieces of unidirectional laminates were cut and mounted in room temperature curing epoxy. After curing, the specimens were polished on a polishing wheel. These polished specimens were used for meso-indentation tests, and the etching and scanning electron microscopy studies.

The coupons used for tensile creep tests measured 6" long and 0.5" wide. Specimens from $(90)_{12}$ laminates and $(0,90_3)_s$ laminates were tested under tensile creep mode. The Dynamic Mechanical Analyzer (DMA) Flexural creep tests were conducted on $(90)_{12}$ specimen measuring 2.5" long and 0.5" wide.

Before leaving the section on material and laminate description, a brief remark (reminder) on the terminology used throughout this report is in order. Since only one laminate configuration is used in this study, the term cross-ply laminate will be used to denote a $(0,90_3)_s$ laminate configuration. Also, the laminates having fibers with 100 % surface treatment and Bisphenol-A sizing have been designated 810 A, those with 200 % surface treatment and Bisphenol-A sizing have been designated 820 A. The laminates with 100 % surface treated fibers and PVP sizing are designated as 810 O laminates.

3.3 Test Procedure

3.3.1 Quasi-Static Testing

All quasi-static tensile tests were performed on a 20 kip servo-hydraulic MTS test machine under load control mode. A loading rate of 3300 lbs /min was used for all tests on $(0,90_3)_s$ laminates. The loading rate used in the transverse tension tests on $(90)_{12}$ laminates was 200 lbs /min, while a loading rate of 5000 lbs/min was used in the unidirectional longitudinal tensile tests on $(0)_8$ laminates. A data collection software (developed in-house) was used to collect and store the load and strain data. 1" long, 0.5" wide and 0.1" thick glass/epoxy end tabs were used in the longitudinal tensile tests on $(0)_8$ laminates. The end tabs and the specimen surfaces were sanded using a 100 grit sandpaper, before gluing the end tabs to the specimen using a room temperature glue (3M#DP-460 Epoxy). In order to minimize grip section damage

in the $(90)_{12}$ and cross-ply $(0,90_3)_s$ laminates, two layers of 60 grit sandpaper with the grit side facing the specimen, were used. At least 1" on each end of the specimen was inserted into the gripping region. A grip pressure of 500 psi was used for the $(0,90_3)_s$ laminates and $(0)_8$ laminates, while a grip pressure of 50 psi was used for the $(90)_{12}$ transverse tensile tests. Strain measurement was done using a 1.0" MTS extensometer. Aluminum V-notched tabs were glued 1" apart, on the specimen using a silicone rubber glue. The knife edges of the extensometer were placed in the V-notch of each tab, and the extensometer was held in position using rubber bands. At least three specimens from each material system were loaded continuously until failure, to obtain the static strength, stiffness and strain to failure of the laminates.

One cross-ply specimen from each of the three material system was loaded monotonically until failure, and the acoustic emission signal was monitored continuously during these tests. A loading rate of 3300 lbs /min was used during these tests. The tests were conducted under load control mode, and a 1" extensometer was used to monitor the strain. The AE transducer was mounted on the back surface of the sample, between the extensometer tabs (in the gauge section), using two layers of mounting tape. The details of the AE setup are described in the next section.

X-ray radiography was performed on one cross-ply specimen from the 810 A, 820 A and 810 O system, to document the progression of damage during quasi-static loading. The laminates were incrementally loaded upto 2000 lbs, 3000 lbs, and 4000 lbs. The specimen was removed from the load frame and x-rayed (details in the next section) to document the damage at each of these load level.

3.3.2 Tensile Fatigue Testing

All fatigue tests were performed on a 20 kip servo-hydraulic MTS test machine under load control mode. Two 60 grit sand papers were used on each end of the specimen to prevent grip section damage. At least 1" of specimen was gripped on either end. A grip pressure of 500 psi was for all tests. Strain measurement was done using a 1.0" extensometer (procedure described in detail in the previous section). The dynamic stiffness was calculated using the dynamic strain (ε) that was monitored continuously as a

function of cycles. In order to compare the results at different load levels, the stiffness was normalized with the initial secant modulus E_o. Since the tests were conducted under load control mode, the normalized stiffness E/E_o was obtained simply by calculating the ratio of the dynamic strain and the initial strain ($\varepsilon/\varepsilon_o$).

Fatigue tests were conducted at three load levels, with the maximum load corresponding to 85, 80, and 75 % of the static strength of the $(0,90_3)_s$ laminate. All tests were conducted at a frequency of 10 Hz, and an R ratio of 0.1. Since the 820 A laminates exhibited run-outs (life greater than 1 million cycles was termed run-out) below the 80 % load level, tests on this material system were conducted at 90%, 85% and 80% load levels.

In addition to these tests, one cross-ply specimen from each material system was fatigued at two load levels for a specific number of cycles. The specimen was removed from the testing machine and x-rayed to document the damage.

3.3.3 Creep Testing

Tensile creep tests were performed on a 20 kip servo-hydraulic MTS test machine under load control mode. Strain measurement was done using a 1.0" extensometer (procedure described in detail in the quasi-static test section). Creep tests were conducted on $(90)_{12}$ and $(0,90_3)_s$ laminates. The load and strain data was collected continuously using data collection software (developed in house). As in the case of fatigue testing, two 60 grit sandpaper pieces were used on each end of the specimen to prevent grip section damage. A 50 psi grip pressure was used for transverse tension tests, and a 500 psi pressure was used for the cross-ply $(0,90_3)_s$ laminates. All tensile creep tests were performed at room temperature.

Short term DMA creep tests were performed on $(90)_{12}$ laminates at various temperatures to generate the master curve for each material system. All tests were performed on a DuPont 983 DMA. A torque of 12 lb-inch was used for gripping the samples in the DMA and an arm displacement of 0.3 mm was used for all tests. In order to generate the master curve, short term creep tests were performed at temperatures

of 100, 110, 120, 130, 140, 150, 160, 165, 170, 175, 180 and 185°C. A cycle that consisted of creep loading at a specific temperature for 10 minutes, followed by a relaxation period of 40 minutes at the next higher temperature was used to generate creep compliance data at the different temperatures. It must be emphasized that the specimen was not removed from the clamps between tests at different temperatures. The 40 minute relaxation period was used to erase all previous loading and thermal history in the specimen.

3.3.4 Interphase Characterization Testing

Single Fiber Fragmentation Test

The single fiber fragmentation tests were performed by Drzal et al under contract from Air Force on the material system that was used in this study. The results are reported in reference [79]. The testing procedure and the modified cure cycle used in the study of this material system are detailed in reference [79]. A brief description of the test method and data analysis are provided here for completeness. A tensile dogbone coupon with a single fiber embedded in the matrix material is used in this test. The specimen is prepared by placing a single fiber in a mold and filling the mold with debulked matrix material. The fiber is aligned and the specimen is cured according to the prescribed curing cycle. The cured specimen are removed from the mold, polished and tested. The prepared specimen is loaded on a stage of a polarized transmitted light microscope. The first fiber fracture occurs when the applied load is greater than the local strength of the fiber. As the applied load is increased, the fiber breaks into progressively smaller fragments until a critical fragment length is reached. At this point, the length of the broken fiber is insufficient to transfer enough shear stress to break the remaining fiber fragments into smaller lengths. The average length of the broken fragments of the fiber is called the "critical length". The interfacial shear strength is then estimated using a shear lag analysis [17] which relates the critical length l_c, fiber diameter (d_f) and fiber strength (σ_f) to the interfacial shear strength (τ) through the following relationship

$$\tau = \frac{\sigma_f \, d_f}{2 \, l_c}$$

It has been observed that in order for the fiber fragments to reach the critical length before catastrophic failure of the specimen occurs, the strain to failure of the matrix must be at least three times the fiber failure strain. Since the 9106-3 matrix has a low strain to failure, the SFFT was carried out at 100°C in order to increase the strain to failure of the matrix. These results were extrapolated to room temperature using a scaling factor of 1.5 (details provided in reference [79]).

Meso-Indentation Technique

Lesko [21] has used the Continuous Ball Indentation Test (CBIT) to estimate the interfacial strength of fiber reinforced composites. In this technique, the test sample was mounted in epoxy with the fibers perpendicular to the free surface. The mounted sample was then polished using standard metallographic polishing techniques. Initial rough polishing was done using a 400 grit emery paper. The fine polishing was done using 3 micron, 1 micron and 0.3 micron alumina powder. The indentation was performed with a 1/16" hardened steel ball under displacement control mode. A loading rate of 4 microns/second was used. The penetration of the indenter was measured using an LVDT. Multiple indentations were made on each sample, with at least 3-5 ball diameter spacing between each indent. The load and displacement data was collected continuously using a computerized data collection system. This data was used in a micromechanics analysis [22] to estimate the interfacial strength. These tests were performed on the material system used in the present study and have been reported by Lesko et al [37], and are reproduced here with permission from the author.

Etching and scanning electron microscopy

The permanganic etching technique described in reference [8] was used to characterize the interphase in the three material system used in this study. The etchant was prepared following the procedure detailed below. One gram of ground potassium permanganate ($KMnO_4$) was added to 40 ml of 85% orthophosphoric acid (H_3PO_4) and 10 ml of distilled water. This solution was stirred for 15 minutes, and the liquid was decanted off the remaining undissolved potassium permanganate. A polished section of the specimen was immersed in freshly prepared etching solution for 5 minutes. While submerged in the

solution, the sample was continuously shaken. After etching for 5 minutes, the sample was washed thoroughly in cold running water. The etched sample was then coated with gold using a sputter coater and observed under the SEM at high magnifications. The 5 minute etching time was found (by trial and error method) to be adequate for the material system used in this study.

3.3.5 Non-Destructive Testing

In order to document the progression of damage in the quasi-static, fatigue and creep tests, various non-destructive testing techniques were used. These include Edge Replication, X-ray radiography, and Acoustic emission. Details about these techniques are discussed in this section

Edge Replication

The edge replication technique has been used previously by many investigators for performing crack density measurements in laminated composites. Reference [80] provides a detailed description of this procedure. In this technique, a strip of acetate tape is held against the specimen edge. Liquid acetone is introduced between the acetate tape and the specimen edge using a syringe. Light, uniform pressure is maintained on the acetate tape for about 30 seconds to obtain the edge replica. The edge replica obtained is then mounted on a microscope stage and the number of edge cracks/inch is counted. In all tests, the edge replication was performed in the gauge section, between the extensometer tabs. It is to be noted that the edge replication technique provides information about the number of edge cracks in the specimen. However, this technique does not provide any details of the extent of propagation of the edge cracks across the width of the specimen.

X-ray radiography

Penetrant enhanced x-ray radiography is one of the most widely used non-destructive technique used to monitor damage in composite materials. Damage modes such as matrix cracking, fiber-matrix debonding, local delaminations, and edge delaminations can be detected using this technique. In this technique, dye penetrant (eg. Zinc Iodide) that is opaque to x-rays is applied generously on all surfaces of

the specimen. The penetrant is allowed to seep in to the specimen for about 3 hours. The specimen is then washed thoroughly using acetone. All traces of zinc iodide is removed from the specimen surface by repeatedly cleaning the surfaces using cotton swabs dipped in acetone. Once the specimen is cleaned, it is exposed to x-ray radiation in a cabinet x-ray machine (Hewlett Packard 43805 N Faxitron series). For all the 8 ply and 12 ply laminates used in this study, a 24 second exposure time at 40 kvp accelerating voltage was used. One main advantage of using this method is that it provides information about the damage in the interior of the laminate also. Some disadvantages of using this technique are listed below. Since a cabinet x-ray machine was used in this study, the specimen had to be removed from the testing machine. This required realignment of specimen in the test frame after x-ray analysis, which could result in some scatter in the data. It must also be borne in mind that zinc iodide is a corrosive material, and leaving a specimen soaked in zinc iodide for even a few hours could degrade the material. Hence, the strength and life data obtained from specimens that were removed for x-ray analysis may not be precise representations of material properties.

Acoustic Emission

Acoustic emission is a non-destructive testing technique used commonly to identify the various damage mechanisms observed in composite materials. In this study, the acoustic emission technique was used to monitor damage progression in the $(0,90_3)_s$ cross-ply laminates under monotonic loading. An Ultran 10 MHz, 0.25 inch diameter transducer was connected to a Physical Acoustics broad band preamplifier set at 40 dB. The preamplifier was connected to a Physical Acoustics SPARTAN 3000 acoustic emission system. The gain was set at 45dB. The other parameters were set at default values. The AE transducer was mounted on the specimen (between the extensometer tabs) using a tape. The number of events, the energy level of the events, and the amplitude of the event were monitored as a function of time during the monotonic tensile test.

3.3.6 Optical and Scanning electron microscopy

Damage and post failure fracture analysis was performed on some specimen using optical and scanning electron microscopy techniques. The presence of some damage modes such as longitudinal splits, local delaminations etc were confirmed using optical microscopy. A small cross-section of a quasi-static test specimen that was loaded upto 4000 lbs was mounted on an epoxy mount, and polished. The polished section was observed under an optical microscope at relatively low magnifications to identify the various damage mechanisms such as longitudinal splitting, local delaminations etc.

Post failure fractographic analysis was done on representative specimen from each material system, subjected to different loads, using an SX 40 International Scientific Instruments (ISI) scanning electron microscope. The specimen surface was cleaned using acetone, and was coated with a thin layer of gold, using a sputter coating machine, before observing under the SEM.

4.0 INTERPHASE CHARACTERIZATION RESULTS

Results from the various interphase characterization tests (both qualitative and quantitative) are presented in this chapter. These results will be discussed in two sections. In the first section, the results from the qualitative interphase characterization tests are presented. Results from the quantitative interphase characterization tests such as the single fiber fragmentation test and meso-indentation test are discussed in section 4.2.

4.1 Qualitative Interphase Characterization

4.1.1 Etching and scanning electron microscopy

Specimens from each of the three material systems were polished and etched using the technique described in the previous chapter. The etched samples were observed under the SEM at high magnifications. Figure 1 shows the scanning electron micrograph of an etched 810 A sample at 20000 X magnification. The fiber used in 810-A material appears to have an irregular shape, with numerous striations visible on the fiber surface. The figure shows an 810 A fiber surrounded by matrix material, with a dark band (that has been etched away) of interphase region between the fiber and the matrix. As mentioned earlier, the function of the etchant is to preferentially etch any uncross-linked material that is present in the system. Looking at figure 1, it may be concluded that the Bisphenol-A sizing (unreacted epoxy) forms an interphase around the fiber, that essentially consists of uncross-linked polymeric material. The interphase formed in the 810 A system is continuous as evidenced by the discountinuous dark band around the fiber (figure 1). This is not very surprising, considering that the sizing material did not contain any hardening agent. Any cross-linking of the sizing material would be due to diffusion of curing agent from the matrix material. Also seen in the figure are numerous dark spots in the matrix material. It has been reported in an earlier study [9] that the PolyEtherSupfone (PES) toughener material phase separates out in the HC 9106-3 matrix material. Since PES is a thermoplastic material (linear chain polymer), it is easily attacked by the etchant used in this study. Based on this, it is claimed that the dark regions in the

matrix material represent the etched PES phase in the matrix.

Figure 2 shows the scanning electron micrograph of an etched 810-O sample at 20000 X magnification. It is again observed that the fiber surface is irregular, with numerous striations visible on the fiber surface. The PES thermoplastic toughener appears as dark spots in the matrix material. The morphology of the interphase revealed in figure 2 is different from that seen in figure 1. It is seen that the fibers in the 810-O system are surrounded by a dark region. This uncross-linked region is surrounded by material that has a gradient morphology. The matrix material near the interphase has a different morphology than the bulk material. The presence of PVP sizing appears to have affected the cure chemistry of the matrix material near the interphase. The matrix material near the interphase is less cross linked. It is also interesting to note that the interphase formed in the 810 O system appears to be continuous and more well defined compared to that in the 810 A system. It is thus concluded that the use of different sizing results in material systems with distinctly different interphases.

In order to determine if there is any preferential distribution of PVP in the 810 O system, some of the etched samples were observed under an optical microscope at low magnification. Figure 3 shows the etched 810 O sample at 390 X magnification. The etched regions appear as dark areas in the photograph. It is seen clearly that the distribution of PVP is highly non-uniform across the specimen section. It appears that some fibers have excess PVP around them, while others do not have any coating. It is also interesting to note the high concentration of PVP at ply and tow boundaries. Since the sizing process essentially consists of pulling a fiber tow through a bath of sizing material, it is hypothesized that in the 810 O system, the fibers on the outside of the tow get coated well with PVP, while the fibers inside the tow do not receive any PVP coating. It must be emphasized here that this non-uniform distribution of PVP must be borne in mind while interpreting the results that will be presented in the following chapters. The author wishes to reiterate that the interphase morphology shown in figure 2 is not representative of the interphase present in the entire laminate. It must be stressed that over 50 % of the fibers in the 810 O system did not reveal this morphology. This leads one to believe that the effects of different fiber sizing

could be either due to the changes in the morphology of the fiber-matrix interphase in some fibers (micro level effects) or due to a meso level effect (such as bundling of fibers, interleaving effect).

The scanning electron micrograph of an etched 820-A sample shown in figure 4 reveals fewer striations on the fibers compared to the 100 % surface treated fibers. The figure also shows that the diameter of the 200 % surface treated fibers are smaller. This is not very surprising, considering that the surface treatment process is known to remove surface layers from the fibers. This removal of surface material could contribute to the reduction in fiber diameter. It is also interesting to note that the dark spots in the matrix that were seen in the 810 A and 820 A system are also seen in the 820 A system. As mentioned earlier, these represent the PES toughener material present in the matrix. What is most striking is the absence of any well defined interphase region near the fiber in this figure. The 200 % surface treated system does not have a low cross-link density region near the fiber surface which was seen in the other two material systems. The matrix appears to have the same morphology at regions near and away from fiber surface. It appears that the 200 % surface treatment imparted to the fiber results in enhanced chemical activity near the fiber surface. This could have resulted in complete cross-linking of the matrix material near the fiber surface. This is somewhat surprising considering that the 200 % surface treated fibers have also been sized with Bisphenol-A epoxy material. This unreacted epoxy sizing produced a discontinuous interphase in the 810 A system. There is no evidence of formation of an interphase with morphology different from that of the bulk matrix material in the 820 A system. The present results indicate that the role of fiber sizing is influenced by the level of surface treatment on the fibers.

Results indicate that the interphase has different morphology in the three system. The 810 A system has a discontinuous region around the fiber which is made of uncross-linked polymeric material. In the 820 A system, this region with uncross-linked polymeric material is absent. In the 810 O system, in addition to the presence of a region with uncross-linked polymeric material, the morphology of the matrix material near the fiber is different. It appears that the cure chemistry of the matrix material near the fiber is affected by the presence of PVP, resulting in a significantly different interphase.

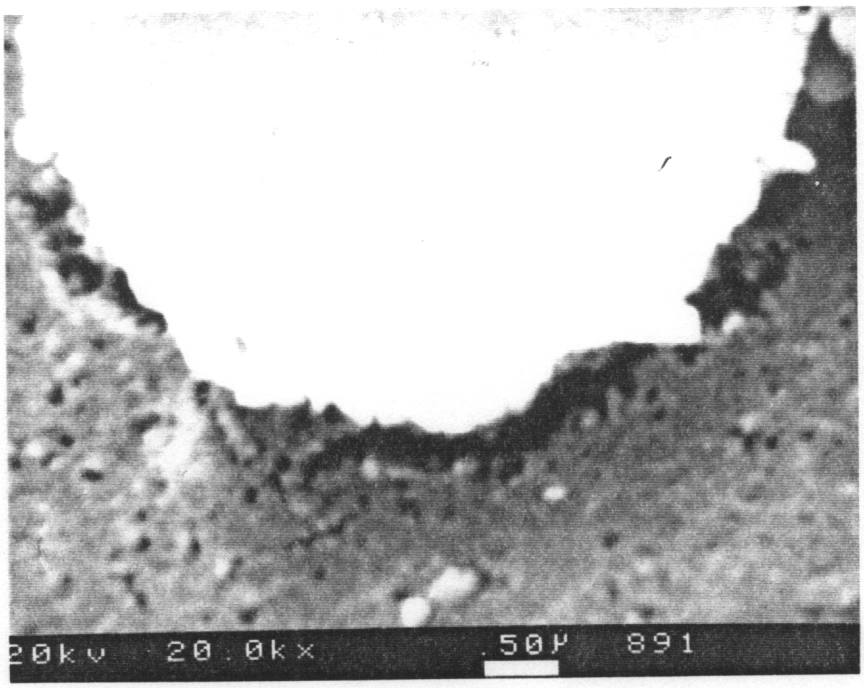

Figure 1 Scanning electron micrograph of an etched 810 A specimen (20000 X).

Figure 2 Scanning electron micrograph of an etched 810 O specimen (20000 X)

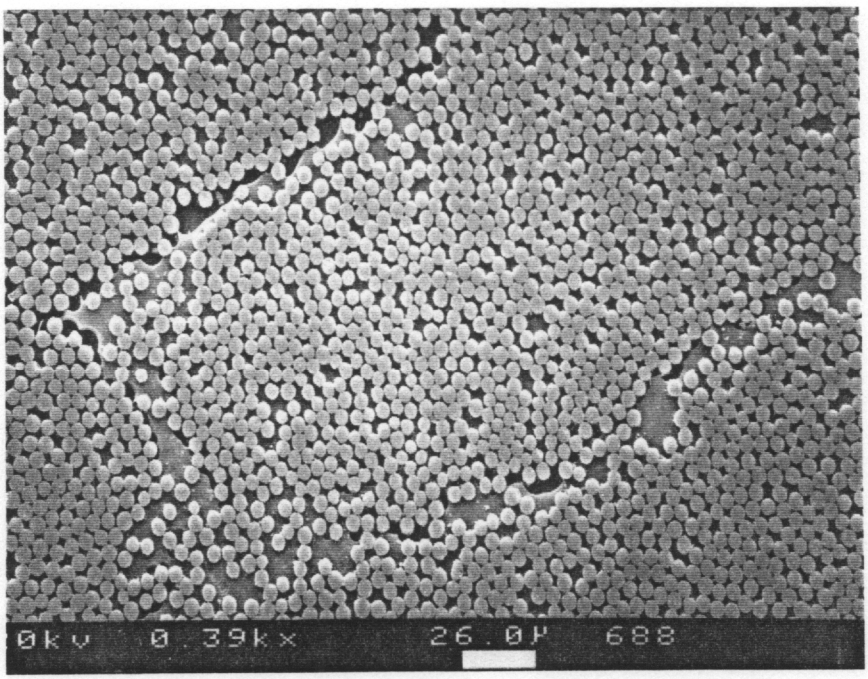

Figure 3 Scanning electron micrograph of an etched 810 O specimen (390 X)

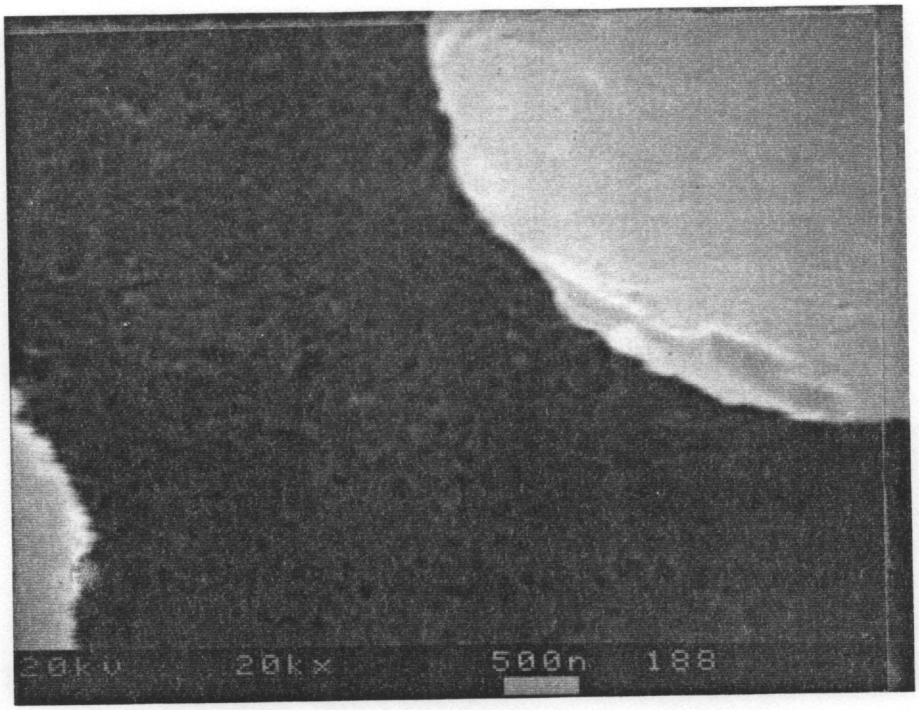

Figure 4 Scanning electron micrograph of an etched 820 A specimen (20000 X)

4.1.2 Scanning electron microscopy

Surface treated and sized fibers that were used in the three material system designated as 810 A, 810 O, and 820 A, were coated with gold and observed under the scanning electron microscope. Figure 5 shows an 810 A fiber at 5000 X magnification. Numerous striations are seen on the fiber surface. Traces of sizing material are also seen on the fiber surface indicating that the sizing does not form a uniform coating around each fiber. Compare this with the 810 O fiber at 5000 X magnification, shown in figure 6. Numerous striations are seen on the fiber surface, but there are no traces of sizing material on the fiber surface. This could indicate that the sizing process does not result in all fibers being coated with the sizing material. Based on the etching results and figure 6, it may be concluded that only the fibers on the outside of the tow get coated with PVP, in the 810 O material system. There is a significant non-uniformity in the distribution of fiber coating in the 810 O system. Figure 7 shows the 820 A fiber at 5000 X magnification. Clearly, there are fewer striations on the fiber surface in the 200 % surface treated fibers compared to the 100 % surface treated fibers (figure 5). There are also traces of sizing material seen on the fiber surface indicating that the distribution of coating on the fiber surface is non-uniform.

Eight fibers from each system were selected randomly, and their diameters were measured from photographs taken at high magnifications. The results are shown in Table V. It is noted that the average diameter of the 200 % surface treated fiber is significantly lower than that of the 100 % surface treated fiber. The diameter of the 810 O fiber is however greater than that of the 810 A fiber. It must be pointed out that only 8 measurements were made on each system, and this may not be a good quantitative measure of the fiber diameters.

Based on the SEM pictures and etching study, it can be concluded that the 200 % surface treatment results in removal of surface layers from the fiber. This results in lower diameter and less striations on the fiber surface. It can also be said that most fibers in the "A" sized systems are coated, while in the "O" sized system, only the fibers on the outside of the tow are coated.

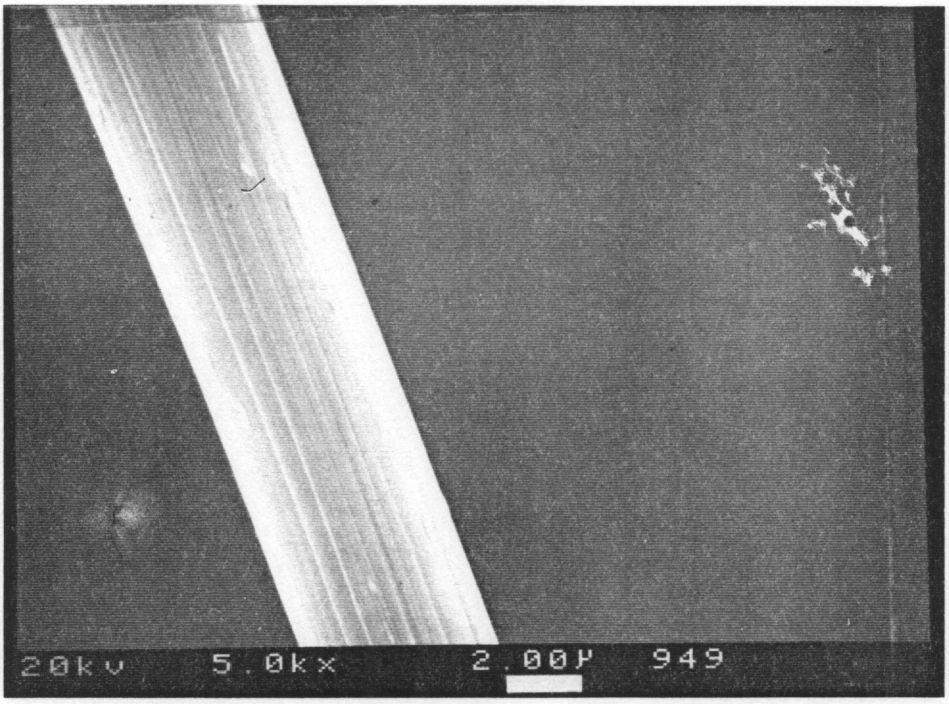

Figure 5 Scanning electron micrograph of an 810 A fiber (5000 X)

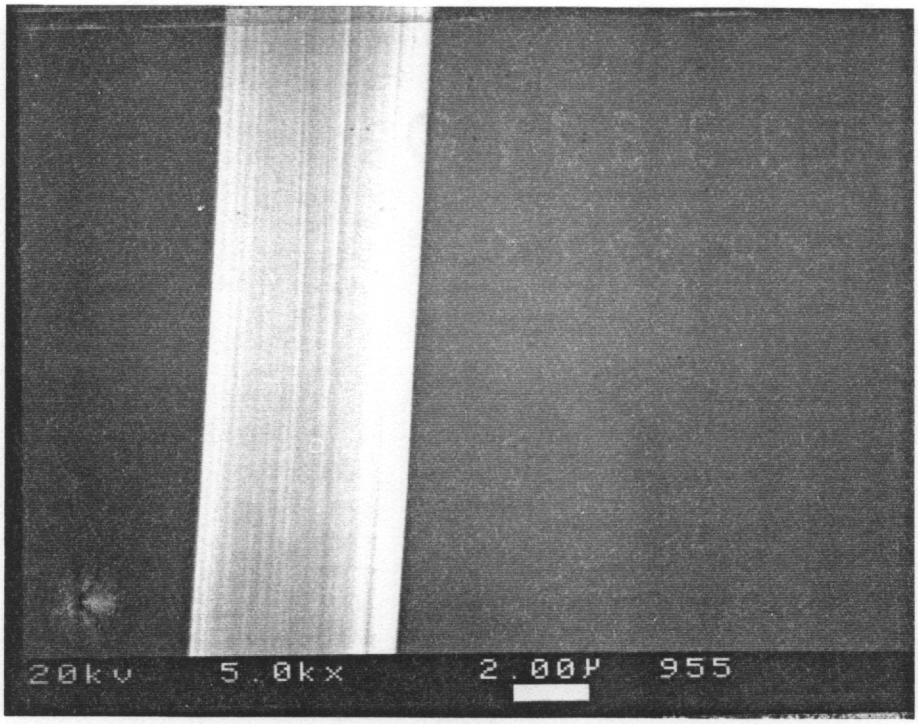

Figure 6 Scanning electron micrograph of an 810 O fiber (5000 X)

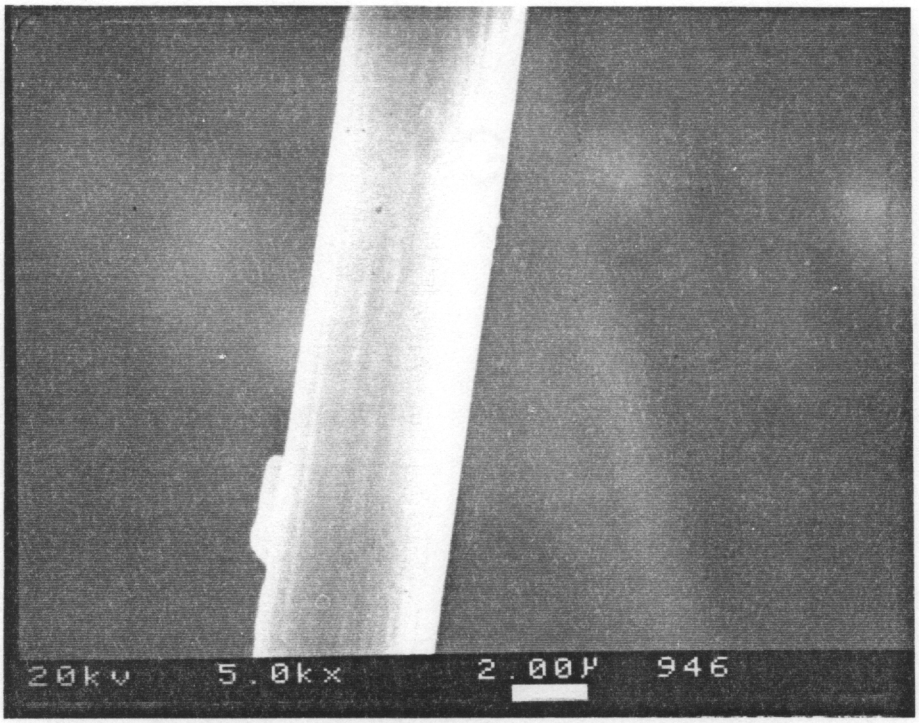

Figure 7 Scanning electron micrograph of an 820 A fiber (5000 X)

Table V Average diameter of the fibers used in the 810 A, 810 O and 820 Asystem.

810 A		810 O		820 A	
Average (Microns)	Std Dev (Microns)	Average (Microns)	Std Dev (Microns)	Average (Microns)	Std Dev (Microns)
5.04	0.16	5.19	0.57	4.4	0.24

4.2 Quantitative Interphase Characterization

4.2.1 Single Fiber Fragmentation Test (SFFT)

The single fiber fragmentation tests were performed by Drzal et al at Michigan State University under contract from the Air Force. These results are reported in reference [79]. Since the same material system was used in the present study, their results are discussed in this section. These results are only intended to provide the reader with a qualitative feel for the trends in the interfacial shear strengths determined from SFFT. Due to the restrictions on the publication of these results, the numerical values of Interfacial shear strength (ISS) are not reported here. All the results are normalized with respect to the ISS of the 810 A system. Detailed description of the test procedure and data reduction technique are provided in reference [79]. Due to the low strain to failure of the matrix material, the SFFT was performed at 100° C. The elevated temperature test results were scaled to 20° C using a multiplicative factor of 1.5 [79].

The results from SFFT on the 810 A, 820 A and 810 O system are presented in Table VI. The table shows the normalized ISS and failure mode for each of the three material system. Results indicate that the ISS of the 810 A and 820 A material system are almost identical. However, the 810 O system possesses a significantly lower ISS. It is also interesting to note that the failure modes are different for the three material system. The 810 O system exhibits 'interfacial failure', while the 810 A system indicates a mixed 'interfacial/matrix failure'. The 820 A system in contrast to the other two material system appears

to exhibit a predominantly 'matrix failure'. It must be added that fiber fractures accompanied by fiber-matrix debonding are termed 'interfacial failures' and those with little or no debonding are classified as 'matrix failures'. It is noted that the results from SFFT on the 810 A, 820 A and 810 O system reveals that the system with the highest ISS exhibits a predominantly matrix failure, while the system with low ISS exhibits interfacial failure.

Table VI Normalized Interfacial Shear Strength and failure modes for the three material system [79].

810 A		810 O		820 A	
Normalized I.S.S	Failure Mode	Normalized I.S.S	Failure Mode	Normalized I.S.S	Failure Mode
1.00	Interface/ Matrix	0.79	Interface	1.02	Matrix

In the author's opinion, the results from SFFT would be more representative of the failures in the 0° ply of a laminate under tensile loading. However, since the tests were performed at elevated temperatures, these results must be treated with caution. The effects of elevated temperature could have significantly influenecd the ISS results in the 810 O system where a PVP sizing was used because the glass transition temperature (T_g) of the PVP material is known to be between 110 and 180° C (depending on the molecular weight) and the SFFT was performed at 100° C. In the author's opinion, these results must be used only as a qualitative measure of the strength of the interphase in these material systems.

4.2.2 Meso-Indentation Test (MIT)

Results from the meso-indentation tests are presented in this section. This data was obtained by Lesko et al [37] working with the same material system. The data is reproduced here with permission from the authors. A representative plot of the Maximum Mean Hardness Pressure (MMHP) and Representative strain (d/D) for the three material system are shown in figures 8, 9 and 10. The MMHP is simply defined as the maximum pressure that is achieved during the test. The d/D ratio represents the ratio of the diameter of the indent to the indenter diameter. The initial data points were discarded in all the tests as there was significant "noise" in the data in this regime. The initial gap in these figures represent the discarded data points. The figures indicate an initial linear region in all the material system. The slope of this linear region indicates the stiffness of the composite material. Results indicate that the stiffness of the 810 O system is significantly lower than that of the 810 A and 820 A system. This is surprising, considering that the stiffness of the unidirectional composite is a fiber dominated property and is not expected to change in these three material system which have the same fiber. This reduction in stiffness is observed in various other laminate configurations under different loading conditions throughout this study. This phenomenon will be discussed in detail in the following chapters. The results from the meso-indentation tests are summarized in Table VII. The table shows the Maximum Mean Hardness Pressure (MMHP) and representative strain at MMHP (d/D) for the three material system. The data indicates that the MMHP value of the 820 A system is significantly higher than that of the other two systems. The MMHP value of the 810 A and 810 O system are almost identical. The d/D ratio at MMHP are significantly different for the three material system. The 810 O system has the highest d/D value and the 820 A system has the lowest d/D value. The 810 A system has a d/D values which is intermediate between the 810 O and 820 A system. Lesko [21] has observed that the MMHP is sensitive to bond strength ; higher the MMHP, stronger the interphase. The micromechanics analysis by Carman et al [22] indicates that the loading results in a predominantly shear stress dominated stress state. The maximum shear stress occurs a few fiber

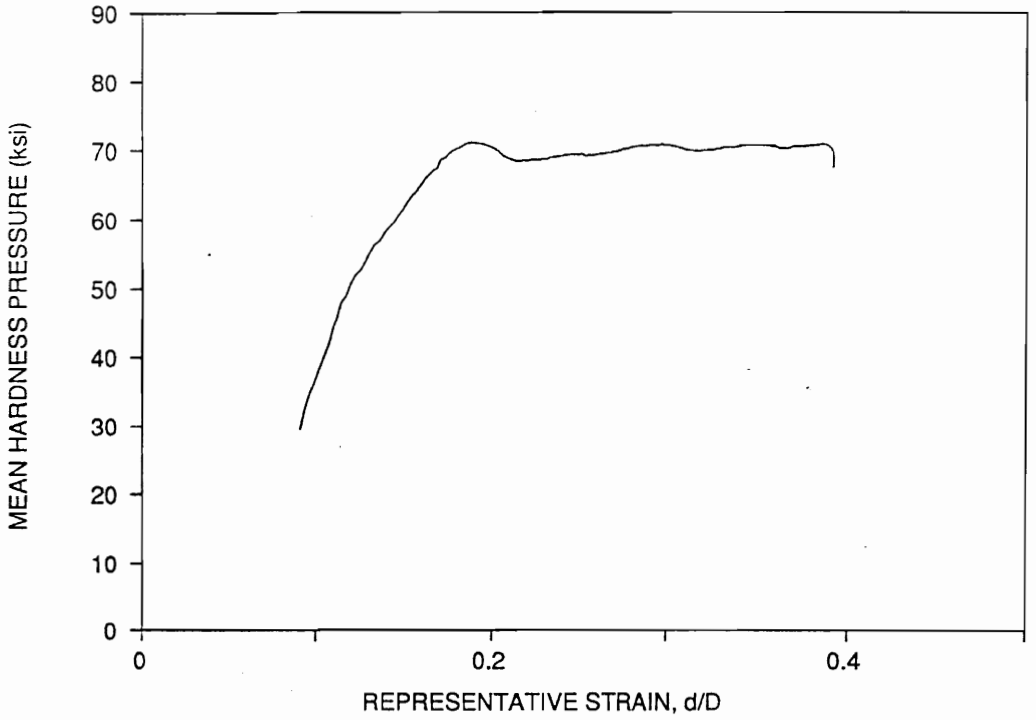

Figure 8 Typical variation of MMHP as a function of d/D for 810 A specimen.

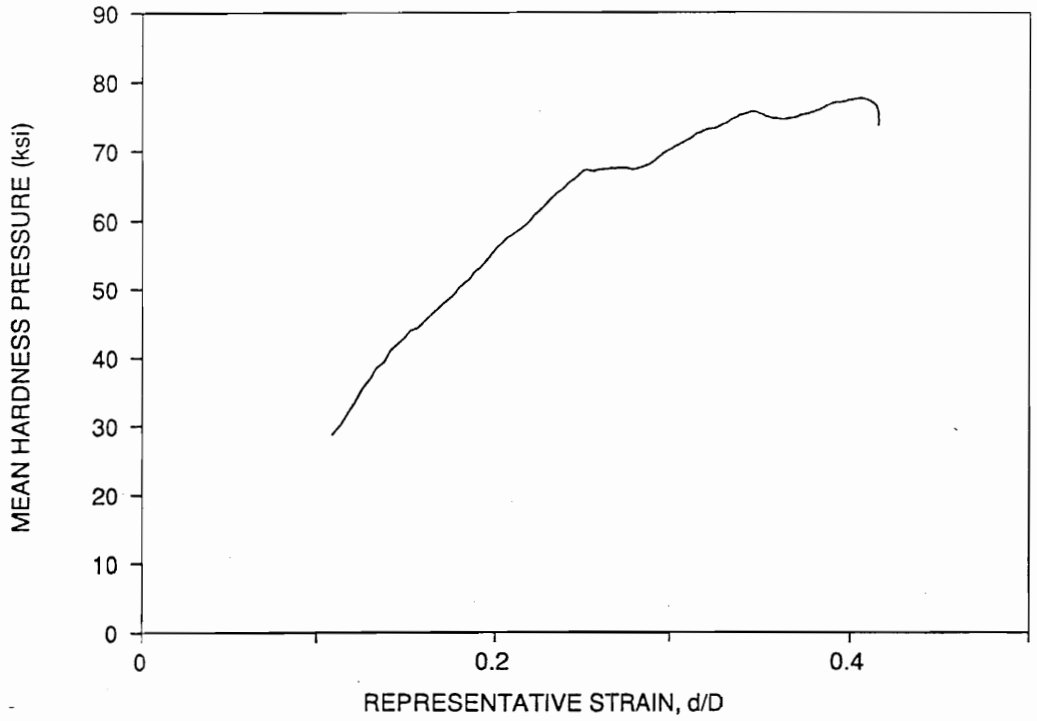

Figure 9 Typical variation of MMHP as a function of d/D for 810 O specimen.

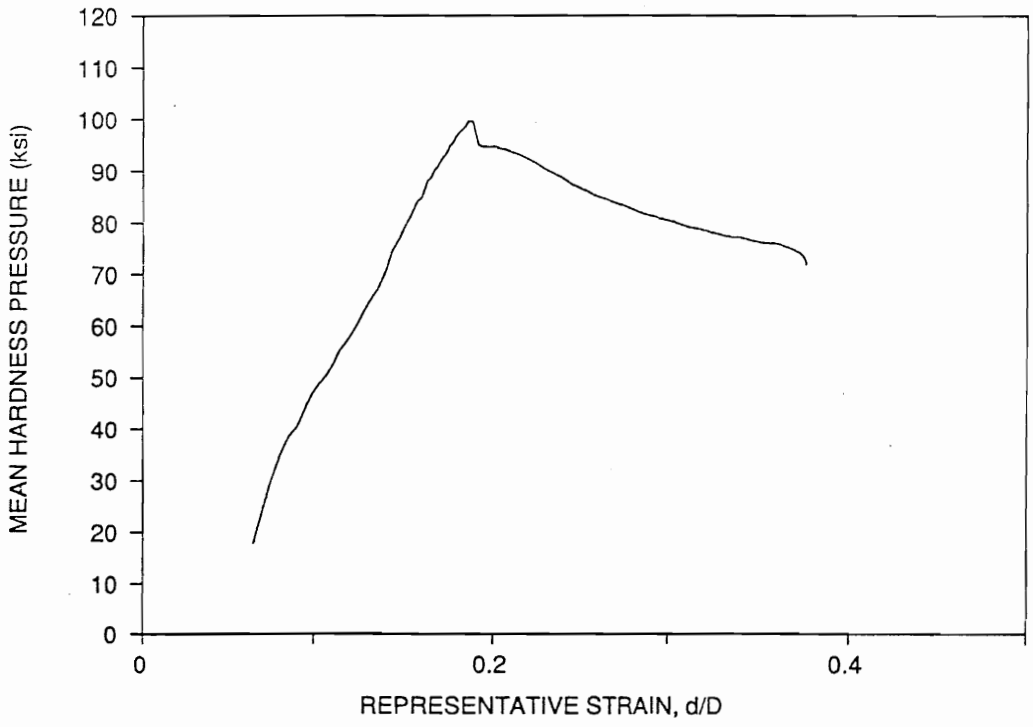

Figure 10 Typical variation of MMHP as a function of d/D for 820 A specimen.

diameters from the free surface. Based on this analysis, it could be said that the MMHP value obtained from this test is a good indicator of the "Interfacial Shear Strength". Lesko [21] has also observed that low d/D ratio at failure indicates a brittle interphase, while a high d/D ratio corresponding to MMHP indicates a compliant interphase. Using these observations as a guide, it could be concluded that the interphase in the 820 A system is strong and brittle. It may be recalled that the fibers used in the 820 A material system had a significantly lower diameter compared to the other two material systems. This suggests that for the same fiber volume fraction, the amount of fiber surface area available for bonding is greater. The increase in interfacial shear strength in the 820 A system (measured using MIT) could be due to the increase in the fiber surface area available for bonding with the matrix material. Comparing the results for the 810 A and 810 O systems, it could be said that the interphase in these two material system possess "similar" shear strength. The interphase in the 810 O system appears to be "Compliant" compared to that in the 810 A system. This conclusion is based on the high d/D ratio at MMHP observed in the 810 O system. It must be pointed out here that the high d/D ratio could be due to other reasons also. The lower stiffness of the 810 O system could have contributed to the increase in d/D ratio in the 810 O system. It is also possible that the interphase in the 810 O system is brittle and undergoes micro-level damage very early on. This kind of a behavior would also result in increased d/D ratios at MMHP. In the author's opinion, the available data is not sufficient to conclusively show if the interphase is compliant or brittle.

It is interesting to compare the qualitative trends obtained from the SFFT and the MIT. Both these tests provide the ISS values for the three material system. Comparing the results from these tests, it may be concluded that even the qualitative trends of ISS for the three material system are not the same. The SFFT results indicate that the 810 A and 820 A system possess similar ISS values while the ISS of the 810 O system is significantly lower. In sharp contrast, the MIT indicates that the 820 A system possesses the highest ISS and the ISS of the 810 A and 810 O system are almost identical. As mentioned earlier, this could be due to differences in loading conditions and the associated failure modes in the SFFT and the MIT.

Table VII Mean Maximum Hardness Pressure and Representative Strain data for the three material system [37].

810 A				810 O				820 A			
MMHP (ksi)	COV (%)	d/D	COV (%)	MMHP (ksi)	COV (%)	d/D	COV (%)	MMHP (ksi)	COV (%)	d/D	COV (%)
68.4	12.9	0.216	8.3	69.6	7.3	0.254	4.3	102.8	10.5	0.185	3.5

4.3 Summary

Results from the etching study indicate that the interphase formed in the three material systems used in this study are different. The interphase in the 810 A system appears to be discontinuous and is made up of uncross-linked polymer material. The 820 A system does not reveal any well defined interphase region between the fiber and the matrix. In sharp contrast, the interphase in the 810 O system has a distinctly different morphology. The interphase appears to be well defined and the cure chemistry of the matrix material appears to have been affected by the presence of PVP. This results in a gradient region near the fiber, where the morphology of the interphase is different from that of the bulk matrix. Optical micrography of the etched samples indicate that the distribution of the uncross-linked material is highly non-uniform in the 810 O system. In the author's opinion, this is a significantly important factor that must be borne in mind while interpreting the results in the following chapters. Since a distinct interphase region is not formed around almost 50 % of the fibers in the 810 O system, the effects of fiber sizing may not necessarily be due to the fiber-matrix interphase. It is possible that the effect of fiber sizing could be influencing the properties of the composite material at a meso level and not at a micro level. Also, the heretogeneity introduced in the composite material by the sizing process (especially in the 810

O system) indicates that the processing variables contribute to some of the differences seen in these material systems.

Scanning electron microscopy of fibers revealed that the fibers in the 820 A system have a significantly lower diameter. There are also less striations on the 820 A fibers. The results from SFFT and MIT indicate conficting trends of ISS values in the three material system. The SFFT results indicates that the interfacial shear strength of the 810 A and 820 A system are almost identical and the 810 O system possesses a significantly lower ISS. The MIT results indicate that the 820 A system has the greatest ISS while the ISS of the 810 A and 810 O system almost identical. Based on the qualitative and quantitative interphase characterization test results, it may be concluded that the interphase in the three material system are different. However, the conflicting ISS results obtained from different tests leaves one with no choice but to speculate on the ordering of the interfacial strength values for these systems. It would suffice to say at this point that the interphase in the three material system are different. More on the strength of these interphases will be discussed in the following chapters.

5.0 UNIDIRECTIONAL LAMINATE TEST RESULTS

5.1 Longitudinal Tensile Test

Quasi-static tests were conducted on three specimens from each of the three material system. The average of three test results are listed in Table VIII. The shows the initial stiffness, strength and strain to failure values for the three material system. The data indicate that varying fiber surface treatment level from 100 % to 200 % does not alter the longitudinal stiffness significantly. However, the strength and strain to failure of the laminate reduces with the increase in surface treatment level. Comparison of the results for the epoxy sized 810 A and PVP sized 810 O system reveals surprising differences. The 810 O system has a significantly greater strain to failure value. It is interesting to note that the strain to failure of the 810 O fiber (obtained from the manufacturer) is 1.66 %. The unidirectional 810 O unidirectional laminates have strain to failure values close to the failure strain of the fiber. This indicates that the failure of the unidirectional laminate is controlled by the global strain to failure of the fiber. The local stress concentration effects do not play an important role in the laminate strength. The strength of the 810 O laminate is 10 % greater than that of the 810 A laminate. It is thus seen that by varying the interfacial bonding, the fiber dominated properties such as longitudinal strength and strain to failure can be affected significantly. Results shown in Table VIII also indicates that the longitudinal stiffness of the 810 O laminate is significantly lower than that of the 810 A laminate. There is a 16 % reduction in the stiffness value going from a Bisphenol-A sized fiber system to a PVP sized system. This surprising considering that the fiber volume fraction in all the panels were almost identical. Varying the interfacial bonding was not expected to change a fiber dominated property such as longitudinal stiffness. There are a couple of explanations that could explain this phenomenon. It is possible that the sizing process results in degradation in the fiber stiffness, which manifests as a reduction in longitudinal stiffness of the laminate. However, this appears less likely, because the sized fibers were tested and the stiffness of these fibers were only 5 % lower than that of the 810 A fibers. It is also possible that the sizing process could have resulted

Table VIII Longitudinal tensile properties of unidirectional $(0)_8$ laminates.

PROPERTY	810 A	810 O	820 A
STIFFNESS (MSI)	27.75 (0.37)	23.43 (0.86)	28.5 (0.21)
TENSILE STRENGTH (KSI)	407 (6.02)	444 (16.42)	400 (3.27)
FAILURE STRAIN (%)	1.31 (0.04)	1.66 (0.05)	1.28 (0.02)

* Values in paranthesis represent the C.O.V

in the breaking of carbon fibers. The presence of broken fibers in the composite could result in reduced longitudinal stiffness. However, since the 810 A, 820 A and 810 O fibers were sized, it could be argued that the sizing process would have resulted in similar damage to the fibers in all three material systems. The only other explanation for the reduced modulus is that there is ineffective load transfer from the matrix to the fiber in the 810 O system, due to the PVP sizing. It is hypothesized that the interphase in the 810 O system results in inefficient load transfer from the matrix to the fiber. This results in the fiber carrying less load. Since the load carrying capacity of the fiber is not fully utilized, the stiffness of the unidirectional laminate is lower. At the present moment, there is no conclusive evidence to back up this claim. However, there are indirect evidences that point to this scenario. It may be recalled that the stiffness of the unidirectional 810 O system was found to be about 10 % lower than the 810 A system in the meso-indentation tests. It must also be pointed out that Lesko et al [37], working with the same material system, have reported similar reduction in unidirectional compressive stiffness. In his work with notched cross-ply laminates, Swain [43] has also observed that the stiffness of the 810 O system was significantly lower than that of the 810 A system. In a recent study, Subramanian et al [81] have reported that the dynamic mechanical characteristics of the 810 O laminates are different from those of the 810 A laminates. They have reported that the storage modulus of the 810 O unidirectional laminates are significantly lower than that of the 810 A laminates. All these results and the results from $(0,90_3)_s$ laminates that will be discussed in the following chapters indicate that the longitudinal stiffness of the unidirectional laminates with PVP sizing is lower than that of the 810 A laminates under tensile and compressive loading.

Figure 11 shows a comparison of typical stress-strain curves for the 810 A, 810 O and 820 A systems. The figure indicates that the stress-strain curves are non-linear for all three material system. This kind of non-linear stress-strain behavior has been reported previously for graphite/epoxy composites by many investigators [38]. This has been attributed to the non-linear stress-strain behavior of the carbon fibers. In order to better understand the differences in the unidirectional tensile stiffness of the

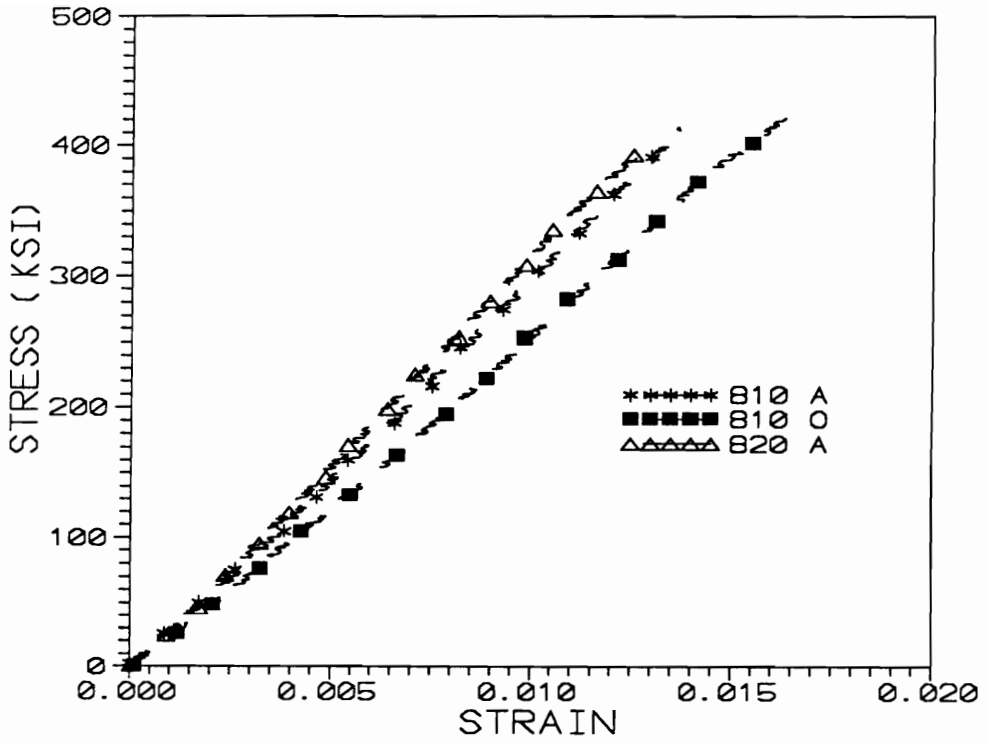

Figure 11 Typical stress-strain diagrams of $(0)_8$ unidirectional 810 A, 820 A and 810 O lamianates.

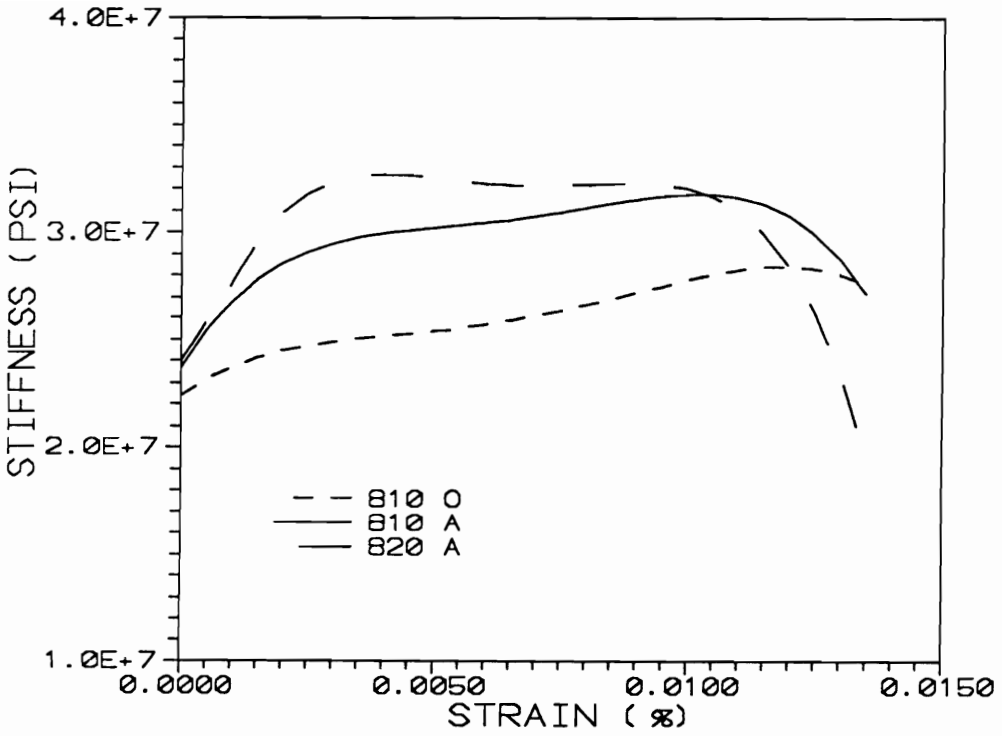

Figure 12 Variation of instantaneous stiffness of $(0)_8$ unidirectional laminates as a function of applied strain.

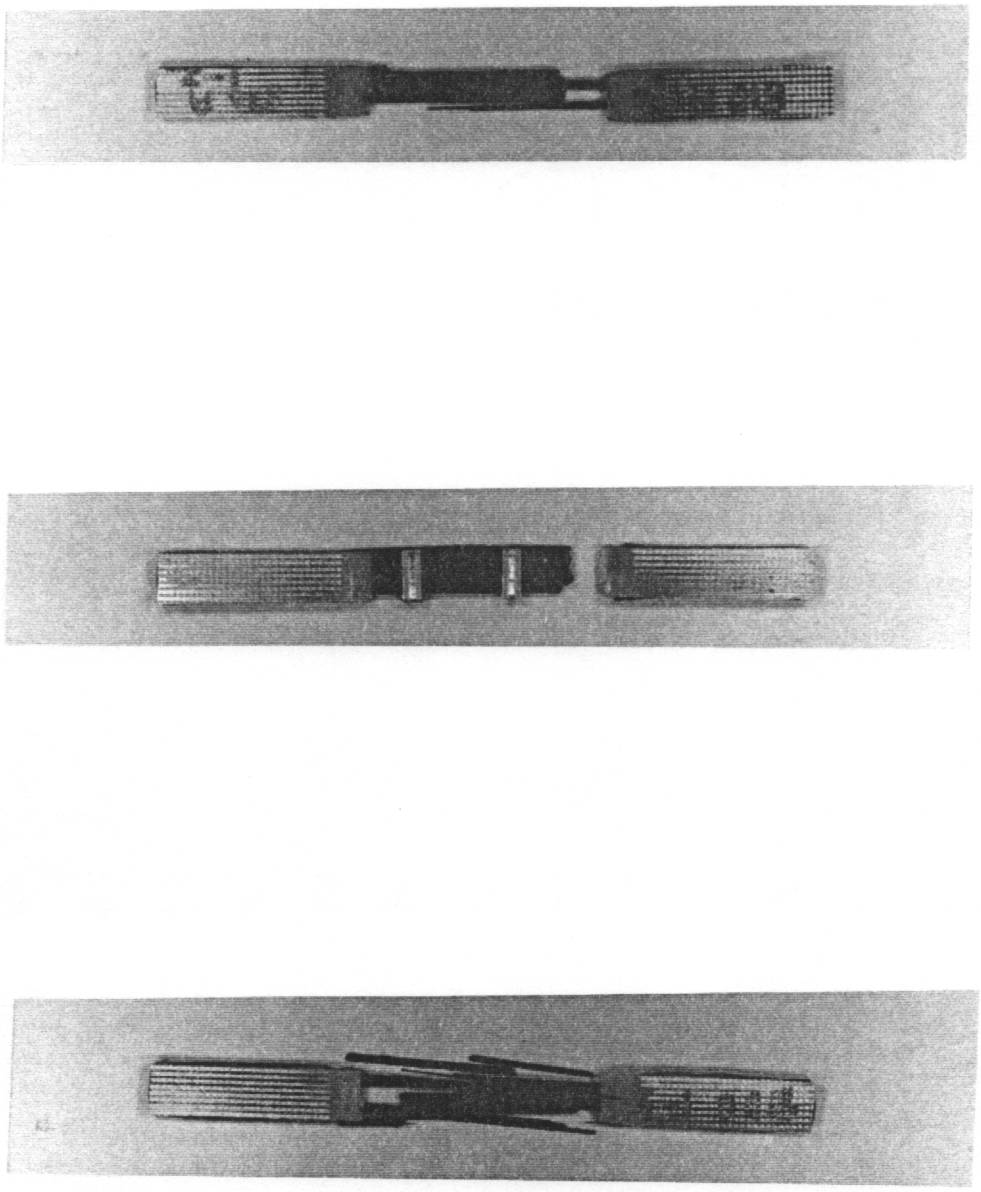

Figure 13 Photograph of failed $(0)_8$ unidirectional laminates;
Top : 810 A; Middle : 820 A; Bottom : 810 O.

three material systems, the stress-strain data was fitted with a fifth order polynomial. Using this fifth order data fit, the variation of instantaneous stiffness (defined as the instantaneous slope of the stress-strain curve) is calculated as a function of applied stain level is calculated. This is plotted as figure 12. From this figure, it is clear that the stiffness of the unidirectional laminate increases initially, and almost plateaus out after about 0.8 % strain. It is interesting to note that the stiffness of the 810 O laminate is lower than that of the 810 A laminate at all strain levels.

Figure 13 shows a comparison of the photographs of failed specimen from the three material system. The figure indicates that the 810 A and 820 A system exhibit a brittle failure, with very little longitudinal splitting. However, the 810 O laminate appears to have more of a "broom failure", with evidence of relatively more longitudinal splitting. This difference in failure modes will be discussed in more detail in the following chapters, where the same trend is seen in the cross-ply laminates under quasi-static and fatigue loading.

Based on the behavior of the unidirectional laminates, the following conclusions are made. The failure of the 810 A and 820 A system is controlled by local stress concentration effects in the vicinity of the broken fibers. This is because of the good fiber-matrix bonding that is seen in these systems. The good bonding precludes the formation of longitudinal splits/debonds near the broken fibers, resulting in the stress concentration effects near broken fibers controlling the final failure of the laminate. In the 810 O system, the lower fiber-matrix bond strength results in the formation of local splits/debonds in the vicinity of the broken fibers, thus reducing the effects of stress concentration in the adjacent fibers. This effectively decouples the broken fiber and isolates it, resulting in a global strain controlled failure of the laminate. The weaker fiber-matrix bonding is probably responsible for the unusually high strain to failure of the 810 O unidirectional laminate.

5.2 Transverse Tensile Test

The transverse tensile strength of the three material systems used in this study was obtained from

Table IX Transverse tensile properties of unidirectional $(90)_{12}$ laminates.

PROPERTY	810 A	810 O	820 A
STIFFNESS (MSI)	1.24 (0.04)	1.22 (0.02)	1.20 (0.02)
TENSILE STRENGTH (KSI)	8.70 (0.45)	8.07 (1.98)	10.80 (3.35)
FAILURE STRAIN (%)	0.70 (0.05)	0.66 (0.18)	0.86 (0.27)

* Values in paranthesis represent the C.O.V

the tests on $(90_{12})_s$ laminates. The stiffness, strength, and strain to failure for the three material systems obtained from 5 tests are displayed in Table IX. Before discussing the results, it must be pointed out that the C-Scan of the 810 O panel indicated that the quality of the 810 O panel was not very good. However, due to lack of availability of any other panels, the specimen from this panel were tested. The results must be interpreted with this in mind. The results indicate that the stiffness of all three material system are almost identical. However, the strength of the 820 A system is highest, while that of the 810 O system is the lowest. It is also interesting to note that the scatter in the strength data is high in the 810 O laminates. The low strength and the greater scatter in the data could be either due to the poor quality of the panel, or due to the PVP sizing used in the material. As will be seen in the next chapter, the data from cross-ply laminates indicate that the transverse strength of the 810 O laminate is indeed lower, and the scatter in the data is also due to the PVP sizing. As mentioned earlier, the sizing process result in a non-uniform distribution of sizing in the 810 O system. Only the fibers on the outside of the tow received PVP coating. If the interphase in the 810 O system is weak, then the non-uniform distribution of PVP could result in a non-uniform distribution of strength in the 90° ply. This would manifest itself as greater scatter in the strength data. It is thus claimed that the "normal strength" of the interphase formed by PVP in the 810 O system is lower than that formed in the 810 A system. Similarly, it could be said that the "normal strength" of the interphase with 200 % surface treatment is greater than that of the 100 % surface treated 810 A system.

Figure 14 shows a comparison of the stress-strain diagrams for the three material system. The stress-strain curve is linear upto failure. As mentioned earlier, the stiffness of the three material system was almost identical. The stiffness of the 810 A system was the highest, while that of the 820 A system was the lowest. This is surprising, because it was expected that the change in interphase would result in changes in the transverse modulus which is a matrix dominated property. In this investigation, the laminates with different interphase possess similar transverse moduli.

Post failure fractography was performed on specimen from each material system using an SEM.

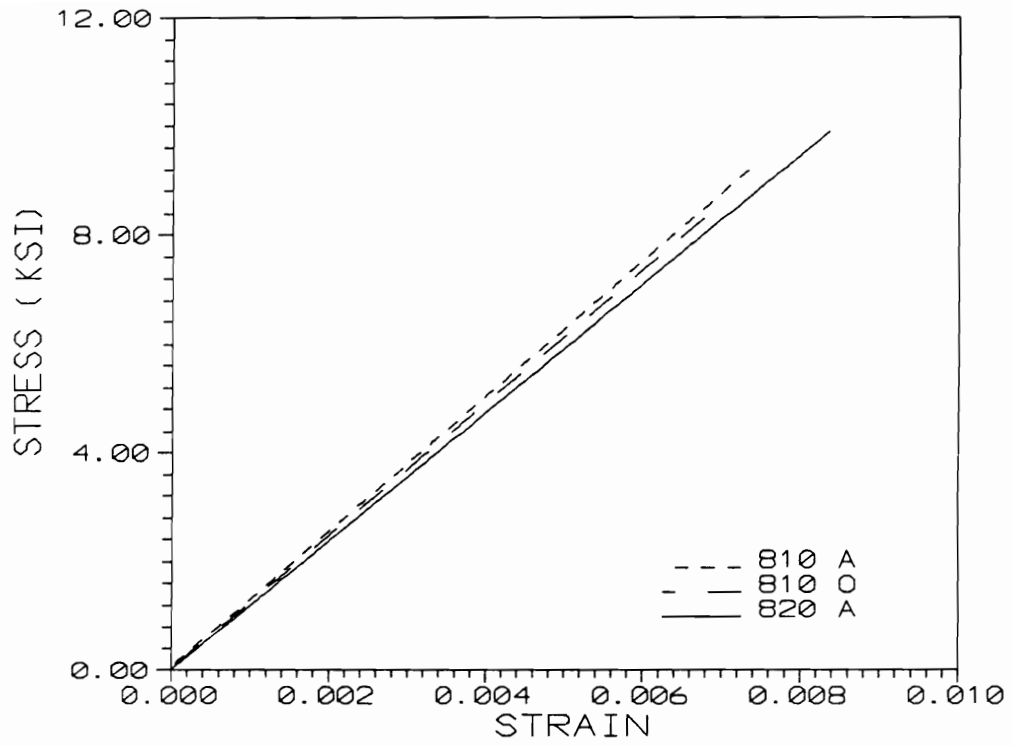

Figure 14 Typical stress-strain diagrams of $(90)_{12}$ unidirectional laminates.

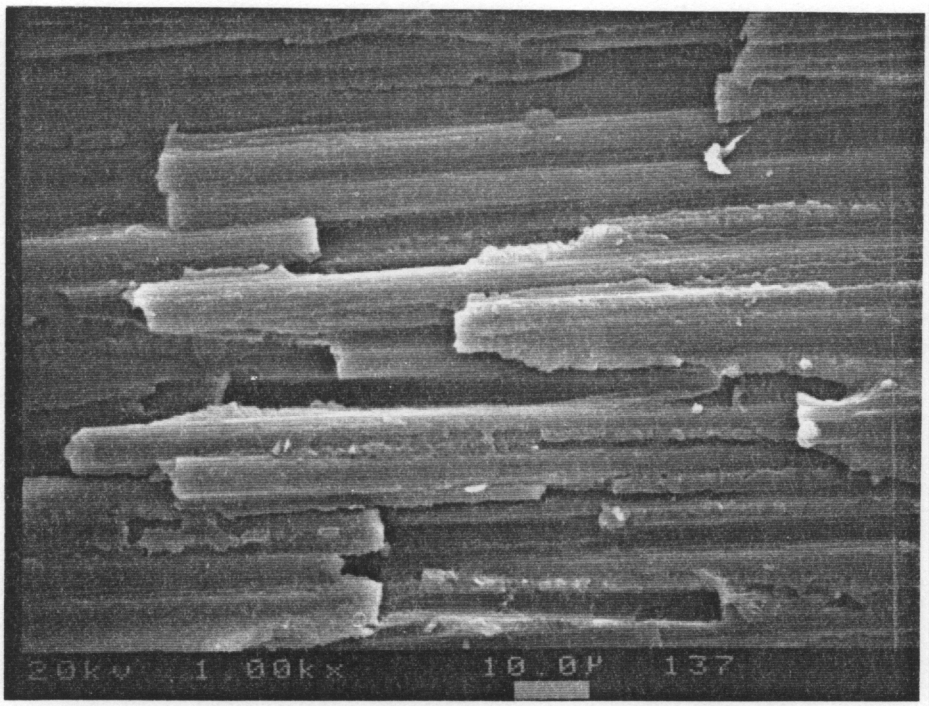

Figure 15 Scanning electron micrograph of failed $(90)_{12}$ 810 A laminate (1000 X magnification).

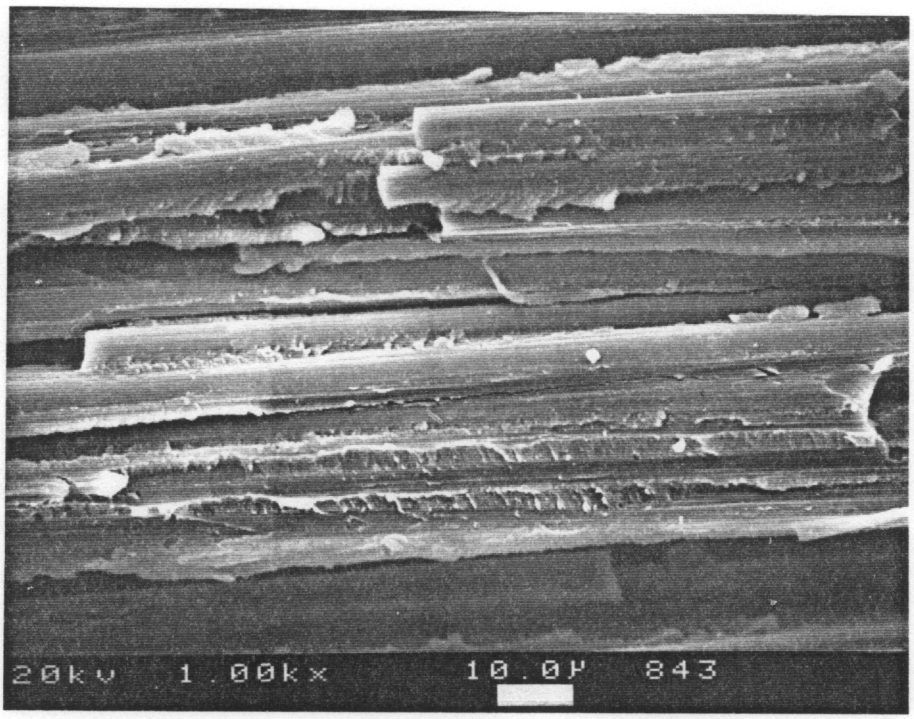

Figure 16 Scanning electron micrograph of failed $(90)_{12}$ 810 O laminate (1000 X magnification).

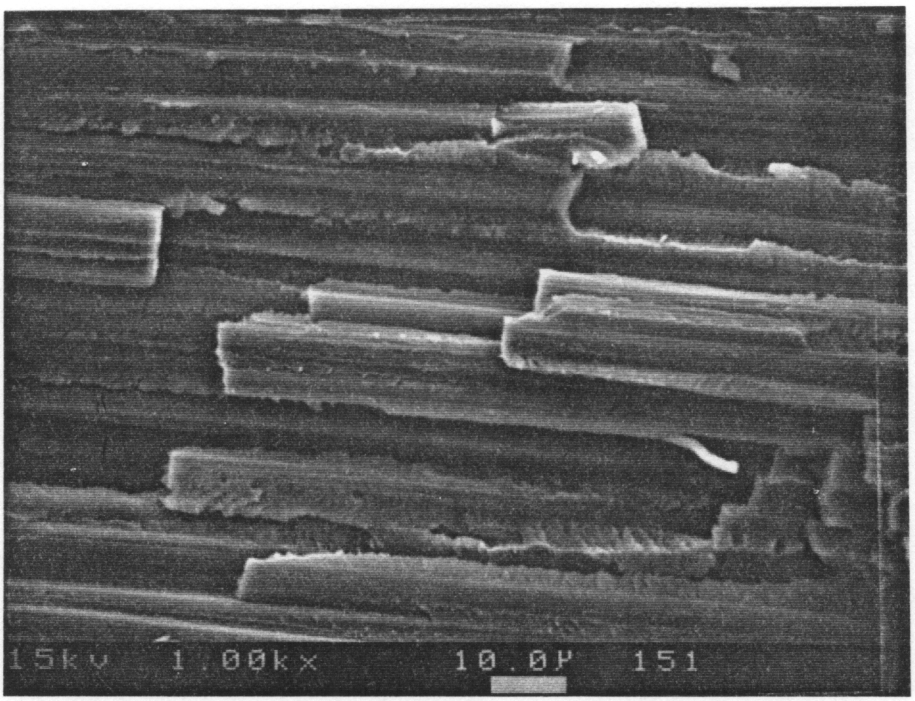

Figure 17 Scanning electron micrograph of failed $(90)_{12}$ 820 A laminate (1000 X magnification).

Figures 15, 16 and 17 show the SEM fractographs of 810 A, 810 O and 820 A laminates respectively, at 1000 X magnification. The fibers in the 810 A systems have more matrix material sticking on it, indicating that the bond strength of the 810 A system could be better than that of the 810 O system. There are also greater number of broken fibers in the 810 A system. Madhukar and Drzal [28] have suggested that in the laminates with good bonding,there are greater numbers of broken fibers. The results in this study are similar to those reported in [28]. In laminates with poor bonding, it is easier to break the fiber-matrix interface. This results in lesser number of fiber breakage. In laminates with higher interfacial normal strength, greater number of fibers are broken when the final failure of the laminate occurs due to better fiber-matrix bonding. The fractograph of the 820 A laminate reveals more matrix material sticking on to the fibers. There are also greater number of broken fibers in this material system. These are again indicative of good fiber-matrix bonding.

5.3 Summary

Results from unidirectional longitudinal tests indicate that the modulus of the 810 A and 820 A system are similar, while the 810 O system has a 16 % lower modulus than the 810 A system. This lower modulus is attributed to poor fiber-matrix bonding and inefficient load transfer between the matrix and the fibers. The tensile strength and strain to failure of the 810 O laminate are significantly greater than that of the 810 A laminate. There is, however, only a slight increase in the tensile strength and strain to failure going from the 810 A to the 820 A system. The 810 A and 820 A system show a brittle failure, controlled by the local stress concentration effects near broken fibers. Failure of the 810 O system appears be controlled by the global strain in the laminate, as evidenced by the high strain to failure value of this system. The transverse tension test results indicate that the 810 O system has a low "normal strength", compared to the 810 A system. The 820 A system has the highest "normal strength". The fractographs indicate that the fiber-matrix bonding in the 820 A and 810 A system are better than that in the 810 O system, under transverse normal loading.

6.0 QUASI-STATIC TEST RESULTS : CROSS-PLY LAMINATES

6.1 Strength Results

Results from quasi-static tests on $(0,90_3)_s$ cross-ply laminates of the three material systems used in this study are discussed in this chapter. The average values of stiffness (as measured by elastic modulus E_{xx}), strength, and strain to failure from three tests are shown in the Table X. The stiffness values reported in the table represent the initial stiffness of the cross-ply laminates obtained by a linear least squares fit of the data between 0 and 1000 lbs (22 ksi). The results indicate that the stiffness of the 810 A laminates are the highest, while the stiffness of the 810 O laminates are significantly lower than that of the 810 A and 820 A laminates. These results are consistent with the unidirectional longitudinal laminate test results discussed in the previous chapter. The 810 O material has the lowest stiffness in both configurations, 0° unidirectional and $(0,90_3)_s$ cross-ply laminates. A simple classical lamination theory based analysis shows that a 16 % change in E_{11} would result in a 10 % change in longitudinal stiffness (E_{xx}) in a $(0,90_3)_s$ laminate. This is consistent with the observed 10 % stiffness reduction in the 810 O laminates, compared to that of the 810 A laminates. The stiffness of the 820 A laminate is 2.5 % lower than that of the 810 A laminate, which is not considered to be experimentally significant.

The tensile strengths of 810 A and 810 O laminates are almost identical, with the 810 O laminates having a 3 % higher strength. This is surprising considering that the 810 O system has a 10 % greater longitudinal strength compared to that of the 810 A system. The strain to failure of the 810 O laminate however is significantly higher. The failure strain of the 810 O laminate is 16 % higher than that of the 810 A laminate. This is consistent with the unidirectional longitudinal strength results. A direct comparison between the unidirectional tensile results and the cross-ply results is made because in the cross-ply laminate, once transverse crack saturation occurs, most of the load is carried by the 0° ply. The failure of the laminate is essentially controlled by the failure of the 0° plies. It is interesting to note that the strain to failure of the cross-ply laminate with PVP sizing is approximately 1.6 %, which is very close to the

Table X Tensile properties of $(0,90_3)_s$ laminates.

PROPERTY	810 A	810 O	820 A
STIFFNESS (MSI)	7.78 (0.12)	7.01 (0.10)	7.57 (0.12)
TENSILE STRENGTH (KSI)	107 (2.16)	111 (4.58)	95.27 (2.16)
FAILURE STRAIN (%)	1.36 (0.02)	1.60 (0.06)	1.23 (0.02)

* Values in paranthesis represent the C.O.V

the strain to failure of the unidirectional laminate and the fiber used in this material system. This indicates that the failure of the 810 O laminate is controlled by the strain to failure of the fiber.

Comparison of the strength of 810 A and 820 A laminates reveal that the 820 A laminate has a significantly lower strength and strain to failure. This is indicative of a brittle local stress concentration controlled failure in the 0° ply of the laminate. As mentioned earlier, Ivens et al [36] have reported similar results in their study with $(0_2,90_2)_s$ graphite/toughened epoxy laminates. Their results indicate that increasing surface treatment levels result in increased bond strength, and also increased notch sensitivity. They have attributed the reduced cross-ply strength at higher surface treatment levels to the increased notch sensitivity. The results in this study follow the trends observed by Ivens et al [36]. The low strength of the 820 A laminate could be due to increased fiber-matrix bond strength and notch sensitivity in this material system.

The presence of transverse matrix cracks is known to influence the local stress state in the plies adjacent to the 90° ply in cross-ply laminates [82,83]. Talug et al [82] have used a finite difference scheme to show that in the presence of transverse matrix cracks, the stresses in the ply adjacent to the 90° ply are significantly greater in the vicinity of the transverse crack tip. Jamison et al [49] have shown experimentally that the stress concentration in the vicinity of transverse cracks precipitate local fiber fractures in the adjacent 0° plies. It is conceivable that in the 820 A system, the presence of 90° ply cracks could initiate early local fiber fractures in the 0° ply. Due to good fiber matrix bonding in this system, the local stress concentration effects near broken fibers could lead to rapid accumulation of local fiber fractures, resulting in lower cross-ply strength and strain to failure. It is hypothesized that the significant reduction in strength and strain to failure of 820 A cross-ply laminates is due to the better fiber-matrix bonding and increased notch sensitivity in this material system. It must also be mentioned here that since the stress concentrations from 90° plies are absent in the unidirectional longitudinal tests, the unidirectional longitudinal strength of the 820 A laminate is not significantly different from that of the 810 A laminate.

A comparison of typical stress-strain curves of the three material systems is shown in figure 18.

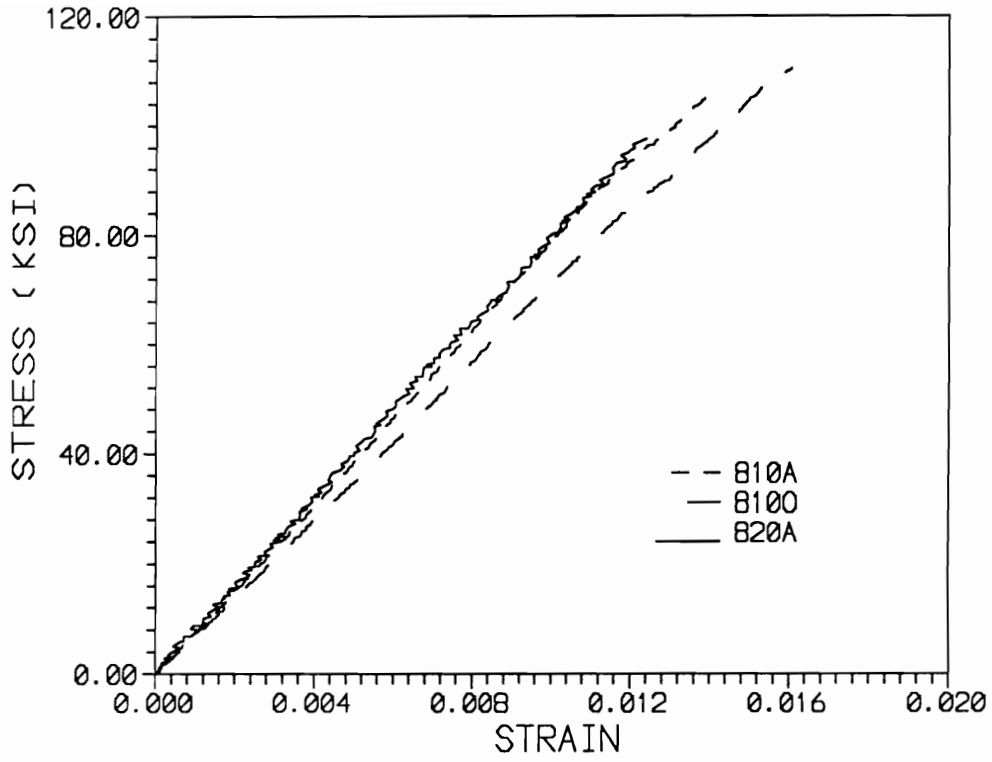

Figure 18 Typical stress-strain curves for the 810 A, 820 A and 810 O cross-ply laminates.

The figure shows that the stress-strain curve of the 820 A laminate is approximately linear to failure. However, the stress-strain curves for 810 A and 810 O laminates exhibit non-linearities close to failure. This is indicative of damage accumulation in the laminate in the form of delaminations and fiber fractures. The 810 O laminate appears to undergo greater amount of damage prior to failure, as evidenced by the high strain to failure.

Figure 19 shows the photographs of the failed 810 A, 820 A and 810 O cross-ply laminates. The damage in the failed specimens correlate with the tensile stress-strain response shown in figure 18. The 820 A laminate, which has an almost linear sttress-strain response, exhibits a brittle failure, with very little evidence of longitudinal splitting in the 0° ply. The 810 A laminate also exhibits a brittle failure, with only little longitudinal splitting in the 0° ply. However, the 810 O laminate exhibits a slightly different failure. There is evidence of relatively more longitudinal splitting in the 0° ply in these laminates. These results are consistent with the unidirectional tensile test results discussed in the previous chapter.

6.2 Damage Analysis

The damage accumulation in the cross-ply laminates of the three material systems was monitored using numerous NDE techniques and the results are discussed in this section. Two specimens from each material system were loaded incrementally, with edge replication being performed at each load level. After edge replication was performed, the specimen was unloaded, and the stiffness was measured by reloading the specimen upto 1000 lbs. The variation of crack density and the corresponding stiffness reductions are plotted as a function of applied load level in figures 20 through 23. The results of the 810 A laminates are compared separately to those of the 820 A laminates and 810 O laminates in order to bring out the influence of fiber surface treatment level and fiber sizing. Figure 20 shows the variation of transverse crack density as a function of applied load in the 810 A and 820 A laminates. The transverse crack density was determined from the crack data on the edge replicas. Data from two tests on each system are presented in the figure. The figure shows that the curves for the two systems are very similar. The onset of matrix

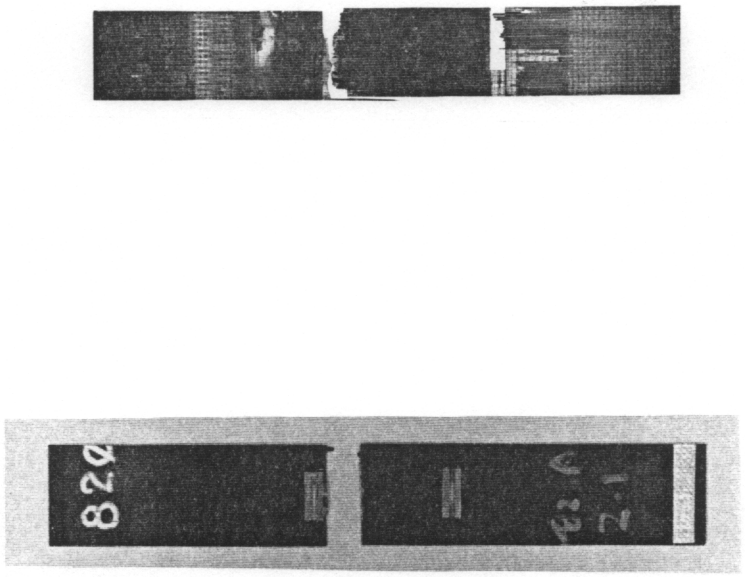

Figure 19 Photographs of the failed 810 A, 820 A and 810 O cross-ply laminates.

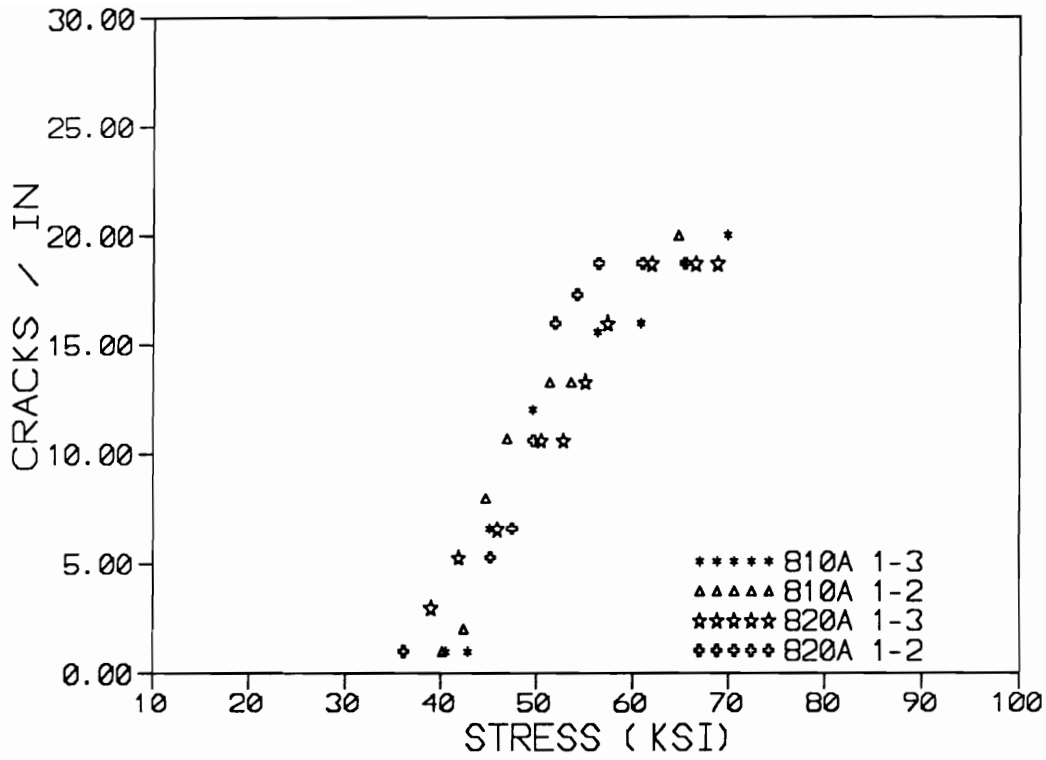

Figure 20 Variation of transverse crack density as a function of applied load for 810 A and 820 A cross-ply laminates.

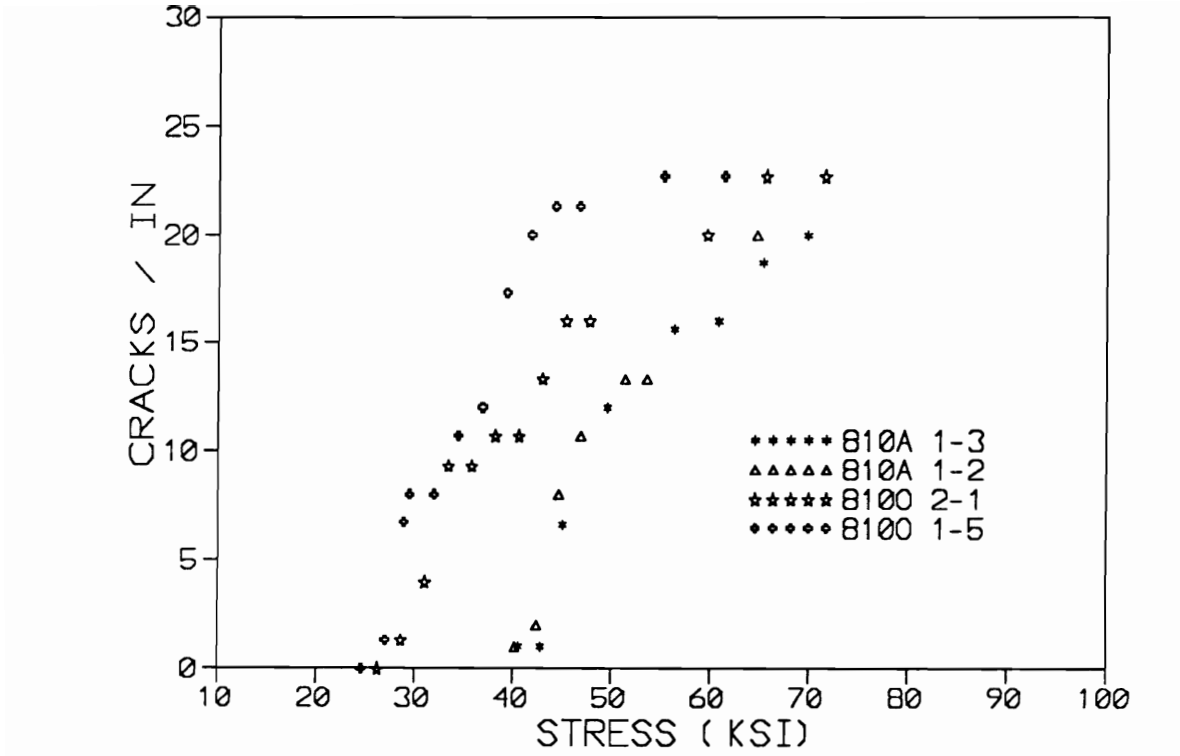

Figure 21 Variation of transverse crack density as a function of applied load for 810 A and 810 O cross-ply laminates.

cracking occurs slightly early in the 820 A system, and the number of cracks (per inch) at saturation is also slightly lower in the 820 A laminates. Figure 21 shows the crack density data for the 810 A and 810 O laminates. As is evident from the figure, there is a significant difference in the matrix cracking characteristics of the two systems with different sizing. The onset of matrix cracking occurs very early in the 810 O laminate. The results indicate that the onset of transverse cracking occurs at approximately 26 ksi in the 810 O laminate; but the first transverse crack appears at approximately 41 ksi in the 810 A laminates. ***By changing the fiber sizing, a 45 % increase in stress to onset of transverse cracking is achieved.*** This is a significant change considering that the sizing material forms less than 1 weight percent of the composite. The figure also indicates that the matrix cracking in the 810 A laminate occurs over a small range of stress values. The saturation of matrix cracking occurs in the 810 A laminates at a stress level of approximately 65 ksi. In contrast, the matrix cracking in the 810 O laminate occurs over a wider range of stress levels. The saturation of matrix cracking occurs at a stress level of around 58 ksi. The saturation crack spacing in the 810 A laminate is 0.05 inches, which is higher than the 0.043 inches saturation spacing in the 810 O laminate.

These results are consistent with some observations reported in the previous chapter. The onset of transverse cracking in the three material system is controlled by two factors; the strength of the 90° ply and the local stresses in the 90° ply. Consider the 810 O and 810 A cross-ply laminate loaded in the axial direction. Since the stiffness of the 0° ply in the 810 O system is lower than that in the 810 A system, the axial stress in the 90° ply of the 810 O system would be greater than that in the 810 A system, for the same external applied load. This would account for some reduction in the stress to onset of matrix cracking. Also, the transverse strength of the 810 O laminate is lower than the transverse strength of the 810 A laminate. This would also result in early transverse cracking in the cross-ply laminate. It is concluded that a combination of increased stress and lower strength in the 90° ply results in early transverse cracking in the 810 O cross-ply laminates.

There are two schools of thought that subscribe to different views, to explain the progressive

cracking in cross-ply laminates. According to some researchers, matrix cracking is accompanied by the strain energy release. Once a matrix crack forms, the strain energy required to form the next crack is greater [84-86]. Hence the next crack forms at a higher load level. According to the other school of thought, the progressive matrix cracking is due to the statistical variation in the local strength in the ply (or in other words, statistical distribution of flaws in the material) [87,88]. If there are fewer flaws or weak sites in the material, then the matrix cracking would occur over small load range. If however, there are more flaws in the material, then the matrix cracking would occur over a larger load range. In the 810 O system, it was observed that the distribution of PVP is non-uniform. Also the transverse strength data indicated greater scatter. This indicates that the distribution of local strength (flaws) in the 90° ply of the cross-ply laminate could have a large scatter. There could be regions in the 90° ply with very high and very low local strengths. If this is indeed the case, then onset of matrix cracking would occur very early, at sites with low strengths. Also, due to the wide distribution of local strength, the progressive cracking would occur over a larger load range. This is exactly what is seen in the 810 O laminate.

The matrix cracking results discussed in the previous paragraph could also be used to make qualitative estimates of the interfacial strength of the material system. It can be argued that if the presence of PVP results in a strong interface, then matrix cracking would initiate at regions away from the tow boundaries which has high PVP concentration. This would mean that matrix cracking would occur at regions where the fiber is bonded directly to the matrix. The interface in this region is similar to that present in the 810 A material system. This would mean that the onset of matrix cracking should occur at similar load levels in the 810 A and 810 O laminates. The experimental results however indicate otherwise. The first matrix crack appears at a significantly lower load level in the 810 O laminate. This leaves one with no choice but to conclude that the interphase formed in the 810 O laminate is the weak link. It is thus concluded that the "interfacial normal strength" of the 810 O system is lower than that of the 810 A system.

Figure 22 shows the variation of stiffness in the 810 A and 820 A cross-ply laminates as a function of applied load. The data for the 810 A and 820 A laminates are similar. This is not very surprising

considering that the crack density curves for these two laminates were almost identical. The maximum stiffness reduction for the 810 A and 820 A laminates is approximately 7 %. The horizontal line in the figure indicates the amount of stiffness reduction in the two systems predicted by a complete ply discount method. The experimental data suggests that the 90° plies in both the 810 A and 820 A laminates carry load even after the saturation crack spacing is achieved. It is also observed that the onset of stiffness reduction coincides with the onset of transverse matrix cracking.

The variation in stiffness as a function of applied load for the 810 A and 810 O laminates are plotted in figure 23. The figure reveals that the stiffness reduction starts at a very low load level in the 810 O laminates. The early stiffness reduction is consistent with the early onset of transverse cracking observed in this material system. It is also noted that the 810 O laminate undergoes 10 % stiffness reduction before transverse crack saturation occurs. This is higher than the 7 % stiffness reduction in the 810 A laminate. The greater stiffness reduction is mainly due to the greater number of matrix cracks seen in the 810 O laminate. It must also be mentioned here that the greater stiffness reduction in the 810 O laminate could be partly due to creep effects. Due to the manner in which the test was performed, there could have been some creep deformation in the laminate. The laminate was held at each load level for about 1 minute for edge replication. This could have resulted in creep deformation in the 90° ply of the laminates. As will be seen in a later chapter, the PVP sized 810 O system exhibits more creep deformation than the 810 A laminate. Thus, time dependent effects could have affected the stiffness of the 810 O laminate more than that of the 810 A laminate. The horizontal lines in the figure indicate the amount of stiffness reduction in the two systems predicted by a complete ply discount method. The experimental data suggest that the 90° plies in both the 810 A and 810 O laminates carry load even after the saturation crack spacing is achieved.

In order to detect the damage in the 0° plies and interlaminar damage in the laminate, x-ray radiography was performed on one specimen from each material system. One specimen from each system was loaded upto 2000, 3000 and 4000 lbs, and x-rayed at each of these load levels. Figure 24 shows the

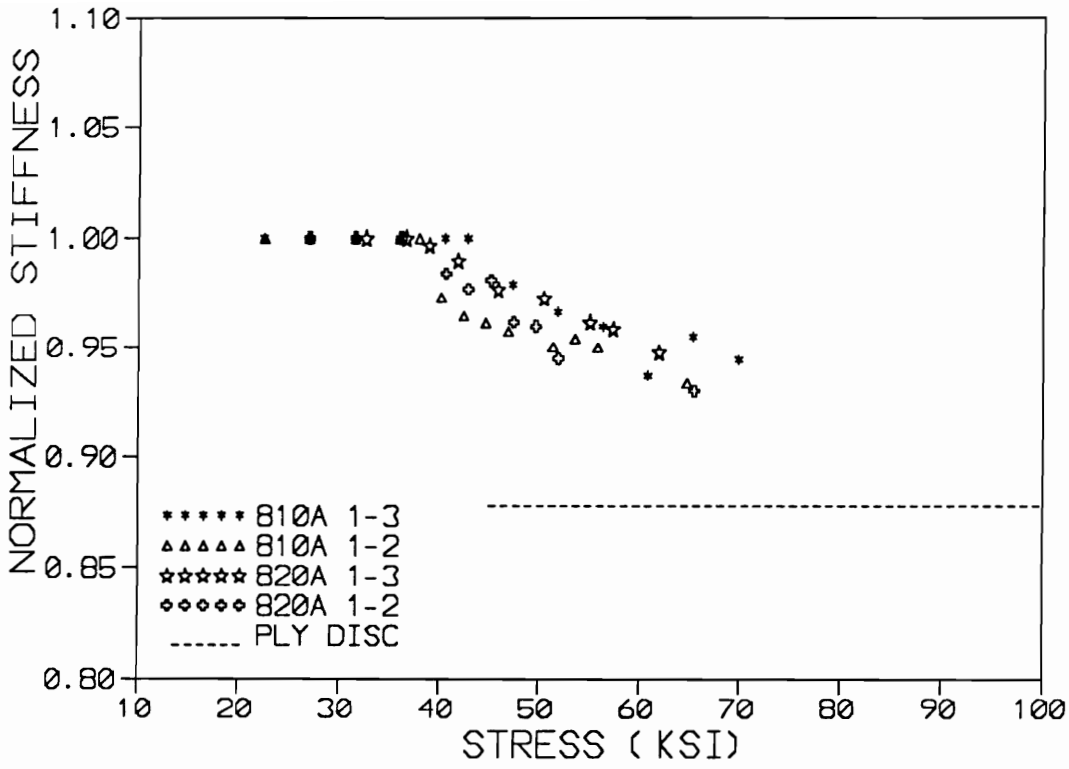

Figure 22 Variation of axial stiffness as a function of applied load for 810 A and 820 A cross-ply laminates.

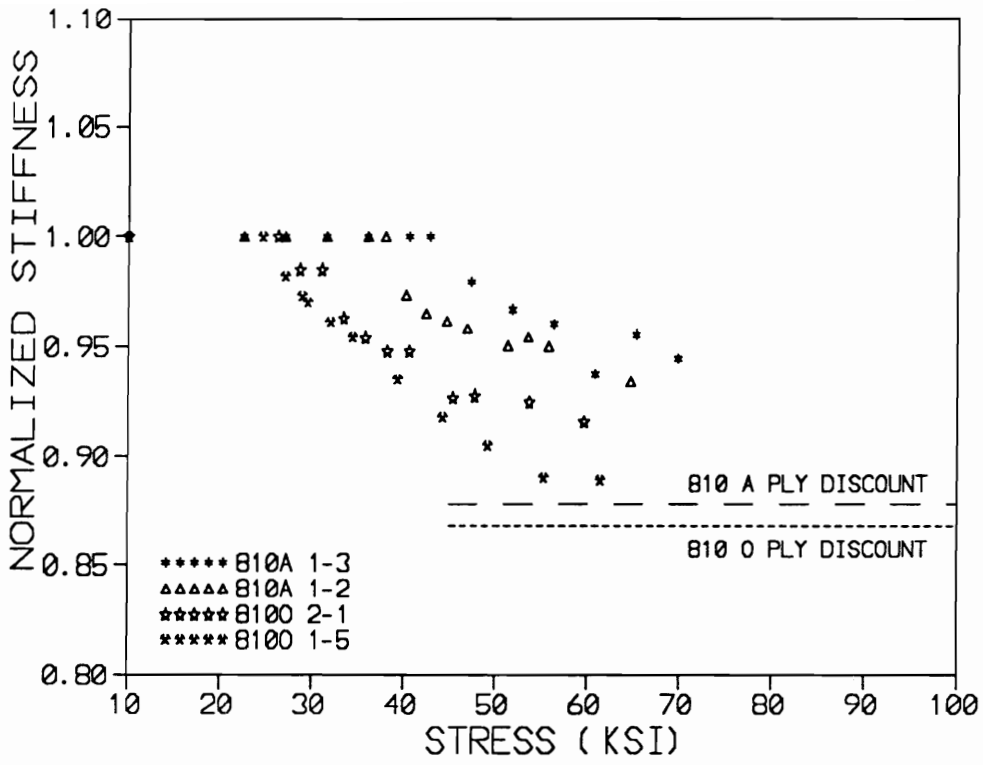

Figure 23 Variation of axial stiffness as a function of applied load for 810 A and 810 O cross-ply laminates.

x-ray radiographs of the 810 A, 820 A and 810 O laminates at the 2000 lbs load level. It is seen clearly that the number of transverse matrix cracks in the 810 A laminate is significantly lower than that in the 810 O laminate after 2000 lbs. A few longitudinal cracks are seen in the 810 A laminate. These cracks were observed before loading, indicating that they could be due to residual thermal stresses. The 820 A laminate shows only 3 transverse cracks/inch after 2000 lbs. This is significantly lower than the number of cracks in the 810 A and 810 O laminates (7 and 20 cracks/inch respectively). Figure 25 indicates that after 3000 lbs, there are 19, 20 and 25 cracks/inch in the 90° plies of the 810 A, 820 A and 810 O laminates respectively. In the 810 O laminate, in addition to the transverse cracks that run through the width of the specimen, there are numerous transverse cracks that do not span the entire width of the laminate. These could be fiber-matrix debonds in the 90° plies. The occurrence of these debonds in only the 810 O laminates could be indicative of weaker fiber-matrix bonding in this material system. The most striking difference between the 810 O laminate and the other two laminates after 3000 lbs load is the presence of numerous longitudinal splits in the 810 O laminate. These splits appear to be local damages, as they do not extend through the length of the laminate. Also, the numerous longitudinal splits are distributed throughout the 0° ply of the 810 O laminate. The appearance of the debonds/splits suggests that they may indeed be fiber-matrix debonding occurring near fiber fractures. In sharp contrast, the 810 A and 820 A laminates do not have any of these longitudinal splits. Figure 26 shows the x-ray radiographs of the 810 A, 820 A and 810 O laminates after 4000 lbs. The 810 A, 820 A and 810 O laminates contains 25,23 and 27 transverse cracks per inch respectively. It may be noted that edge replication studies revealed a saturation of transverse cracks after about 65 ksi (corresponding to about 3000 lbs load). At this load level, the number of matrix cracks per inch in the 810 A, 820 A and 810 O laminates were found to be 20,19 and 25 respectively. As mentioned earlier, the 90° ply carries load even after saturation of matrix cracks occur at around 65 ksi. Due to this kind of behavior, the 90° ply could undergo further cracking at loads greater that 65 ksi. The greater number of cracks per inch (25,23 and 27 in the 810 A,820 A and 810 O laminates respectively) at 4000 lbs could be a result of transverse cracks forming between cracks

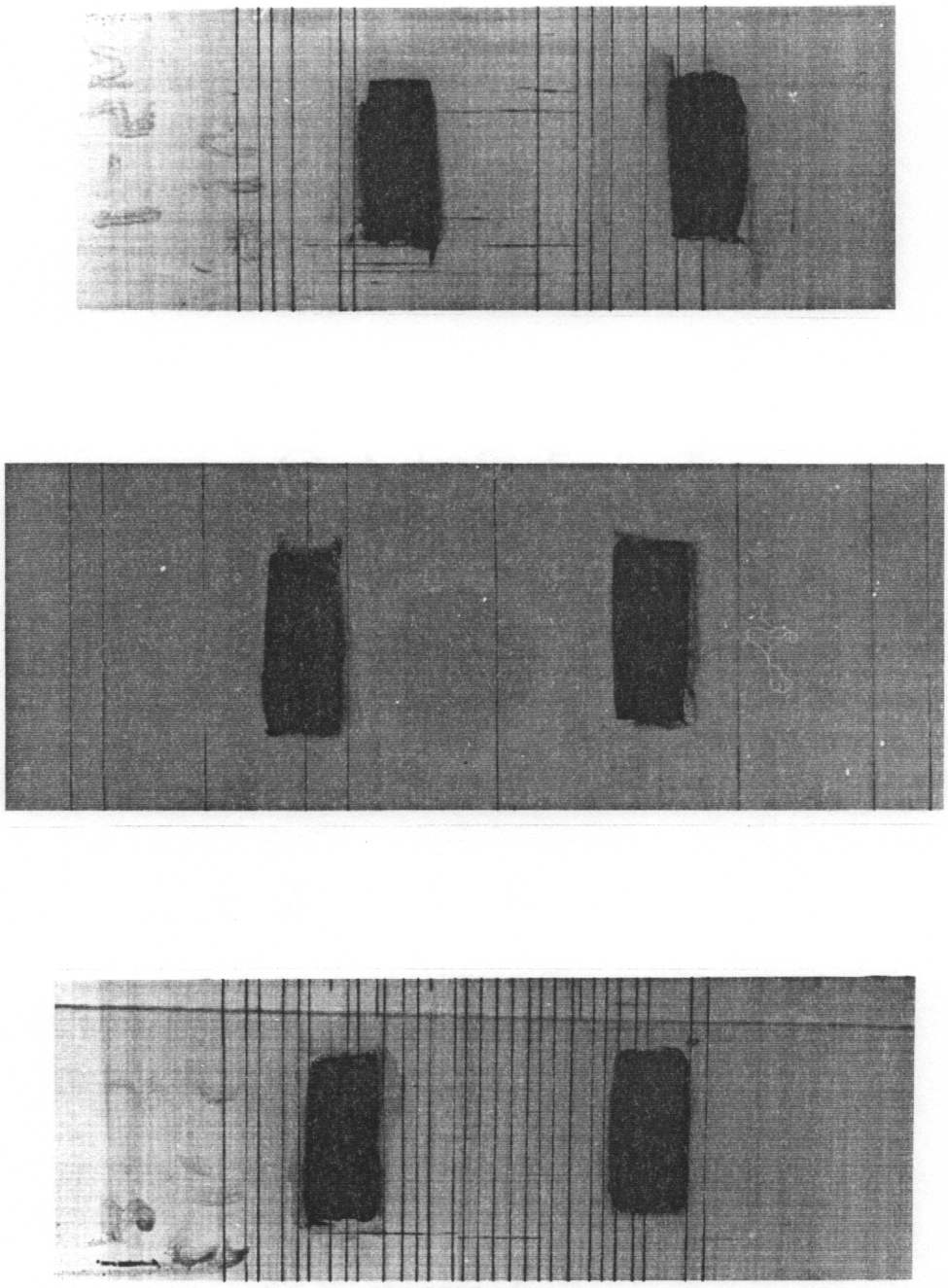

Figure 24 X-ray radiograph of the cross-ply laminates after 2000 lbs ;
Top : 810 A; Middle : 820 A; Bottom : 810 O

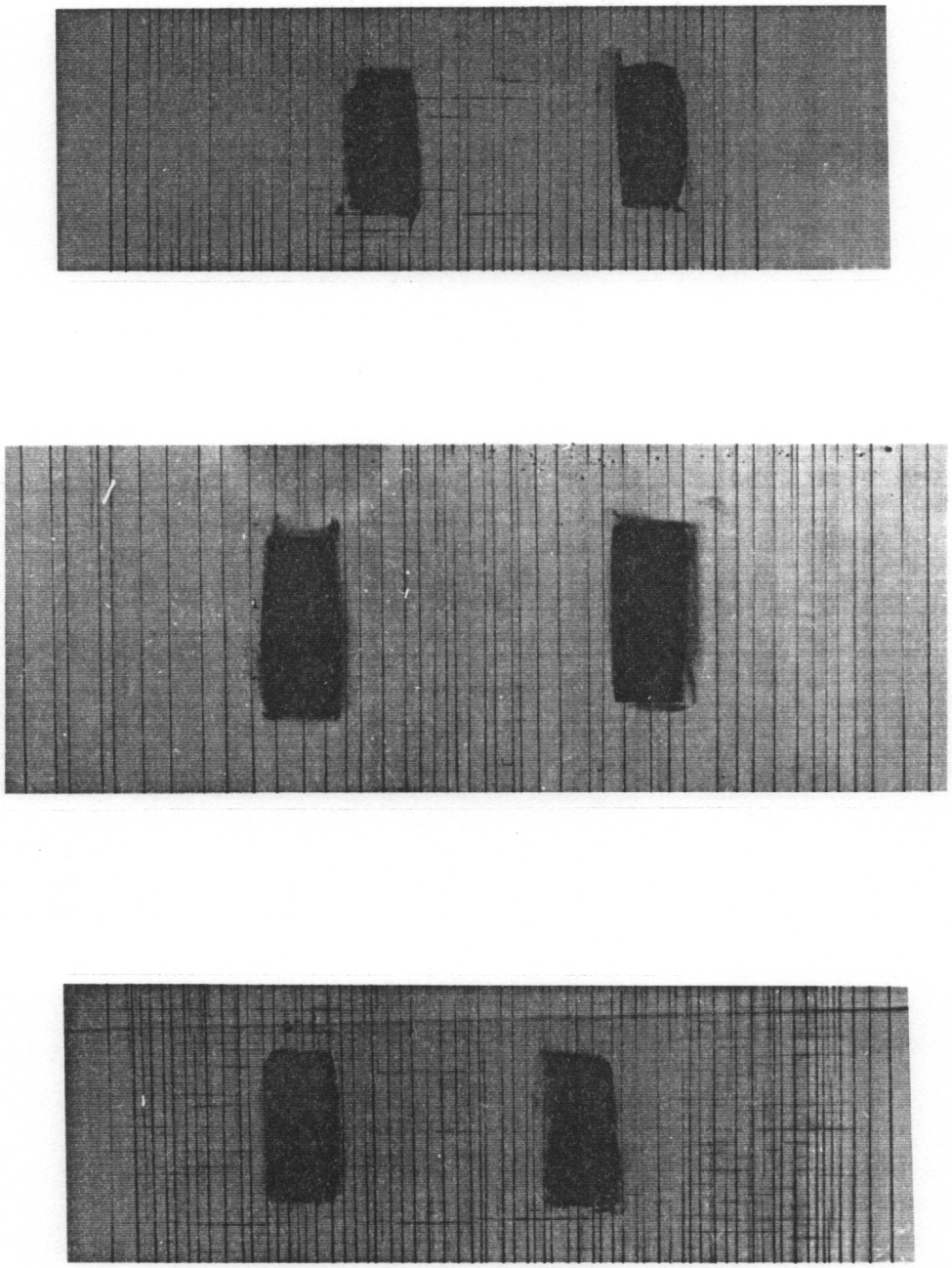

Figure 25 X-ray radiograph of cross-ply laminates after 3000 lbs;
Top : 810 A; Middle : 820 A; Bottom : 810 O.

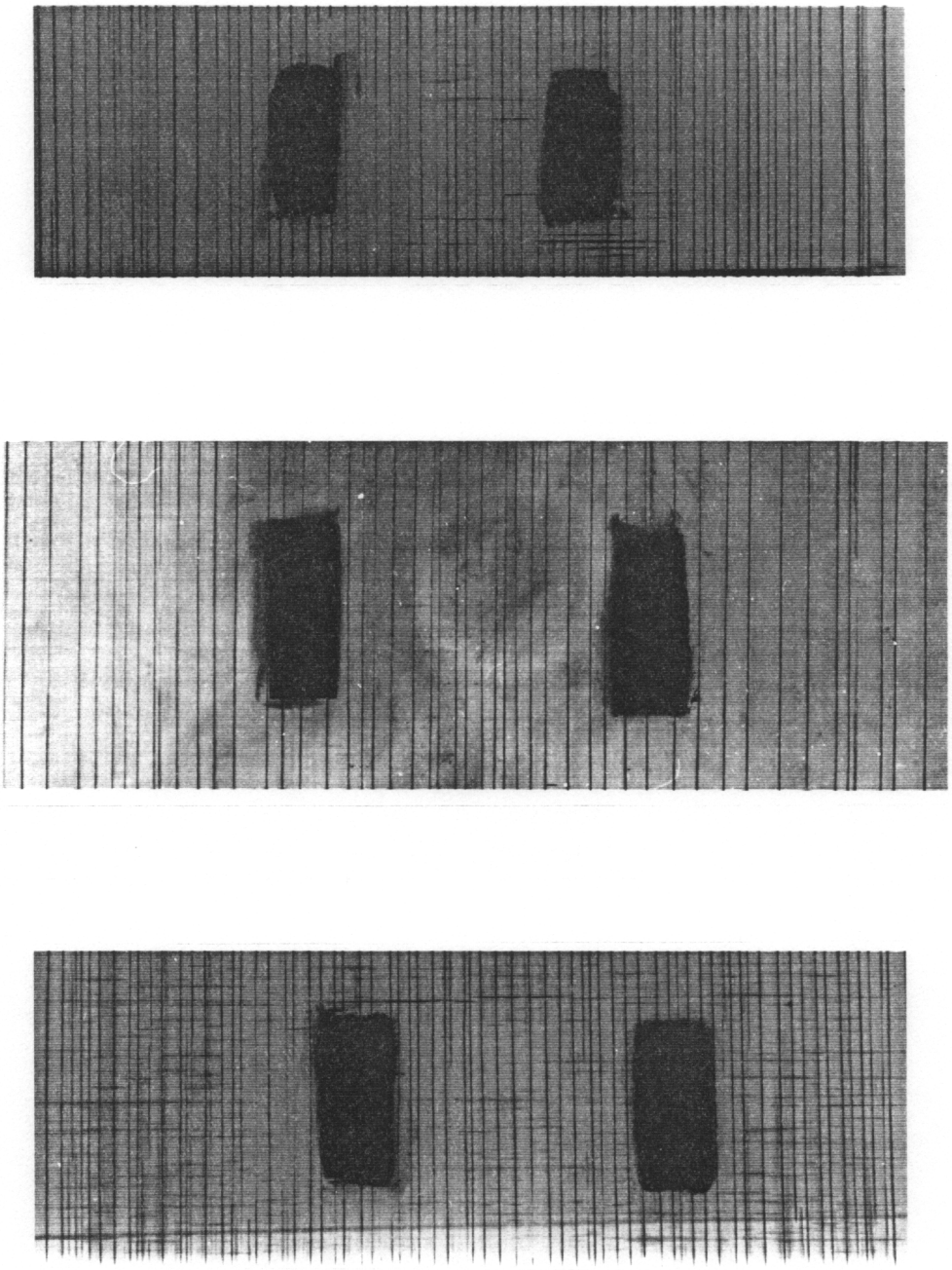

Figure 26 X-ray radiograph of cross-ply laminates after 4000 lbs;
Top : 810 A; Middle : 820 A; Bottom : 810 O.

that occurred prior to saturation. Figure 26 reveals numerous local longitudinal splits in the 810 O laminate. Surprisingly, there are no new longitudinal splits in the 0° ply of the 810 A and 820 A laminates, even at this load level. In the 810 A laminate, an edge delamination is found to occur at the 0/90 interface. The 820 A and 810 O laminate do not reveal any edge delamination. The figure also reveals numerous local delaminations on the 0/90 interface, located at the intersections of the 90 and 0 degree ply cracks, in the 810 O laminate. It has been previously reported [15] that a three dimensional stress state occurs at the region near the intersection of the 90 and 0 degree ply cracks. These stresses have been reported to cause local delaminations in other material systems, in similar laminate configurations [82]. The results from this study are consistent with the results reported in [82]. In contrast, the 810 A and 820 A laminates do not reveal longitudinal splitting or local delaminations. It is thus seen that by varying the fiber sizing, entirely different damage mechanisms are observed in the $(0,90_3)_s$ laminates under monotonic loading.

In order to verify the presence of longitudinal splits and local delaminations in the 810 O laminates after 4000 lbs, the specimen was sectioned across the width. The sectioned sample was mounted on epoxy, polished and observed under an optical microscope. Figure 27 shows the optical micrograph of this sample at 400 X magnification. The figure shows the outer 0° ply in the cross-ply laminate, with fibers running perpendicular to the polished surface. The presence of the longitudinal split in the 0° ply is seen clearly in this photograph. It is also interesting to note that the crack turns into a local delamination when it hits the 0/90 interface. The optical micrograph shown in figure 27 thus confirms the x-ray radiography results.

One specimen from each material system was load monotonically upto failure, and the acoustic emission signals were monitored. The acoustic emission results for the 810 A laminate are shown in figure 28. The number of AE activities at various energy levels are displayed in figure 28a. Most AE events are low energy activities, between 10 and 40 KJ energy levels. A few intermediate energy level activities between 40 and 70 KJ are also recorded. Very few high energy activities (greater than 70 KJ) are recorded during the test in the 810 A laminate. In figure 28b, the amplitude of the AE events are plotted as a

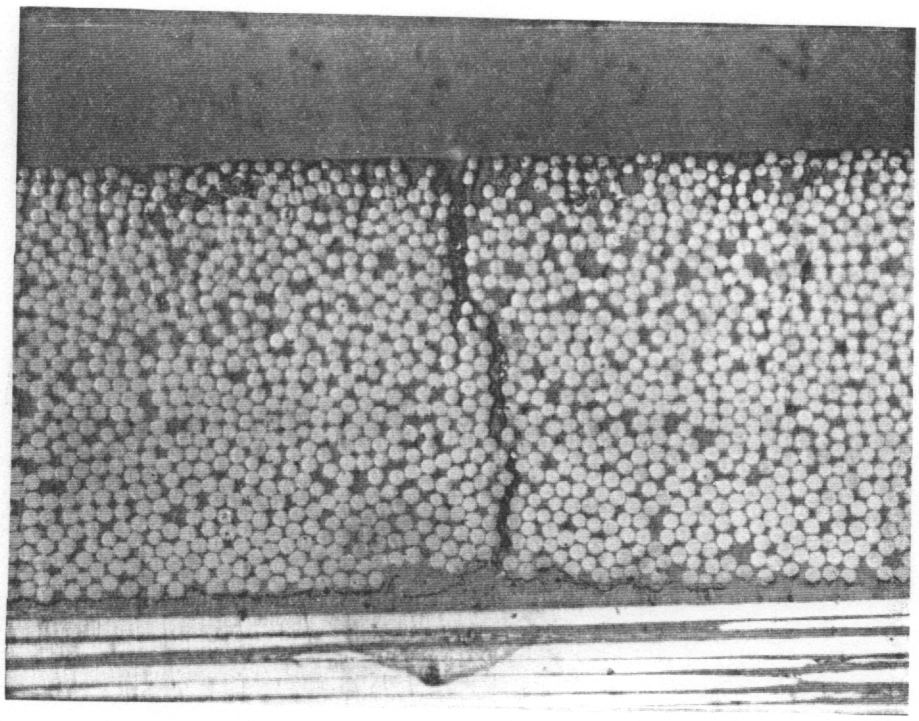

Figure 27 Optical micrograph of 810 O laminate after 4000 lbs revealing the longitudinal split in the 0° ply and local delamination on the 0/90 interface (400 X magnification).

function of time. It is seen that most of the AE activities have low amplitude (between 40 and 60 dB), while some activities between 80 and 100 dB are also recorded towards the end of the test. No AE activities in the 60-80 dB range are recorded during the entire test.

Figure 29 shows the energy and amplitude data for the 810 O laminate. The 810 O laminate shows greater amount of low energy and high energy activities. In addition, there are a few intermediate energy activities (40-70 KJ level). Figure 29b indicates that there are numerous low, intermediate and high amplitude activities recorded during the 810 O laminate test. A total of 398 AE events are recorded during the entire test. This is significantly greater than the 195 events recorded during the 810 A laminate test.

Figures 30a and 30b indicate that the number of activities are significantly lower in the 820 A laminate. There are no activities in the intermediate energy and intermediate amplitude levels, as in the 810 A laminates. Also the total number of AE activities recorded during the test is only 23, which is significantly lower than that seen in the 810 A and 810 O laminates.

It is thus seen that the AE response of the three material system are significantly different. Recently, some investigators [89-92] have used the AE response to identify the various damage mechanisms in composite materials. In his work with glass/epoxy laminates, Kander [89] has concluded that matrix cracking produces low amplitude AE signals (between 40-60 dB), while the fiber-matrix debonding is characterized by intermediate amplitude AE signals between 60 and 80 dB. The fiber fracture has been identified with the high amplitude activities in the 80-100 dB range. The results reported in [89] will be used as a guide, to interpret our data. It must be mentioned here that there is general agreement in the literature that the high energy, high amplitude AE events represent fiber fractures, while matrix cracking is characterized by the low energy, low amplitude AE events. However, there is some disagreement over the identification of intermediate energy and amplitude activities with fiber-matrix debonding. It can be argued that low energy and amplitude events could represent fiber-matrix debonding when the bonding is weak. Similarly, in well bonded systems, the fiber matrix debonding could release a lot of energy and in this case a high amplitude, high energy event could represent fiber-matrix debonding. For the above

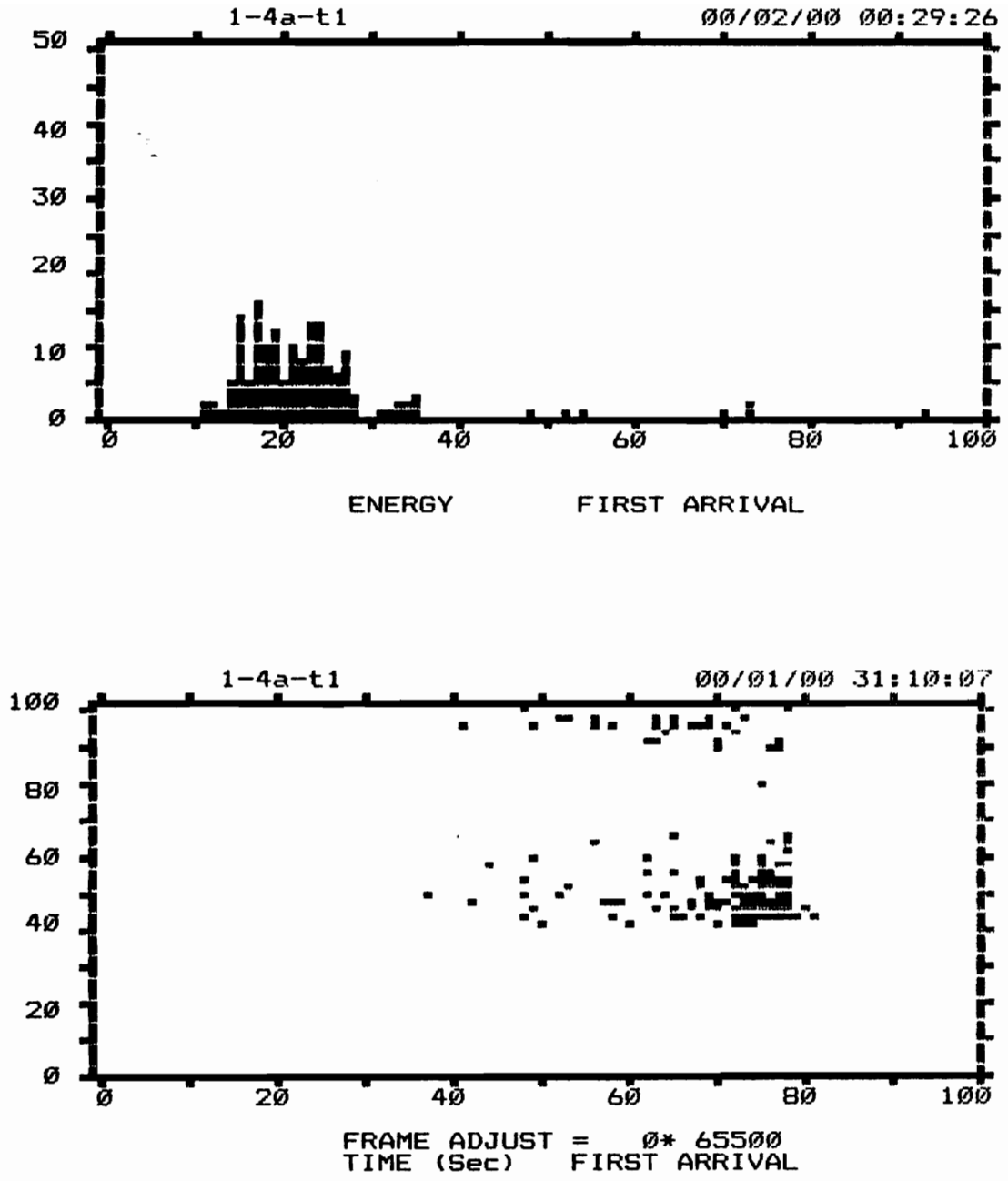

Figure 28 AE results for the 810 A cross-ply laminate; a) Number of AE activities at various energy levels; b) Amplitude of AE event as a function of time.

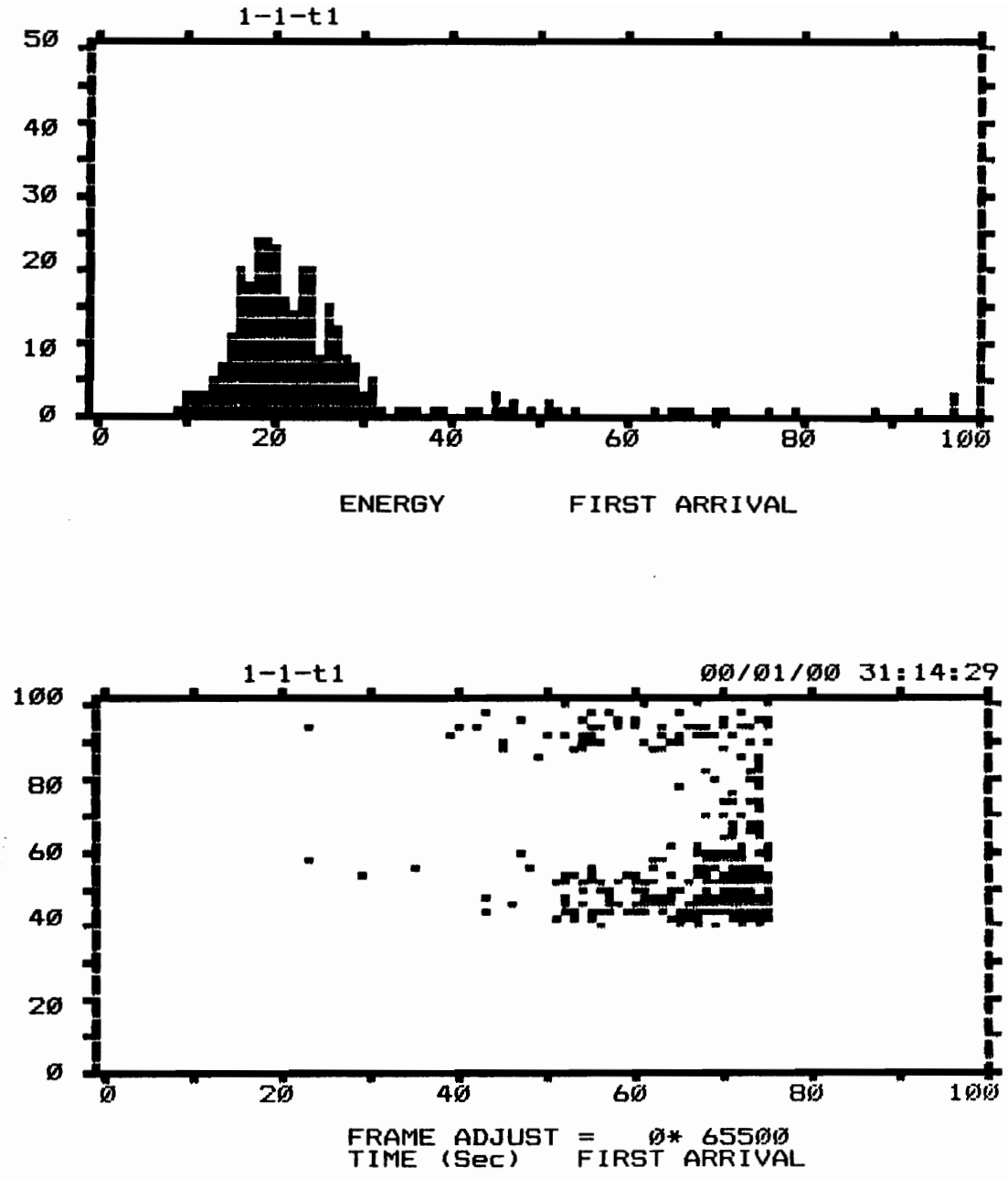

Figure 29 AE results for the 810 O cross-ply laminates; a) Number of AE activities at various energy levels; b) Amplitude of AE events as a function of time.

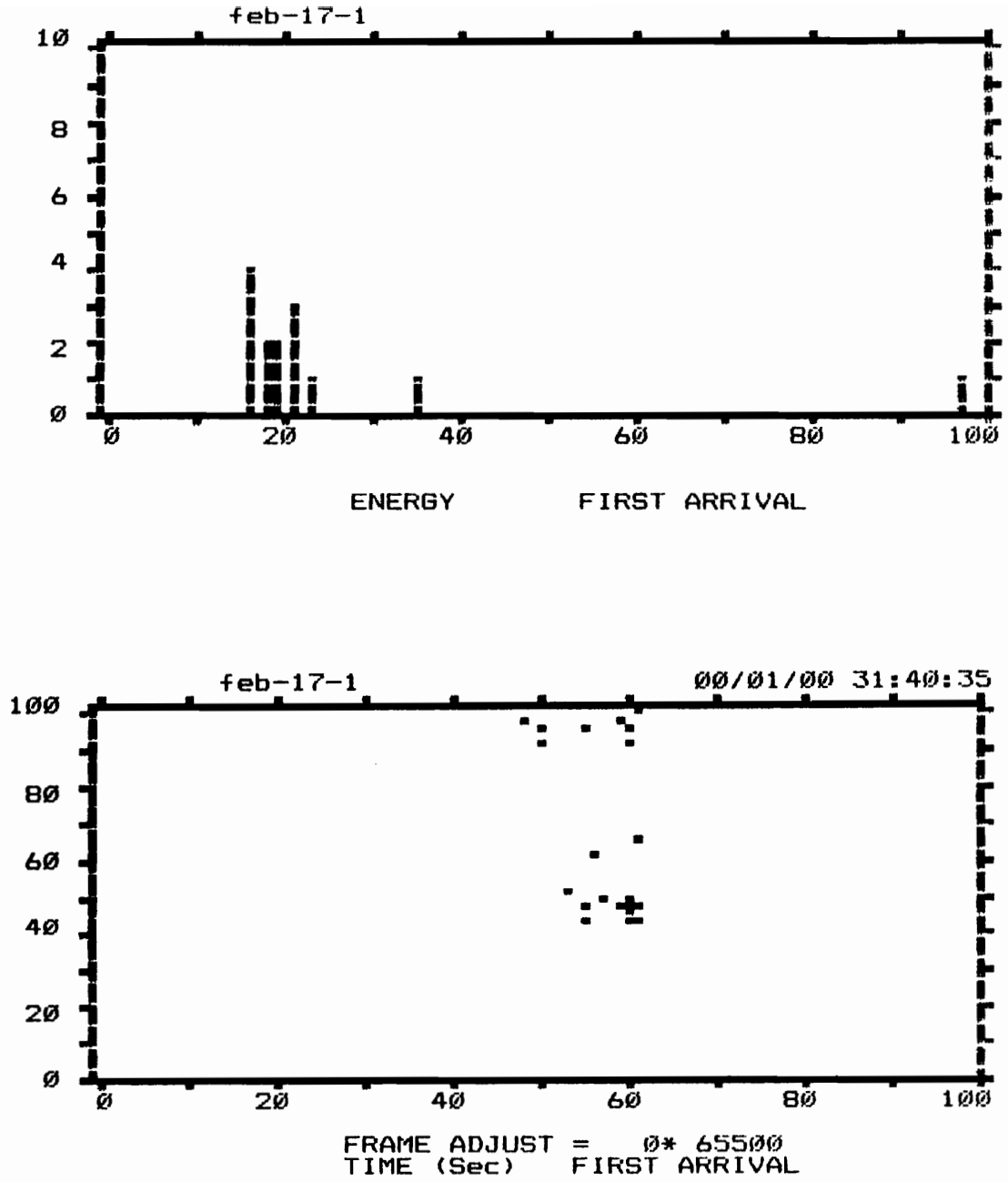

Figure 30 AE results for the 820 A cross-ply laminates; a) Number of AE activities at various energy levels; b) Amplitude of AE events as a function of time.

mentioned reason, the intermediate level events need to be interpreted with caution. **The mere absence of intermediate level AE activities does not necessarily mean absence of fiber-matrix debonding.** The intermediate level AE signals in this study will be used in conjunction with the x-ray radiography results (discussed earlier) to estimate the damage mechanism associated with it. Since there is general agreement about the damage mechanism associated with low and high energy level activities, they will be interpreted as matrix cracking and fiber fracture respectively, in this study.

If we assume that the low amplitude events between 40 and 60 dB indicate matrix cracking activity in the 90° ply, the AE results indicate that the matrix cracking starts around 43 ksi, 60 ksi and 25 ksi in the 810 A, 820 A and 810 O laminates. The onset of matrix cracking determined from edge replication compare well for the 810 A and 810 O laminates. The results for the 820 A laminate however do not correlate well. It must be borne in mind that the AE transducer picks up activities occurring close to the location of the transducer in the specimen. As was seen in the x-ray of the 820 A specimen after 2000 lbs (figure 24), there were only three cracks in the gauge section of the specimen. It could very well be possible that some cracking occurred in the 820 A laminate away from the location of the transducer, that was not recorded. It is also observed that the number of low amplitude activities are greatest in the 810 O laminates, followed by the 810 A and 820 A laminates. This corresponds well with the edge replication results reported earlier. The most interesting feature of the AE results is the presence of intermediate amplitude signals (60-80 dB range) in the 810 O laminate. These activities could be due to the longitudinal splits/fiber-matrix debonds in the 0° ply of the 810 O laminate. Since extensive splitting was seen only in the 810 O laminates, and the intermediate range amplitude events were seen only in the 810 O laminate, it is concluded that the AE signal in the intermediate amplitude range indicate longitudinal splitting (possibly fiber-matrix debonding in the 0° ply). A comparison of the high amplitude activities representing fiber fractures in the laminate yields some more interesting information. Very few fiber fracture are recorded in the 820 A laminate. There are greater number of fiber fractures in the 810 A laminate, while the 810 O laminate shows the highest number of fiber fracture. These results correlate very well with the

fractured specimen shown in figure 19. Based on the AE results and the photographs of failed specimen, it is concluded that the 820 A laminate exhibits very few fiber fractures prior to final failure, and the failure is controlled by the local stress concentration effects near broken fibers, in the 0° ply. In the 810 A laminate, there is a greater number of fiber fractures, but the failure is still controlled by stress concentration effects near broken fibers. The failure mode of the 810 O laminate is different from the other two systems. It is concluded that the presence of longitudinal splits relieves the stress concentration effects near broken fibers, and this results in greater number of distributed fiber fractures. The final failure is controlled by global strain in the laminate, and not by the local stress concentration effects.

Post failure fractography was performed on one specimen from each material system using the SEM. Figure 31 shows the scanning electron micrograph of the 0° ply of the 810 A laminate at 1500 X magnification. The figure indicates clean fibers with evidence of very little matrix ductility. The fractograph of the 820 A laminate shown in figure 32 indicates that the fibers have greater amount of matrix material sticking on its surface, indicating better fiber-matrix bonding. Scanning electron micrographs of the 0° ply in the failed 810 O laminate are displayed in figures 33 and 34. Figure 33 shows the failed 0° ply at a region away from the fracture surface at 290 X magnification. It is seen that there are numerous distributed fiber fractures in the 0° ply even at regions away from the fracture surface. This confirms the AE results that indicated greater amount of high amplitude activities representing fiber fractures. The fracture surface of the 0° ply at 1500 X magnification is shown in figure 34. It is interesting to note that the broken fibers in the 810 O system appear to be clumped together, forming a bundle. The figure also reveals that the fibers are covered by a thin layer of material indicating that failure could have initiated in the interphase or between the interphase and the matrix. Since the interphase material is seen sticking on to the fibers, it is concluded that the interphase bonds well with the fibers. The interphase material appears to be discontinuous, revealing the fiber surface at various locations. This indicates that the interphase material itself could possesses lower strength/strain to failure and the failure could have initiated in the interphase region.

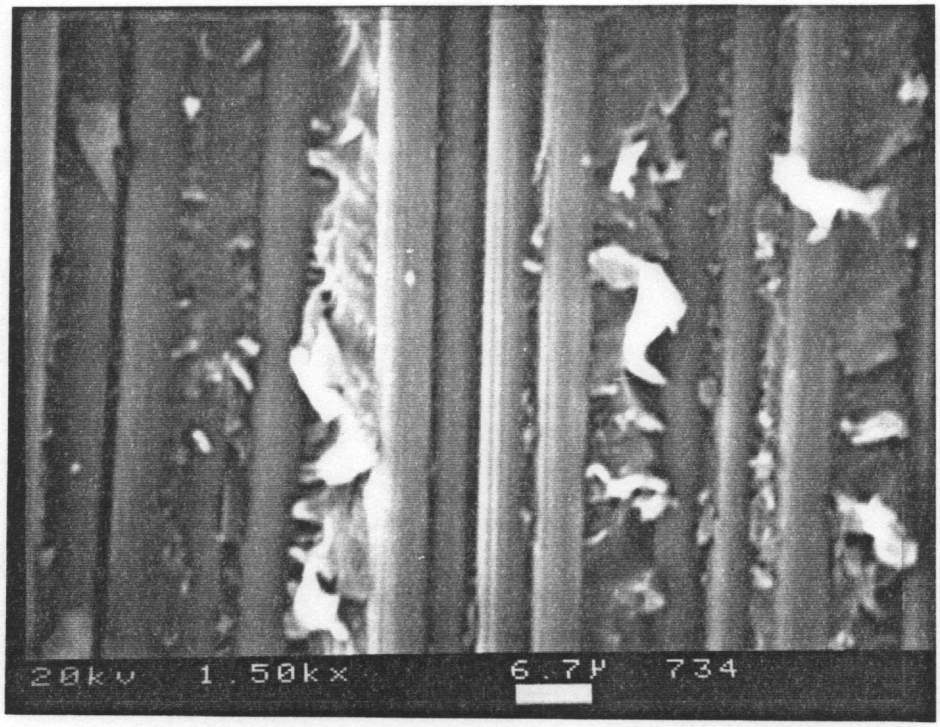

Figure 31 Scanning electron micrograph of 0° ply of failed 810 A cross-ply laminate (1500 X magnification).

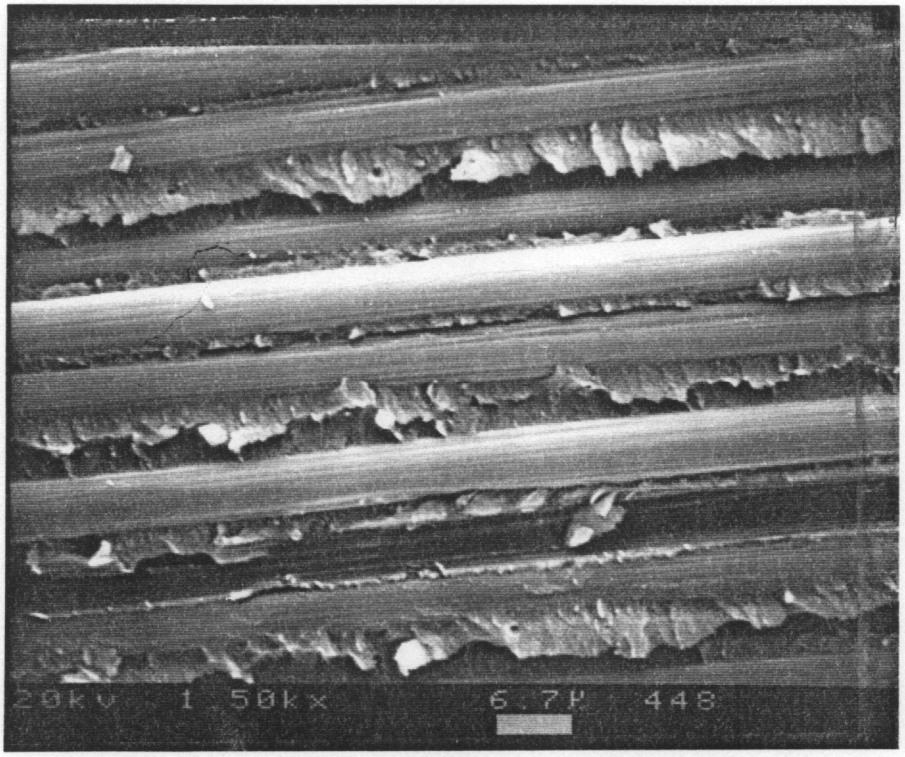

Figure 32 Scanning electron micrograph of 0° ply of the failed 820 A cross-ply laminate (1500 X magnification).

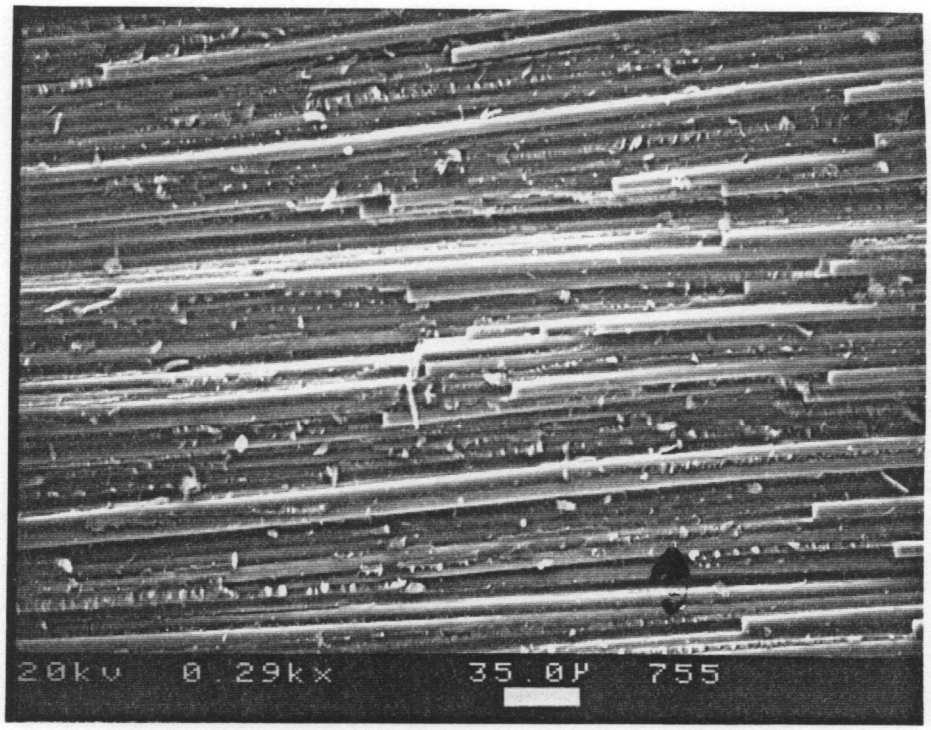

Figure 33 Scanning electron micrograph of 0° ply of the failed 810 O cross-ply laminate revealing numerous broken fibers at a region away from the fracture area (290 X magnification).

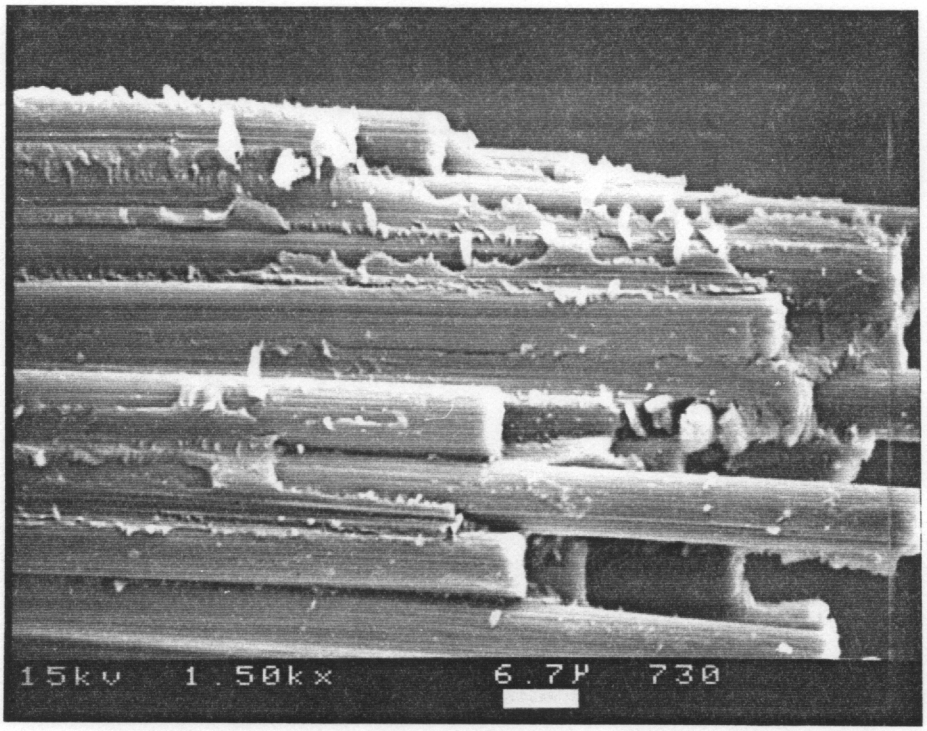

Figure 34 Scanning electron micrograph of 0° ply of the failed 810 O cross-ply laminate (1500 X magnification).

It may be recalled that etching studies (chapter 4) revealed that the distribution of PVP was highly non-uniform. The PVP appeared to be concentrated on the outer fibers of tows (bundles) of fiber. This non-uniform distribution of PVP and the presence of bundles of broken fibers forces one to raise the following question " **Does the sizing process (specially the use of PVP) influence the properties of the composite at a micro level (individual fiber-matrix level) or does it affect the composite at a meso level (tow level) ?**" The available results are not sufficient to support any conclusions. However, it is the authors opinion that the changes observed in the PVP sized 810 O system is due to a combination of the effects at micro and meso levels. If indeed some of the effects seen in the 810 O system are due to changes at a meso (tow) level, then it would open a whole new field of meso-mechanics. If these results can be reproduced using other fibers and matrices, then the composites engineer would have the option of improving the performance of the material by tailoring the material at a tow level. Since these changes can be made at no added manufacturing costs, this would prove to be an attractive way of toughening the composite. However, more work needs to be done to better understand the failure mechanisms and isolate the actual cause for the changes in properties of laminates manufactured with fiber having different sizing.

6.3 Summary

The 810 A laminate exhibits delayed onset of transverse matrix cracking, no longitudinal splitting in the 0° ply, no local delaminations on the 0/90 interface and few fiber fractures. The final failure is controlled by the local stress concentration effects near broken fibers in the 0° ply. In contrast, the 810 O laminate exhibits early transverse cracking, numerous longitudinal splits, a few local delaminations on the 0/90 interface, and a lot of fiber fractures. The final failure is controlled by global strain in the laminate. The 820 A laminate exhibits delayed transverse cracking, no longitudinal splitting or local delaminations, and very few fiber fractures. The final failure is controlled by local stress concentration effects near broken fibers in the 0° ply of the laminate. ***The damage mechanisms and failure modes in cross-ply laminates with different fiber-matrix interphase are different.*** It may be recalled that the interfacial strength (measured

using SFFT) of the 820 A laminate was the highest, followed by the 810 A and 810 O laminates. However, the ordering of the tensile strength of the cross-ply laminates is reversed. ***It is thus seen that high interfacial strength does not translate into better tensile strength of cross-ply laminates.***

7.0 FATIGUE CHARACTERIZATION OF CROSS-PLY LAMINATES

7.1 Fatigue S-N Characterization

Results from fatigue tests on $(0,90_3)_s$ laminates at various load levels are discussed in this section. The fatigue lives of the 810 A, 820 A and 810 O systems at the three load levels are displayed in Figure 35. The lines represent linear least squares approximations. For comparison purpose, the fatigue lives are plotted against the normalized stress levels ($\sigma_{max}/\sigma_{ult}$) in figure 35a. Results indicate that the fatigue lives of 810 O laminates are greater at higher normalized load levels, while the 810 A laminates have longer lives at lower normalized load levels. The 820 A laminates have the longest lives at all normalized load levels. The 810 A and 820 A laminates exhibit run outs at 75 % and 80 % load levels respectively (fatigue lives greater than 1 million cycles are termed run outs). The 810 O laminates possess lives less than 1 million cycles at all three load levels. However, it must be borne in mind that the static strength of the 820 A laminate was significantly lower than that of the other two systems. Hence, at the same normalized stress level ($\sigma_{max}/\sigma_{ult}$), the 820 A laminate is subjected to a lower absolute applied stress level. This is seen clearly from figure 35b which shows the fatigue lives of these laminates at various load levels. The 820 A laminates have the lowest fatigue lives at any given stress level. Also, the slope of the S-N curve of the 810 O laminate is significantly greater than that of the other two material systems. **Results indicate that cross-ply laminates of materials with the same fiber and matrix, but with different interphase, exhibit varied fatigue response.** This observation is even more surprising if we consider that the strength and life of $(0,90_3)_s$ is essentially determined by the 0° ply in the laminate. **This means that the fatigue response of the fiber dominated 0° ply, in the cross-ply laminate configuration, is sensitive to the interfacial bonding condition.** It is believed that the damage mechanisms and failure modes in the 810 A, 820 A and 810 O cross-ply laminates are vastly different which results in significantly altered fatigue performance characteristics in these materials. This claim is supported by the damage analysis results which are discussed in the following section.

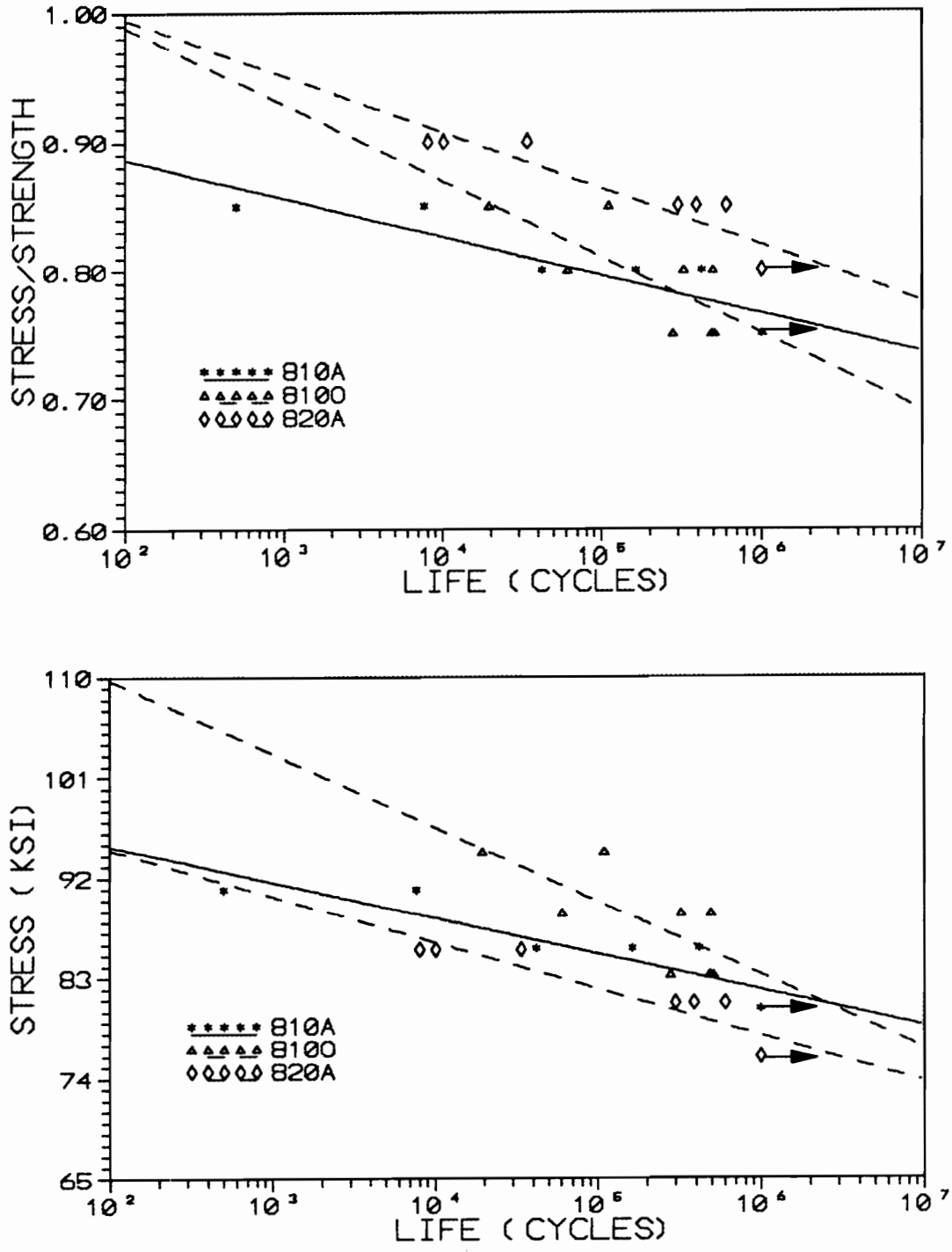

Figure 35 Comparison of the S-N curves of the 810 A, 810 O and 820 A cross-ply laminates. Top : Normalized stress vs Life Bottom : Applied Stress vs Life

7.2 Damage Analysis

Stiffness degradation has been used as a non destructive testing parameter to measure damage in laminated composites in a number of previous studies [50-53]. In this study, dynamic stiffness reduction was monitored for one specimen at each load level, as a function of cycles. The normalized stiffness (E/E_o) is plotted against the normalized life (N/N_f) in Figures 36,37 and 38 for the 810 A, 820 A and 810 O cross-ply laminates respectively. Results indicate that the damage evolution, as indicated by stiffness reduction, is significantly different for the three material system. Figure 36 reveals two distinct stages in the life of the 810 A laminates. Most of the stiffness reduction occurs in the first stage, during the first 10 % of the life of the specimen. The stiffness remains relatively unchanged throughout the remaining life. At all load levels, the maximum stiffness reduction is 7-9 %. The 810 A specimens do not exhibit any accelerated damage near the end of the life, and appear to fail suddenly, in a brittle fashion. The stiffness reduction curves for the 820 A laminates at the three load levels are plotted in Figure 37. The 820 A laminates also show two distinct stages, with most of the stiffness reduction occurring in the first 10 % of the life of the laminate. The stiffness does not change appreciably after the first 10 % of the life. The total stiffness reduction in the 820 A laminates range between 3 and 8 %. Figure 38 shows that there are three distinct phases in the life of the 810 O laminates at all three load levels. Significant damage occurs in the first stage of the life of the laminate that lasts 10-20 % of the life. The stiffness change occurring in this stage is significantly higher than that measured in the 810 A and 820 A laminates. In the second stage, which continues until 90 % of the life, there is no appreciable damage occurring in the laminate. The stiffness reduces by about 2-3 % during the second stage which spans 70-80 % of the life of the laminate. In the third stage, during the last 10 % of the life, an appreciable amount of damage occurs in the laminate, as indicated by the rapid reduction in stiffness of the laminate before final failure occurs. This third stage is observed at all three load levels in the 810 O system. It is also interesting to note that the total stiffness reduction in the 810 O laminate before failure occurs ranges between 13 and 20 %. This is significantly

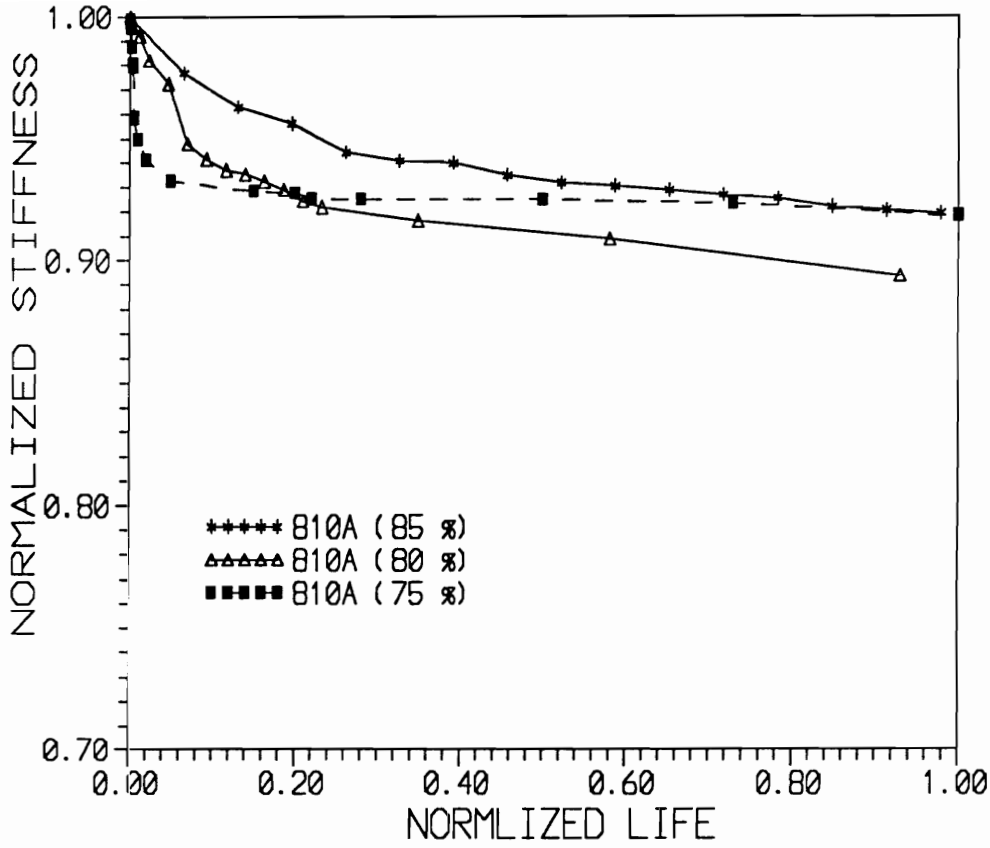

Figure 36 Variation of normalized stiffness as a function of normalized cycles for the 810 A cross-ply laminates at various load levels.

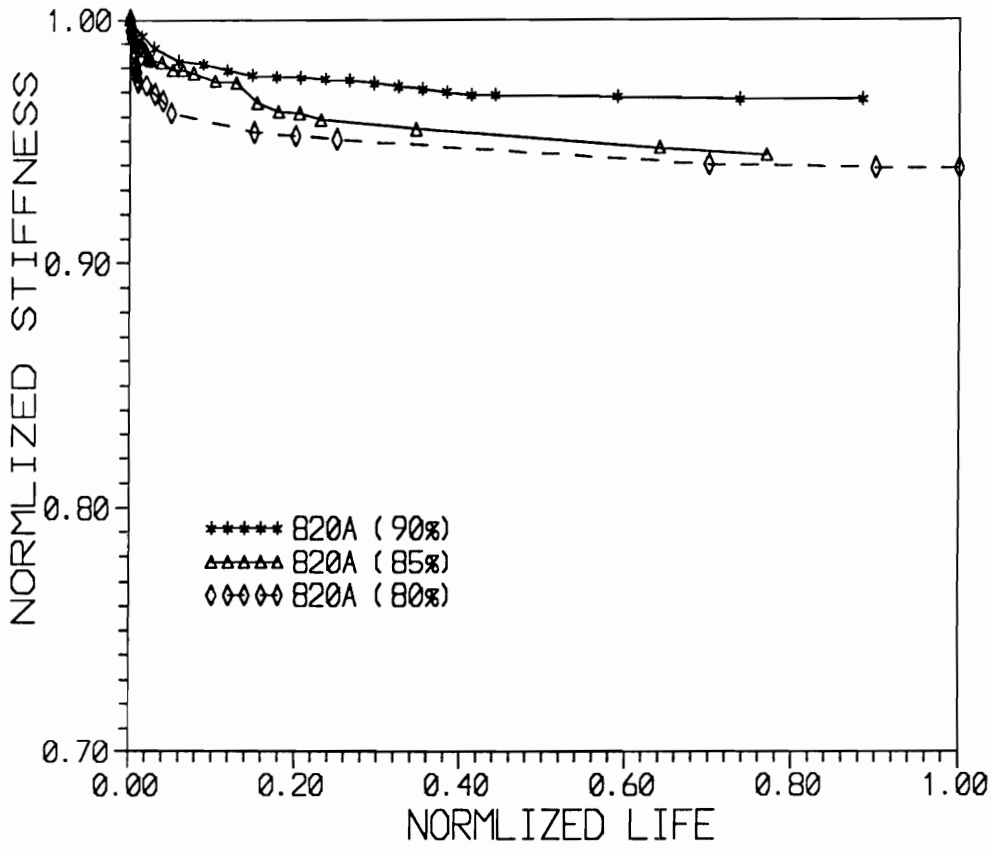

Figure 37 Variation of normalized stiffness as a function of normalized cycles for the 820 A cross-ply laminates at various load levels.

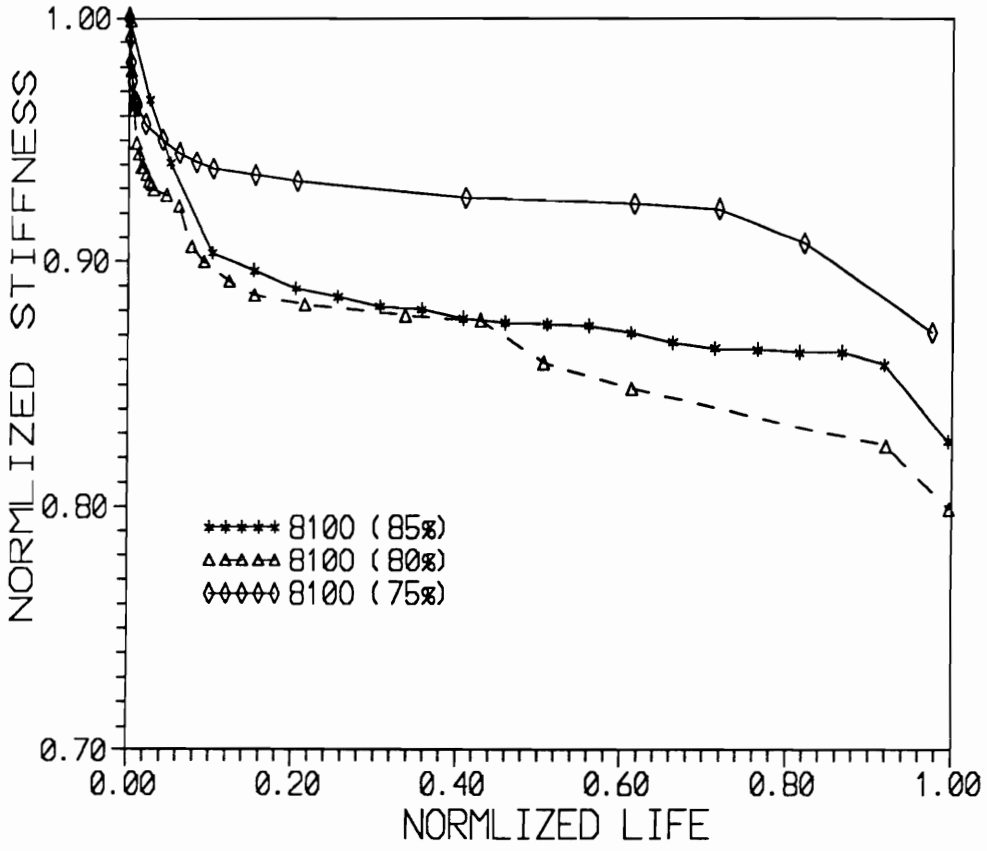

Figure 38 Variation of normalized stiffness as a function of normalized cycles for the 810 O cross-ply laminates at various load levels.

higher than the stiffness reduction observed in the 810 A and 820 A laminates. It should be noted that the 13-20 % reduction in stiffness is significantly greater than the 12 % stiffness reduction predicted by a total ply discount theory. This leads one to believe that there is significant damage occurring the 0° ply of the 810 O cross-ply laminate in the form of fiber fractures. The presence of local delaminations on the 0/90 interface (to be discussed in the next section) could also account for some of the stiffness reduction in these laminates. It is concluded that the higher stiffness reduction in the 810 O laminate is due to the greater amount of damage in the form of matrix cracking, fiber-matrix debonding, local delaminations and fiber fracture. In sharp contrast to the failure process of 810 A and 820 A laminates, the 810 O laminates exhibit accelerated accumulation of damage at the end of the life.

In order to get a better understanding of the damage mechanisms, one specimen from each material system was fatigued at different load levels for specific number of cycles and removed for penetrant enhanced x-radiography. Figure 39 shows the x-ray radiograph of 810 A laminates at 80 % and 75 % load levels after 50,000 cycles and 1 million cycles respectively. The two dark, rectangular areas in the radiographs are the extensometer mounting tabs. The x-ray radiograph reveals numerous transverse cracks in the 810 A laminates at both load levels. The 810 A laminates have 21 and 28 transverse cracks/inch at 80 % and 75 % load levels. A few longitudinal splits are also present in the 0° ply of the 810 A laminates at both load levels. There are however no local delaminations on the 0/90 interface at both the load levels. The x-ray radiograph of the 810 A laminate after 50,000 cycles at the 80 % load level reveals an edge delamination. There is no edge delamination present in the 810 A laminate after 1 million cycles at 75 % load level. The x-ray radiographs of the 810 O laminates after 50,000 cycles and 200,000 cycles at 80 % and 75 % load levels respectively are displayed as Figure 40. The figure reveals 21 and 30 transverse cracks/inch at the 80 % and 75 % load levels respectively. In sharp contrast to the 810 A laminates, the 810 O laminates exhibit extensive longitudinal splitting at both load levels. The longitudinal splits do not extend throughout the length of the specimen and appear to be local splits/debonds. These longitudinal splits are dispersed throughout the 0° ply of the 810 O laminate. It is also interesting to note

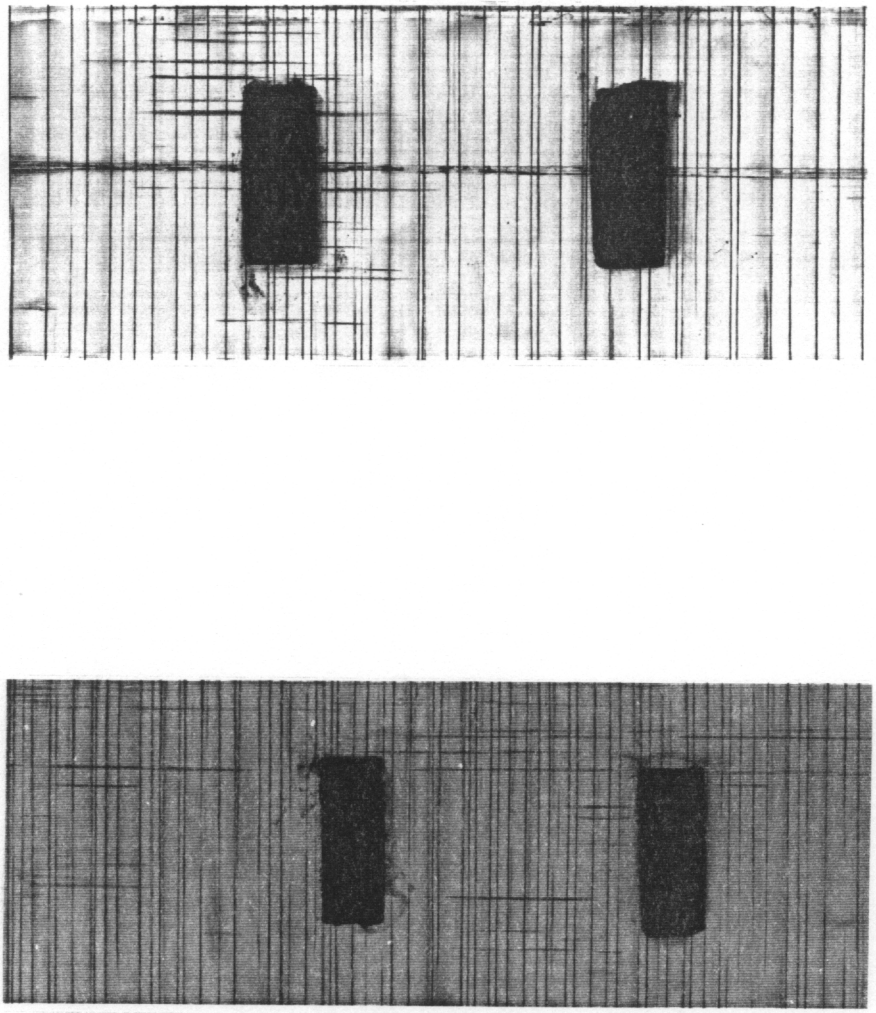

Figure 39 X-ray radiograph of the 810 A cross-ply laminate
Top : 80 % load level after 50000 cycles.
Bottom : 75 % load level after 1 million cycles.

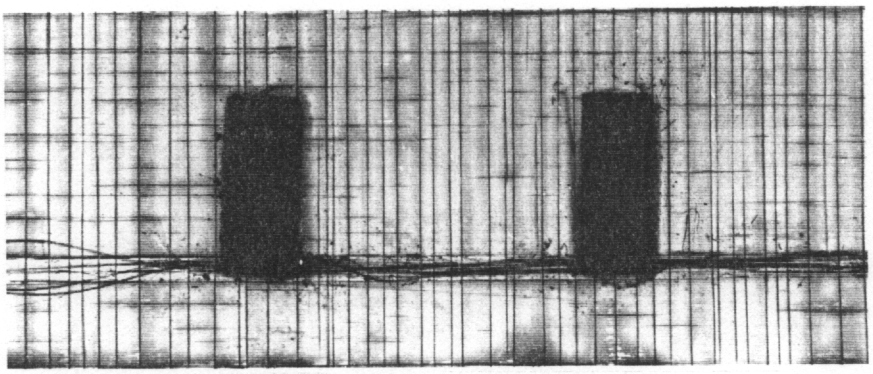

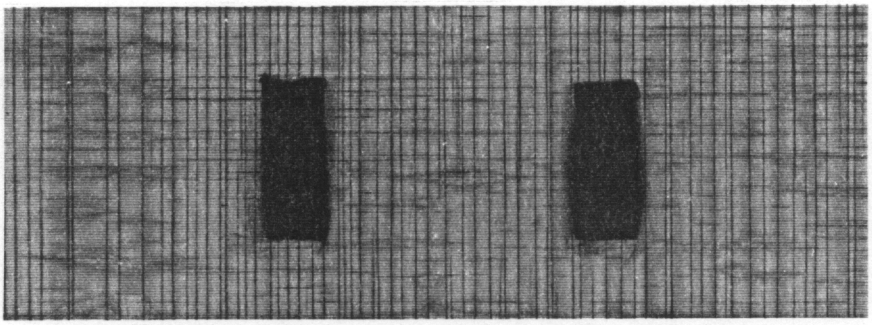

Figure 40 X-ray radiograph of the 810 O cross-ply laminate
Top : 80 % load level after 50000 cycles.
Bottom : 75 % load level after 200000 cycles.

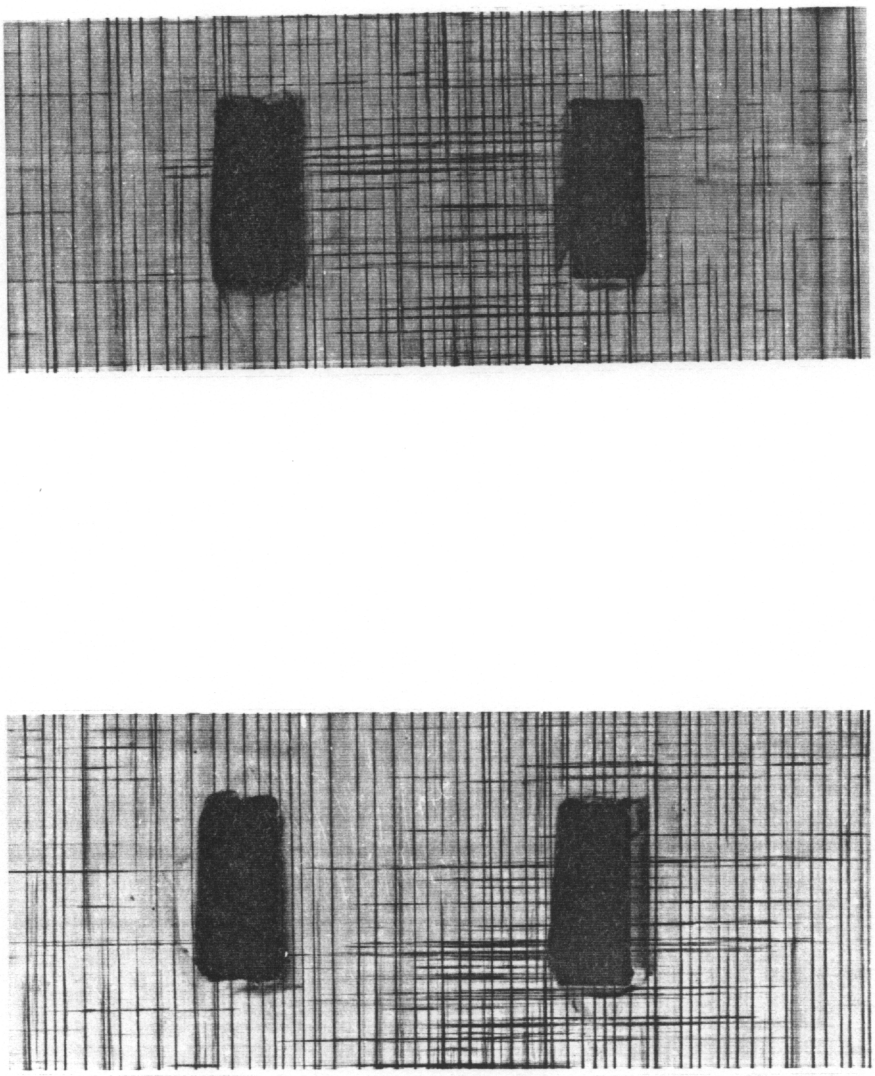

Figure 41 X-ray radiograph of the 820 A cross-ply laminate
Top : 85 % load level after 250000 cycles.
Bottom : 80 % load level after 1 million cycles.

that numerous local delaminations are present on the 0/90 interface at both load levels. These local delaminations appear at intersections of the 90° and 0° ply cracks. The x-ray radiographs of 820 A laminates after 250,000 cycles and 1 million cycles at 85 % and 80 % load levels respectively are shown in Figure 41. The figure reveals 29 transverse cracks/inch at both load levels. In addition to the transverse cracks, numerous longitudinal cracks in the 0° ply are also seen in the laminates at both load levels. However, it appears that the longitudinal cracks in the 820 A laminates are longer than those seen in the 810 O laminates. The 820 A laminates do not reveal any edge or local delaminations at both load levels. Comparing the x-ray radiographs in figures 39,40 and 41, it is clear that the damage mechanisms in the cross-ply laminates of the three material systems used in this study are significantly different.

It is worth mentioning here that damage analysis (using x-ray radiography) on cross-ply laminates under quasi-static tension loading (discussed in the previous chapter) indicated no longitudinal splitting in the 810 A and 820 A laminates. In contrast, the 810 A laminates exhibit a few longitudinal splits under fatigue loading. The 820 A laminates reveal greater amount of longitudinal splitting under fatigue loading at all load levels. The 810 O laminates exhibit numerous distributed longitudinal splits under quasi-static and fatigue loading. It is also interesting to note that the longitudinal splits in the 810 A and 820 A laminates are longer, and appear well defined under x-ray radiographic inspection. In comparison, the splits in the 810 O laminates are smaller and bear the appearance of localized damage.

Based on the damage analysis results, one can speculate on the strength of the fiber-matrix interphase under fatigue loading. The presence of numerous distributed longitudinal splits in the 810 O laminates leads one to believe that the interphase in this system is weaker under fatigue loading. The absence of appreciable longitudinal splits in the 810 A cross-ply laminates can be interpreted as an indication of good fiber-matrix bond in this material system. These results are consistent with the quasi-static test results discussed in the previous chapter. This leads one to believe that the performance of the interphase in these two material system are qualitatively similar under static and fatigue loading. The 820 A laminates however exhibit surprisingly different behavior under static and fatigue loading. There was

no evidence of longitudinal splitting in these laminates under static loading even at very hig load levels. In sharp contrast, the 820 A laminates exhibit appreciable amount of longitudinal splitting at all load levels under fatigue loading. This leads to the question of the behavior of the interphase under static and fatigue loading. One is forced to ask the question **" Does the interphase behave differently under static and fatigue loading conditions ?"** The results from the present study do not provide a definitive answer to this question. However, there is reason to suspect that the behavior of the interphase could be different under static and fatigue loading. More systematic studies need to be performed to conclusively establish the significance and relevance of this issue.

Figures 42, 43 and 44 show the photographs of failed 810 A, 820 A and 810 O laminates fatigued at different load levels. The figure indicates that the 810 A laminate exhibits catastrophic brittle failure, with little evidence of longitudinal splitting in the 0° ply. The 820 A laminate exhibits a brittle failure with some evidence of longitudinal splitting. In contrast, when the 810 O laminate fails, the outer 0° ply shatters completely, resulting in a brush like failure. The failed specimens indicate that the failure of the 810 A and 820 A laminates are controlled by local stress concentration effects in the 0° ply, while the 810 O laminates exhibits a global failure. Since significant stiffness reduction occurs at all three load levels in the 810 O laminates prior to final failure, and the strain in the laminate exceeds 1.5 %, it can be said that the failure of the 810 O laminates is controlled by global strain to failure in the 0° ply.

Post failure fractography was performed on specimen subjected to fatigue loading at different load levels. The scanning electron micrographs of the 0° ply of the failed 810 A, 820 A and 810 O laminates are shown as figures 45, 46 and 47 respectively. The failure surface of the 810 A laminates fatigued at 85 % and 80 % load levels are shown in figure 46a and 46b respectively. The figures reveal clean fibers, with very little evidence of matrix plasticity. It is also interesting to note that the fiber surface reveals striations at high magnification. The failure surfaces of the 820 A laminates at 90 % and 85 % load levels are displayed in figures 46a and 46b respectively. These figures again reveal clean fibers, but at high magnification (figure 46b), the fibers do not reveal any striations. Also, the fibers in the 820 A system

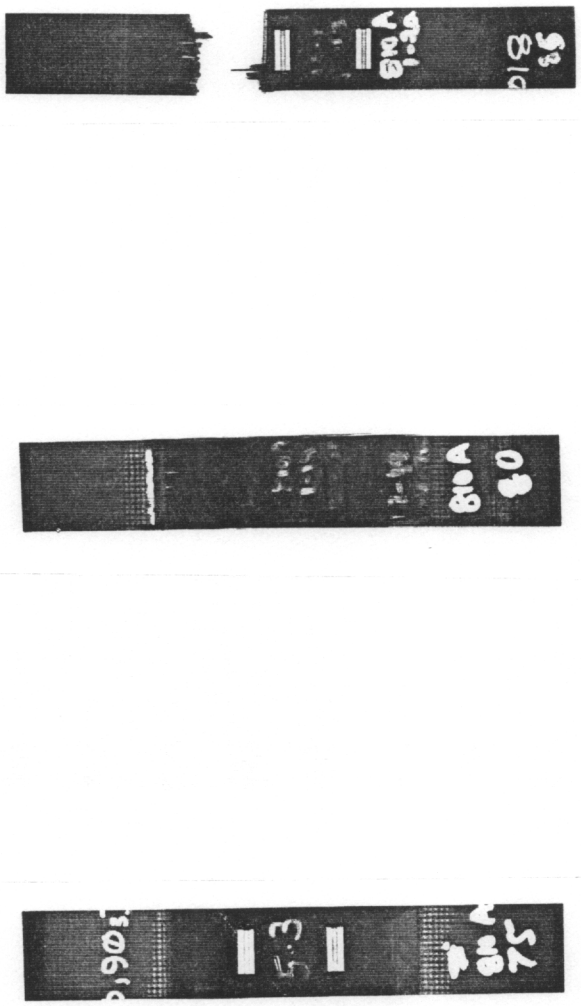

Figure 42 Photograph of failed 810 A cross-ply laminate
Top : 85 % load level Middle : 80 % load level Bottom : 75 % load level.

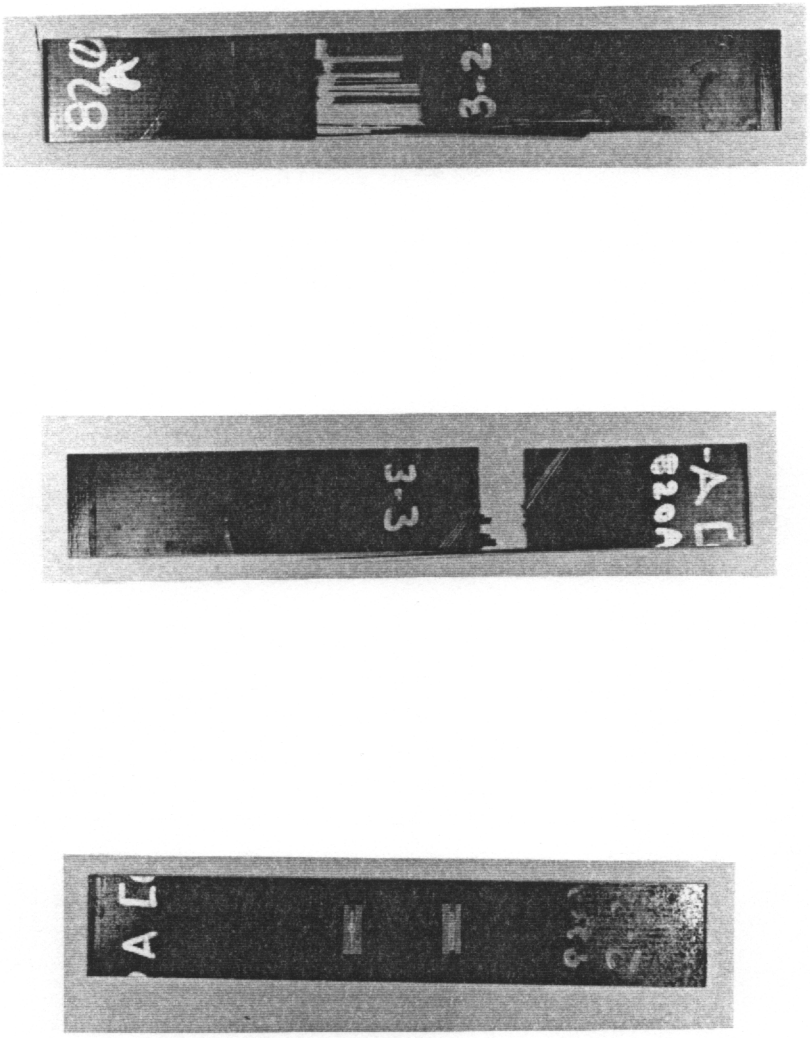

Figure 43 Photograph of failed 820 A cross-ply laminate
Top : 90 % load level Middle : 85 % load level Bottom : 80 % load level.

Figure 44 Photograph of failed 810 O cross-ply laminate
Top : 85 % load level Middle : 80 % load level Bottom : 75 % load level.

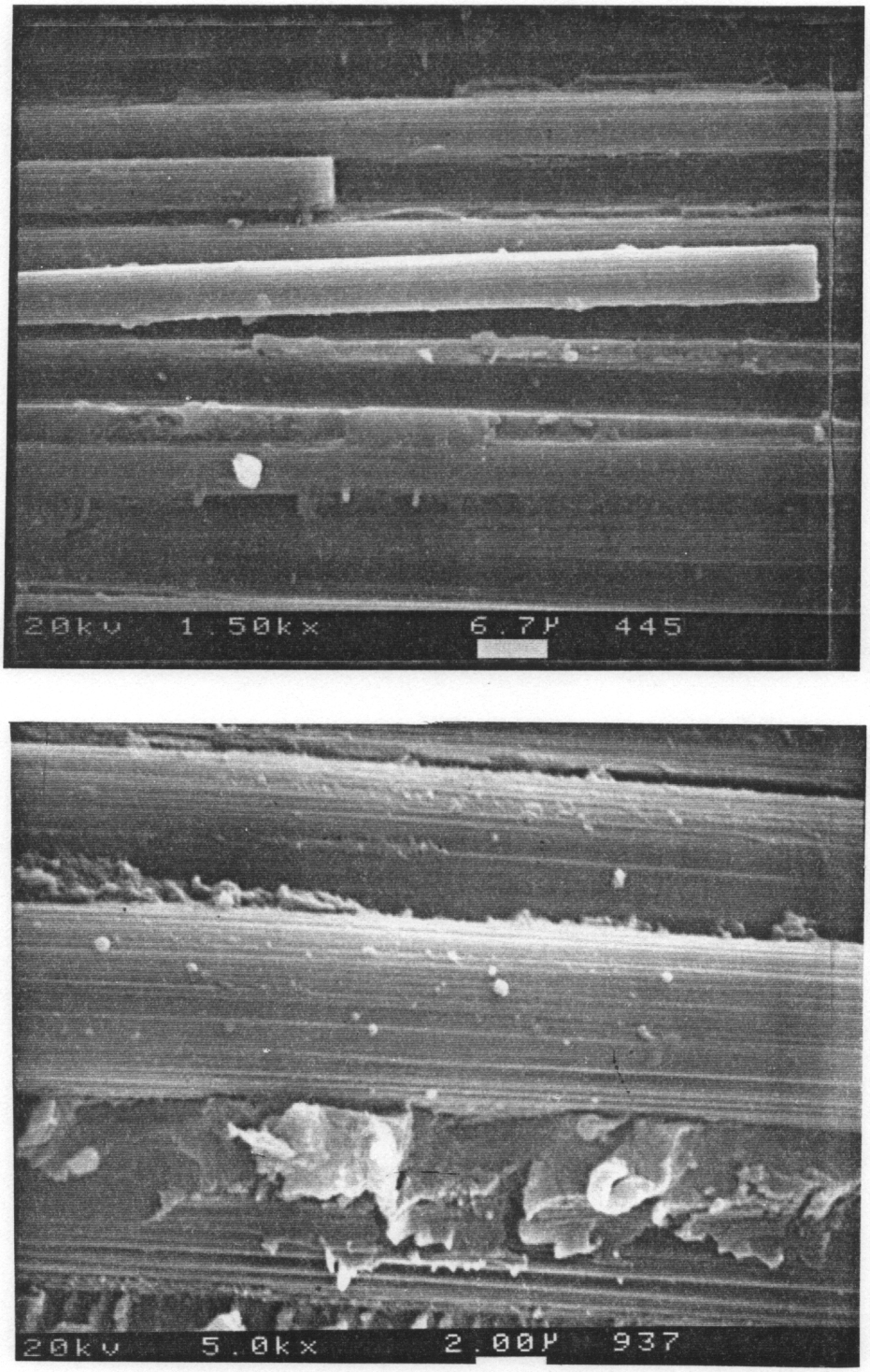

Figure 45 Scanning electron micrograph of failed 810 A laminate
Top : 85 % load level (1500 X).
Bottom : 80 % load level (5000 X).

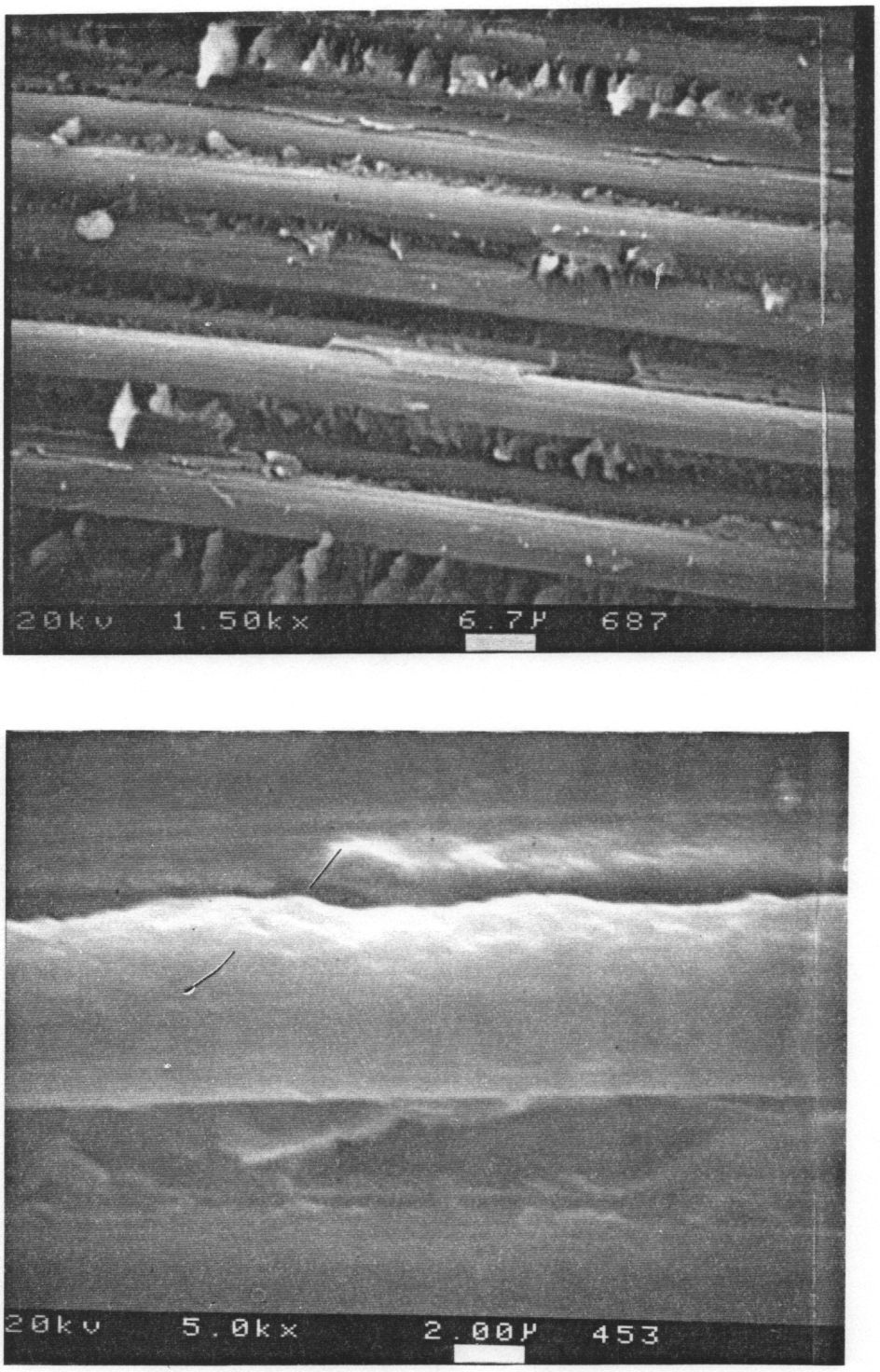

Figure 46 Scanning electron micrograph of failed 820 A laminate
Top : 90 % load level (1500 X).
Bottom : 85 % load level (5000 X).

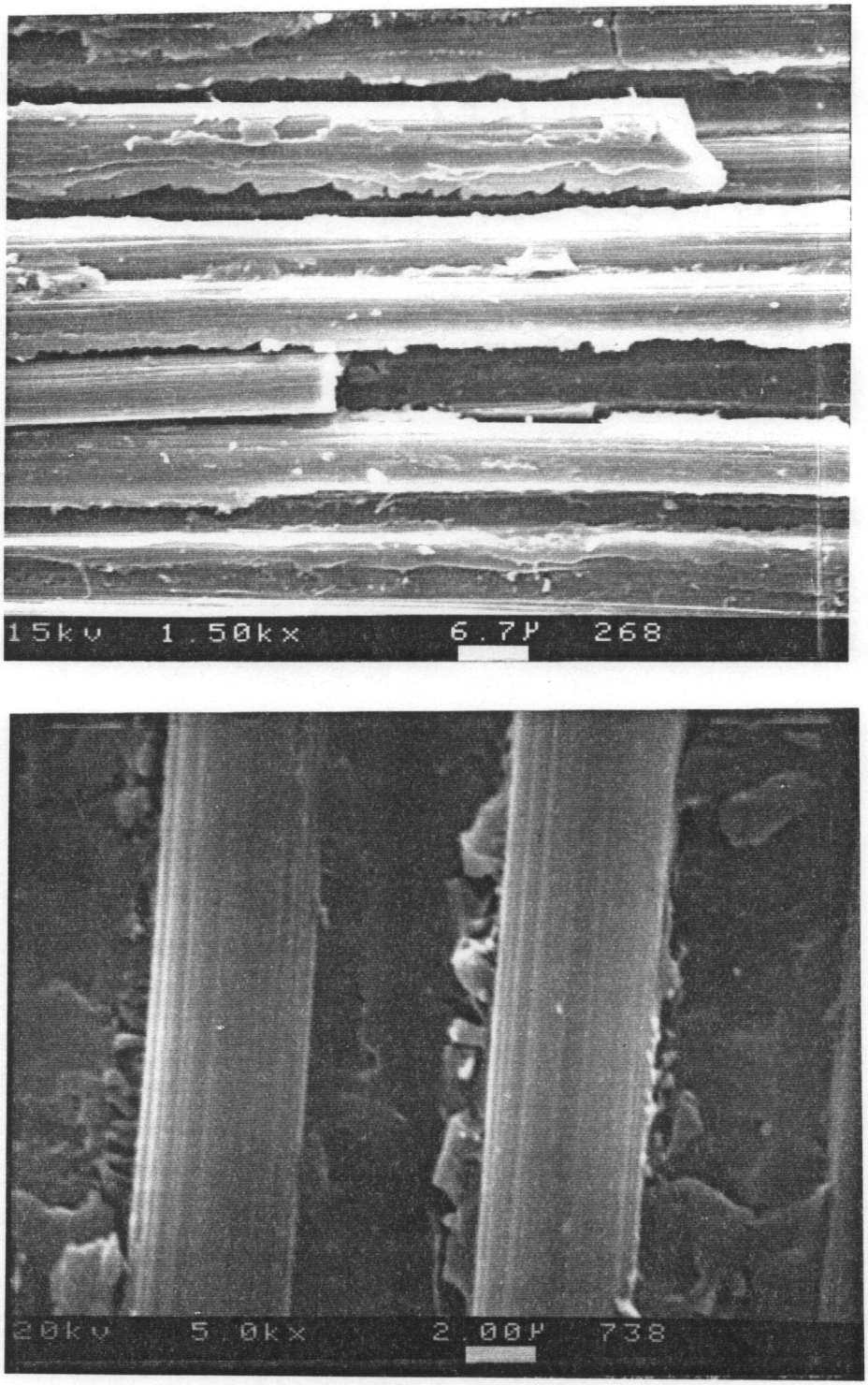

Figure 47 Scanning electron micrograph of failed 810 O laminate
Top : 85 % load level (1500 X).
Bottom : 80 % load level (5000 X).

appear to be covered by matrix/interphase material. This could be indicative of good fiber-matrix bonding. In comparison, the failure surface of 810 O laminates reveal a different morphology. This is shown in figure 47a and 47b. The fibers in the 810 O laminates subjected to fatigue loading at 85 % load level (at 5000 X magnification) reveal damage in a small region near the fibers (the interphase region). The interphase region surrounding the fiber exhibits extensive micro-damage. This leads one to believe that the longitudinal splits seen in the 810 O laminates (using x-ray radiography) is interphasial damage. This belief is further confirmed by figure 47b which shows the fractograph of the 810 O laminate subjected to fatigue loading at 80 % load level. A discontinuous layer of interphase material covers the fibers in these laminates. The figure indicates that the interphase material bonds well to the fibers, but has low strength/strain to failure. The fiber-matrix debonding initiates in the interphase region, in the 0° ply of the 810 O laminates. These results are consistent with the x-ray radiography results that revealed different longitudinal splitting characteristics in the 810 O laminates. Based on these fractographs, it is concluded that the longitudinal splits in the 810 O laminates are local interphasial debonds.

From the stiffness reduction results, damage analysis, and the appearance of the failed specimen, it is concluded that the fatigue failures of the 810 A and 820 A systems are controlled by stress concentration effects near broken fibers in the 0° ply. In the 810 O system, there is more damage in the 0° ply in the form of longitudinal splitting and local delamination. It appears that these damage modes provide an energy absorbing mechanism and reduce the local stress concentration effects near broken fibers. The final failure of the 810 O cross-ply laminate is controlled by the global strain in the 0° ply. More about these effects will be discussed in the tensile strength modelling section in chapter 9.

The damage analysis and fatigue life results presented in this section indicate clearly that the damage mechanisms and failure modes in cross-ply laminates of the three material system used in this study are vastly different. Since the same fiber and matrix were used in these material systems, the changes could be attributed to the presence of the different interphases. **One is left with no choice but to believe that changes in fiber-matrix bonding conditions effected through subtle changes in the form of varied fiber**

surface treatment levels and sizing (which constitute < 1 % of the composite), alter the damage mechanisms and failure modes of cross-ply laminates under fatigue loading. This results in fatigue lives that are different by orders of magnitude. It must however be admitted that the exact mechanism by which these changes are brought about is not fully known at the present moment.

In this section, a brief discussion is provided to explain the varied fatigue behavior (Figure 35) of the 810 A, 820 A and 810 O laminates based on the damage analysis results. It is well known that in a $(0,90_3)_s$ cross-ply laminate configuration, the final failure of the laminate is controlled by the failure of the 0° ply. The 90° ply undergoes early cracking during the first 10 % of the life, and as a result most of the load is carried by the 0° ply. Thus, in order to predict the strength and life of the laminate, the strength and life of the 0° ply needs to be estimated accurately. Recent analytical investigations [62,93] have revealed that the strength of unidirectional 0° laminate is controlled by two factors ; the stress concentration effects near broken fibers and the ineffective length. The strength reduces as the stress concentration factor increases and as the ineffective length increases. The damage analysis results indicate that the 810 O and 820 A laminates (to a lesser extent) exhibit more longitudinal splitting compared to the 810 A laminates. The effect of these splits on the stress concentration factors and ineffective length are different. The presence of longitudinal splits reduce the stress concentration effects near broken fibers and increase the ineffective length (details in the modelling chapter). This means that the presence of splits would improve strength and life of the laminate when stress concentration effects control the failure, and reduce the strength and life when ineffective length controls the final failure. It is postulated that in the material system used in this study, failure at high load levels (greater than 80 %) are controlled by stress concentration effects and at lower load levels, the ineffective length controls the failure. The S-N curves of the three material system can be explained using this hypothesis. Comparing the S-N curves of the 810 A and 810 O laminates, it could be said that at high load levels, the presence of longitudinal splits reduce the stress concentration effects in 810 O laminates. This results in longer fatigue lives in 810 O laminates, compared to the 810 A laminates, at higher load levels. At lower load levels, the distributed longitudinal

splitting results in increased ineffective length in the 810 O laminates. The lower fatigue life of 810 O laminates at the lower load level could be attributed to this. Comparing the S-N curves for the 810 A and 820 A laminates, it can be said that the 820 A laminates have longer lives at higher load levels because of the longitudinal splits and lower absolute load levels applied in these tests (due to the lower static strength of the laminates). However, as was seen in the 810 O laminates, the slope of the S-N curve of the 820 A laminate is greater than that of the 810 A laminate. This is probably due to the presence of greater number of longitudinal splits, at lower load levels, in the 820 A laminates. These longitudinal splits increase the ineffective length and reduce the strength and life of the laminate.

The results from this study could be generalized and the following conclusion could be made. The presence of longitudinal splits result in the shifting of the S-N curve of the cross-ply laminate (whose failure is controlled by 0°ply) to the right. The longitudinal splits also appear to increase the slope of the S-N curve, resulting in poor performance under low-load long-life situations.

7.3 Summary

Based on the results from tension-tension fatigue tests on cross-ply laminates of the three material system used in this study, the following observations are made. The fatigue life of cross-ply laminates are sensitive to the nature of interphase present in the material system. The cross-ply laminates with different fiber-matrix interphase exhibit varied damage mechanisms and failure modes. The 820 A laminates have greater life at all load levels used in this study. A comparison of the fatigue lives of the 810 A and 810 O laminates reveals that the 810 O laminates have longer fatigue lives at higher load levels and lower lives at lower load levels. Damage analysis results indicate that all three material system exhibit extensive transverse ply cracking at all load levels. In addition, the 810 A laminate reveals edge delamination at high load levels, very little longitudinal splitting and no local delaminations. The 820 A laminates exhibit moderate amount of longitudinal splitting and no local or edge delaminations. In contrast, the 810 O laminates exhibit extensive distributed longitudinal splitting and local delaminations at all load levels. The

stiffness reduction results also confirm the presence of greater amount of damage in the 810 O laminates. Fractographic analysis of failed specimen indicates that the longitudinal splits in 810 O laminates are interfacial debonds. Photographs of the failed specimen from the three material system show that the failure of the 810 A and 820 A laminates are controlled by stress concentration effects in the 0° ply while the failure of the 810 O laminate is controlled by the global strain to failure of the 0° ply.

8.0 CREEP CHARACTERIZATION

Numerous tests were performed to characterize the creep response of $(90)_{12}$ and $(0,90_3)_s$ laminates of the 810 A, 820 A and 810 O material system. Results from these tests are presented in this chapter. The results will be discussed in two sections. The flexural creep response of $(90)_{12}$ laminates obtained using the dynamic mechanical analyzer will be presented in the first section. The room temperature tensile creep response of the $(90)_{12}$ and $(0,90_3)_s$ laminates at various load levels will be discussed in the following section.

8.1 Flexural Creep Response (Using DMA)

Short term (10 minute) flexural creep tests were performed at various temperatures on $(90)_{12}$ laminates using a DuPont-983 DMA. Tests were conducted at 10° C temperature intervals between 110 ° C and 150° C. Since the glass transition temperature (T_g) of the matrix material is around 185° C, tests were conducted at 5°C intervals above 150°C. The variation of creep compliance of the 810 A laminate at various temperatures is displayed as figure 48. The figure indicates that at lower temperatures, there is very little change in creep compliance . However, at temperatures close to the T_g of the matrix, appreciable variation in creep compliance is observed. It is also noted that the initial creep compliance increases with temperature. Creep compliance curves were obtained for the 810 O and 820 A laminates also, using the 10 minute creep test. The data obtained from these tests were then used to generate master curves for these material systems. The Time Temperature Superposition Principle (TTSP) described in reference [64] was used to shift these curves along the horizontal and vertical axes to obtain the master curves. The master curves for the 810 A, 820 A and 810 O laminates at a base temperature of 110° C are plotted in figure 49. The figure indicates that the initial compliance of the three material system are different. The 820 A laminate has the highest compliance, followed by the 810 O laminate. The 810 A laminate has the lowest initial compliance at 110° C. It must be mentioned here that these trends are qualitatively similar to the room temperature tensile test results discussed in chapter 5. The difference in the compliance values

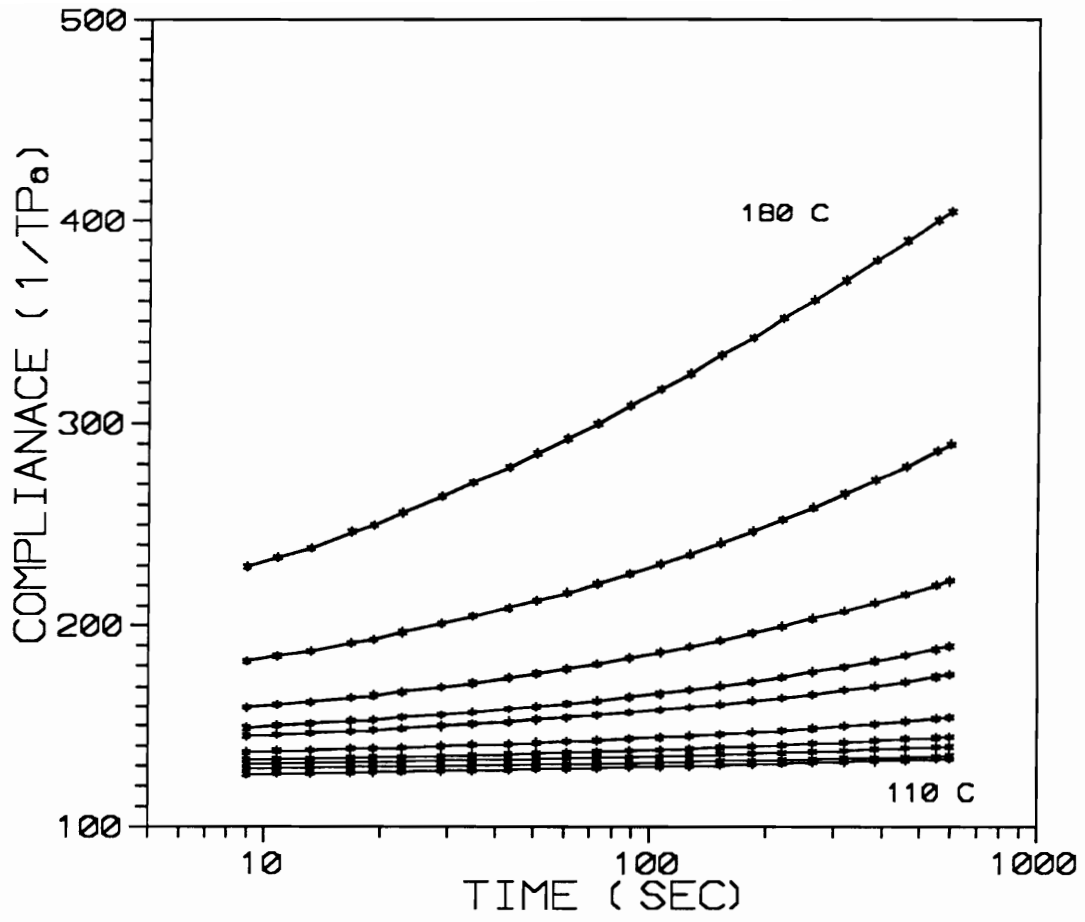

Figure 48 Creep compliance curves for the 810 A $(90)_{12}$ laminate at various temperatures.

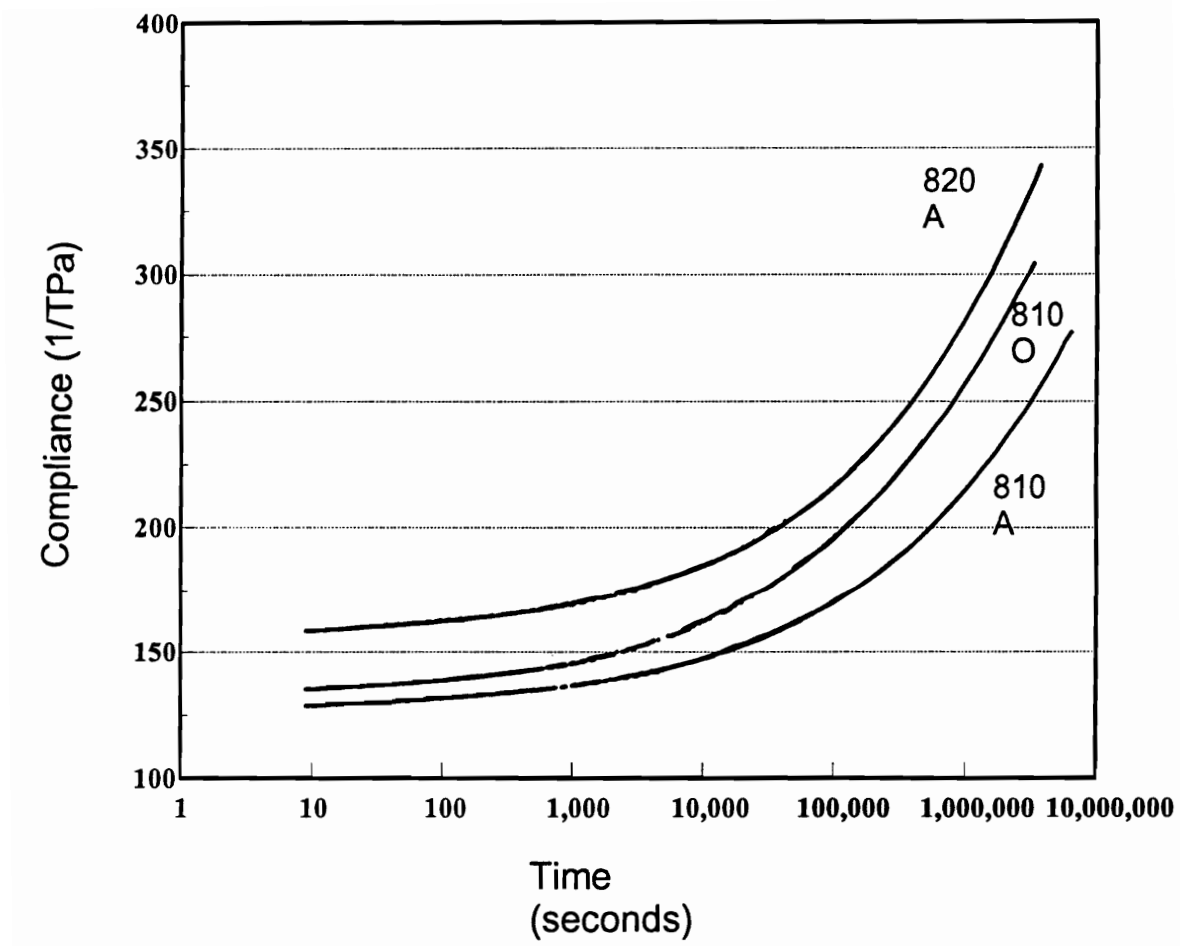

Figure 49 Comparison of creep compliance master curves at 110° C of 810 A, 820 A and 810 O $(90)_{12}$ laminates.

between the three material system is however different. This could be due to a combination of the following reasons. The tensile creep response was measured at room temperature, while the flexural creep response master curve was obtained for an elevated temperature of 110 ° C. Also, the material system may exhibit inherently different response under tensile and flexural loading. Finally, it must be mentioned that the software used in the DMA to calculate the flexural compliance does not consider the orthotropic nature of the composite material.

The horizontal shift factors for the three material systems obtained by TTSP is plotted against the reciprocal of the absolute temperature in figure 50. All three material system exhibit a biliniear behavior. The slope of the curve is greater at temperatures near the glass transition temperature. The variation of shift factor with temperature is represented using an Arrhenius type equation of the following form

$$\log(a_T) = -\frac{H_a}{2.303R}\left(\frac{1}{T}-\frac{1}{T_o}\right)$$

where H_a is the activation energy, T_o is the reference temperature (110°C). The Arrhenius equation is usually valid at temperatures below the T_g. The activation energy is obtained by fitting a straight line through the $\log(a_T)$ vs (1/T) plot shown in figure 50. Since the data indicates a bilinear behavior, the data for each material system are fitted with two straight lines. It is observed that the change in slope occurs for the 810 A, 820 A and 810 O system at 145, 153, 150° C respectively. These temperatures correspond to the beginning of transition from the glassy state to rubbery state. Since a bilinear behavior is observed in figure 50, two activation energy values are obtained for each material system. These values are shown in table XI. Notice that the activation energy value for the three material system at higher temperatures (near the T_g) is higher. Similar behavior has been reported in some earlier studies [12,95]. This behavior has been attributed to the different molecular motions associated with the transitions at the lower temperatures and at temperatures close to the T_g.

In order to verify that there is no damage induced by temperature or mechanical loads during

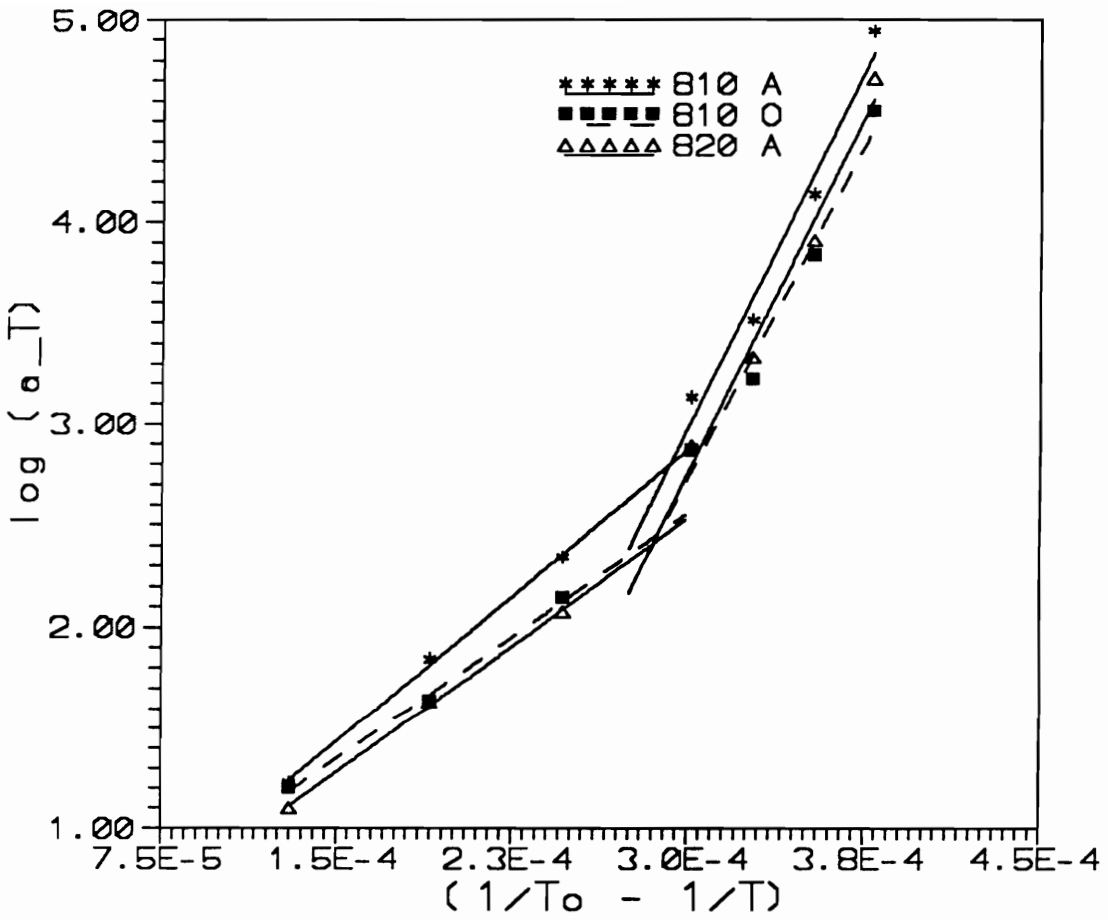

Figure 50 Variation of horizontal shift factor with temperature for the three material system.

Table XI Activation energy values for 810 A, 820 A and 810 O system obtained from figure 50.

	Activation Energy (H_a) 110°C < T < 145°C	Activation Energy (H_a) 145°C < T < 180°C
810 A	9579	23558
810 O	8078	21996
820 A	8364	23471

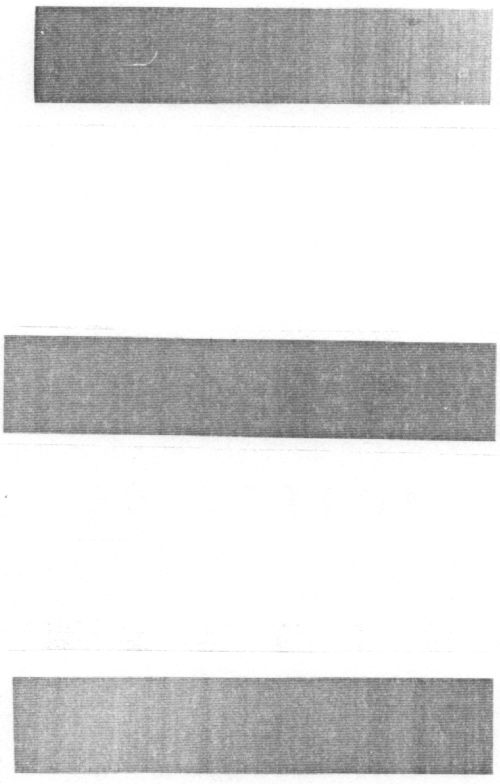

Figure 51 X-ray radiograph of $(90)_{12}$ specimen after short term DMA creep tests; Top : 810 A; Middle : 820 A; Bottom : 810 O.

the DMA test, specimen from each of the three material system was x-rayed. Figure 51 shows the x-ray radiograph of the 810 A, 820 A and 810 O specimen. The figure does not reveal any damage in the form of transverse matrix cracking or fiber-matrix debonding.

8.2 Tensile Creep Response

8.2.1 Room temperature tensile creep response of $(90)_{12}$ laminates

The room temperature tensile creep response of 810 A $(90)_{12}$ laminates at three different load levels is displayed in figure 52. The variation of normalized creep compliance at three different load levels is plotted against time in this figure. The figure indicates that the 810 A laminates exhibit limited time dependent response. The maximum increase in compliance after 15,000 seconds is only about 5 %. It is also noticed that in the range of loads tested, the creep response of the 810 A laminates is independent of load level. Thus, it could be said that the material system exhibits linear viscoelastic creep response in the range of loads tested. Since the creep response is independent of load in this load range, a power law curve is fitted through all the data points in figure 52. The solid line in the figure represents a power law best fit curve for the 810 A system. The variation of normalized creep compliance of the 820 A $(90)_{12}$ laminates at two load levels are displayed in figure 53. The figure indicates that most of the creep compliance change occurs initially. As in the 810 A laminates, the creep compliance appears to be independent of the applied load in the load range tested. The maximum creep compliance change after 15,000 seconds is around 5 %. Recall that a similar response was observed in the 810 A laminates. The solid line in the figure represents a power law best fit curve through all the data points (obtained at the two different load levels). Figures 52 and 53 indicate that the creep response of $(90)_{12}$ laminates of the 810 A and 820 A system are almost identical. The change of surface treatment level from 100 % to 200 % does not appear to affect the room temperature creep response of the $(90)_{12}$ laminates.

The creep response of the 810 O 90_{12} laminates are shown in figure 54. In sharp contrast to the creep response of the 810 A and 820 A system, the 810 O laminates exhibit greater creep response. The

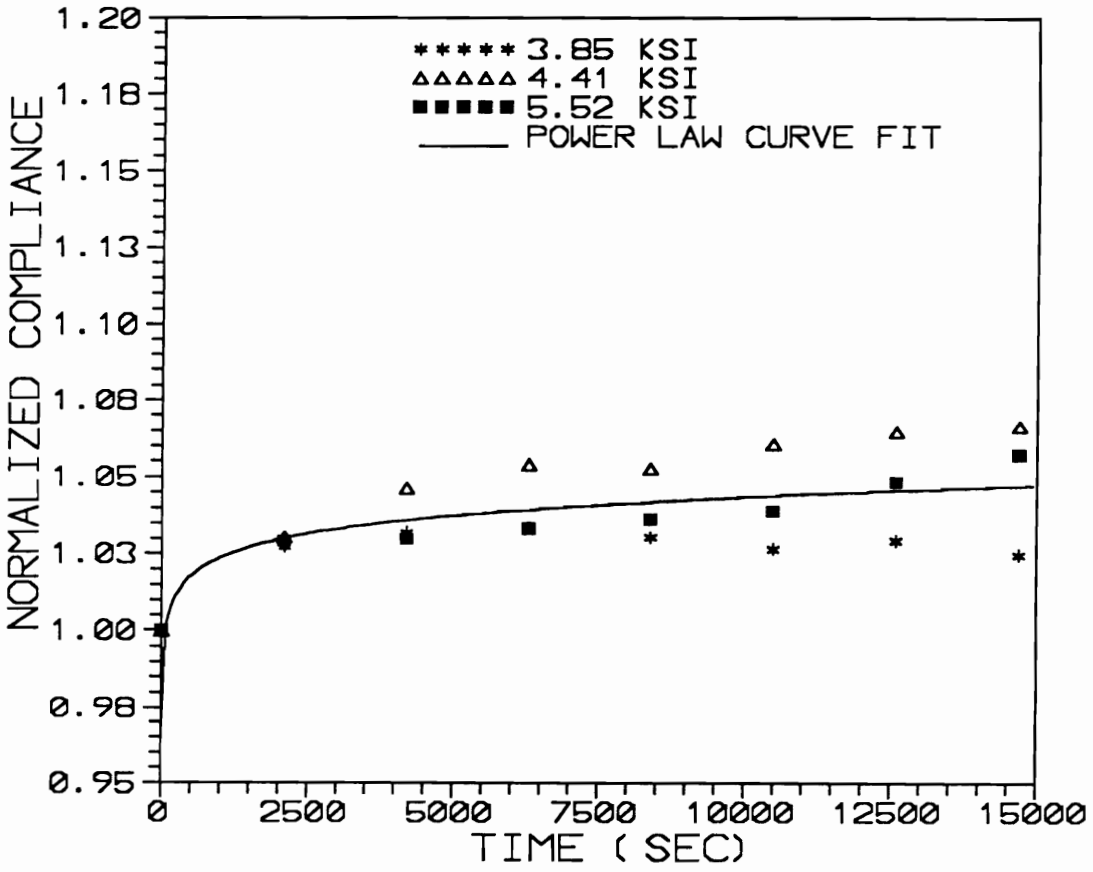

Figure 52 Variation of room temperature tensile creep compliance of $(90)_{12}$ 810 A laminates at various load levels.

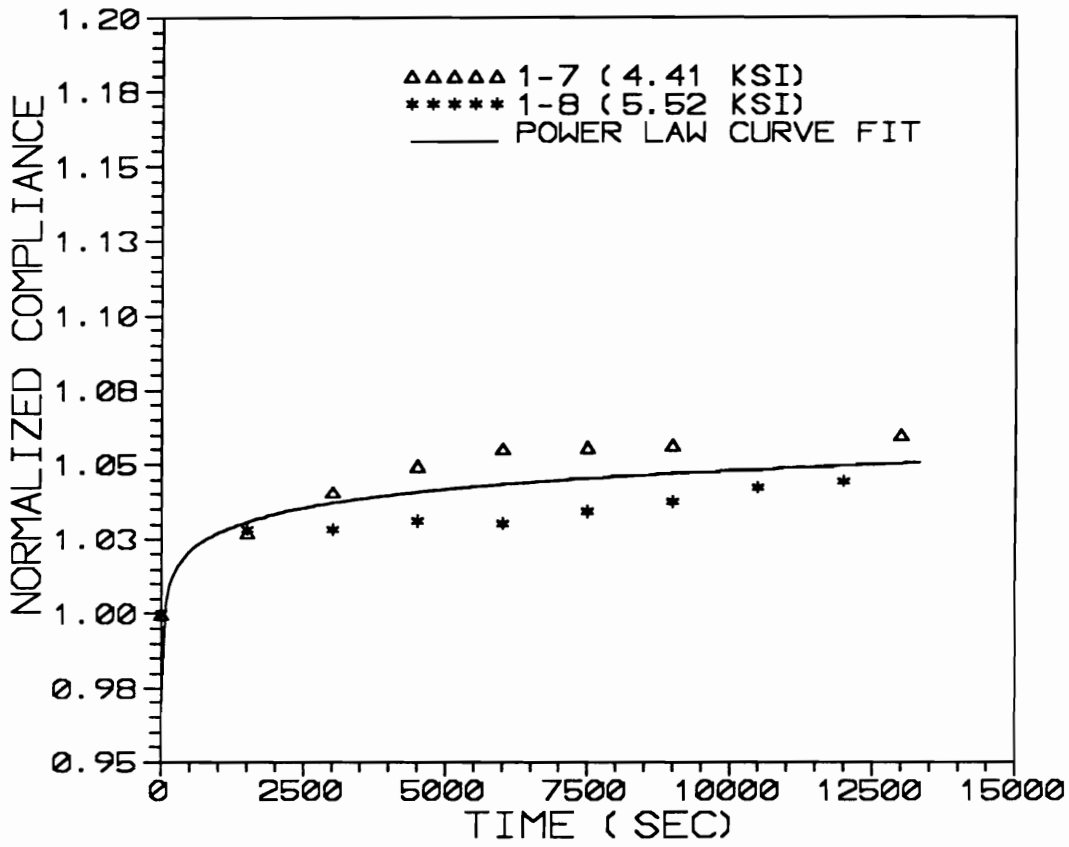

Figure 53 Variation of room temperature tensile creep compliance of $(90)_{12}$ 820 A laminates at various load levels.

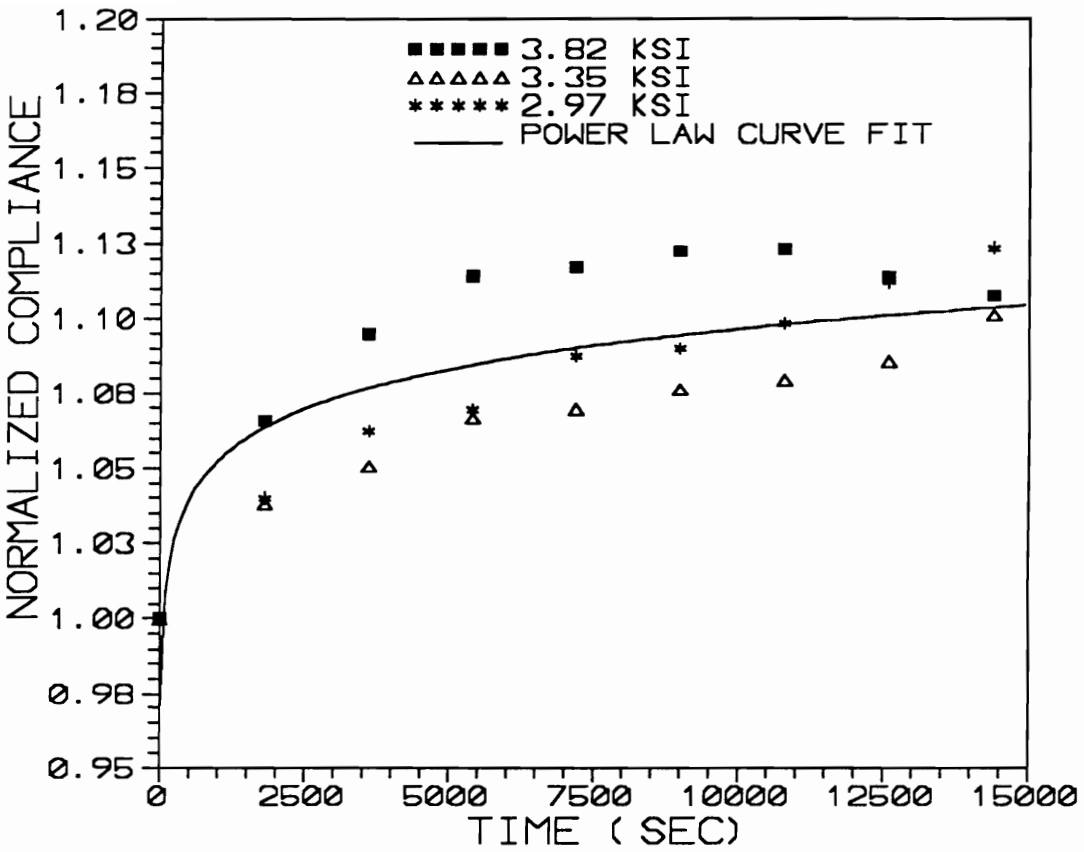

Figure 54 Variation of room temperature tensile creep compliance of $(90)_{12}$ 810 O laminates at various load levels.

maximum creep compliance change after 15,000 seconds is about 13 %. This is significantly greater than the 5 % change observed in the other two material system. The data also indicate slight stress dependence in the load range used in this study. However, for comparison purpose, a power law best fit curve is drawn through all the data points in figure 54. The solid line in the figure represents the best fit curve. The constant and exponent obtained by fitting the data for 810 A, 820 A and 810 O laminates with a power law curve are displayed in Table XII. Comparing the value of exponent obtained for the three material system, it can be concluded that the 810 O system exhibits greater creep response. This is not very surprising considering that the 810 O system contains a thermoplastic sizing material. It is well known that the thermoplastic materials exhibit greater creep response. Even though the sizing forms less than 1 % of the material, the creep response of the material system is dramatically changed. This indicates that the fiber-matrix interphase plays a significant role in the time dependent response of composite materials.

In order to verify the presence of damage in the form of matrix cracks and/or fiber-matrix debonding, one laminate from each material system was x-rayed. Figure 55 shows the x-ray radiograph of the 810 A, 820 A and 810 O laminates after 15,000 seconds loading at 5, 4 and 5 ksi stress level respectively. These represent the highest load levels used for each material system. The figure does not reveal any damage in the form of matrix cracks or fiber/matrix debonding in either of the three material system. It is thus concluded that the changes in compliance displayed in figures 52 through 54 represent changes in creep compliance.

It is interesting to compare the room temperature tensile creep response of the three material system with the flexural creep response obtained using short term DMA tests. Both tests indicate that the 810 O system exhibits greater creep response. The 810 A and 820 A system exhibit similar DMA flexural creep response but the changes in creep compliance are lower in these materials when compared to that seen in the 810 O system. The initial flexural creep compliance of the 810 O laminates is greater, and the laminates undergo greater changes in creep compliance at any given instant in time. These results are consistent with the room temperature tensile creep response. It must however be mentioned here that even

Table XII Constants and exponents for the 810 A, 820 A and 810 O laminates obtained from figures 52-54.

	Constant	Exponent
810 A	0.966	0.0084
810 O	0.912	0.0199
820 A	0.967	0.0086

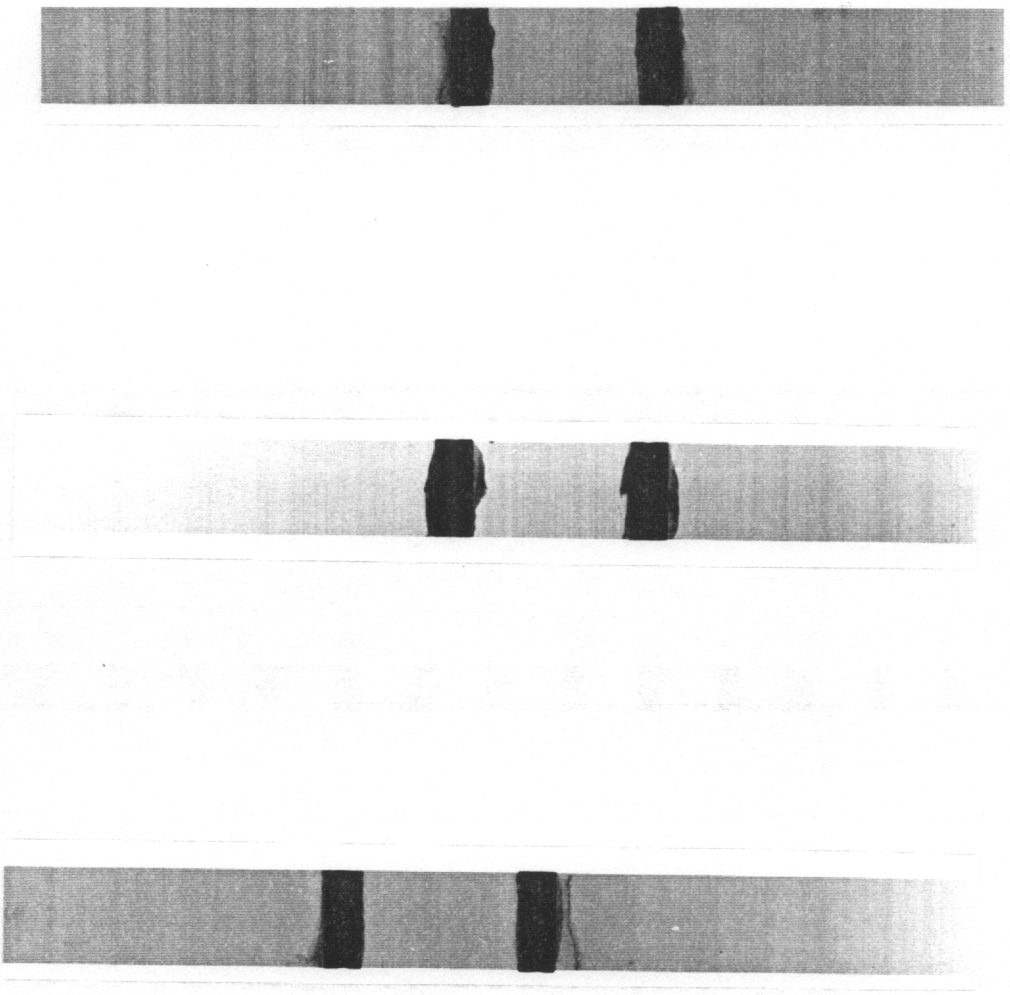

Figure 55 X-ray radiographs of $(90)_{12}$ laminates after tensile creep tests;
Top : 810 A; Middle : 820 A; Bottom : 810 O.

though the qualitative trends are similar, the amount of compliance changes observed under tensile and flexural creep loading are different. Both the tensile creep test and DMA creep tests indicate that the presence of PVP (thermoplastic) sizing results in greater creep, even when the amount of sizing material used in the composite material is very small. The difference in the amount of compliance changes observed during tensile and flexural creep tests could be due to reasons discussed in the previous section.

8.2.2 Room Temperature tensile creep response of cross-ply laminates

The normalized creep compliance of the 90° ply in the 810 A cross-ply laminate at 50 ksi load level is shown in figure 56. The creep compliance of the 90° ply was obtained by measuring the compliance of the cross-ply laminate and estimating the change in compliance of the 90° ply using classical lamination theory. In obtaining this curve, it was assumed that the 0° ply behaves as a perfectly elastic material, and the compliance change in the cross-ply laminate is due to creep and damage in the 90° ply. The solid line in the figure indicates the variation in creep compliance of the 90° ply obtained from the $(90)_{12}$ laminate tests discussed in the previous section. The figure indicates that the constrained 90° ply undergoes greater compliance changes compared to the unconstrained 90° laminates. This is somewhat surprising because the constrained ply is expected to undergo less creep. However, it must be borne in mind that the constrained 90° ply could also undergo damage, while it was established that the unconstrained 90° laminates did not undergo any damage. Also interesting is the increase in compliance observed after about 12,000 seconds. This could be indicative of damage in the form of matrix cracking in the 90° ply of the cross-ply laminate. In order to verify the presence of damage in the cross-ply laminates, x-ray radiography was performed on this laminate. The damage analysis results of the three material system will be discussed later in this section.

The variation of normalized tensile creep compliance of the 90° ply in the 820 A cross-ply laminate at 50 ksi load level is shown in figure 57. The variation of compliance of the unconstrained 90° laminate is shown in the figure as a solid line. The figure indicates that greater compliance variation occurs

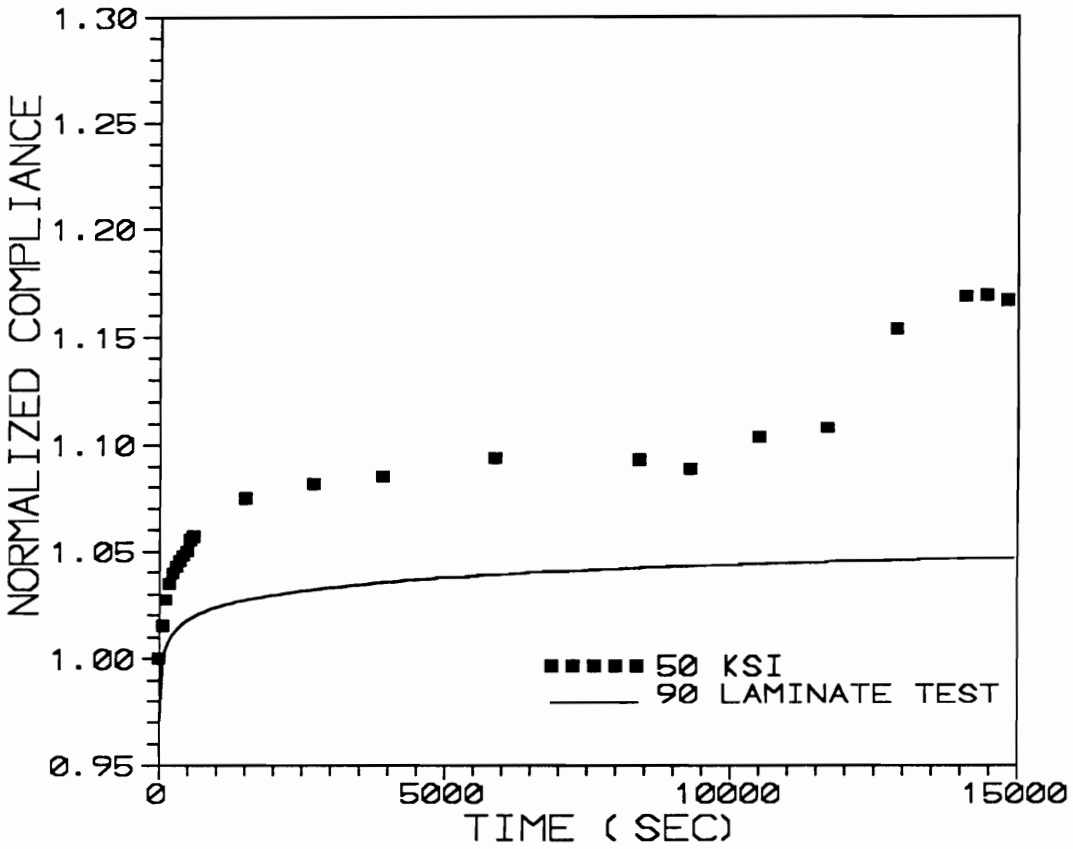

Figure 56 Variation of creep compliance in the 90° ply of the 810 A cross-ply laminate (50 ksi load).

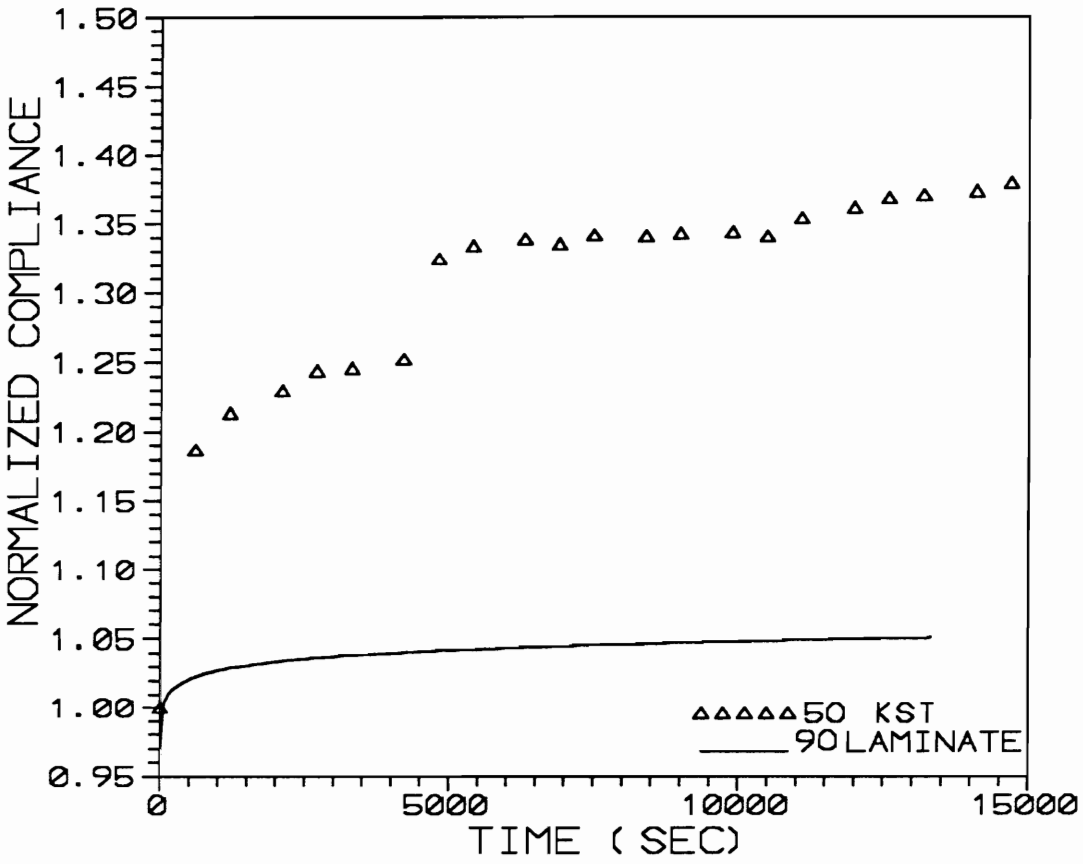

Figure 57 Variation of creep compliance in the 90° ply of the 820 A cross-ply laminate (50 ksi load level).

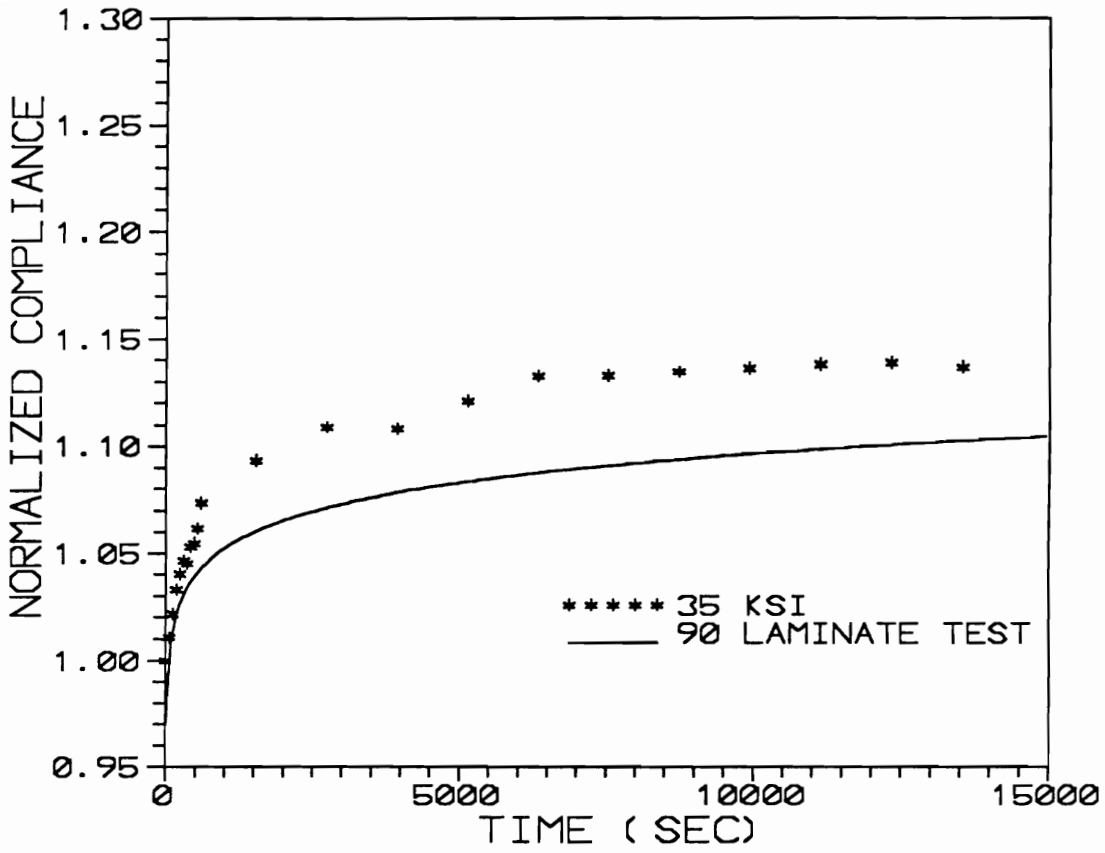

Figure 58 Variation of creep compliance in the 90° ply of the 810 O cross-ply laminate (35 ksi load level).

in the constrained 90° ply. Again, this could be due to damage in the form of matrix cracks in the 90° ply of the cross-ply laminate. It is interesting to note that the deviation of the compliance curve of the constrained 90° ply from that of the unconstrained 90° ply is the greatest in the 820 A system.

The room temperature creep compliance of the unconstrained and constrained 90° ply of the 810 O system at 35 ksi load level are plotted in figure 58. The 90° plies in the 810 O cross-ply laminate exhibits greater compliance changes compared to the unconstrained 90° laminate. It is interesting to note that the contribution of damage to the compliance change in the cross-ply laminate is the lowest in the 810 O laminate. This is somewhat surprising, considering that the 810 O laminates exhibited greater damage under quasi-static and fatigue loading. But it must be borne in mind that the 810 O laminate was subjected to a lower load compared to the 810 A and 820 A laminates.

In order to verify if there is any damage in the constrained 90° ply of the cross-ply laminate, specimen from all three material system were x-rayed. Figure 59 shows the x-ray radiographs of these laminates after 15,000 seconds. The figure clearly shows damage in all three laminates in the form of transverse matrix cracks in the 90° plies. This explains the greater compliance changes in the constrained 90° plies of the three material system. It is well known that the presence of transverse matrix cracks reduces the stiffness of the laminate, and hence results in increased compliances. It is interesting to note that in the 810 O laminate, there are no transverse cracks extending throughout the width of the laminate. However, there are numerous small transverse cracks in the 90° ply that do not extend through the width of the laminate. The 810 O laminate also reveals a few longitudinal splits in the 0° ply. This is not very surprising considering that the 810 O system exhibited longitudinal splitting under quasi-static and fatigue loading. In comparison, the 810 A laminate has two transverse cracks extending through the width of the laminate, in the gage section. There are no longitudinal splits in the 0° ply of the 810 A laminate. The x-ray radiograph of the 820 A laminate reveals two transverse cracks extending through the width of the laminate. A few longitudinal splits are also seen in the 0° ply of the cross-ply laminate. While comparing the damage in the three laminates displayed in figure 59, it must be borne in mind that the 810 A and 820

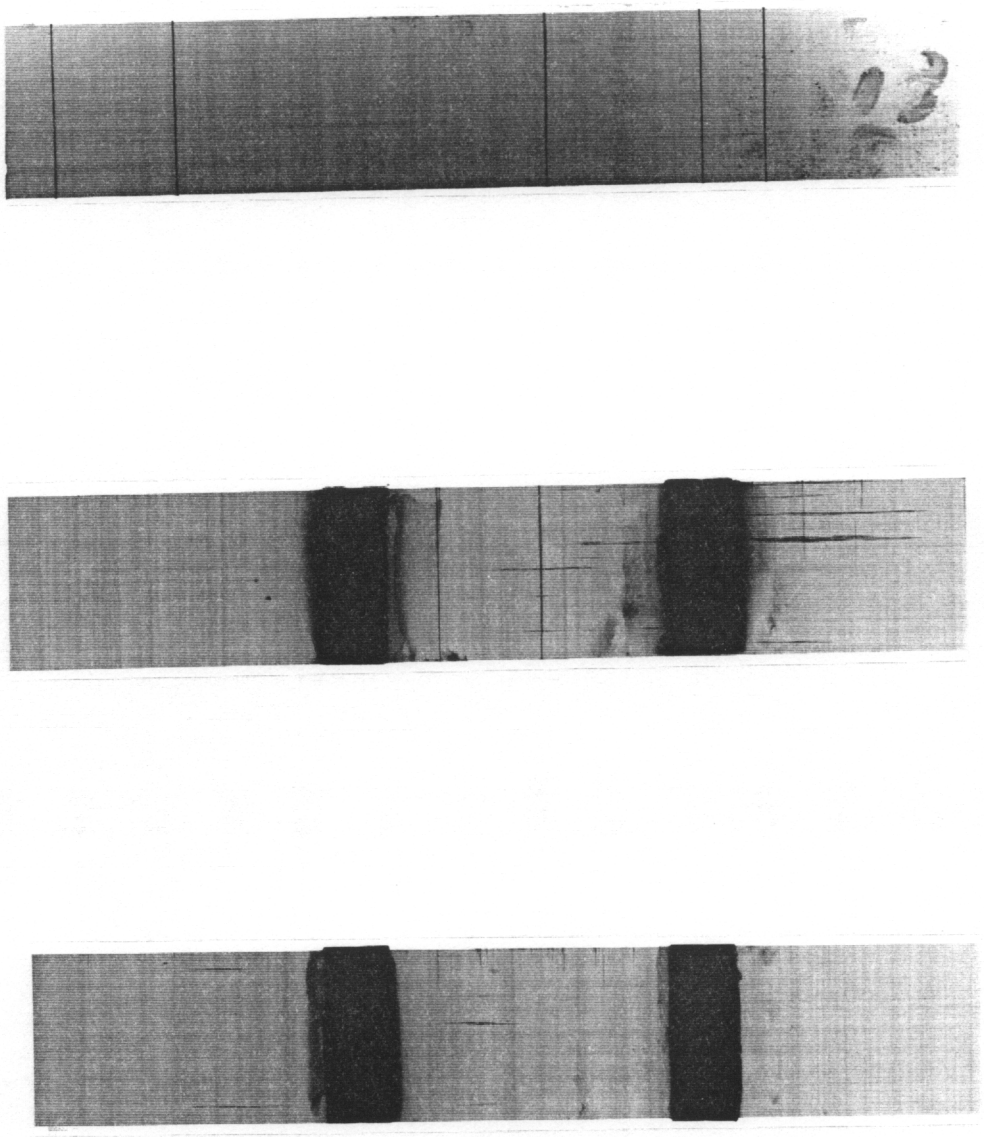

Figure 59 X-ray radiograph of cross-ply laminate after 15000 seconds;
Top : 810 A; Middle : 820 A; Bottom : 810 O.

A laminates were subjected to a higher load compared to the 810 O laminate. This could explain the lesser amount of damage seen in the x-ray radiograph of the 810 O laminate. It is however surprising to see longitudinal splits in the 820 A laminate. Recall that the 820 A laminates did not exhibit any longitudinal splitting during quasi-static loading. However, the 820 A laminates did reveal extensive longitudinal splitting under fatigue loading. Even though the 820 A cross-ply laminates did not exhibit longitudinal splitting under quasi-static loading, numerous longitudinal splits in the 0° ply of the cross-ply laminates are seen under fatigue and creep loading. In contrast, the 810 A laminates exhibit no splitting under quasi-static and creep loading. A few longitudinal splits are observed at high loads under fatigue loading. Since the only difference in the three material system is the interphase, the different damage characteristics under quasi-static, fatigue and creep loading can be attributed to the interphase.

The compliance variation curves (figure 52-54) indicate that the compliance change due to damage is greatest in the 820 A laminate, and lowest in the 810 O laminate. This is consistent with the damage revealed by x-ray radiographs shown in figure 59. The 820 A laminate exhibits more damage than the other two laminates, while the damage is the least in the 810 O laminate.

8.3 Summary

The short term DMA creep results indicate that the initial compliance of the $(90)_{12}$ laminates of the 820 A system is greater than that of the other two material system. The 810 A $(90)_{12}$ laminates possess the lowest initial creep compilance. The 810 O laminates exhibit significantly greater amounts of changes in flexural creep compliance compared to the other two material system. The room temperature tensile creep test on $(90)_{12}$ laminates indicates a similar response. The room temperature tensile creep tests on cross-ply laminates indicate that the 90° plies in the laminate exhibits creep deformation and damage in the form of transverse matrix cracks and longitudinal splits in the 0° ply.

9.0 STATIC STRENGTH AND FATIGUE LIFE PREDICTION MODELS

In order to predict the influence of fiber-matrix interphase on the long term behavior of cross-ply laminates, a few strength and damage prediction models were developed in this study. These include models that consider the effect of an interphase at a micro-level and at a ply level. These models were used in a cumulative damage scheme to predict the fatigue lives of cross-ply laminates. The cumulative damage scheme is based on the philosophy used in the 'Critical Element Model' proposed by Reifsnider and Stinchcomb [58]. The damage progression in a cross-ply laminate has been studied extensively by numerous researchers [84-87]. It is well established that the main damage mechanisms in this laminate configuration include the transverse matrix cracking, longitudinal splitting, and delaminations (both local and free edge). The final failure of this laminate is controlled by the tensile failure of the 0° ply in the laminate. It is also well established in the literature that the failure of the 0° ply is essentially controlled by the accumulation of fiber fractures in the ply [93,94,96]. Hence, in order to predict the strength and life of cross-ply laminates, the accumulation of matrix damage (transverse, longitudinal cracks and delamination) as well as the accumulation of fiber fractures need to be predicted accurately. In this study, a model that includes the effect of fiber-matrix interphase, has been developed, to predict the tensile strength of the unidirectional laminates. In order to predict the accumulation of transverse matrix cracks, the 1-D shear lag model proposed by Reifsnider [97] has been modified to include the effects of an interphase. Results from these two models have been used in a cumulative damage scheme to predict the fatigue life of cross-ply laminates. These modelling efforts will be discussed in three sections. In the first section, the tensile strength prediction model is described and some salient features of this model are highlighted. In the next section, the shear lag model used to predict the progressive transverse cracking in cross-ply laminates is described. Finally, these models are used in a cumulative damage scheme to predict the damage evolution and life of cross-ply laminates under fatigue loading. The damage and fatigue life predictions are compared with experimental values that are reported in chapter 7.

9.1 Unidirectional Tensile Strength Prediction Model

The tensile failure of unidirectional composites has been studied by numerous researchers [98-103] in the past two decades. It is well recognized that the tensile failure of unidirectional laminates is best described by a cumulative damage process. The final failure results from the accumulation of damage in the form of fiber fractures in the unidirectional laminate. The properties of the fiber and matrix such as strength and stiffness, have been shown to influence the tensile strength of the unidirectional laminate significantly. Some recent experimental [12,31,36] and analytical efforts [93,94,104,105] have, however, brought out the importance of the role of the fiber-matrix bonding (also referred to as the interface/interphase) in determining the tensile failure process. Before going into the details of the limitations of the tensile strength prediction models available currently, it will be appropriate to trace the history of the evolution of the various tensile strength prediction schemes.

Recognizing that the tensile strength of a single fiber is not uniform, Weibull [106] used the weakest link theory to predict the fracture of a single fiber. The fracture of a bundle of fibers, referred to as the bundle strength, was then worked out by Coleman [107] and Rosen [108]. In calculating the bundle strength, Rosen [108] assumed that individual fibers in the bundle fail only once. The statistical distribution of strength of the fibers determines the failure of each fiber. The failure of the bundle of fibers is due to the accumulation of fiber fractures. Hahn [109] has presented a simple argument based on these assumptions that lead to Rosen's bundle strength equation

$$X_b = \frac{E_f \, \varepsilon_o}{(L \, \alpha \, e)^{(1/\alpha)}} \tag{1}$$

where X_b is the bundle strength, E_f is the tensile modulus of the fiber, L is a characteristic length, α and ε_o are the shape factor and location parameter of the weibull strength distribution of the fiber, and e is the Napierian logarithm. Hence, the bundle strength of the fibers is a function of the Weibull parameters.

The failure of fiber bundles in the presence of matrix material was first tackled by Zweben and

Rosen [110]. They assumed that the matrix material does not carry any axial load in the composite material, and all the load is carried by the fibers. However, near fiber breaks, the matrix material serves to transfer the load to the adjacent fiber by a shear transfer mechanism. The length over which this stress transfer takes place is known as the 'ineffective length'. Based on these assumptions, they used the classical shear lag model to show that the ineffective length is approximated by the following formula

$$\delta = \frac{d_f}{2}\left[\frac{1}{2}\left(\frac{1-v_f^{1/2}}{v_f^{1/2}}\right)\frac{E_f}{G_m}\right]^{1/2} \ln\left(\frac{1}{1-\phi}\right) \qquad (2)$$

where δ is the ineffective length, d_f is the diameter of the fiber, v_f is the fiber volume fraction, E_f is the fiber modulus, G_m is the matrix shear modulus and ϕ is an efficiency parameter normally chosen to be 0.99. Using the ineffective length calculated above in the rule of mixtures, the tensile strength of the composite is estimated as

$$X_c = v_f\, X_b(\delta) + v_m\, X_m(\varepsilon_f) \qquad (3)$$

where v_f and v_m are the volume fractions of the fiber and matrix phases, X_b is the bundle strength calculated using $L=\delta$, and X_m is the stress in the matrix when the strain in the fiber is ε_o. It must be pointed out that this analysis assumes perfect bonding between the fiber and the matrix, and that the matrix behaves in a perfectly elastic manner. Even though the analysis shows that the stresses in the fibers adjacent to the broken fiber are greater, the strength prediction does not explicitly consider the effects of this stress concentration.

Batdorf [111,112] argued that the stress concentrations in the adjacent fibers would result in local accumulation of fiber fractures and this would lead to the final failure of the composite. He considered that the stresses in the adjacent fibers vary linearly from $c_i\sigma$ to σ, where c_i is the stress concentration in the adjacent fiber. Based on this assumption, he calculated the probability of a single fiber fracture (called a singlet) becoming a doublet, and so on. He showed that as the applied external load increases, fiber

fractures accumulate resulting in the formation of "i-plets". He was able to demonstrate that the accumulation of a critical number of fiber fractures ("i-plets") leads to an instability (i.e.) the load required to form the (i+1)-plet is lower than the load required to form the i-plet. This signifies catastrophic failure. The load level at which this instability occurs was considered to be the failure strength of the laminate. The salient features of this approach are that it considers the effect of stress concentrations near broken fibers and that the final failure of the composite is a result of the accumulation of fiber fractures that are estimated from the stress concentration effects. In this analysis, perfect fiber-matrix bonding was assumed and the matrix was assumed to behave as a perfectly elastic material.

Based on these models, it is clear that the tensile strength of the unidirectional laminate is dependent on the ineffective length and the stress concentration effects near fiber fractures. Recently, Reifsnider et al. [93,94] realized that the assumption of a perfectly elastic matrix may not reflect the physics of the problem accurately. The high shear stresses in the matrix material near broken fibers could lead to local matrix plasticity and/or fiber matrix debonding. They also observed that both the ineffective length and stress concentration factors could vary as a function of the number of fiber fractures. Based on this, they constructed a model that considers elasto-plastic matrix deformation near fiber fractures. They estimated the ineffective length and stress concentration factors using shear lag analysis and used this in Batdorf's model to predict the tensile strength. This model shows that when the fiber-matrix bond strength is low, debonding occurs. Under these conditions, the failure of the laminate is controlled by the ineffective length. However, when the fiber-matrix bond strength is high, elastic failure (controlled by stress concentration effects near broken fibers) is observed. In the elastic failure regime, higher bond/yield strength results in greater stress concentrations, leading to reduced strength. When the failure is accompanied by debonding/yielding, higher bond/yield strength reduces the ineffective length and hence increases the tensile strength. **This analysis clearly indicates that, generally speaking, when elastic failure occurs, the tensile strength reduces with increasing fiber-matrix bond strength values. However, when interfacial debonding occurs in the material, the tensile strength increases with increasing interfacial strength**

values. The model predicts the existence of an optimum interfacial strength value for which the tensile strength is maximum.

Using this scheme, the authors were able to predict a maximum of 7-8 % changes in tensile strength for graphite/epoxy laminates. Recent experimental efforts [12,31,36], however, have shown that by changing fiber surface treatment and sizing in graphite/epoxy laminates, 40-50 % changes in tensile strength could be obtained. However, these experimental results must be interpreted with some degree of caution. Higher levels of surface treatment are known to remove weak outer carbon fiber layers and improve fiber-matrix bonding. But, during this process, the fiber strength could also be degraded significantly. This could result in lowered tensile strength at higher surface treatment levels. However, in the authors opinion, the model described in reference [93] captures the qualitative trends reported in references [12,31,36], but does not predict the actual changes in strengths observed experimentally. This could be due to one or a combination of the following reasons. This model considers perfect bonding between fiber and matrix prior to interfacial debonding. There is some experimental evidence that shows that this may not be true. The longitudinal stiffness of the unidirectional laminate calculated assuming perfect bonding (using the rule of mixtures) appears to over predict the stiffness values in laminates where poor fiber-matrix bonding is observed. In their study with AU4, AS4 and AS4C fibers in Epon 828 matrix, Madhukar and Drzal [29] have observed over 10 % increase in longitudinal modulus going from an untreated AU4 system to a surface treated AS4 system. They have also reported a 5 % increase in tensile modulus in the AS4C laminates compared to the AS4 laminates. Similarly, Ivens et al [38] have reported upto 20 % increase in longitudinal modulus of $(0_2,90_2)_s$ laminates going from an untreated system to a 100 % surface treated system. Since the transverse modulus of a unidirectional graphite/epoxy composite is almost 20 time lower than its longitudinal modulus, it can be easily shown that the contribution of the 90° ply to the overall stiffness of the cross-ply laminate used in their study is less than 5 %. This being the case, the 20 % stiffness change between the untreated and 100 % surface treated system must be a direct consequence of stiffness changes in 0° ply. Ivens et al have used the argument of unbonded fibers proposed

by Gresczuk [113] to explain this behavior. They claim that the reduction in longitudinal stiffness could be due to a certain volume fraction of fibers not being bonded to the matrix material. In the present study, 16 % reduction in the longitudinal modulus of unidirectional laminates were observed going from a Bisphenol-A sized fiber to a PVP sized fiber system. These and numerous other investigations indicate that the longitudinal modulus of unidirectional laminates could be altered by a significant amount by varying the interphase. In the authors's opinion, this indicates that the longitudinal stiffness of unidirectional laminate is influenced significantly by the nature of bonding that exists between the fiber and matrix. In systems with good bonding, the matrix transfers the load to the fiber effectively and the stiffness of the laminate approaches the value predicted by a rule of mixtures. The assumption of perfect bonding between fiber and matrix is valid under those conditions. However, when the bonding between the fiber and the matrix is poor (as in the case of untreated fiber systems and also in the systems with certain sizings), there could be inefficiency in the load transfer between the matrix and the fiber. This could result in a discontinuity in displacement between the fiber and the matrix. Since the matrix does not transmit all the load into the fiber, the stiffness of the laminate is reduced. Under such conditions, the perfect bonding assumption is not valid. Hence, while modelling interphase problems, the perfect bonding assumption must be used with caution. The model in reference [93] uses a perfect bonding assumption. This could be one reason for the difference in the experimental and predicted tensile strength values.

In the model developed in reference [93], it is assumed that the matrix material undergoes plastic deformation even after the first fiber fracture. However, it is often observed that the first fiber fracture occurs at load levels that are almost half the failure loads. At such load levels, the interface may not fail. In the authors opinion, in order to accurately predict the tensile strength, the failure of the interface should be checked after each fiber fracture. If the interface does not fail, then elastic analysis must be performed. If interfacial failure occurs before the final failure of the laminate, then a plastic analysis must be performed. In most brittle matrix systems, the interfacial shear strength is lower than the matrix failure strength. This would result in interfacial debonding occurring prior to gross matrix plasticity. Once

debonding occurs, the stress is transferred to the matrix through friction at the fiber/matrix interface. Under this condition, the shear stress in the matrix could be assumed to be constant along the debonded length and the assumption of a perfectly plastic matrix behavior would be valid.

Most of the tensile strength prediction models available in the literature do not consider the interphase as a distinct region around the fiber. In the author's opinion, in order to obtain an accurate estimate of tensile strength, the interphase must be modeled as a distinct region, with properties different from those of the matrix and fiber. As mentioned in chapter 2, there is no reliable method available to estimate the properties (such as Young's modulus, Shear modulus, Coefficient of thermal expansion etc) of the interphase region. This has prompted researchers to reduce the interphase into a one dimensional interface region, and characterize the interphase with a single parameter, the interfacial shear strength.

In this study, the tensile strength prediction model proposed in reference [93] is modified to account for some of the factors discussed in this section. A brief description of the model is given below. Following the work of Gao and Reifsnider [93], the broken fibers are assumed to form a central core with a layer of matrix material around it. The nearest neighboring row of fibers are assumed to be arranged such that it forms a concentric cylinder around the central core of broken fibers. Concentric cylinders of matrix material and average composite material are assumed to be wrapped around this. Figure 60 shows a schematic of the arrangement described above. The nomenclature used in this chapter is described in Appendix 1. The calculation of the geometric parameters and the average properties of the central core are described in Appendix 2. The force equilibrium equations for the central core of broken fibers and the adjacent fibers are written in the following form

$$E_{fl}\pi r_{fl}^2 \frac{d^2u_{fl}}{dx^2} + 2\pi r_{fl}\tau_{m1} = 0 \qquad (4)$$

$$n_i E_{c2}\pi r_{c2}^2 \frac{d^2u_{c2}}{dx^2} + 2\pi r_m\tau_{m2} + 2\pi r_{c2}\tau_{m3} = 0 \qquad (5)$$

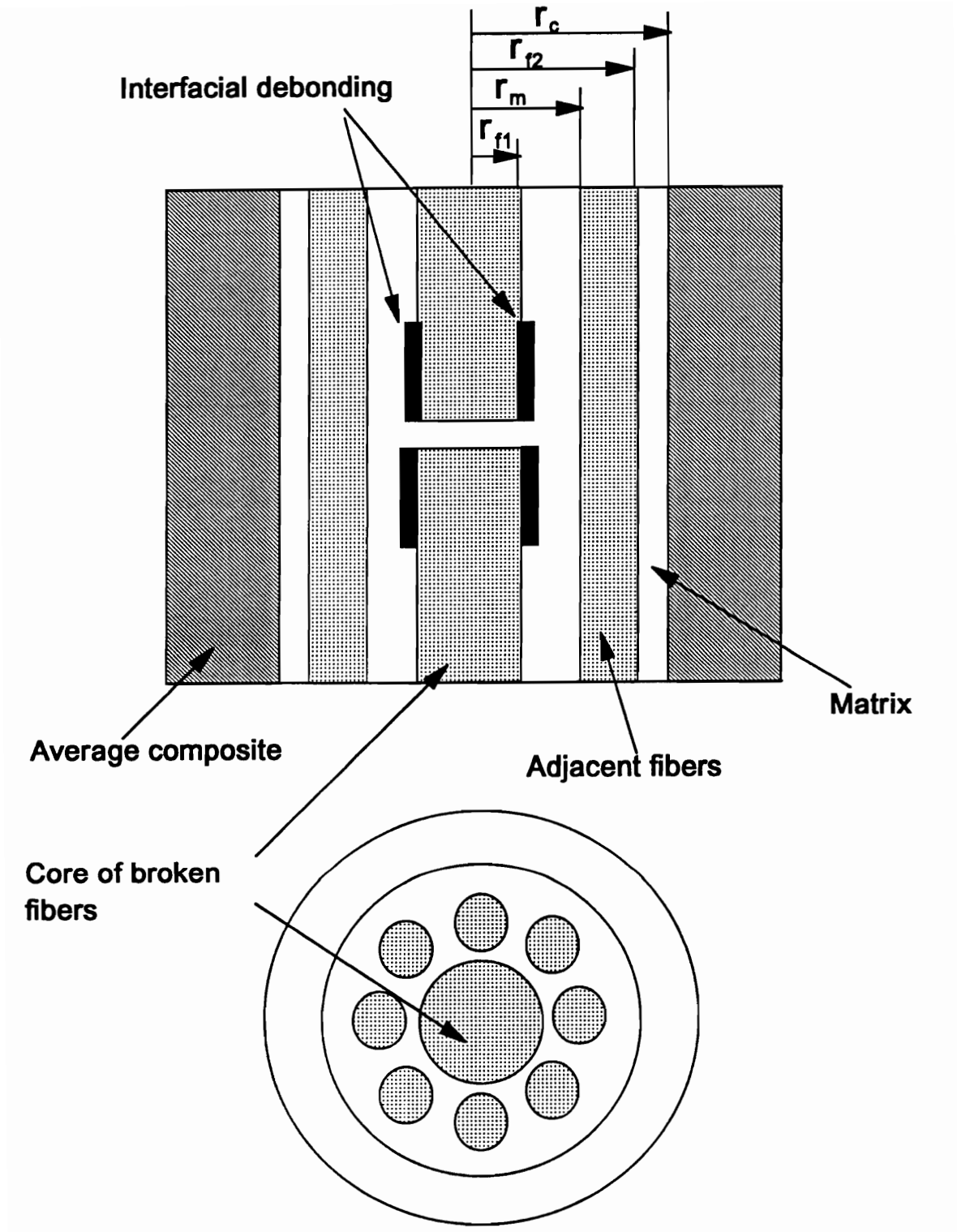

Figure 60 Schematic of unidirectional laminate with a core of broken fiber.

where

$$\tau_{m1} = \left(\frac{u_{m2} - u_{m1}}{b}\right) G_i$$

$$\tau_{m2} = \left(\frac{u_{m1} - u_{m2}}{b}\right) G_i \qquad (6)$$

$$\tau_{m3} = \left(\frac{u_c - u_{m2}}{b}\right) G_i$$

In writing these relationships, it is assumed that the displacement varies linearly in the radial direction, in the matrix material. Assuming that the displacement in the fiber and matrix at the fiber-matrix interface is discontinuous, and that the displacement in the average composite is uniform, the following expressions can be written

$$u_c = \frac{\sigma_a \, x}{E_x} \qquad (7)$$

$$u_{m1} = \eta \, u_{f1} \qquad (8)$$

$$u_{m2} = \eta \, u_{f2} \qquad (9)$$

where η is the 'efficiency factor' that determines how well the load is transferred from the matrix into the fiber. $\eta = 1$ indicates perfect bonding and good load transfer at the interface, while $\eta = 0$ indicates complete debonding with no transfer of load from the matrix into the fiber. It must be mentioned here that this 'efficiency factor' may be estimated using the measured tensile modulus of the unidirectional laminate. A detailed description of the procedure used for estimating the 'efficiency factor' from the longitudinal modulus is given in Appendix 3.

Using equations 6,7 and 8, the equilibrium equations (4 and 5) are written in the following form

$$\frac{d^2u_n}{dx^2} + k_1\, u_n + k_2\, u_{f2} = 0 \tag{10}$$

$$\frac{d^2u_{f2}}{dx^2} - k_3\, u_{f2} + k_4\, u_n + k_5\, x = 0 \tag{11}$$

where

$$k_1 = -\frac{2\, r_n\, \eta\, G_i}{b\, E_n\, r_n^2}$$

$$k_2 = -k_1 \tag{12}$$

$$k_3 = \frac{2\, r_m\, \eta\, G_i}{n_i\, b\, E_{f2}\, r_{f2}^2} + \frac{2\, r_{f2}\, \eta\, G_i}{n_i\, b\, E_{f2}\, r_{f2}^2}$$

$$k_4 = \frac{2\, r_m\, \eta\, G_i}{n_i\, b\, E_{f2}\, r_{f2}^2}$$

$$k_5 = \frac{2\, r_{f2}\, \eta\, G_i\, \sigma_a}{n_i\, b\, E_{f2}\, r_{f2}^2\, E_x}$$

Equations 10 and 11 have to be solved subject to the following boundary conditions

$$\left(\frac{du_n}{dx}\right)_{x=0} = 0 \tag{13}$$

$$\left(u_{f2}\right)_{x=0} = 0 \tag{14}$$

Simplifying equations 10 and 11 we obtain

$$[D^4 + D^2\,(k_1 - k_3) - (k_2k_4 + k_1k_3)]\, u_{f2} - k_2k_5x = 0 \tag{15}$$

Solving for the homogeneous part of the above equation yields

$$\alpha,\beta = \left[\frac{(k_3-k_1) \pm \sqrt{(k_1+k_3)^2 + 4k_2k_4}}{2}\right]^{1/2} \tag{16}$$

Assume a solution of the following form

$$u_{f1} = C_1 e^{-\alpha x} + C_2 e^{-\beta x} + C_3 x + C_4 e^{\alpha x} + C_5 e^{\beta x} \tag{17}$$

$$u_{f2} = D_1 e^{-\alpha x} + D_2 e^{-\beta x} + D_3 x + D_4 e^{\alpha x} + D_5 e^{\beta x} \tag{18}$$

In order for the fiber displacements to be finite as x->∞, the constants C_4,C_5,D_4 and D_5 should be set equal to 0. Substituting the assumed displacement functions in the governing differential equations (10 and 11), the following set of 6 equations are obtained

$$C_1\alpha^2 + k_1C_1 + k_2D_1 = 0 \tag{19}$$

$$C_2\beta^2 + k_1C_2 + k_2D_2 = 0 \tag{20}$$

$$k_1C_3 + k_2D_3 = 0 \tag{21}$$

$$D_1\alpha^2 + k_4C_1 - k_3D_1 = 0 \tag{22}$$

$$D_2\beta^2 + k_4C_2 - k_3D_2 = 0 \tag{23}$$

$$k_4C_3 - k_3D_3 + k_5 = 0 \tag{24}$$

The constants C_1 through C_3 and D_1 through D_3 are obtained by solving equations 13,14,19,20,21 and 24 and are listed below

$$C_3 = \frac{-k_2 k_5}{k_1 k_3 + k_2 k_4} \tag{25}$$

$$D_3 = -C_3 \tag{26}$$

$$C_1 = \left(-\frac{k_2}{\alpha^2 + k_1} \right) D_1 \tag{27}$$

$$C_2 = \left(-\frac{k_2}{\beta^2 + k_1} \right) D_2 \tag{28}$$

$$D_1 = \frac{C_3}{\left[\frac{\beta k_2}{\beta^2 + k_1} - \frac{\alpha k_2}{\alpha^2 + k_1} \right]} \tag{29}$$

$$D_2 = -D_1 \tag{30}$$

Thus, the solution to the problem is obtained as

$$u_{f1} = C_1 e^{-\alpha x} + C_2 e^{-\beta x} + C_3 x \tag{31}$$

$$u_{f2} = D_1 e^{-\alpha x} + D_2 e^{-\beta x} + D_3 x \tag{32}$$

The constants are given by equations 25-30, and α and β are given by equation 16.

The strains and stresses in the central core and the adjacent fibers are obtained using the strain-displacement and constitutive relationships as

$$\varepsilon_m = \frac{du_m}{dx} \quad ; \quad \sigma_m = E_m \, \varepsilon_m \tag{33}$$

$$\varepsilon_f = \frac{du_f}{dx} \quad ; \quad \sigma_f = E_f \, \varepsilon_f \tag{34}$$

The elastic stress concentration factor in the adjacent fiber is then written as

$$C_i = (\sigma_f)_{x=0} \tag{35}$$

The elastic ineffective length is obtained by determining the length over which the inner core recovers 99 % of the applied stress. It is obtained by solving the following equation for x

$$\sigma_m (x) = 0.99 \, \sigma_a \tag{36}$$

Having obtained the elastic stress concentration factor (C_i) and the elastic ineffective length(δ_i), the corresponding plastic stress concentration factor C^*_i and the plastic ineffective length (δ^*_i) are obtained using the following approximation. It is assumed that the matrix exhibits an elastic-perfectly plastic behavior. If the average shear stress in the interphase exceeds the interfacial shear strength, the interface is assumed to debond. Once debonding occurs, the shear stress in the matrix is assumed to be constant over the region defined as the plastic ineffective length, and zero elsewhere. The plastic stress concentration factor is estimated by calculating the average stress in the adjacent fiber as follows

$$\overline{\sigma_f} = \frac{1}{\delta} \int_0^{\delta} \sigma_f \, dx \tag{37}$$

$$\overline{\sigma_f} = \frac{E_f}{\delta} \left[D_3 \delta - D_1 - D_2 \right] \tag{38}$$

$$C_i^* = \frac{\overline{\sigma_2}}{E_2 D_3} \tag{39}$$

It turns out that the plastic stress concentration factor calculated in this manner is 1. In order to estimate the plastic ineffective length, the force balance argument is used to obtain

$$\delta_i^* = \frac{\overline{\sigma_1} r_1}{2 \eta \tau_i} \tag{40}$$

where $\overline{\sigma_1}$ is the average stress in the inner core and is given by

$$\overline{\sigma_1} = \frac{E_1}{\delta} \int_0^{\delta} \varepsilon_1 \, dx \tag{41}$$

$$\overline{\sigma_1} = \frac{E_1}{\delta} (C_3 \delta - C_1 - C_2) \tag{42}$$

Note that in writing the force balance equation, it has been assumed that due to interfacial debonding, the shear stress in the matrix is not equal to the interfacial shear strength, but is multiplied by the 'efficiency factor' η. This is because once debonding occurs, the stress transfer occurs essentially by means of friction. It is expected that the stress transfer in this region after debonding occurs will not be perfect. The shear stress is multiplied by the efficiency factor to reflect this behavior. Knowing the stress concentration factors and ineffective lengths (elastic and plastic) for the different fiber breakages (i-plets), the tensile strength is predicted following Batdorf's analysis.

Batdorf has shown that the stress level at which the first fiber fracture occurs (singlet) is given by

$$\sigma_1 = \left(\frac{1}{N L}\right)^{\frac{1}{m}} \sigma_0 \tag{43}$$

where N = Total number of fibers in the specimen

L = Normalized length of the specimen

m = Weibull strength shape factor for the fiber

σ_0 = Weibull strength location parameter for the fiber

The stress level at which the subsequent fiber fractures occur is given by

$$\sigma_i = \left(\frac{1}{N\ L\ \pi\ n_{i-1}\ \lambda_{i-1}} \right)^{\frac{1}{im}} \sigma_0 \qquad i = 2,3,..... \tag{44}$$

where

$$\lambda_i = 2\ \delta_i \left[\frac{C_i^{m+1} - 1}{(C_i - 1)\ (m+1)} \right] \tag{45}$$

and n_i are the number of nearest neighbors around a core of i broken fibers. The number of nearest neighbors are estimated assuming that the fibers are arranged in a hexagonal packed system. The number of nearest neighbors for the first 25 fiber fractures are given in Table XIII.

The procedure used for estimating the tensile strength is detailed below. The stress required for breaking the first fiber is first estimated using equation 43. At this stress level, the average shear stress in the matrix region is estimated by integrating the shear stress in the matrix over the elastic ineffective length as follows

$$\overline{\tau_m} = \frac{1}{\delta} \int_0^{\delta} \left(\frac{u_{2m} - u_{1m}}{b} \right) G_i\ dx \tag{46}$$

$$\overline{\tau_m} = \frac{G_i\ \eta}{\delta\ b} \left[\frac{(D_1 - C_1)}{\alpha} + \frac{(D_2 - C_2)}{\beta} \right] \tag{47}$$

It is assumed that interfacial debonding occurs when the average shear stress in the matrix exceeds the

interfacial shear strength. Subsequent fiber failure loads are calculated using equation 44. At each load level, it is checked to see if interfacial failure occurs. The elastic stress concentration factors (SCF) and ineffective lengths are used in equation 44 until interfacial failure is observed. Once interfacial failure occurs, the plastic SCF and ineffective lengths (equations 39 and 40) are used in equation 44 to predict subsequent fiber fractures. If there is no interfacial failure until instability occurs, then the final failure is classified as elastic failure. If debonding occurs prior to final failure, the failure is termed plastic.

Using the model described above, the tensile strength and the failure mode of unidirectional laminates can be predicted. It must be mentioned here that the prediction scheme requires that the Weibull strength parameters for the fiber be known. It is also required to normalize the lengths used in the analysis with a characteristic length value. In this study, all the lengths are normalized by a factor of $100*r_f$. The typical radius of a carbon fiber is around 3 microns. The factor $100*r_f$ is chosen because 500 microns is very close to the typical critical length value obtained for graphite/epoxy composites using the single fiber fragmentation test. Parametric studies were conducted to investigate the influence of various parameters on the failure mode and tensile strength of unidirectional graphite/epoxy composites. The results from these studies are discussed below. The following parameters were used in all the calculations discussed in this section.

N = 1 Million (Total number of fibers)

L' = 5 inch (Length of the specimen)

l = $100*r_f$ (Normalization length)

r_f = 2.5 microns (Fiber radius)

v_f = 0.60 (Volume fraction)

σ_0 = 500 ksi (Fiber strength Weibull location parameter)

E_f = 44 msi (Fiber stiffness)

E_x = $E_c*(\eta)^{0.66}$ (where E_x is the composite stiffness, E_c is the composite stiffness predicted using the rule of mixtures and η is the efficiency factor) [This relationship was obtained

using the CCM detailed in Appendix 3]

Using these parameters, the influence of the interfacial shear strength, efficiency factor, matrix shear modulus, and Weibull strength shape factor on the tensile strength of the unidirectional laminate was investigated. In all the figures, the tensile strength of the laminate has been normalized with the Weibull location parameter σ_0. Figure 61 shows the variation of normalized tensile strength with the interfacial shear strength for different values of Weibull shape factor (m). The figure shows clearly that the tensile strength increases with 'm'. The figure also indicates that high interfacial strengths result in elastic failures, while low interfacial strengths result in plastic failures. In the elastic failure range, the strength of the unidirectional laminate is independent of the interfacial shear strength. This is because the elastic stress concentration factors and ineffective lengths used to estimate the strength are independent of the interfacial shear strength. When the interfacial shear strength is low, early debonding occurs. Under these conditions, the tensile strength reduces rapidly as the interfacial shear strength decreases. For intermediate interfacial shear strength values, the transition from elastic to plastic failure is observed. In this region, even though the failure is plastic, the plastic ineffective length is small and the failure is still controlled by the stress concentration factor. Since debonding reduces the stress concentration factor, the tensile strength increases with reducing interfacial strength values. It is thus observed that when the failure is controlled by stress concentration effects, interfacial debonding increases the tensile strength. This makes physical sense in that debonding results in decoupling the broken fiber from the rest of the composite and alleviates the stress concentration effects. However, when the plastic ineffective length controls the failure, debonding reduces the tensile strength. This is because the plastic ineffective length increases with debonding very rapidly, and the tensile strength reduces with increasing ineffective length. In figure 62, the variation of tensile strength as a function of the efficiency factor η is plotted for various values of 'm'. It is observed that when the failure is elastic, the tensile strength reduces with increasing η. However, when the composite material failure is preceded by interfacial failure, the trends are reversed. Tensile strength in this regime increases with increasing values of η. It is also interesting to note that as the value of 'm' increases, the

tensile strength increases. Since the tensile strength is low for small values of 'm', the shear stress in the matrix material is low, and hence most of the failures are elastic. For high values of 'm', the shear stresses in the matrix are significantly higher. This results in early debonding at the interface and most failures are plastic. It is also noted that elastic failure occurs when η is large and plastic failure occurs when η is small. Let us take a moment to consider the physical significance of η. As mentioned earlier, large values of η indicates effective load transfer at the interface (good bonding) and low values of η results in ineffective load transfer which is indicative of poor fiber-matrix bonding. This means that when fiber-matrix bonding is good, elastic failure (controlled by SCF) occurs, and poor bonding results in plastic failure accompanied by fiber-matrix debonding.

The variation of tensile strength as a function of the interfacial shear strength for two different values of η are shown in figure 63. The figure reveals that for a given value of η, an optimal interfacial shear strength value exists, for which the tensile strength of the composite is maximum. However, it is observed that the optimal interfacial strength value is a function of η. As η reduces, the optimal interfacial strength value and the maximum tensile strength achievable increases.

Based on the predictions of this model, it is claimed that the interface can be characterized completely by the two parameters η and τ. For example, changes in the interfacial conditions effected through fiber surface treatment and sizing can be fully represented using these two parameters. Knowing these two parameters, the tensile strength of the unidirectional laminate can be predicted. It is also interesting to note that by varying these two parameters slightly, the tensile strength of the unidirectional laminate could be altered significantly. This is especially true when the failure mode changes from elastic to plastic or vice-versa.

Using the scheme described, the tensile strength of the 810 A, 820 A and 810 O laminates were estimated. It must be mentioned here that most of the data necessary for the strength prediction are not available. However, since the same fiber and matrix material has been used in the three systems, and only the interphase has been changed, the necessary values were assumed but kept constant for the three systems.

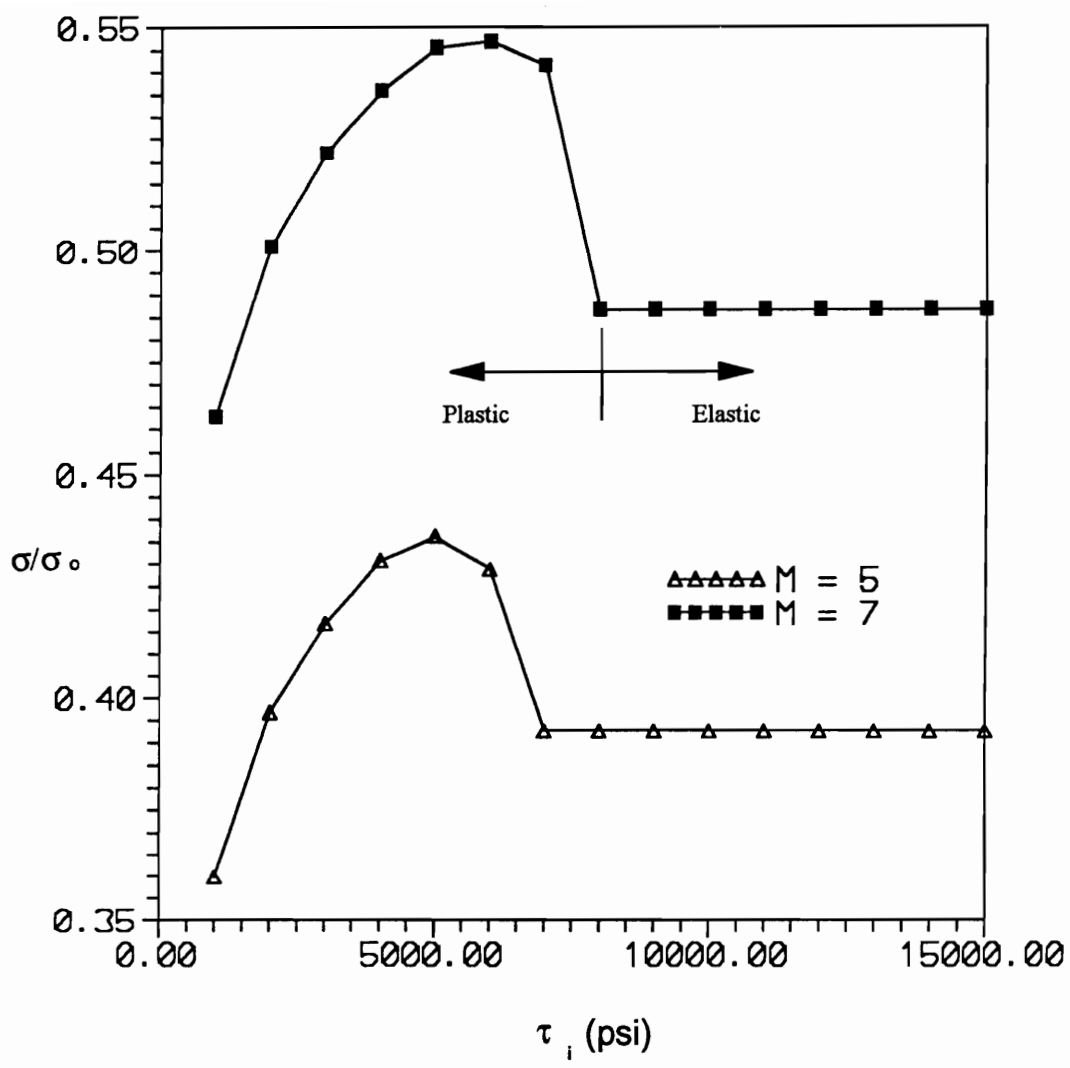

Figure 61 Variation of predicted tensile strength as a function of τ_m.

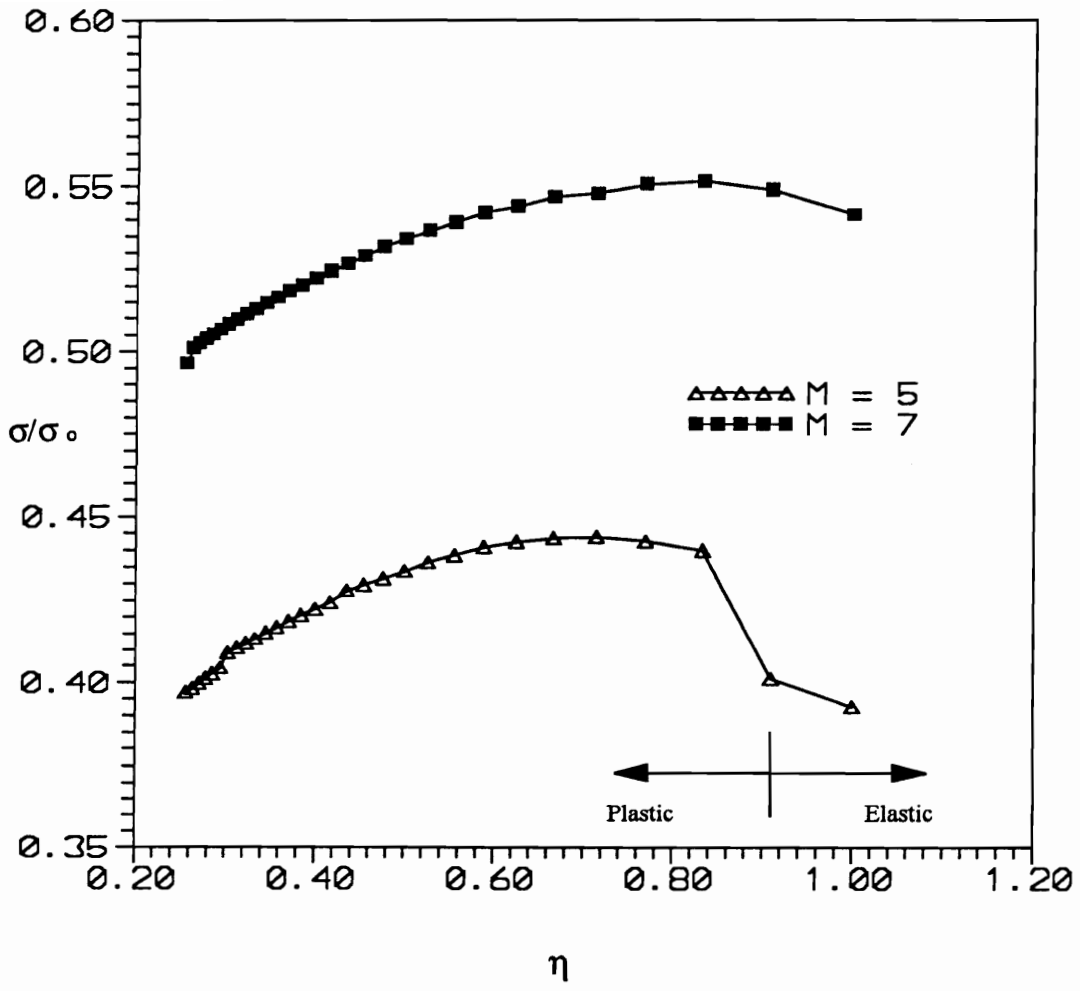

Figure 62 Variation of predicted unidirectional tensile strength as a function of η.

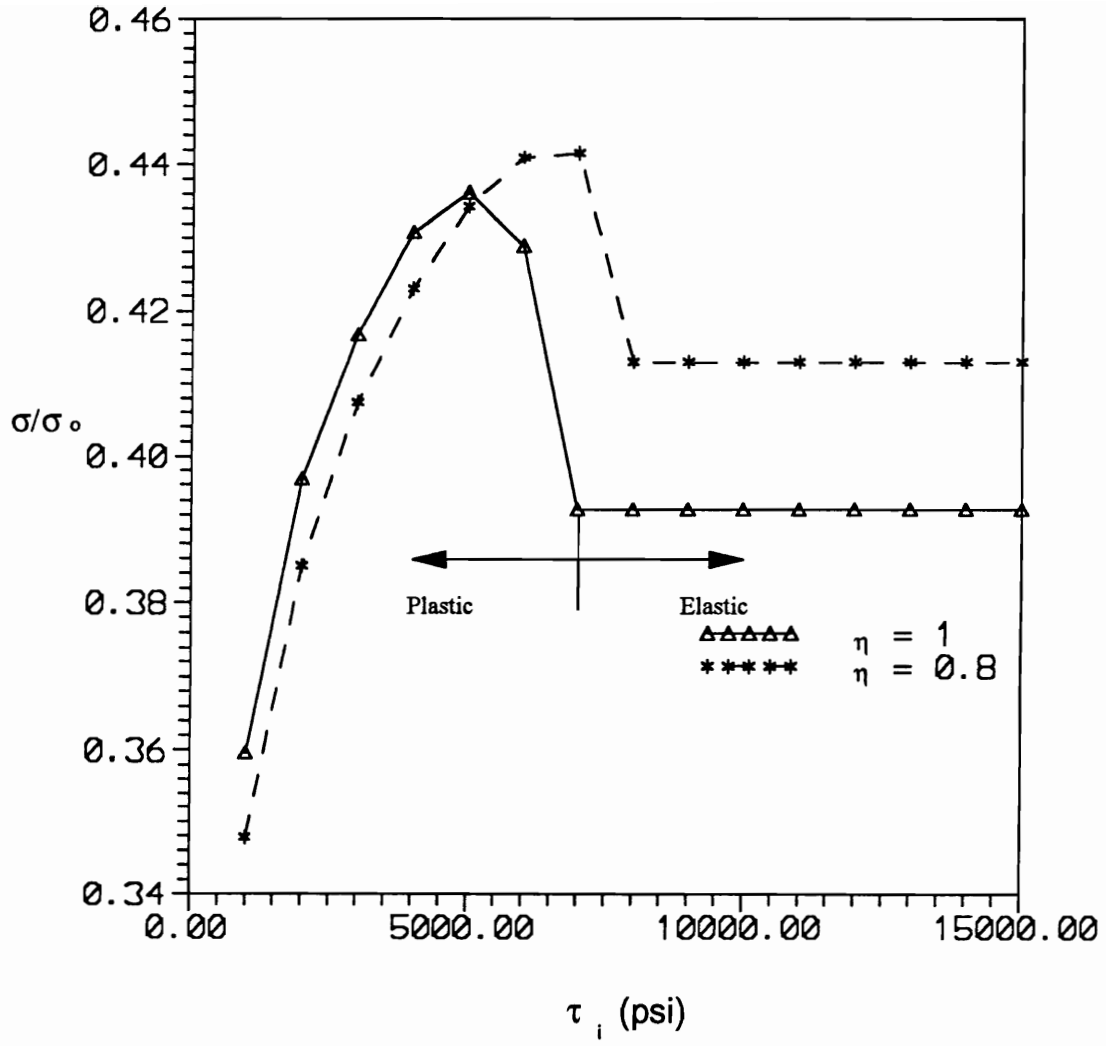

Figure 63 Predicted variation of unidirectional tensile strength as a function of τ_m for different η.

Only the interfacial shear strength and efficiency factor values were altered to reflect the changes in interphase. This enables us to compare the predicted values of tensile strength with the experimental values reported in chapter 5. It must be mentioned here that as far as possible, most of the values used in the model were assumed to be typical values used for most graphite/epoxy composites. Some of the properties used in the strength prediction model are listed below

N = 1 Million (Total number of fibers)

L = 5 inch (Length of the specimen)

l = $100*r_f$ (Normalization length)

r_f = 2.5 microns (Fiber radius)

v_f = 0.60 (Volume fraction)

σ_0 = 1000 ksi (Fiber strength Weibull location parameter)

m = 5

E_f = 44 msi (Fiber stiffness)

E_x = $E_c*(\eta)^{0.66}$ (where E_x is the composite stiffness, E_c is the composite stiffness predicted using the rule of mixtures and η is the efficiency factor)

G_m = 0.18 msi

810 A		**820 A**		**810 O**	
η	= 0.9	η	= 0.95	η	= 0.77
τ_m	= 12 ksi	τ_m	= 12 ksi	τ_m	= 10 ksi

The above properties were chosen based on experimental data on these material systems. The experimental results indicate that the interface is weakest in the 810 O system and strongest in the 820 A system. Hence, the ISS of the 810 O was assumed to be lower than that of the other two systems. Also, the experimental data from unidirectional laminate tests indicate that the stiffness of the 820 A laminates is very close to the values predicted by the rule of mixtures. The experimental values diverge very

significantly for the 810 O system. Using the procedure described in Appendix 3, the efficiency factors for the three system were estimated. **It must be emphasized that these values are based on experimental data on these material system and were not chosen arbitrarily.**

Using the properties listed above, the tensile strength of the three material system were predicted. Table XIV shows the predicted and experimental tensile strength values for the three material systems. The table also shows the predicted failure modes and number of i-plets formed before final failure occurs. The model predicts that the 810 A and 820 A laminates do not exhibit interfacial failure prior to final failure. However, the 810 O system exhibits plastic failure. It may be recalled that the non-destructive testing results for the cross-ply laminates discussed in chapter 6 indicated similar results. The NDE results revealed that the 810 A and 820 A laminates exhibit less interfacial debonding and the failed specimen suggest that the failure is elastic. In sharp contrast, the 810 O laminate exhibits extensive fiber-matrix debonding and the failed specimen suggests a global strain controlled failure. These observations are consistent with the predictions shown in Table XIV. The AE results indicate that the number of fiber fractures in the 0° ply of the cross-ply laminate is highest in the 810 O laminate and lowest in 820 A laminates. The tensile strength model predicts the observed trends very well. Maximum fiber fractures are predicted by the tensile strength prediction model in the 810 O system, followed by the 810 A and 820 A system respectively. It is thus seen that the failure modes and the tensile strength values predicted by the model agree very well with the experimental values. It must be added here that the NDE results are from cross-ply laminates, while the theoretical predictions described in this section are for unidirectional laminates. In the authors opinion, this is justified for the following reason. In $(0,90_3)_s$ laminate, most of the load is carried by the 0° ply, once saturation of matrix cracks occurs in the 90° ply. Subsequently, the laminate behaves like a unidirectional material. Under these conditions, qualitative comparisons of damage in the 0° ply of the cross-ply laminate with those in the unidirectional laminates is reasonable.

Table XIII Number of nearest neighboring fibers

i	1	2	3	4	5	6	7	8	9	10	11	12	13	14	15	16	17	18	19	20	21	22	23	24	25
n_i	6	8	9	10	11	12	12	13	14	14	15	15	15	16	17	18	18	18	18	20	20	20	20	20	20

Table XIV Comparison of experimental and predicted unidirectional static strength

	Strength (ksi) (Expt)	Strength (ksi) (Pred)	Fiber Fractures (Expt)	Fiber Fractures (Predicted i-plets)	Debonding (Expt)	Debonding (Pred)
810 A	407	392	Few	18	None	No
810 O	444	432	Numerous	25	Extensive	Yes
820 A	400	388	Very Few	18	None	No

9.2 Prediction of matrix cracking and damage in cross-ply laminates

9.2.1 Introduction

Numerous models are available in the literature to predict the onset of transverse matrix cracking in laminated composites. Most of these models use modified forms of shear lag analysis to estimate the stresses in the laminate with a transverse crack [114-124]. These stresses are used in some stress/strain/strain energy based failure criterion to predict the onset of transverse matrix cracks in laminated composites. Wang et al. [60] have used a Monte-Carlo simulation scheme to predict the onset and progression of transverse cracking under static and fatigue loading. In their analysis, it was assumed that numerous flaws, of varying dimensions are present in the 90° ply of the cross-ply laminate. A normal distribution function was used to describe the size of these distributed microcracks. It was assumed that these cracks developed into transverse matrix cracks in the 90° ply under applied external loading. They have used a fracture mechanics based approach (strain energy release rate criterion) to predict the formation of matrix cracks from these microcracks. More recently, some models based on 'Damage Mechanics' concepts have been proposed to model the transverse cracking problem in composites. These include models advanced by Talreja [54], Allen et al [56], Joshi et al [57] etc. In these models, the thermodynamic principles are used to derive the constitutive relationships and damage parameters. Talreja [54] has used a vector to represent damage in his model and has demonstrated that an initially orthotropic material becomes anisotropic in the presence of damage. His model contains a few phenomenological constants that have to be determined through a set of experiments on specific laminates.

In this study, the one dimensional shear lag model proposed by Reifsnider [97] has been used to determine the saturation crack spacing and the stress state in the cross-ply laminates with transverse matrix cracks. A novel scheme that uses the Weibull strength parameters of the 90° ply is used in conjunction with the shear lag analysis results to predict the onset and progression of transverse matrix cracks. It is well known that the strength of the 90° ply is dependent on the volume of the 90° ply. It has been

observed that as the volume of the 90° ply increases, the strength reduces [85-87]. This behavior has been explained using the following arguments. As the volume of the 90° ply increases, the number of flaws present in the ply also increases. The presence of a greater number of flaws increases the probability of failure and reduces the strength of the laminate. In the present model, similar arguments are used to account for the changes in the transverse cracking characteristics due to changes in volume of the 90° ply. A brief description of the model is given in the next section. First, a brief description of the shear lag model is provided. This is followed by a description of the scheme that uses the results from shear lag analysis to predict the onset and progression of matrix cracking.

9.2.1 Shear Lag Analysis

The one dimensional shear lag model proposed by Reifsnider [97] has been used to study the matrix cracking behavior in $(0,90_3)_s$ cross-ply laminates. Since detailed descriptions of the problem formulation and solution technique are available in the literature [97], the discussion here will be limited. The schematic of the matrix cracking problem to be solved using the shear lag analysis is shown in figure 64. The figure shows a transverse matrix crack in the 90° ply constrained by 0° plies on either side. The thickness of the 90° ply and the 0° ply are denoted by 'a' and 'c' respectively. It is assumed that the stresses are transferred from the 90° ply to the 0° ply through a shear transfer mechanism over a small region. This region is assumed to have a thickness of 'b'. Let U_0 and U_{90} represent the axial displacement of the 0° ply and the 90° ply respectively. The force equilibrium equations for the 0° ply and the 90° ply are written as

$$a\, E_{90} \frac{d^2U_{90}}{dX^2} + \frac{2\,G}{b}(U_0 - U_{90}) = 0 \tag{48}$$

$$c\, E_0 \frac{d^2U_0}{dX^2} + \frac{G}{b}(U_{90} - U_0) = 0 \tag{49}$$

where E_0, E_{90} are axial stiffness of the 0° and 90° ply respectively and G is the shear modulus of

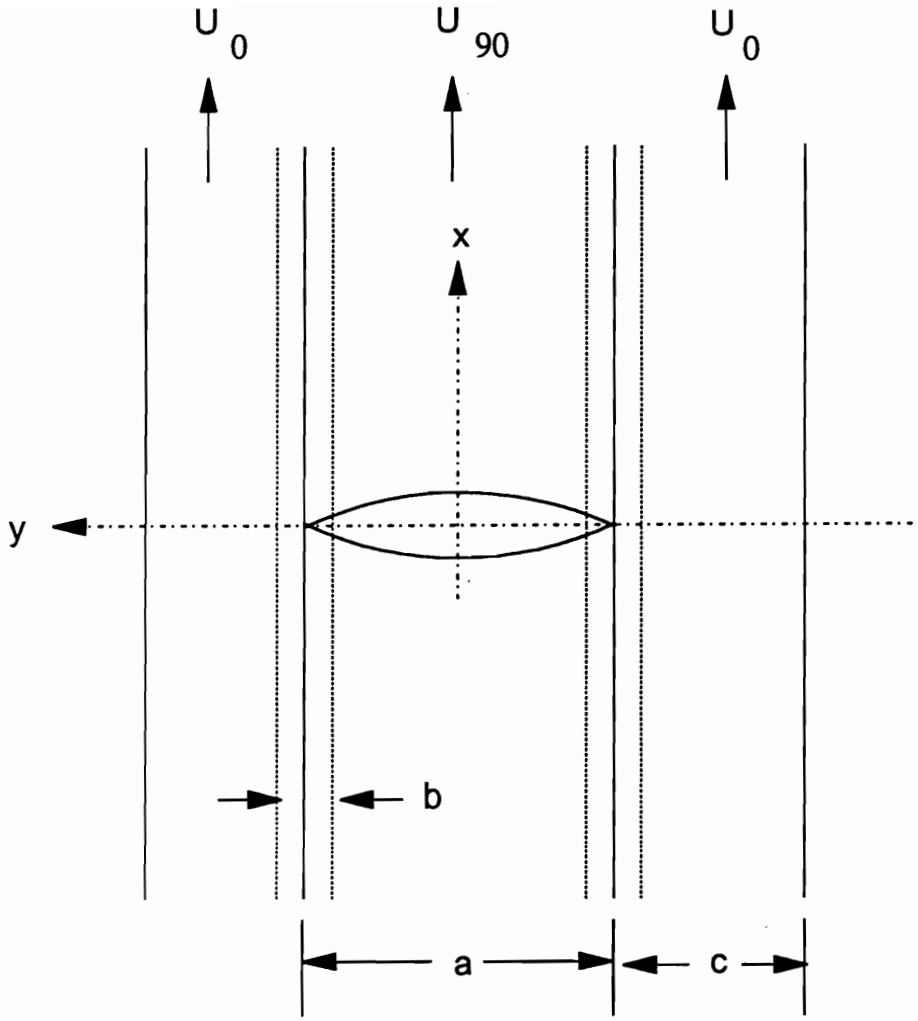

Figure 64 Schematic of the shear lag model showing a transverse ply crack in the central 90° ply with the constraining 0° plies

the interply stress transfer region.

The displacements and distance coordinates are normalized using the following scheme

$$U = \left(\frac{\sigma_a \, a}{\sqrt{E_x \, G}} \right) u \tag{50}$$

$$X = \left(\sqrt{\frac{E_x}{G}} \, a \right) x \tag{51}$$

where σ_a is the remote applied stress and E_x is the axial stiffness of the laminate. Note that X and U represent the actual distance coordinate and displacement and x and u represent the normalized quantities. Using this normalization, the equilibrium equations reduce to the following form

$$A \frac{d^2 u_{90}}{dx^2} + (u_0 - u_{90}) = 0 \tag{52}$$

$$B \frac{d^2 u_0}{dx^2} + (u_{90} - u_0) = 0 \tag{53}$$

where

$$A = \frac{E_{90} \, b}{2 \, E_x \, a}$$
$$B = \frac{E_0 \, b \, c}{E_x \, a^2} \tag{54}$$

Equations 52 and 53 are solved subject to the following boundary conditions

$$\left(\frac{du_{90}}{dx} \right)_{(x \to \infty)} = 1 \tag{55}$$

$$\left(\frac{du_0}{dx}\right)_{(x\to\infty)} = 1 \tag{56}$$

$$\left(\frac{du_{90}}{dx}\right)_{(x=0)} = 0 \tag{57}$$

$$(u_0)_{(x=0)} = 0 \tag{58}$$

Assume a solution of the following form

$$u_{90} = x + C_1 e^{-\alpha x} + C_2 e^{-\beta x} \tag{59}$$

$$u_0 = x + C_1 D_1 e^{-\alpha x} + C_2 D_2 e^{-\beta x} \tag{60}$$

Substituting the assumed displacement functions in the equilibrium equation (equations 53 and 54) yields the following set of algebraic equations

$$D_1 = 1 - A \alpha^2 \tag{61}$$

$$D_2 = 1 - A \beta^2 \tag{62}$$

$$B D_1 \alpha^2 - D_1 + 1 = 0 \tag{63}$$

$$B D_2 \beta^2 - D_2 + 1 = 0 \tag{64}$$

Substituting the displacement function in the boundary conditions (equations 55 through 58) we obtain

$$1 - \alpha C_1 - \beta C_2 = 0 \tag{65}$$

$$C_1 D_1 + C_2 D_2 = 0 \tag{66}$$

The six unknowns C_1, C_2, D_1, D_2, α and β are obtained by solving equations 61-66 and are listed below

$$\alpha = \sqrt{\frac{A + B}{A B}} \qquad \beta = 0 \tag{67}$$

$$C_1 = \frac{1}{\alpha} \qquad C_2 = A \alpha^2 - \frac{1}{\alpha} \tag{68}$$

$$D_1 = 1 - A \alpha^2 \qquad D_2 = 1 \tag{69}$$

Having obtained the complete solution, the stresses in the 90° ply and the 0° ply are written as

$$\sigma_{90} = \frac{\sigma_a E_{90}}{E_x} \left[1 - \alpha C_1 e^{-\alpha x} - \beta C_2 e^{-\beta x}\right] \tag{70}$$

$$\sigma_0 = \frac{\sigma_a E_0}{E_x} \left[1 - \alpha C_1 D_1 e^{-\alpha x} - \beta C_2 D_2 e^{-\beta x}\right] \tag{71}$$

9.2.3 Damage Prediction

In chapter 6 it was reported that the accumulation of transverse matrix cracks occurs over a range of applied external load. It was observed that gradual accumulation of transverse matrix cracks in the 90° ply of the cross-ply laminate occurs as the applied external load is increased incrementally, until a

Characteristic Damage State (CDS) is reached. Beyond this, the transverse crack density does not change as the applied external load increases. The matrix cracking is accompanied by reduction in the axial stiffness of the laminate. Experimental data indicated that the onset and rate of accumulation of transverse cracks was different for the three material system examined. It must be mentioned that when the applied load level is significantly greater than the load level at which CDS is achieved, new transverse cracks appear at locations between the existing cracks. In this analysis, only the transverse cracking characteristics before the CDS is reached, is modeled. The onset and progression of transverse cracking in the cross-ply laminate is predicted using the results from the shear lag analysis (described in the previous section) and the Weibull strength parameters for the 90° laminate.

The shear lag analysis is used to determine the saturation crack spacing and the characteristic damage state (CDS). The saturation crack spacing (SCS) is the distance from the crack face, over which 99.9 % of the applied external stresses are recovered in the 90° ply of the laminate. The CDS is obtained by calculating the reciprocal of the SCS (CDS = 1/SCS). The CDS essentially represents the number of cracks/inch in the 90° ply of the laminate, when saturation of transverse matrix cracking occurs. This is a function of the material properties and laminate configuration.

It is claimed that the accumulation of transverse matrix cracks occur over a range of applied external load because of the non-uniform distribution of flaws/defects in the 90° ply. The distribution of flaws would essentially result in a non-uniform distribution of local strength in the 90° ply. Due to the spatial distribution of strength in the 90° ply, the transverse cracks would form at different locations in the 90° ply, at different applied load levels. Under these assumptions, matrix cracks would occur at locations in the 90° ply where the local stresses exceed the local strength. It must be mentioned here that a scheme similar to this was used by Wang et al. [60], to predict the progressive matrix cracking in cross-ply laminates. They assigned values for the flaw dimensions in the 90° ply using a normal distribution function, and used a fracture mechanics based approach predict the formation and progression of matrix cracks. In the present analysis, a different scheme is used to represent the spatial distribution of strength

in the 90° ply. It is postulated that the spatial distribution of local strength in the 90° ply is directly related to the Weibull strength parameters of 90° laminates. The shape factor (α) and location parameter (β) for the 90° laminate can be obtained by fitting the experimental transverse strength data with a two parameter Weibull fit. The Weibull shape factor α indicates the distribution of the strength about the mean value, and β is a measure of the mean strength. In this study, only 5 specimens were tested from each material system under a transverse tensile loading mode. The results from these tests are reported in chapter 5. The data were fitted with a two parameter Weibull distribution, and the corresponding α and β values (Maximum Likelihood Parameter estimates) for the three material system are located in Table XV. The data clearly indicates that the spread in the strength is more in the 810 O and 820 A laminates. Also, the location parameter (β) is highest for the 820 A system and lowest for the 810 O system. Since very few tests were performed, the values of α and β obtained from the transverse test data may not be accurate. However, the trends obtained from these results are used to estimate the values α and β to be used in the model. The assumed values of α and β used in this analysis are shown in Table XVI. Using these values of α and β in conjunction with the results from the shear lag analysis, the onset and progression of matrix cracking is predicted.

For an applied external stress σ_a, the strain (ε_{90}) in the 90° ply is calculated using CLT. Knowing the Weibull strength parameters for the 90° laminate, the probability of failure of the 90° ply in the cross-ply laminate at a strain level ε_{90} is written as

$$p\ (\varepsilon_{90}) = 1 - \exp\left(-\frac{\varepsilon_{90}}{\beta}\right)^{\alpha} \tag{72}$$

It is postulated that the number of transverse matrix cracks/inch at a strain level ε_{90} is related to the probability of failure of the 90° ply in the cross-ply laminate by the following linear relationship

$$n_{cr} = n_{CDS}\ p(\varepsilon_{90}) \tag{73}$$

Table XV Weibull strength parameters for the 810 A, 820 A and 810 O 90° laminates estimated from experimental transverse strength results

	810 A	810 O	820 A
α	22.2	4.3	4.0
β (%)	0.719	0.726	0.992

Table XVI Weibull strength parameters for the 810 A, 820 A and 810 O 90° laminates used in the shear lag model.

	810 A	810 O	820 A
α	9	5	6
β (ksi)	0.718	0.655	0.833

where n_σ is the number of cracks at any applied external stress σ_a, n_{CDS} is the number of cracks in the 90° ply when saturation of matrix cracking occurs, and $p(\varepsilon_{90})$ is the probability of failure of the 90° ply in the cross-ply laminate at that strain level. This functional representation essentially indicates that when the probability of failure of the 90° ply is less than 1 %, there is no transverse matrix cracking. As the probability of failure increases, the number of transverse matrix cracks also increase. When the probability of failure is 100 %, saturation of matrix cracking occurs (the Characteristic Damage State is reached).

It is well known that the formation of transverse matrix cracks is accompanied by a stiffness reduction in the laminate. The presence of transverse cracks reduces the load carrying capacity of the 90° ply. This results in a reduction in the stiffness of the 90° ply and the whole laminate. In order to estimate the reduction in stiffness of the 90° ply and the laminate due to the formation of a single transverse crack, results from the shear lag analysis are used. The stiffness reduction scheme proposed by Lim and Hong [115] is used in this analysis. The average strain in the 0° ply, in the presence of a single transverse crack in the 90° ply is determined as

$$\overline{\varepsilon_0} = \frac{\sigma_a}{l\, E_x} \int_0^l (1 - \alpha\, C_1\, D_1\, e^{-\alpha x} - \beta\, C_2\, D_2\, e^{-\beta x})\, dx \tag{74}$$

which yields

$$\overline{\varepsilon_0} = \frac{\sigma_a}{l\, E_x} (l + C_1\, D_1\, (e^{-\alpha l} - 1) + C_2\, D_2\, (e^{-\beta l} - 1)) \tag{75}$$

It is assumed that the crack occurs at a constant applied external load and the constitutive relations for the uncracked and cracked laminates are written as

$$\sigma_x = \varepsilon_0\, E_x \qquad \text{(Uncracked laminate)} \tag{76}$$

$$\sigma_x = \overline{\varepsilon_0}\ \overline{E_x} \qquad \text{(Cracked laminate)} \tag{77}$$

Combining equations 73, 74 and 75, the stiffness reduction due to the formation of a single transverse matrix crack in the 90° ply of the cross-ply laminate is written as

$$\frac{\overline{E_x}}{E_x} = \frac{1}{1 + C_1 D_1 (e^{-\alpha l} - 1) + C_2 D_2 (e^{-\beta l} - 1)} \tag{78}$$

where $\overline{E_x}$ is the stiffness of the laminate in the presence of a single transverse crack, E_x is the undamaged initial stiffness of the laminate, l is the distance over which the stresses are perturbed due to the presence of the crack, and the other parameters such as α, β, C_1, C_2, D_1 and D_2 are shear lag parameters defined earlier. Having estimated the stiffness reduction in the laminate, the stiffness reduction in the 90° ply can be estimated easily using CLT (assuming that the stiffness of the 0° ply does not change). Since a cross-ply laminate is used in this study, this can be estimated by using the rule of mixtures in the following way

$$\overline{E_{90}} = \frac{\overline{E_x} - E_0\ v_0}{v_{90}} \tag{79}$$

where E_0 is the axial stiffness of the 0° ply, v_0 and v_{90} are the volume fractions of the 0° and 90° plies in the laminate respectively.

The variation of transverse matrix crack density with the applied load is given by equation 71 and the corresponding stiffness reduction in obtained from equation 77. The accumulation of damage in the cross-ply laminate is predicted using these equations as follows. The applied external load is increased incrementally and the load level required to initiate the first transverse crack is calculated using equation 71. The stiffness reduction associated with the formation of the first crack is then estimated using equation 77. Using the reduced stiffness, the shear lag analysis is performed and the new values of α, β, C_1, C_2, D_1 and D_2 are calculated. Using these values, the load level required to initiate the next crack and the

corresponding stiffness reduction are calculated using equations 71 and 77. This procedure is repeated until the saturation of matrix cracking is achieved.

Using the cumulative damage scheme described in the previous paragraph, the matrix cracking characteristics of 810 A, 820 A and 810 O laminates predicted. The material properties used in the model to predict this are displayed in Table XVII. The variation of transverse matrix crack density and the associated stiffness reduction for the 810 A and 810 O laminates predicted using this scheme are compared with the experimental data in figures 65 and 66. The figures show good correlation between the experimental and predicted values. The model predicts the early onset of transverse cracking in the 810 O laminate very well. It also predicts a greater number of transverse matrix cracks in the 810 O laminate when saturation occurs. This compares well with the experimental data. It is also interesting to note that even though the load level at which onset of matrix cracking occurs is significantly different for the 810 A and 810 O laminates, the difference in the load level at which saturation of matrix cracking occurs is not much. It is concluded that the differences in the load required to initiate the transverse matrix cracking is due to a combination of reduction in the stiffness of the 0° ply and the greater distribution in the strength of the transverse (90°) ply. This analysis brings out the importance of the Weibull strength parameters in the onset and progression of transverse matrix cracking very well. It is observed that even when the average transverse strength of the 90° ply in two material systems is not very different, the onset of matrix cracking in the 90° ply could occur very early if the distribution of strength in the 90° ply is not uniform. As was mentioned earlier, the distribution of PVP in the 810 O laminate was uneven. It was observed that fibers on the outside of the tow had excess amounts of PVP and those on the inside of the tow had lesser or no PVP. This could have resulted in the wider distribution of strength (weak links) in the 810 O laminates. This is confirmed by the greater scatter in the transverse strength data of the 810 O laminates and the early onset of matrix cracking in the cross-ply laminate.

The experimental and predicted variation of transverse crack density and stiffness reduction in the 810 A and 820 A laminates are displayed as figures 67 and 68. It is again observed that the predictions

Table XVII Material properties for 810 A, 820 A and 810 O material system used for static damage prediction

	810 A	810 O	820 A
E_{11} (msi)	27	24	27
E_{22} (msi)	1.24	1.22	1.2
G_{12} (msi)	0.7	0.7	0.7
ν_{12}	0.3	0.3	0.3
E_{xx} (msi)	7.68	6.91	7.68
G_m (msi)	0.15	0.15	0.15
t_{ply} (in)	0.0055	0.00525	0.0055
b (in)	0.00055	0.000525	0.00055

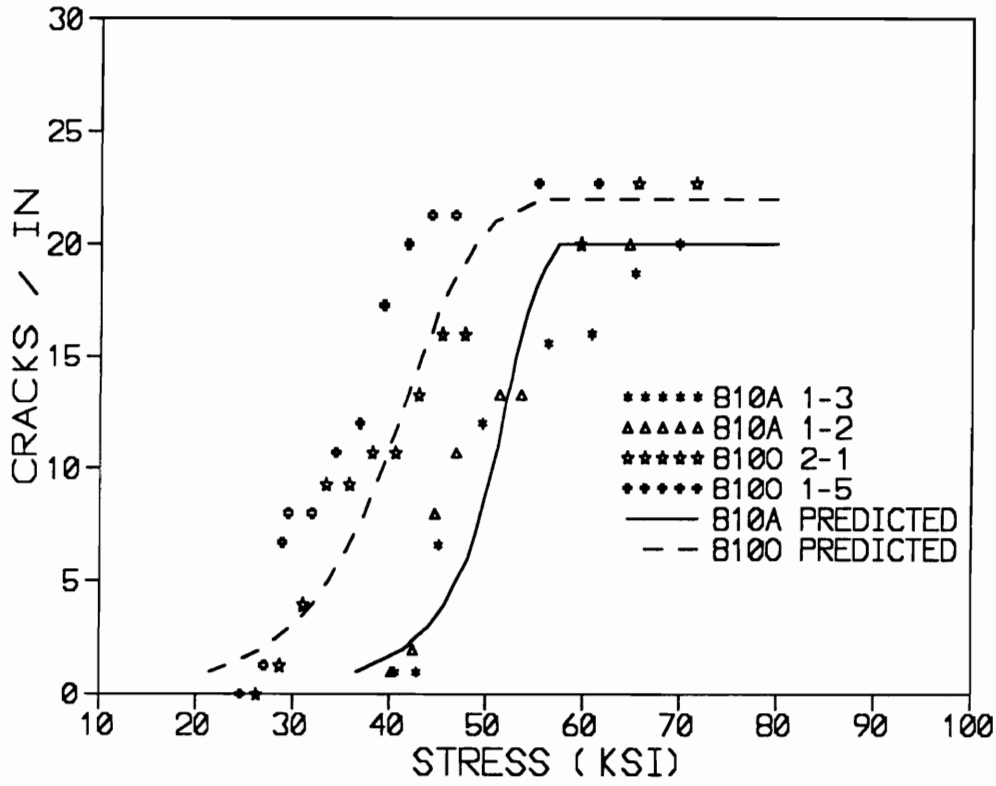

Figure 65 Comparison of experimental and predicted variation of static transverse crack density in the 810 A and 810 O cross-ply laminates

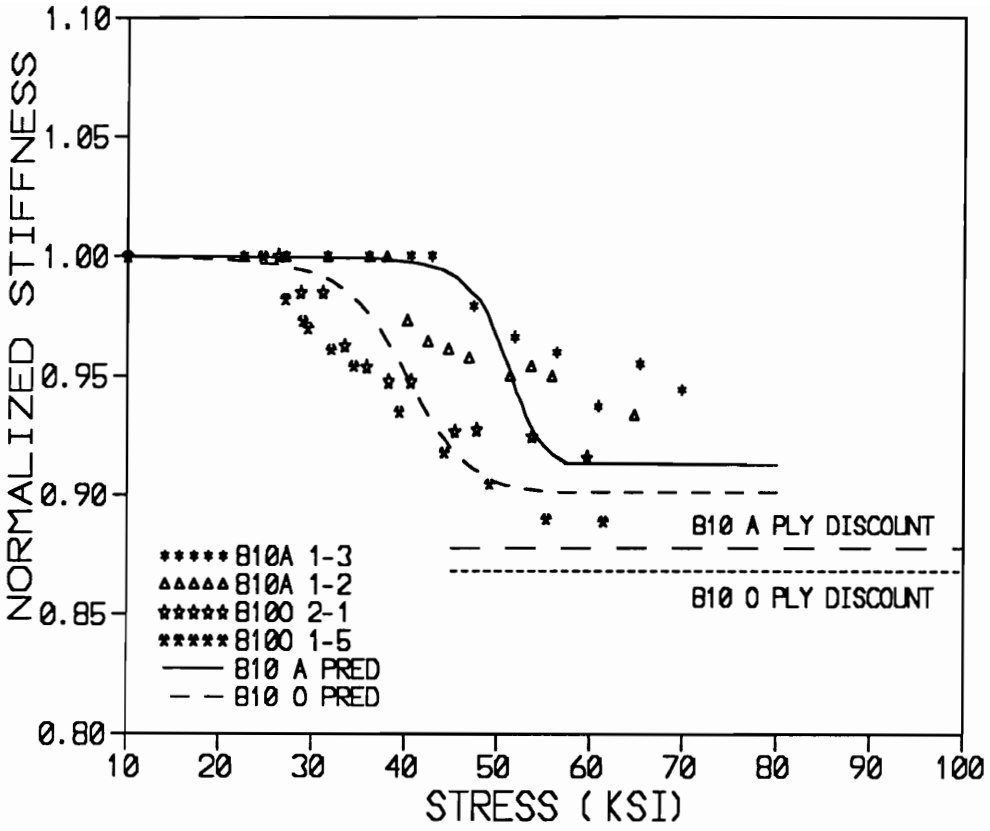

Figure 66 Comparison of experimental and predicted variation of static stiffness reduction in the 810 A and 810 O cross-ply laminates

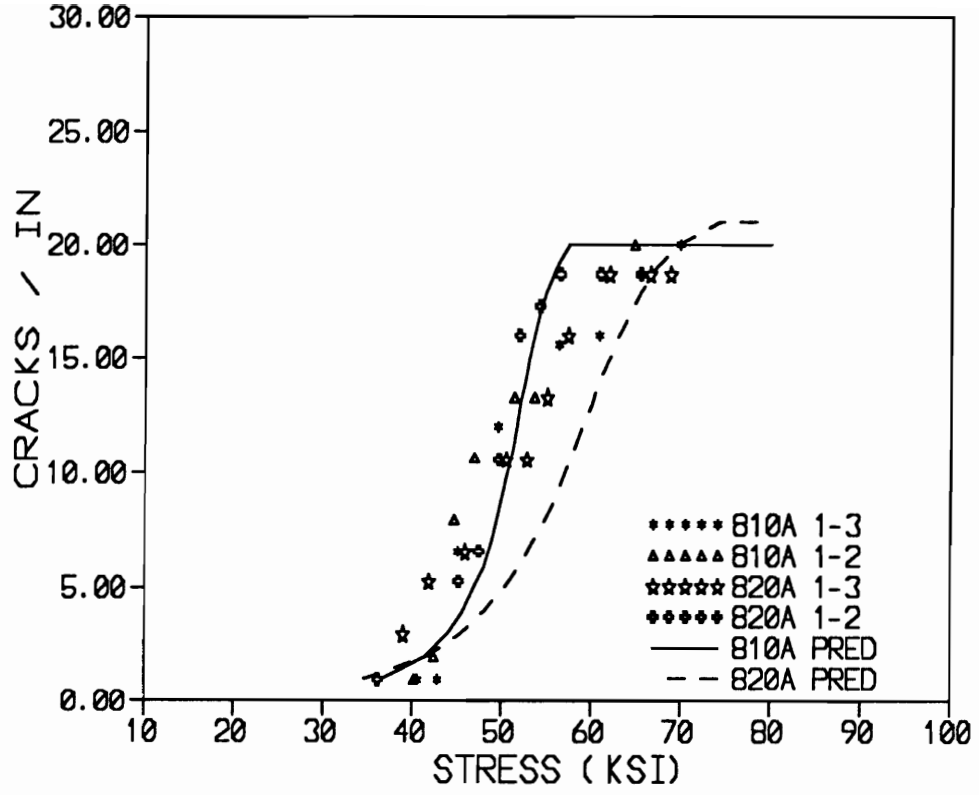

Figure 67 Comparison of experimental and predicted variation of static transverse crack density in the 810 A and 820 A cross-ply laminates

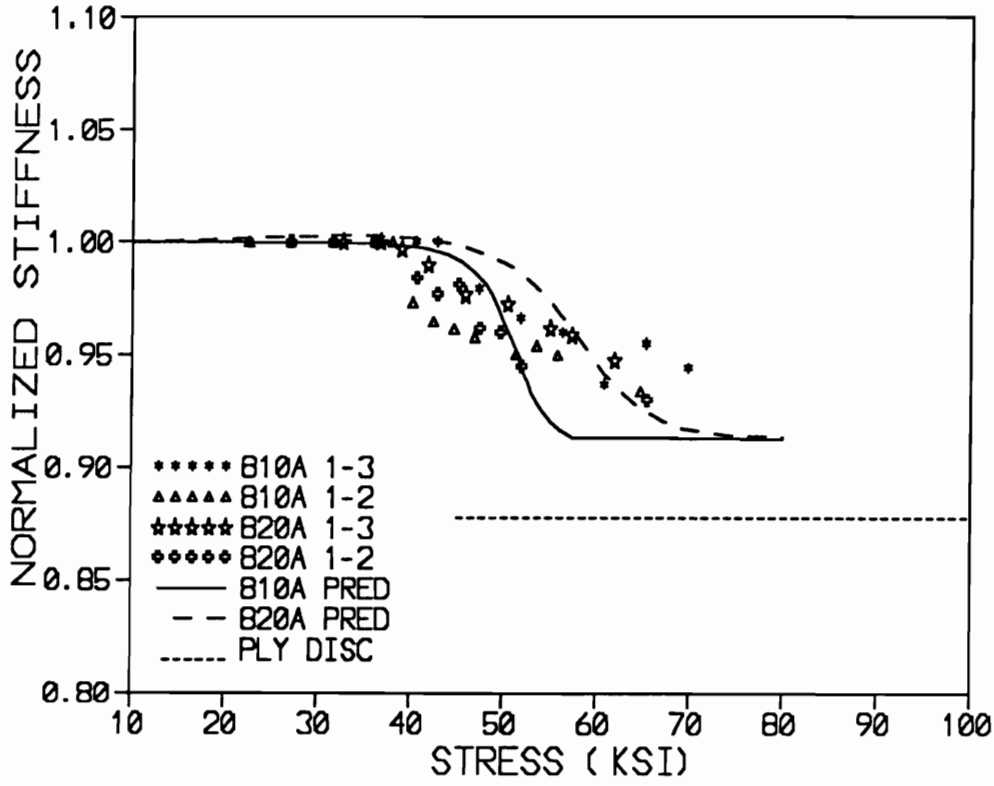

Figure 68 Comparison of experimental and predicted variation of static stiffness reduction in the 810 A and 820 A cross-ply laminates

820 A laminate is greater than the 810 A laminate, the onset of transverse cracking occurs at almost the same load levels in the two material system. This is due to the greater variation in the transverse strength of the 820 A laminate that is reflected by the lower value of α for this system. The horizontal lines in figures 66 and 68 indicate the stiffness reduction predicted using the ply discount method which assumes the stiffness of the 90° ply is zero. The experimental data and the present analysis indicate that the 90° ply carries load even after saturation of matrix cracking occurs.

9.3 Fatigue Damage and Life Prediction

9.3.1 Introduction

Numerous models have been forwarded in recent years for predicting the long-term behavior of laminated composite materials. Some of the commonly used methods have been discussed in the literature review section. In this study, a cumulative damage scheme based on the Critical Element Model [58] has been used to predict damage and fatigue life of cross-ply laminates. This model uses a semi-empirical approach, where the results from the damage analysis (discussed in chapters 6,7,8) are used in conjunction with the models described in sections 9.1 and 9.2, to predict the long-term behavior of cross-ply laminates. Figure 69 shows a schematic of the outline of the critical element model. The laminate is considered to be composed of sub-critical elements and critical elements. The sub-critical elements are defined as those elements that undergo damage during fatigue loading, but the failure of these elements does not result in the final failure of the laminate. In contrast, the primary load carrying member in the laminate, is designated as the critical element. The failure of the whole laminate is controlled by the failure of this element. In $(0,90_3)_s$ laminates, the 90° ply is the sub-critical element, and the 0° ply is the critical element. It is assumed that most of the damage occurs in the sub-critical element, while the final failure of the laminate is considered to coincide with the failure of the critical element. The damage in the sub-critical element results in degradation of properties (eg. stiffness) and this results in redistribution of stresses.

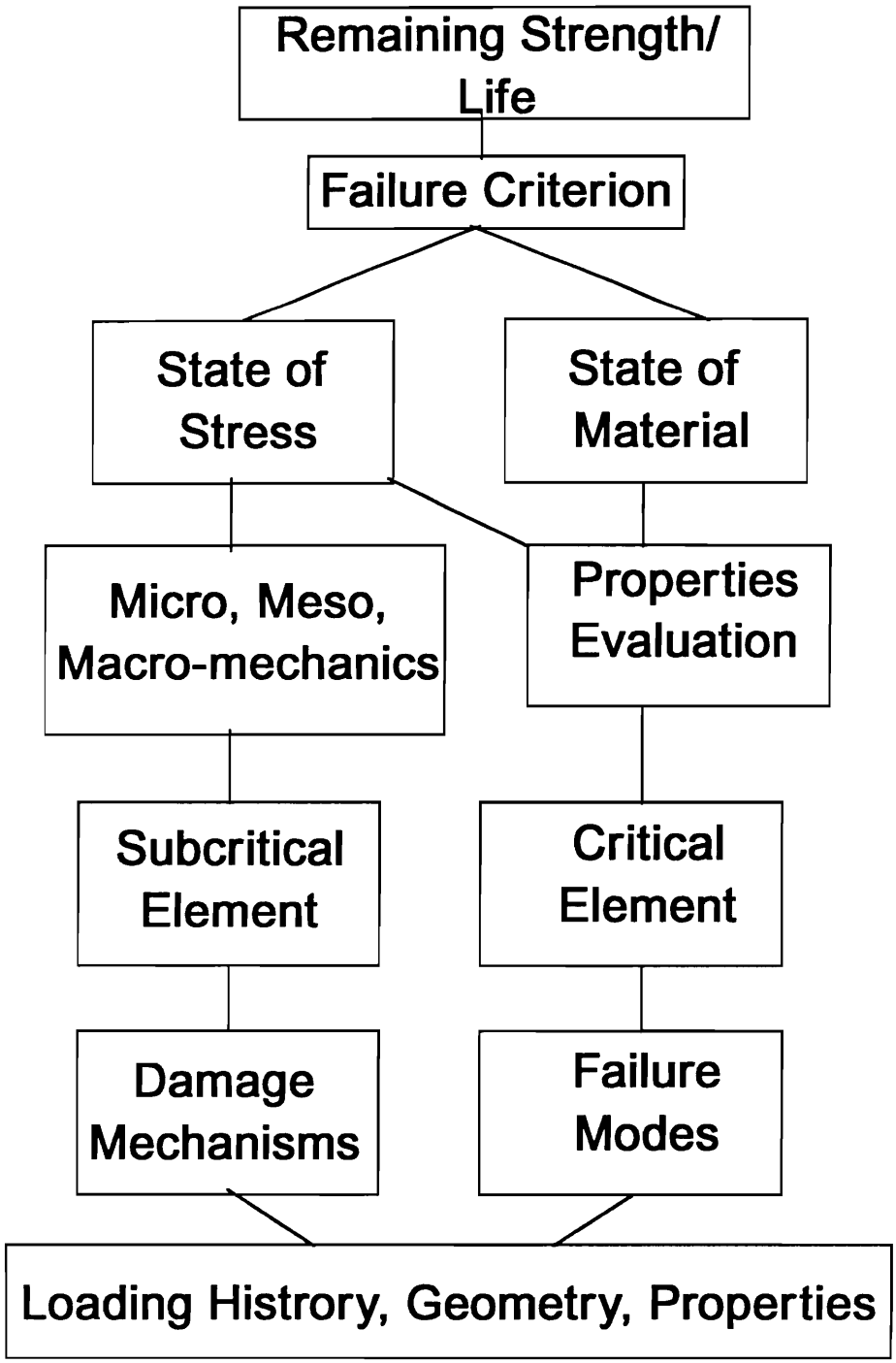

Figure 69 Schematic of Critical Element Model.

Based on the damage in the sub-critical element, the stresses in the critical element are calculated as a function of cycles. The critical element itself would exhibit time dependent property degradation (eg. strength degradation of 0° ply under fatigue loading represented by the S-N curve for the 0° ply, damage in the 0° ply in the form of interfacial damage, etc). This is obtained from experiments performed on 0° laminates. After each block of loading cycles, the stress and strength of the critical element are used in an appropriate failure function (eg. maximum stress/strain, Tsai-Hill etc) to predict the failure of the critical element. It is assumed that the failure of the laminate coincides with the failure of the critical element. The fatigue life is defined by the number of cycles required for the failure of the critical element.

9.3.2 Fatigue Life Prediction

The damage analysis results discussed in chapters 6,7 and 8 indicate that transverse matrix cracking, creep deformation in the 90° ply and local delaminations on the 0/90 interface are the main damage mechanisms associated with the sub-critical element. In the critical element, other than the strength reduction in the 0° ply characterized by the S-N curve of the 0° laminate, fiber-matrix debonding is observed in some laminates. Based on these experimental observations, a cumulative damage scheme is constructed to predict the fatigue life of cross-ply laminates. A schematic of the cumulative damage scheme is shown in figure 70. A detailed description of the scheme is provided in this section. The variation of the transverse crack density as a function of cycles is determined experimentally for the three material systems at different load levels. In order to construct a master curve, independent of the applied load level, the crack density is multiplied by a factor $\left[1 - \left(\frac{\sigma_{max}}{\sigma_{static}}\right)\right]$ and plotted against the number of cycles.

These data are fitted with a power law curve to obtain a single master curve that describes the variation of crack density as a function of cycles. The master curves for the three material systems are shown in figure 71. The master curve that describes the variation in crack density in the different material system

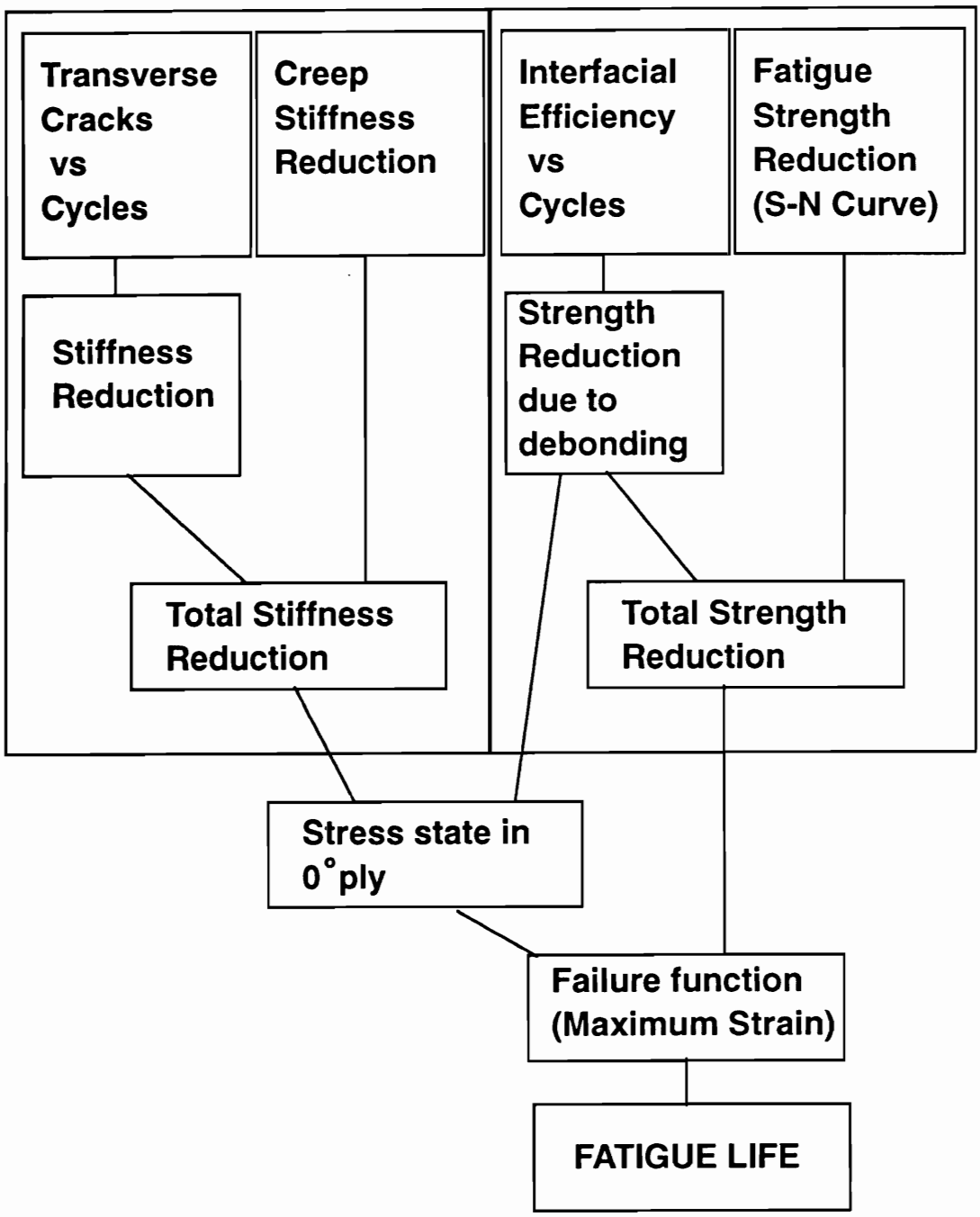

Figure 70 Schematic of cumulative damage scheme used for fatigue life prediction.

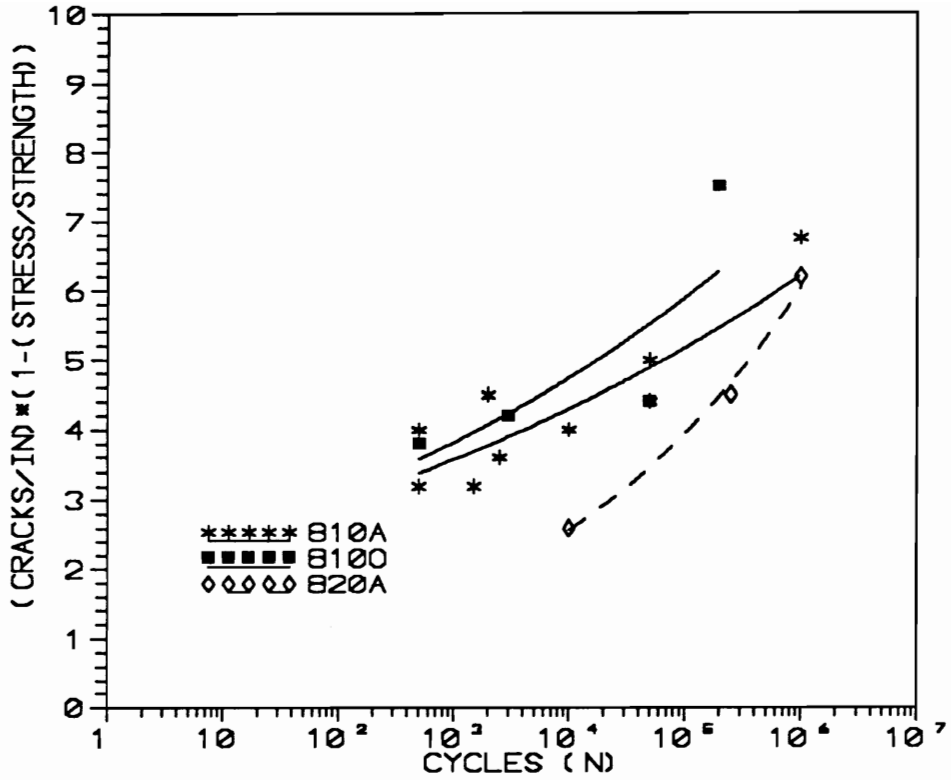

Figure 71 Variation of transverse crack density as a function of cycles in the cross-ply laminates of 810 A, 820 A and 810 O system

at different load levels (in the form of a power law curve) is provided as an input to the model. Using the shear lag model described in section 9.2, and the crack density variation provided as an input, the stiffness reduction in the 90° ply is calculated after each block of cycles. The stiffness reduction in the 90° ply due to creep (determined experimentally and discussed in detail in chapter 8) is also input into the model in the form of a power law curve. The total stiffness reduction in the 90° ply (due to damage and creep) after each block of cycles is estimated by adding the individual components. The stiffness of the entire laminate is then calculated using the rule of mixtures (equation 30). Classical Lamination Theory is used to calculate the stresses and strains in the 0° ply (using the damaged properties of the 90° ply), after each block of cycles. It must be mentioned here that this scheme neglects the interaction between the damage and creep phenomena.

The S-N curves for the 0° laminates of the three material system used in this study were not available. Hence, an S-N curve was assumed for each of the three material systems. Since the same fiber and the same matrix material were used, the same S-N curve was used for the three material systems. It must be mentioned here that the insitu S-N curve of the 0° ply in the cross-ply laminate could be different from that of the 0° laminate. This is because of the transverse stresses that are present in the 0° ply of the cross-ply laminate. These transverse stresses could initiate debonding in the 0° ply. As was discussed in section 9.1, the debonding in the 0° ply would result in a reduction in the efficiency of load transfer from the matrix to the fiber and vice-versa. This is accounted for by varying the efficiency factor η in the 0° ply as a function of cycles. Since there is no direct way to experimentally determine this variation, a polynomial function is assumed to describe the variation of η as a function of cycles. In section 9.1, a tensile strength model was described which predicts the tensile strength of a unidirectional laminate including the efficiency factor η. The polynomial describing the variation of η with cycles was used in conjunction with the tensile strength model to predict the insitu tensile strength variation of the 0° ply as a function of cycles. The predicted tensile strength is then used in the assumed S-N curve of the 0° ply to estimate the degradation of the insitu tensile strength of the 0° ply as a function of cycles.

The tensile strength and the tensile stress estimated thus are used in a maximum strain failure criterion after each block of cycles to check for the failure of the critical element. If the critical element fails, then the calculation is terminated and the number of cycles at which this occurs is assumed to be the fatigue life.

The influence of fiber-matrix interphase is included in the present model in a number of different levels. Different creep stiffness reduction curves and crack density variation curves are input into the model for the three material system with different interphases. The calculation of stiffness reduction using the shear lag model also includes the effects of interphase at a lamina level. The influence of interphase on the behavior of the critical element is also included in this model. This is done by varying the efficiency factor η which reflects the interfacial bonding condition.

In this section, the rationale behind using some specific forms of equations (which were not generated experimentally) to predict the fatigue life of cross-ply laminates with different interphase is discussed. The S-N curve for the 0° laminate was not experimentally generated because of the lack of availability of specimens for testing. As mentioned earlier, since the same fiber and matrix material were used in the three material systems, and since the influence of the interphase is introduced in the model through the efficiency factor η, the same S-N curve equation was used for all three material systems. An equation that is consistent with the typical S-N curves of graphite/epoxy 0° laminates was used. It was experimentally observed that the debonding characteristics in the 0° ply of the three material system were significantly different. This was used as a guide while choosing the functional relationships describing the variation of η as a function of cycles. It was reported in chapter 7 that the 810 O laminates exhibit extensive debonding in the 0° ply, while the 810 A laminates exhibit very few debonds. The 820 A laminates revealed intermediate amount of debonding in the 0° ply. In order to reflect this, it was assumed that η remains unchanged in the 810 A laminates and 820 A laminates. The stiffness reduction data reported in chapter 7 also indicate these trends. As was mentioned in the tensile strength modeling section, the interfacial efficiency (η) is directly related to the longitudinal stiffness. Degradation in η results in a

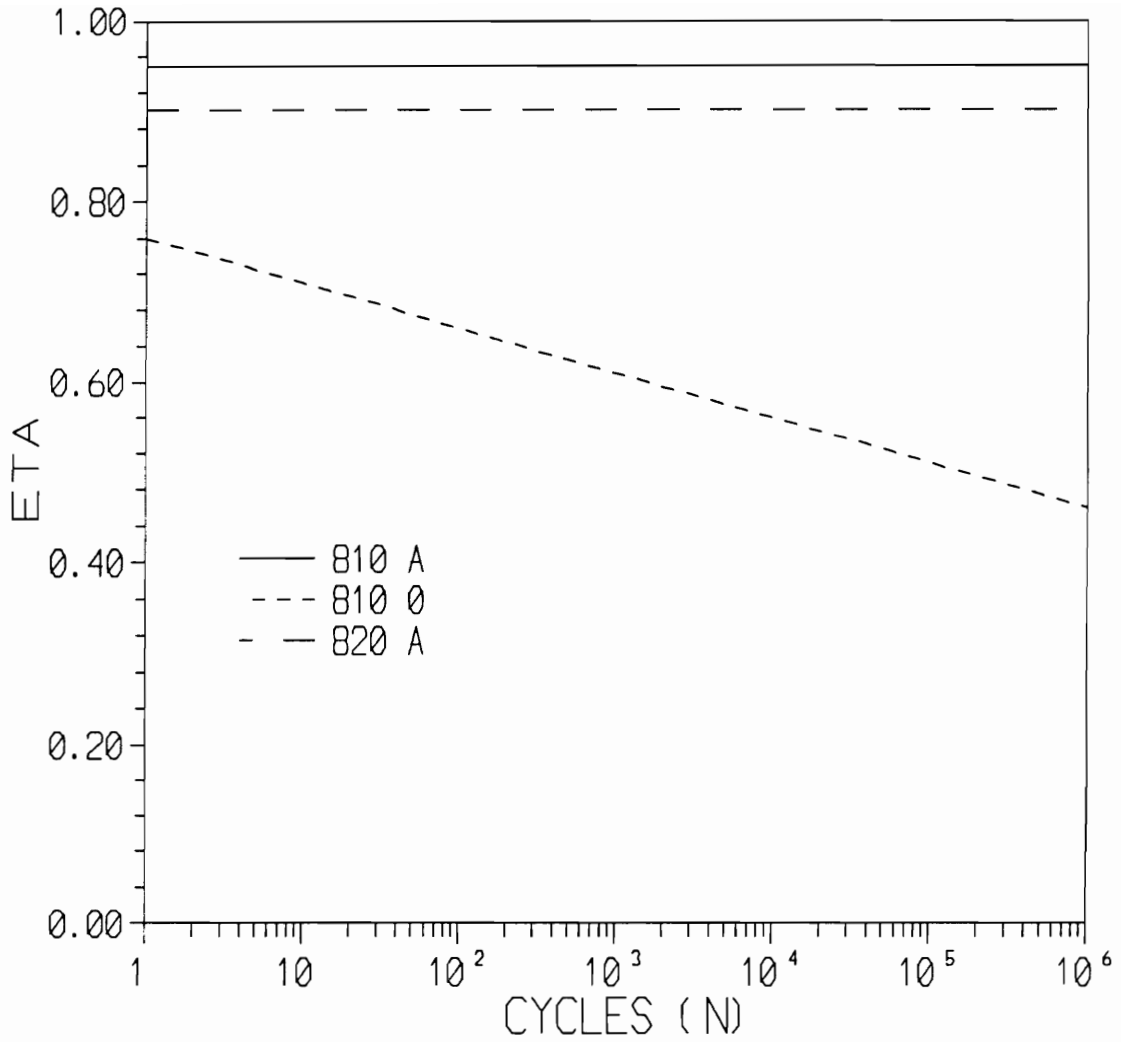

Figure 72 Variation of efficiency factor η as a function of cycles in the 810A, 820 A and 810 O system

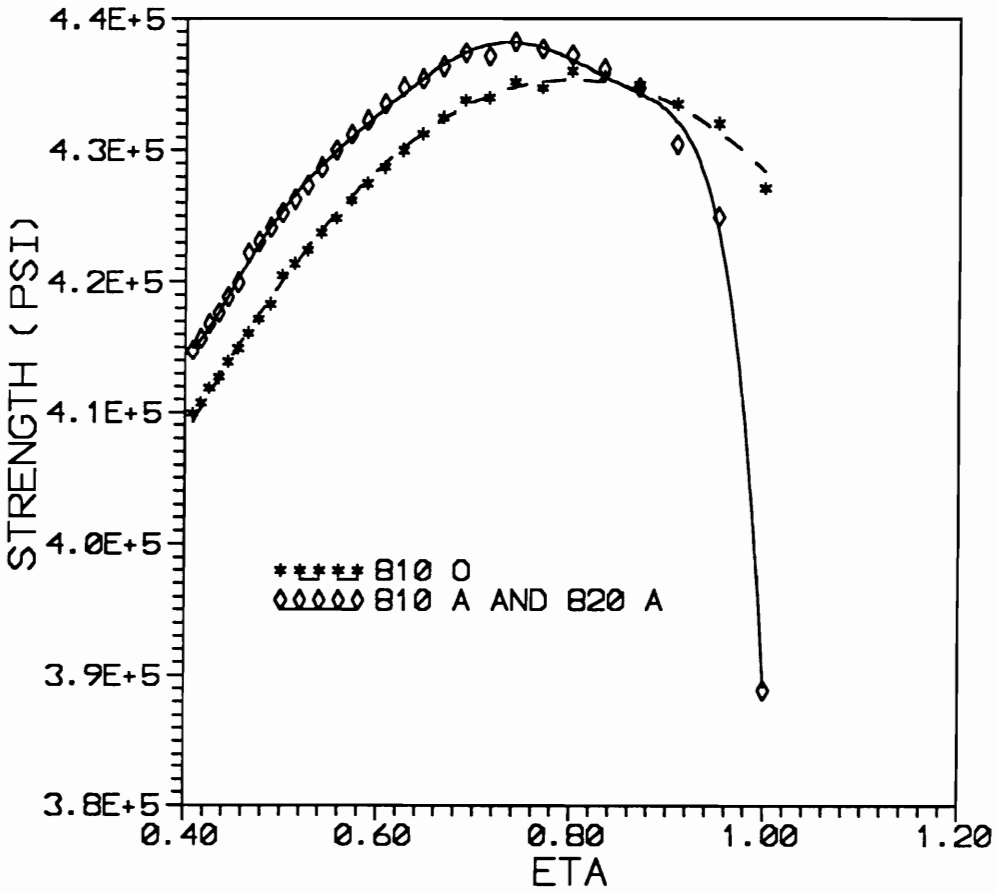

Figure 73 Variation of unidirectional tensile strength as a function of efficiency factor η for the 810 A, 820 A and 810 O system

reduction in the longitudinal modulus of the 0° ply of the laminate. Hence, the experimentally measured stiffness reduction data can be used directly to estimate the changes in η as a function of cycles. The stiffness reduction data (chapter 7) indicate that there is very little stiffness reduction in the 810 A and 820 A systems after the first 10 % of the life. Also, the amount of stiffness reduction is small, indicating that it is primarily due to matrix cracking in the 90° ply. This indicates that there is no significant stiffness reduction in the 0° ply of the laminate. Hence, it is assumed that η remains constant under fatigue loading in these two material systems. In contrast, there is significantly greater amount of stiffness reduction in the 810 O laminate. Also, there is appreciable stiffness reduction occuring in the laminate after the intial stiffness drop in the first 10 % of the life. This indicates that the stiffness of the 0° ply reduces as a function of cycles in this material system. In order to reflect this, a linear stiffness reduction equation is used for the 810 O system. The assumed variations of η as a function of cycles are shown in figure 72. The variation of tensile strength with η for the three material system, predicted by the model described in section 9.2 is depicted in figure 73. Note that the 810 A and 820 A system are represented by the same curve because all the parameters for these two system used in the model are identical. However, the interfacial shear strength for the 810 O system was assumed to be lower than that of the 810 A and 820 A system. This results in a different curve for the 810 O laminate. The figure suggests that the tensile strength increases initially as η reduces. However, for small values of η, the strength starts reducing significantly. Combining the relationship that describes the variation in η with cycles and the relationship that describes the variation in tensile strength with η, the variation in tensile strength with cycles can be obtained. This is combined with the assumed S-N curve to obtain the variation of insitu strength of the 0° ply of the three material systems.

Using these experimental data along with the assumed functional relationships described earlier, the fatigue lives of the 810 A, 820 A and 810 O laminates are predicted at various applied load levels. All the equations used for the three material system are listed in Table XVIII.

A comparison of the experimental and predicted fatigue lives for the three material system at the

Table XVIII Equations for the 810 A, 820 A and 810 O material system used in the fatigue damage and life prediction model

810 A	810 O	820 A
$n[1-(\sigma_{max}/\sigma_{ult})] = 2\ (N)^{0.08}$	$n[1-(\sigma_{max}/\sigma_{ult})] = 2\ (N)^{0.09}$	$n[1-(\sigma_{max}/\sigma_{ult})] = 0.4\ (N)^{0.2}$
$\varepsilon_0^{fat} = \varepsilon_0^{st}\ (1.06 - 0.012\ \ln(N)^{0.9})$	$\varepsilon_0^{fat} = \varepsilon_0^{st}\ (1.06 - 0.012\ \ln(N)^{0.9})$	$\varepsilon_0^{fat} = \varepsilon_0^{st}\ (1.06 - 0.012\ \ln(N)^{0.9})$
$\eta = 0.95$	$\eta = 0.76 - 3e\text{-}7*N$	$\eta = 0.90$
$E_{90}^{crp} = E_{90}\ [1.03\ (t)^{-0.008}]$	$E_{90}^{crp} = E_{90}\ [1.09\ (t)^{-0.020}]$	$E_{90}^{crp} = E_{90}\ [1.03\ (t)^{-0.008}]$

n = Number of transverse cracks/in

N = Number of cycles

t = Time (sec)

η = Efficiency factor

E_{90} = Unidirectional transverse stiffness (msi)

E_{90}^{crp} = Unidirectional transverse stiffness including creep effects (msi)

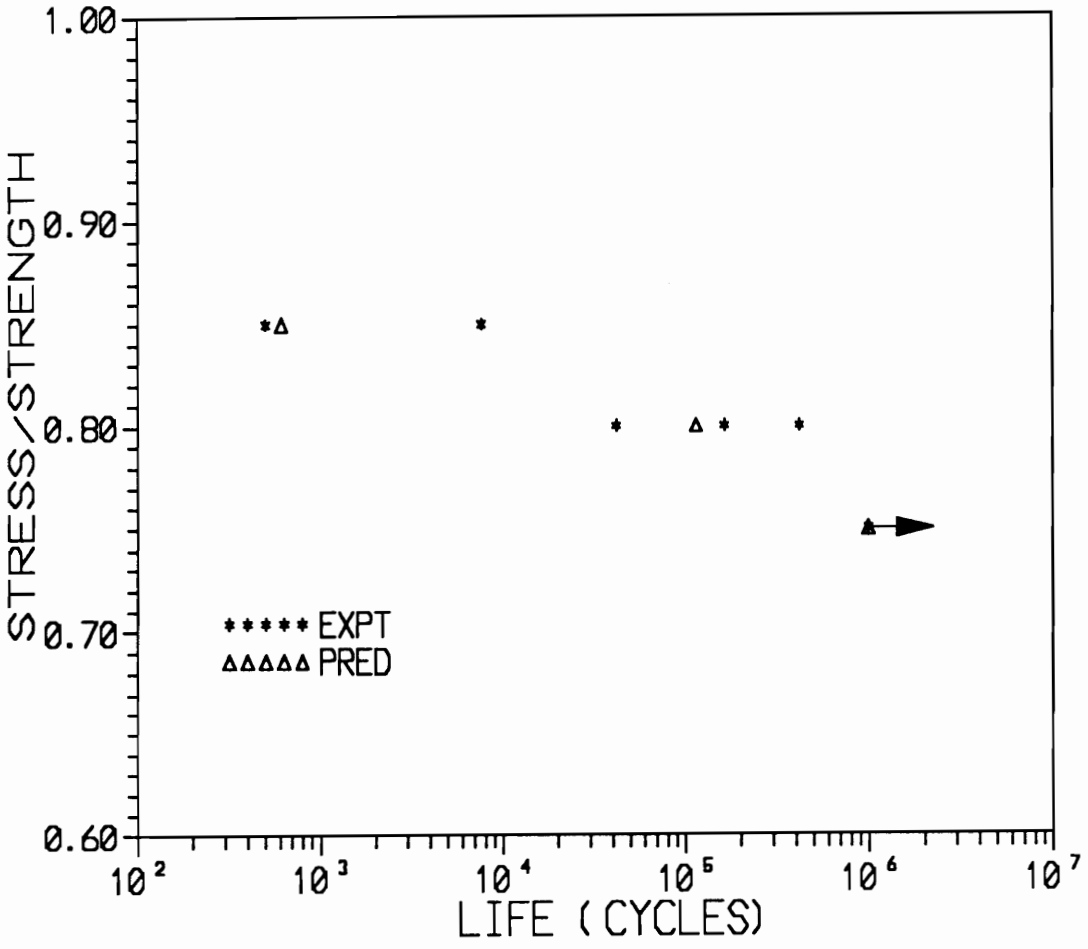

Figure 74 Comparison of the experimental and predicted fatigue life of the 810 A cross-ply laminates.

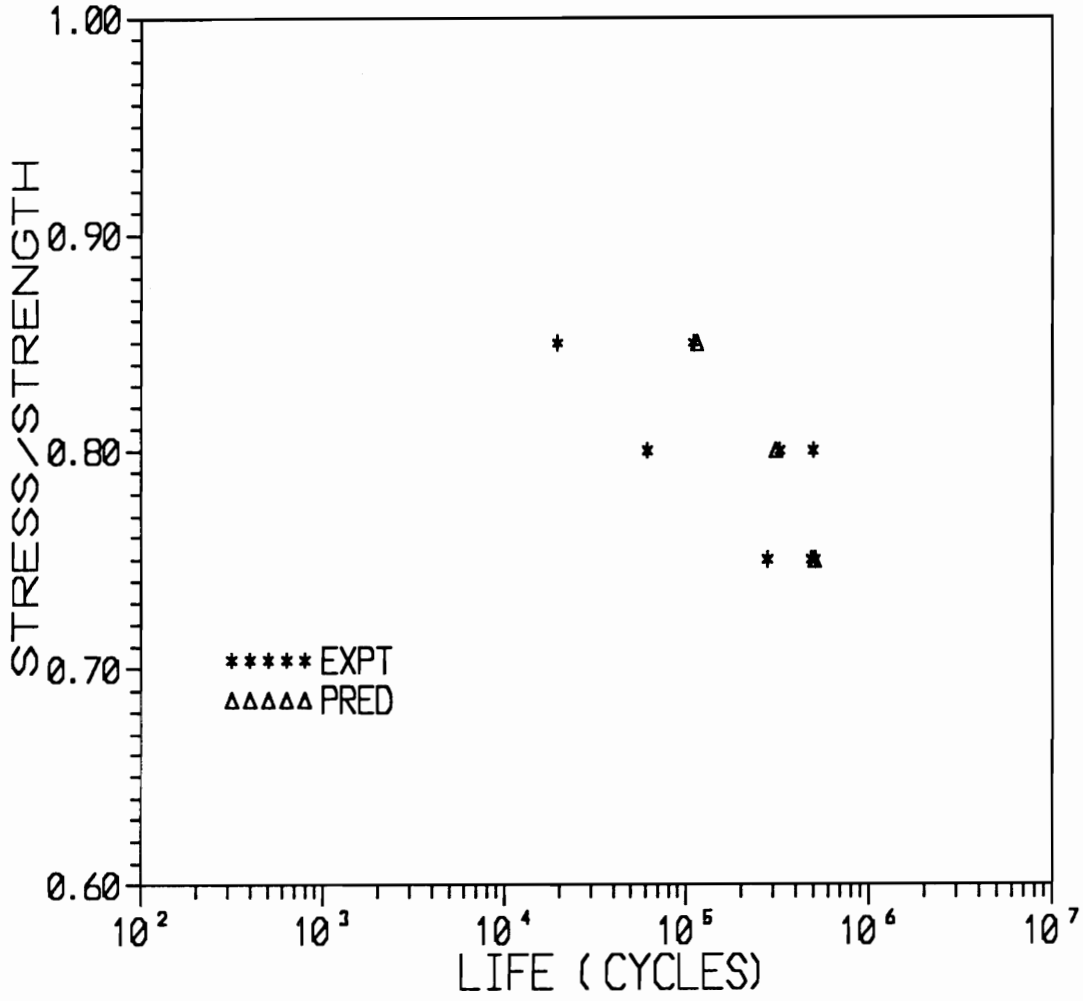

Figure 75 Comparison of the experimental and predicted fatigue life of the 810 O cross-ply laminates.

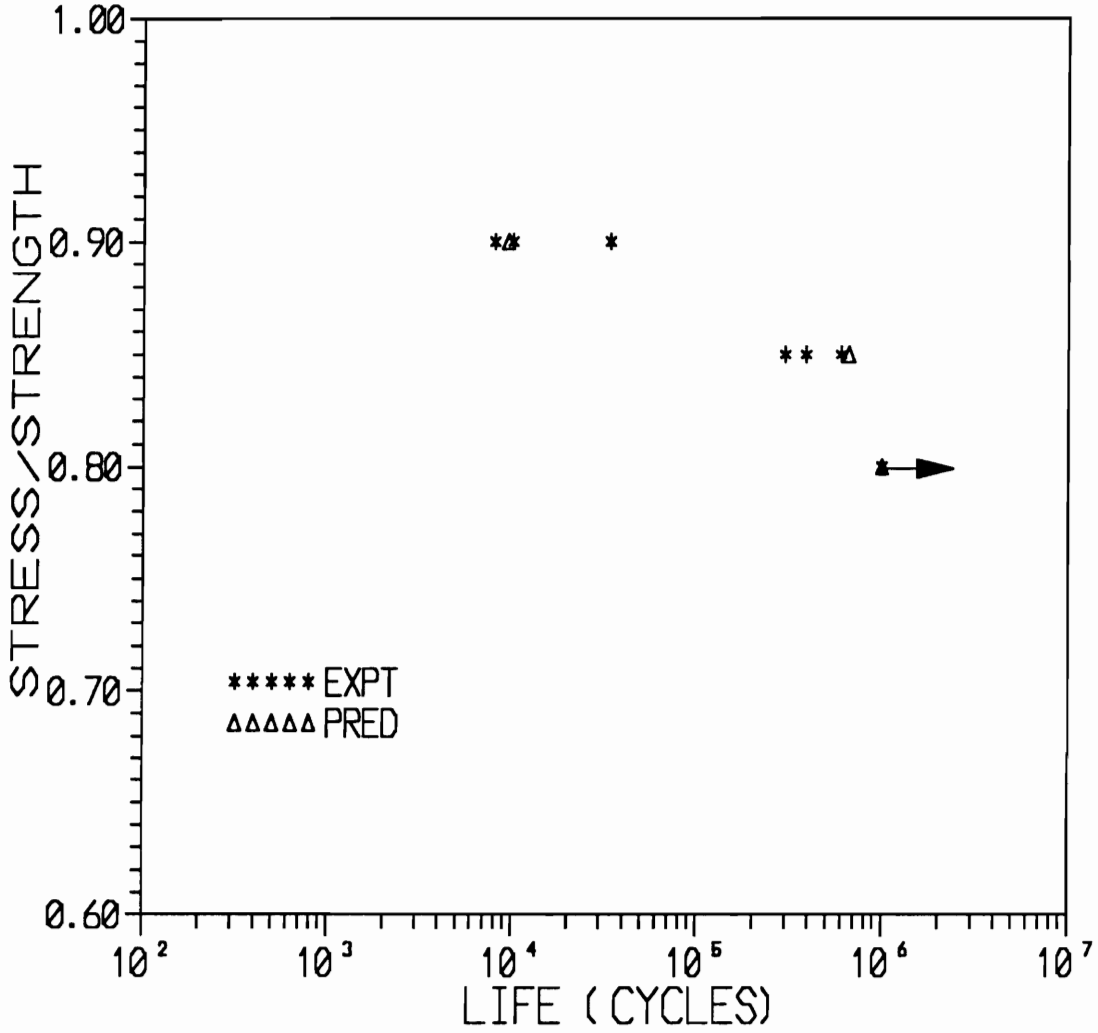

Figure 76 Comparison of the experimental and predicted fatigue life of the 820 A cross-ply laminates.

different load levels is shown in figures 74 through 76. The figures show good correlation between experimental and predicted fatigue lives. Some of the experimental observations that are predicted well by the model and some limitations of the model are listed below

- The fatigue lives of the 820 A laminates are higher than those of the 810 A and 810 O laminate at all three load levels.
- The 810 A laminates have lower life at 85 % load level and higher life at 75 % load level compared to the 810 O laminate.
- The S-N curve for the 810 O laminate has the highest slope, followed by the 820 A and 810 A laminates.

It must be pointed out that in order to obtain better estimates of fatigue lives and minimize the assumptions involved in the life prediction scheme, the following approach should be used.

- The S-N curves for the 0° laminates must be obtained experimentally.
- The variation of η as a function of cycles should be experimentally determined. It must be mentioned here that a method that involves the measurement of hysteresis loss as a function of cycles has been used in ceramic matrix composites to measure the effect of sliding friction at fiber-matrix debonds. This could yield quantitative information about the extent of debonding in the material. This method could be used to obtain the variation of η as a function of cycles.
- The interaction between damage and creep must be experimentally characterized and used in the model.

Based on the experimental results and the predictions from the model, it is claimed that the presence of interfacial debonding influences the fatigue behavior in the following manner. In general, the presence of fiber-matrix debonding reduces the stress concentration effects and increases the ineffective length. In the high stress, low life situation, the stress concentration effects control the laminate failure. The presence of debonds in the 0° ply alleviates the stress concentration effects in this regime and increases the fatigue life of the 810 O laminates. In the low load, long life regime, the ineffective length controls

the final failure. The presence of debond increases the ineffective length and reduces the fatigue life under these conditions. This is reflected in the greater slope of the S-N curve of the 810 O laminates. It can thus be concluded that for the material system under investigation, the presence of fiber-matrix debonds in the 0° ply shifts the S-N curve to the right and also increases the slope of the S-N curve. Depending upon the extent of debonding, the fatigue lives of the cross-ply laminates are altered differently.

9.3.3 Fatigue Damage Prediction

The stiffness reduction in the cross-ply laminate predicted using shear lag analysis results (equation 29) is used to estimate the amount of damage in the laminate as a function of cycles. Here, damage is defined as

$$D(n) = 1 - \left(\frac{E(n)}{E_o} \right) \tag{80}$$

where D(n) and E(n) are damage and stiffness after n cycles, and E_o is the initial stiffness of the laminate. In the fatigue experiments described in chapter 7, the dynamic stiffness was monitored as a function of cycles. These values could be used in equation 31, instead of the quasi-static stiffness values, to obtain an estimate of the damage in the laminate. The experimental and predicted variation of damage with normalized cycles for the three material system at different load levels are displayed in figure 77, 78 and 79. The figures indicate that the damage accumulation predicted by the model agrees well with the experimental data.

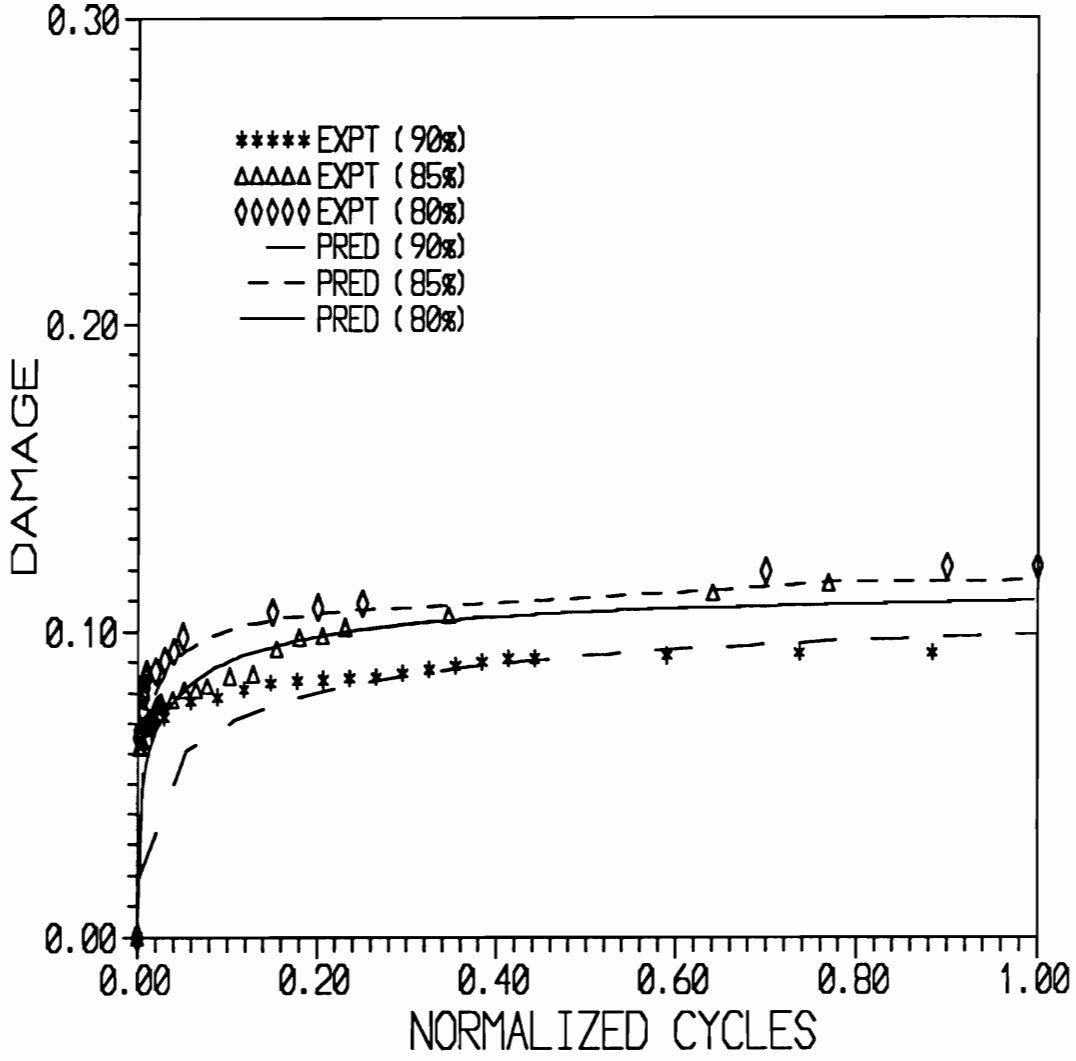

Figure 77 Comparison of the experimental and predicted variation of damage in 820 A cross-ply laminates.

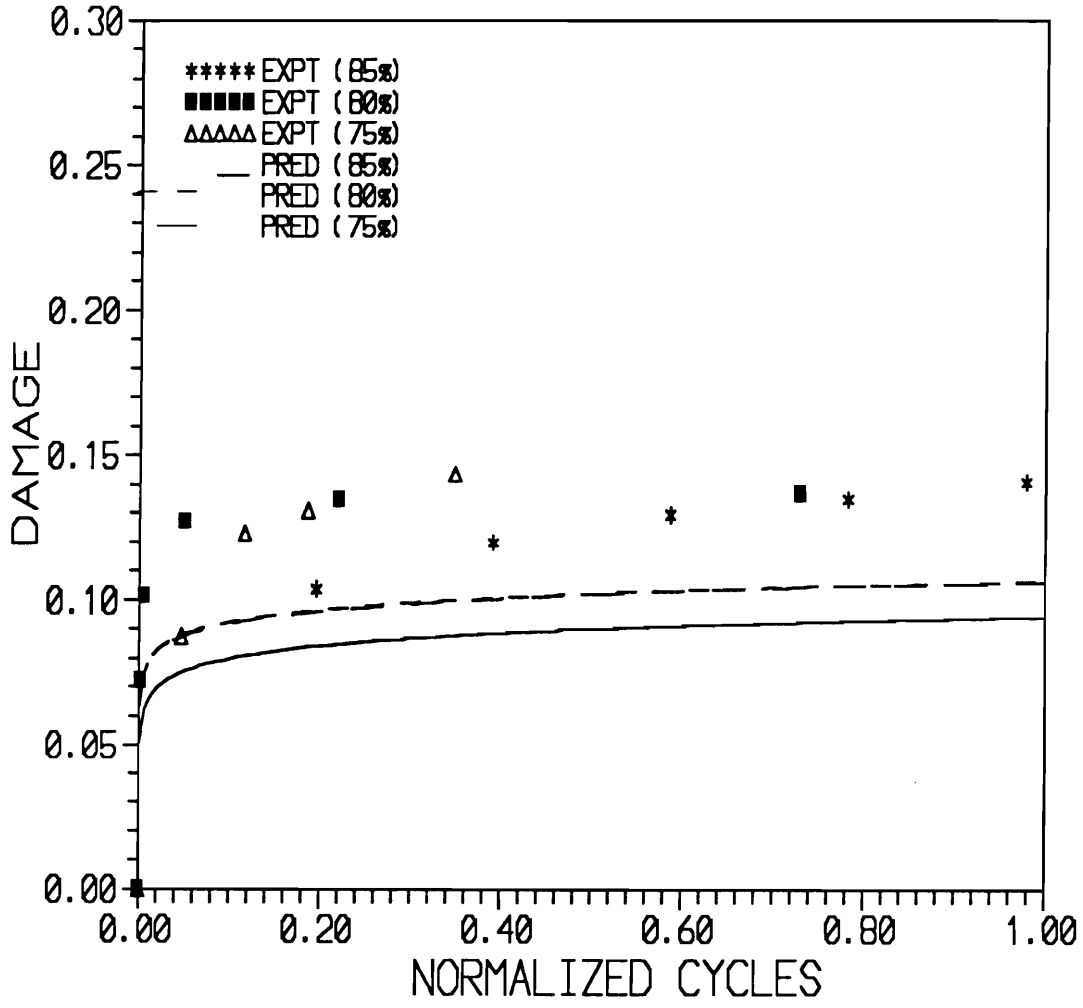

Figure 78 Comparison of the experimental and predicted variation of damage in 810 A cross-ply laminates.

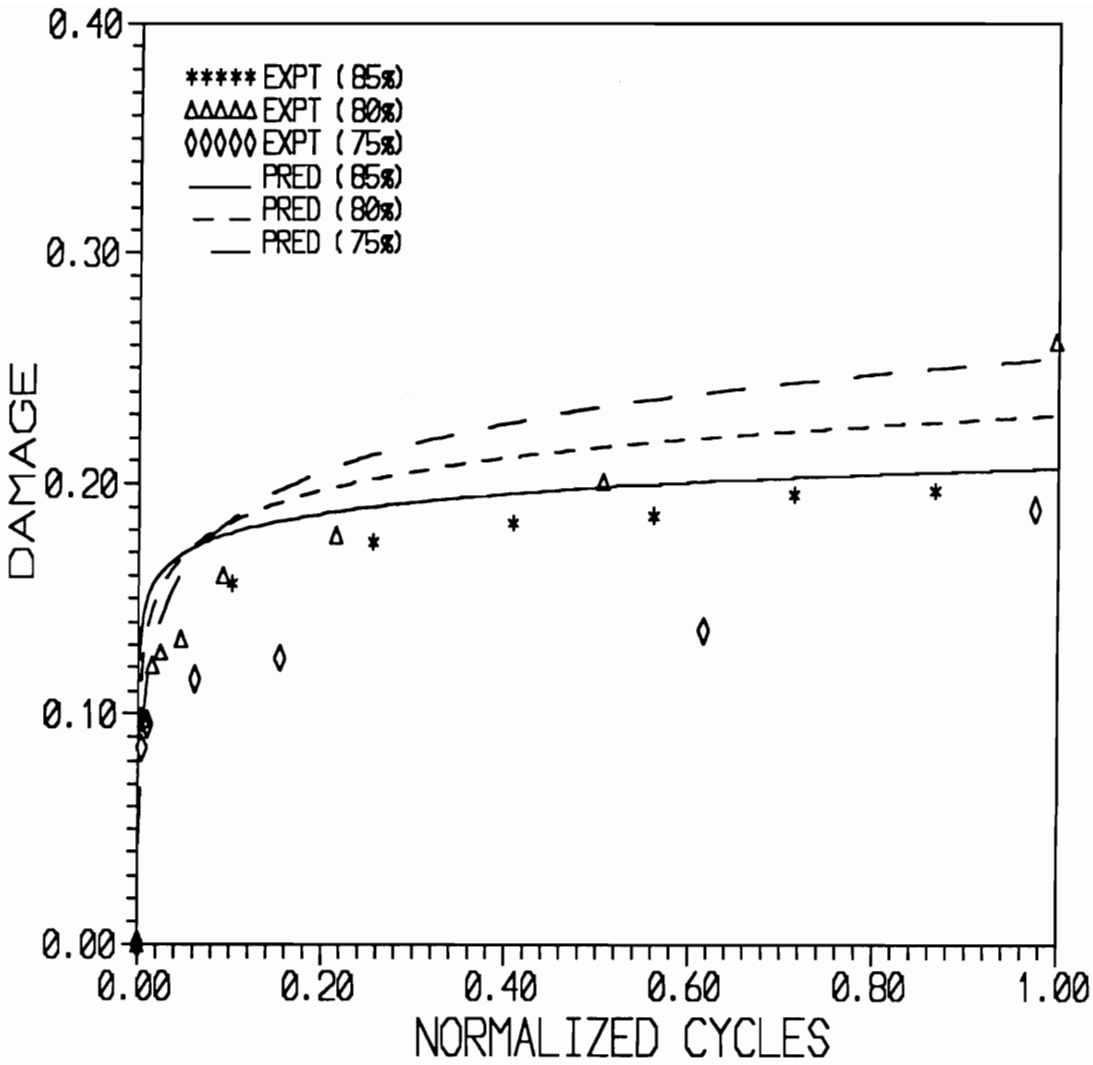

Figure 79 Comparison of the experimental and predicted variation of damage in 810 O cross-ply laminates.

10.0 CLOSURE

In this study, the influence of fiber surface treatment and fiber sizing on the mechanical properties of unidirectional and $(0,90_3)_s$ cross-ply laminates was studied. Three material systems having the same Apollo carbon fiber and HC 9106-3 toughened epoxy matrix, but with different fiber surface treatment and fiber sizing, were used in this study. Detailed description of the material systems is given in section 3.1. For convenience, description of the three material systems provided in Table I (section 3.1) is reproduced here.

	810 A	820 A	810 O
Fiber	Apollo	Apollo	Apollo
Matrix	HC 9106-3	HC 9106-3	HC 9106-3
Surface Treatment	100 %	200 %	100 %
Sizing	Bisphenol-A	Bisphenol-A	PolyVinylPyrrolidone

The presence of different interphase in the three material system was confirmed using a permanganic etching technique. The single fiber fragmentation test (SFFT) results indicate that the interfacial shear strength (ISS) of the 810 O system is significantly lower than that of the other two system. The 810 A and 820 A material system possess similar ISS. The ISS estimated using the meso-indentation technique (MIT) indicates that the 820 A system has the highest ISS, and the 810 A and 810 O system possess similar ISS.

The unidirectional longitudinal and transverse properties were obtained from tensile tests on $(0)_8$

and $(90)_{12}$ laminates. Results indicate that the longitudinal tensile strength and strain to failure of the 810 O system is greater than that of the other two system, while the stiffness of this material system is lower than that of the other two material system. The 810 A and 820 A system possess similar longitudinal tensile strength and failure strain and longitudinal stiffness. The transverse tensile tests indicate that the 820 A system has the greatest strength, while the 810 O system has the lowest strength. Post failure SEM analysis reveals good bonding between the fiber and the matrix in the 820 A system and poor fiber-matrix bonding in the 810 O system.

The tensile test results on cross-ply laminates indicate that the 810 A and 810 O system possess similar strength, while the strength of the 820 A system is significantly lower. The 810 O laminates have the highest failure strain while the 820 A laminates have the lowest failure strain. Nondestructive test results reveal that the 810 A laminate exhibits delayed onset of transverse matrix cracking, no longitudinal splitting in the 0° ply, no local delaminations on the 0/90 interface and few fiber fractures. The final failure is controlled by the local stress concentration effects near broken fibers in the 0° ply. In contrast, the 810 O laminate exhibits early transverse cracking, numerous longitudinal splits, a few local delaminations on the 0/90 interface, and a lot of fiber fractures. The final failure is controlled by global strain in the laminate. The 820 A laminate exhibits delayed transverse cracking, no longitudinal splitting or local delaminations, and very few fiber fractures. The final failure is controlled by local stress concentration effects near broken fibers in the 0° ply of the laminate. ***The damage mechanisms and failure modes in cross-ply laminates with different fiber-matrix interphases are different.***

Results indicate that the fatigue life of cross-ply laminate is sensitive to the nature of interphase present in the material system. The 820 A laminates have greater life at all load levels used in this study. A comparison of the fatigue lives of the 810 A and 810 O laminates reveals that the 810 O laminates have longer fatigue lives at higher load levels and lower lives at lower load levels. The cross-ply laminates with different fiber-matrix interphases exhibit varied damage mechanisms and failure modes. Damage analysis results indicate that all three material system exhibit extensive transverse ply cracking at all load levels.

In addition, the 810 A laminate reveals edge delamination at high load levels, very little longitudinal splitting, and no local delaminations. The 820 A laminates exhibit moderate amounts of longitudinal splitting and no local or edge delaminations. In contrast, the 810 O laminates exhibit extensive distributed longitudinal splitting and local delaminations at all load levels. The stiffness reduction results also confirm the presence of greater amount of damage in the 810 O laminates. Fractographic analysis of failed specimens indicates that the longitudinal splits in 810 O laminates are interfacial debonds. Photographs of the failed specimens from the three material system show that the failure of the 810 A and 820 A laminates are controlled by stress concentration effects in the 0° ply while the failure of the 810 O laminate is controlled by the global strain to failure of the 0° ply.

The short term DMA creep results and the room temperature tensile creep test results indicate that the 810 O laminates exhibit significantly greater amounts of changes in flexural creep compliance compared to the other two material systems. The room temperature tensile creep tests on cross-ply laminates indicate that the 90° plies in the laminate exhibits creep deformation and damage in the form of transverse matrix cracks and longitudinal splits in the 0° ply.

In this study, a model was developed to predict the tensile strength of unidirectional laminates including the effect of interphase. The model uses a shear lag analysis in conjunction with Batdorf's tensile strength prediction scheme. The model predicts the tensile strength, failure mode (presence/absence of fiber-matrix debonding prior to final failure) and the number of fiber fractures. The tensile strength and failure mode predicted using this model agrees well with the experimental observations for the 810 A, 810 O and 820 A material system. Parametric studies were conducted to study the influence of interfacial shear strength, weibull parameters (fiber) and 'efficiency factor (η) on the tensile strength and failure modes of unidirectional laminates. ***Results indicate that the tensile strength of the unidirectional laminates can be optimized by tailoring the interphase.***

The onset and progression of transverse matrix cracking in cross-ply laminates was predicted using a modified form of 1 dimensional shear lag model. A novel scheme that uses the weibull strength statistics

of the 90° ply, was used to predict the number of transverse matrix cracks and the corresponding stiffness reduction as a function of applied load. The predicted matrix cracking characteristics for the 810 A, 810 O and 820 A laminates agree well with the experimental values.

The unidirectional tensile strength prediction model and the transverse crack prediction model were used in a cumulative damage scheme, to predict the fatigue life of cross-ply laminates. The cumulative damage scheme used in this study is based on the critical element model. A schematic of the fatigue life prediction model is shown in the figure below (reproduction of figure 76). The predicted fatigue life matches well with the experimental values for the three material systems at the different load levels.

Appendix 1

NOMENCLATURE USED IN THE MODEL

r_f = Fiber radius

r_{fi} = Radius of inner core

E_{f2} = Fiber modulus

E_{fi} = Stiffness of the inner core

i = Number of broken fibers in the inner core

v_f = Fiber volume fraction in the average composite

v_f' = Fiber volume fraction in the inner core

u_{fi} = Displacement of inner core

u_{f2} = Displacement of adjacent fiber

u_c = Displacement of the average outer composite ring

$d = r\,(1/v_f) - 1))$

b = Thickness of the matrix region over which stress transfer occurs (2*d)

η = Efficiency factor

G_m = Shear modulus of the matrix material

E_x = Axial modulus of the average composite material

σ_a = Applied external stress

E_m = Young's modulus of matrix

τ_i = Interfacial shear strength

m = Weibull shape factor for the fiber

σ_0 = Weibull location parameter for the fiber

N = Total number of fibers in the composite

L = Length of the test specimen

δ_i = Elastic ineffective length

δ_i^* = Plastic ineffective length

C_i = Elastic stress concentration factor

C_i^* = Plastic stress concentration factor

n_i = Number of nearest neighboring fibers

Appendix 2

Calculation of geometric parameters

Consider a single fiber with matrix material around it. If the radius of the fiber is r_f, and the fiber volume fraction is v_f, then the thickness of the matrix layer is calculated as follows

$$v_f = r_f^2 / r_m^2$$

$$r_m = r_f / (v_f)^{0.5}$$

The thickness of the matrix layer is obtained as

$$d = r_m - r_f$$

$$d = r_f \left(\frac{1}{\sqrt{v_f}} - 1 \right)$$

Consider an inner core of radius r_{fi} that consists of i broken fibers. Let r'_m be the radius of the matrix material that surrounds the inner core of broken fibers. For this arrangement, the various geometric parameters are calculated as follows

$$v_f = i\, r_f^2 / r'^2_m$$

$$r_m' = \frac{\sqrt{i}\, r_f}{\sqrt{v_f}}$$

The radius of the inner core of broken fibers can be written as

$$r_{fi} = r_m' - d$$

$$r_{fi} = \frac{\sqrt{i}\, r_f}{\sqrt{v_f}} + r_f - \frac{r_f}{\sqrt{v_f}}$$

$$r_{fi} = r_f \left[\frac{\sqrt{i} - 1}{\sqrt{v_f}} + 1 \right]$$

The various geometric parameters used in the tensile strength prediction model are listed below

$$d = r_f \left(\frac{1}{\sqrt{v_f}} - 1 \right)$$

$$r_{fl} = r_f \left(\frac{\sqrt{i} - 1}{\sqrt{v_f}} + 1 \right)$$

$$r_m = r_{fl} + 2\,d$$
$$r_{f2} = r_m + 2\,r_f$$
$$r_c = r_{f2} + 2\,d$$

The damaged modulus of the inner core is calculated using the rule of mixture. However, the fiber volume fraction in the inner core is different from that of the composite material. The fiber volume fraction of the inner core is calculated as follows

$$v_f' = i\, r_f^2 / r_n^2$$

This new volume fraction is used to estimate the stiffness of the inner core as

$$E_n = (v_f' * E_f) + (1 - v_f') * E_m$$

Appendix 3

Longitudinal stiffness prediction using Concentric Cylinders Model (CCM)

1. Auxiliary Problem

A solution (using CCM) to the problem of a single fiber embedded in an infinite matrix is outlined in this section. The solution procedure used in this analysis is similar to that described in reference [25]. A displacement formulation is used to solve the problem, and the external loads are applied in the form of tractions. Figure A1 shows the schematic of the concentric cylinders assemblage model. Since the problem is axisymmetric, the polar coordinates are used to solve the problem. Throughout this section, superscripts f and m represent the quantities in the fiber and matrix phases respectively. It is assumed that the fiber and matrix are homogeneous, linearly elastic materials. The matrix is assumed to be isotropic and the fiber transversely isotropic. Due to axisymmetry, the displacement field in the two domains can be expressed in the following form

$$u_r^{(m)} = B_1^{(m)} r + \frac{B_2^{(m)}}{r}$$
$$u_\theta^{(m)} = 0$$
$$u_z^{(m)} = D z$$

(a1)

$$u_r^{(m)} = B_1^{(f)} r + \frac{B_2^{(f)}}{r}$$
$$u_\theta^{(f)} = 0$$
$$u_z^{(f)} = \eta D z$$

Note that in writing the above displacement fields, it has been assumed that the axial displacement is not continuous at the fiber-matrix interface. The efficiency factor η has been introduced in these relationships such that $\eta = u_f/u_m$. For such a displacement field, the equations of elasticity reduce to the following simple form

Strain-Displacement Relationship

$$\varepsilon_{rr}^{(n)} = \frac{du_r^{(n)}}{dr}$$
$$\varepsilon_{\theta\theta}^{(n)} = \frac{u_\theta^{(n)}}{r} \qquad \text{(a2)}$$
$$\varepsilon_{zz}^{(n)} = \frac{du_z^{(n)}}{dz}$$
$$\varepsilon_{rz} = \varepsilon_{\theta z} = \varepsilon_{r\theta} = 0$$

Constitutive Relationship

$$\sigma_{zz}^{(n)} = C_{11}^{(n)} \varepsilon_{zz} + C_{12}^{(n)} \varepsilon_{rr}^{(n)} + C_{13}^{(n)} \varepsilon_{\theta\theta}^{(n)}$$

$$\sigma_{rr}^{(n)} = C_{12}^{(n)} \varepsilon_{zz} + C_{22}^{(n)} \varepsilon_{rr}^{(n)} + C_{23}^{(n)} \varepsilon_{\theta\theta}^{(n)} \qquad \text{(a3)}$$

$$\sigma_{\theta\theta}^{(n)} = C_{12}^{(n)} \varepsilon_{zz} + C_{23}^{(n)} \varepsilon_{rr}^{(n)} + C_{22}^{(n)} \varepsilon_{\theta\theta}^{(n)}$$

where $C_{ij}^{(n)}$ are the elements of the reduced stiffness matrix of the constituent phases. Substituting the assumed displacement functions in equations a2 and a3 yields the various components of the stress tensor in the fiber and matrix phases.

In order to evaluate the constants that appear in the assumed displacement functions, the displacement and traction continuity conditions are enforced at the fiber-matrix interface. It is required that the radial displacements and radial stresses in the fiber and matrix be equal at the fiber-matrix interface. This is expressed as

$$u_r^{(f)} = u_r^{(m)} \qquad \text{(a4)}$$

$$\sigma_{rr}^{(f)} = \sigma_{rr}^{(m)} \qquad \text{at} \qquad r = r_f \qquad \text{(a5)}$$

In this analysis, loads are applied in the form of tractions. Since the stresses in the fiber and matrix are different, the traction boundary condition is applied by considering that the applied longitudinal load is equal to the sum of the volume averaged stresses in the longitudinal direction. This expressed

mathematically as

$$\int \sigma_{zz}^{(f)}\, dV + \int \sigma_{zz}^{(m)}\, dV = \sigma_{zz}^{app} \tag{a6}$$

It is also required that the radial stress σ_{rr} vanish as r -> ∞ . This is expressed as

$$\left(\sigma_{rr}^{(m)}\right)_{r \to \infty} = 0 \tag{a7}$$

In order for the displacement to be finite at the center of the fiber, the constant $B_2^{(f)}$ is set equal to 0. The other four constants $B_1^{(f)}$, $B_1^{(m)}$, $B_2^{(m)}$ and D are evaluated by solving equations a4-a7.

2. Complete Solution

The fiber-fiber interactions are accounted for in an approximate sense using the Mori-Tanaka average stress scheme. A detailed description of this method is available in reference [25]. The general procedure is outlined here for completeness.

The solution of a single fiber embedded in an infinite matrix subjected to uniform longitudinal loading, is obtained first using the method outlined in the previous section (Auxiliary problem). The stresses obtained from the auxiliary problem are written in the following form

$$\sigma_{rr}^{(n)} = h_{rr}^{(n)}\, \sigma_0 \tag{a8}$$

$$\sigma_{zz}^{(n)} = h_{zz}^{(n)}\, \sigma_0 \tag{a9}$$

where h_{rr} and h_{zz} are defined as the concentration factors in the fiber and matrix phases. These concentration factors are averaged over the entire volume of the composite to obtain the volume averaged concentration factors as follows

$$\left\langle h_{\alpha\beta}^{(n)} \right\rangle = \frac{1}{\pi \left(r_o^2 - r_i^2\right)} \int_0^{2\pi} \int_{r_i}^{r_o} h_{\alpha\beta}^{(n)}\, r\, dr\, d\theta \tag{a10}$$

where n = fiber, matrix

$\alpha\beta$ = rr and zz

In order to account for the fiber-fiber interactions in an approximate sense, the applied external load is replaced by the unknown average stress $\langle\sigma_{zz}^{(m)}\rangle$ and $\langle\sigma_{rr}^{(m)}\rangle$. These average stresses are estimated using the solution to the auxiliary problem and the rule of mixtures approximation written in the following form

$$v_f \left\langle \sigma_{zz}^{(f)} \right\rangle + v_m \left\langle \sigma_{zz}^{(m)} \right\rangle = \sigma_0 \tag{a11}$$

$$v_f \left\langle \sigma_{rr}^{(f)} \right\rangle + v_m \left\langle \sigma_{rr}^{(m)} \right\rangle = 0 \tag{a12}$$

The volume averaged stresses $\langle\sigma_{zz}^{(n)}\rangle$ and $\langle\sigma_{rr}^{(n)}\rangle$ can be written in terms of the volume averaged concentration factors in the following form

$$\left\langle \sigma_{\alpha\beta}^{(n)} \right\rangle = \left\langle h_{\alpha\beta}^{(n)} \right\rangle \left\langle \sigma_{zz}^{(m)} \right\rangle \tag{a13}$$

where n = fiber, matrix

$\alpha\beta$ = rr and zz

Using equation a13 in equations a11 and a12 we obtain

$$v_f \left(\left\langle h_{zz}^{(f)} \right\rangle \left\langle \sigma_{zz}^{(m)} \right\rangle \right) + v_m \left\langle \sigma_{zz}^{(m)} \right\rangle = \sigma_0 \tag{a14}$$

$$v_f \left(\left\langle h_{rr}^{(f)} \right\rangle \left\langle \sigma_{zz}^{(m)} \right\rangle \right) + v_m \left\langle \sigma_{rr}^{(m)} \right\rangle = 0 \tag{a15}$$

The average stresses $\langle\sigma_{zz}^{(m)}\rangle$ and $\langle\sigma_{rr}^{(m)}\rangle$ are estimated by solving equations a14 and a15. The complete solution to the problem is obtained by replacing the applied external load with $\langle\sigma_{zz}^{(m)}\rangle$ and $\langle\sigma_{rr}^{(m)}\rangle$. The longitudinal stresses in the fiber and matrix are written as

The strains in the fiber and matrix are estimated using the constitutive relationships (equation a3). The average strain in the composite is estimated using the rule of mixtures as

$$\sigma_{xx}^{(n)} = h_{xx}^{(n)} \left\langle \sigma_{xx}^{(m)} \right\rangle \tag{a16}$$

$$\varepsilon_{xx}^{tot} = v_f \, \varepsilon_{xx}^{(f)} + v_m \, \varepsilon_{xx}^{(m)} \tag{a17}$$

The average stiffness of the laminate in the longitudinal direction is calculated as

$$E_{11} = \frac{\sigma_0}{\varepsilon_{xx}^{tot}} \tag{a18}$$

Note that the average stiffness estimated using the above equation is a function of the efficiency factor η. The efficiency factor can be estimated using this equation, if the longitudinal stiffness of the unidirectional composite is known. Using the properties for the Apollo fibers and HC 9106-3 matrix [16] in the above analysis, the variation of longitudinal stiffness with η was determined and is plotted as figure A2. Results indicate that the longitudinal stiffness is a non-linear function of η. As η -> 1, the stiffness of the composite approaches the value predicted by the rule of mixtures, which assumes perfect bonding. As η -> 0, the stiffness of the composite approaches the stiffness of the matrix. This is because no load is being transferred to the fiber, and all the load is being carried by the matrix material. The efficiency factor η for a given material system can be estimated using the longitudinal modulus (determined from a tensile test on a unidirectional composite) in equation a18.

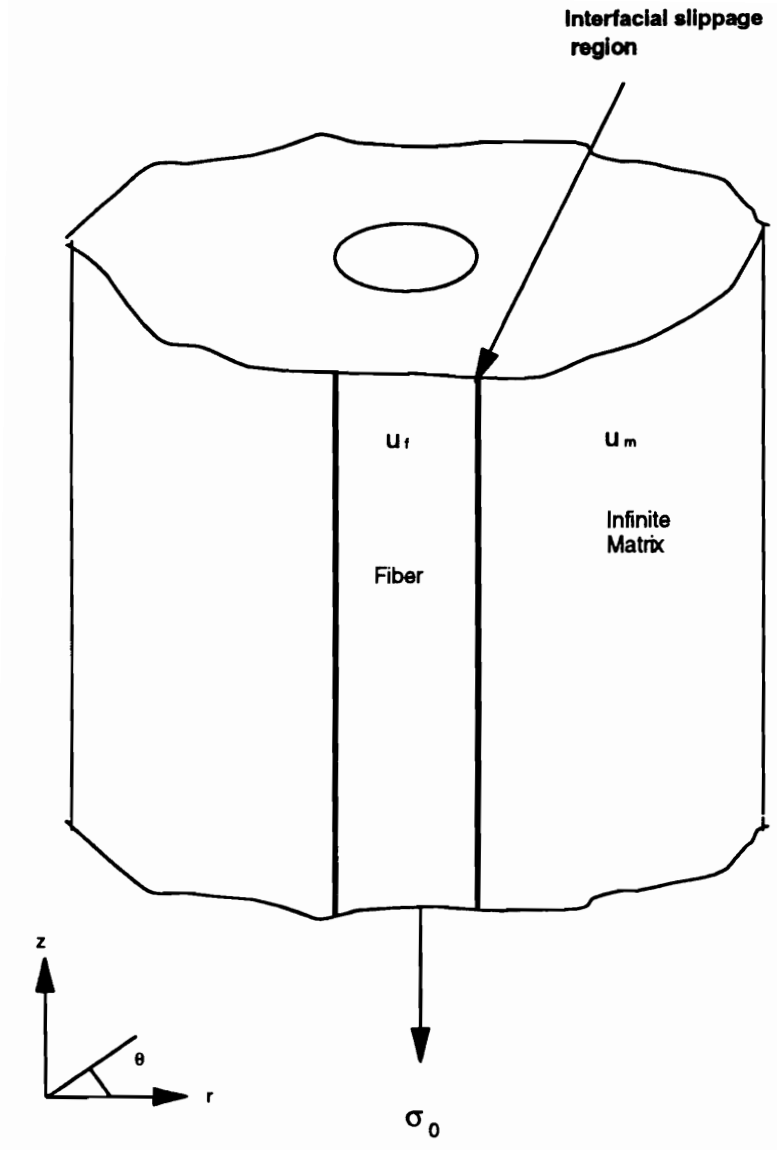

Figure A1 Schematic of concentric cylinders assemblage (CCA) used to solve the auxilary problem

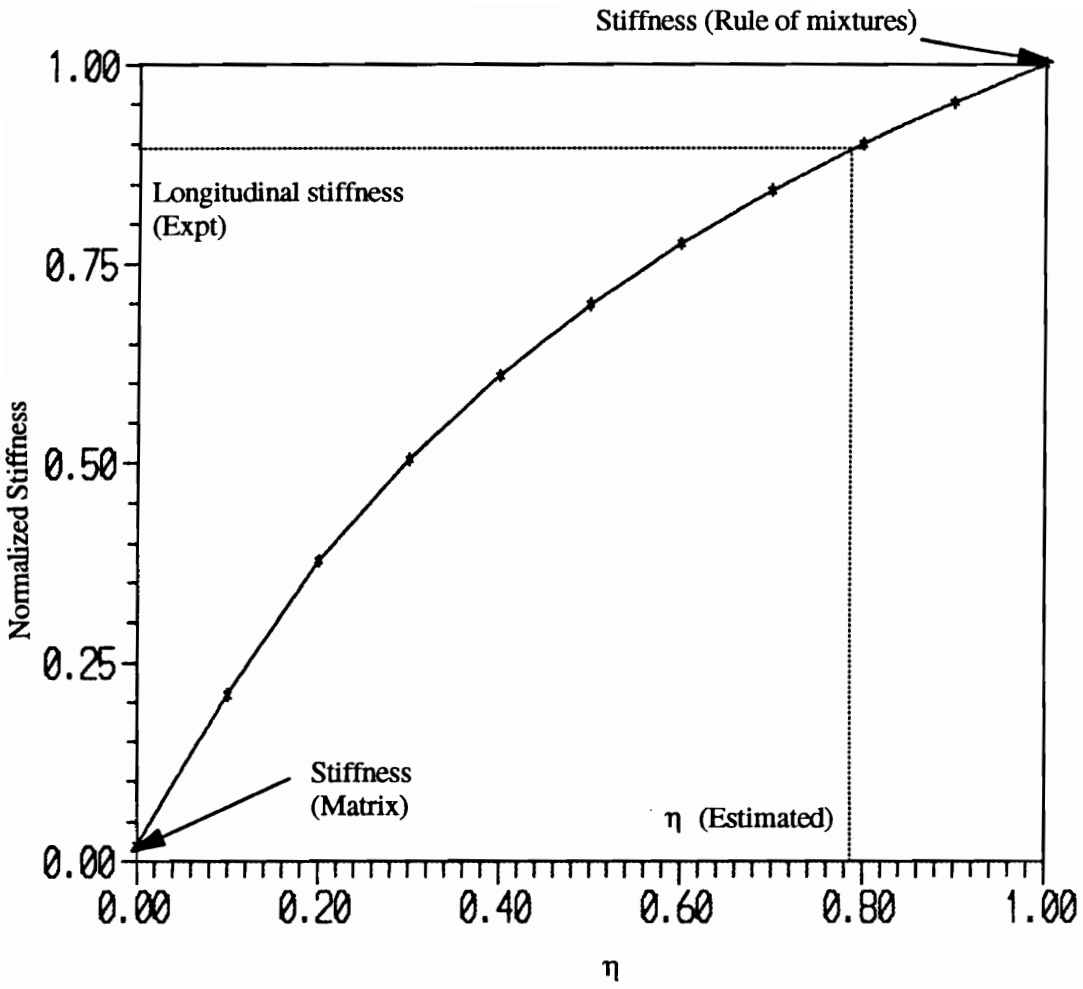

Figure A2 Variation of longitudinal stiffness with efficiency fator η

REFERENCES

1. Jayaraman, K.," Effect of the Interphase on the Thermo-Mechanical Response of Unidirectional Fiber-Reinforced Epoxies : Modeling, Analyses and Experiments," Ph.D. Dissertation, Virginia Polytechnic Institute and State University, 1992.

2. Jayaraman, K., Reifsnider, K. L., and Swain, R. E., "The Interphase in Unidirectional Fibrous Composites,I. A Review of Characterization Methods," submitted to Journal of Composites Technology and Research, 1991.

3. Jayaraman, K., Reifsnider, K. L., and Swain, R. E., "The Interphase in Unidirectional Fibrous Composites,II. A Review of Modeling Studies," submitted to Journal of Composites Technology and Research, 1991.

4. Reed, K. E., "Dynamic Mechanical Analysis of Fiber Reinforced Composites," Polymer Composites, V. 1(1), 1980, pp. 44-49.

5. Thomason, J. L., "Investigation of Composite Interphase Using Dynamic Mechanical Analysis: Artifacts and Reality," Polymer Composites, Vol. 11, No. 2, April, 1990, pp. 105-113.

6. Gerard, J. F., Perret, P., and Chabert, B., "Study of Carbon/Epoxy Interphase: Affect of Surface Treatment of Carbon Fibers on the Dynamic Mechanical Behaviour of Carbon/Epoxy Unidirectional Composites,' Controlled Interphases in Composite Materaials, H. Ishida, ed., Elsevier Science Publishing, 1990, pp. 449-456.

7. Peacock, J., Fife, B., Nield, E., and Crick, R. A., "Examination of the Morphology of Aromatic Polymer Composites (APC-2) Using an Etching Technique," in Composte Interfaces, H. Ishida and J. L. Koenig, eds., Elsevier Science Publishing Co., pp. 299-306, 1986.

8. Olley, R. H., Bassett, D. C., Blundell, D. J., "Permenganic Etching of PEEK," Polymer, Vol. 27, March 1986, pp. 344-348.

9. Peters, P. W. M, and Albertsen, H., "The Fiber-Matrix Interphase in CFRP with a phase separating Matrix System," Interfacial Phenomena in Composite Materials, Leuven, Sept. 17-19, 1991, pp. 101-104.

10. Hodge, D. J., Middlemiss, B. A., and Peacock, J. A., "Correlation Between Fiber Surface Energetics and Fiber-Matrix Adhesion in Carbon Fiber Reinforced PEEK Composites," in Materials Research Society Symposium Proceedings, Vol. 170, ED. by Pantano, C. G. and Chen, E. J., H., pp. 339 -344.

11. Bascom, W. D., Yon, K. J., Jensen, R. M., Cordner, L., "The Adhesion of Carbon Fibers to Thermoset and Thermoplastic Polymers," Journal of Adhesion, Vol. 34, 1991, pp. 79-98.

12. Chang, Y. S.," The affect of the Interphase/Interface Region on Creep and Creep Rupture of Thermoplastic Composites," PhD. Dissertation, Virginia Polytechnic Institute and State University, 1992.

13. Bacon, C. R., William, J. G., and Cornilsen, C. C., "Interphase Chemistry via Micro-Raman Spectroscopy," Proceedings of the Fifth Technical Conference of the American Society for Composites, Technomic Publishing Co., pp. 137-143, 1990.

14. Bolvari, A. E., and Ward, T. C., "Determination of Fiber-Matrix Adhesion and Acid-Base Interactions," in Inverse Gas Chromatography : Characterization of Polymers and Other Materials, Ed. Lloyd, D. R., Ward, T. C., and Schreiber, H. P., ACS Symposium Series 391, 1989.

15. Yip, P. W., and Lin, S. S., "Effect of Surface Oxygen on Adhesion of Carbon Fiber Reinforced Composites," in Materials Research Society Symposium Proceedings, Vol. 170, Ed. by Pantano, C. G., and Chen, E. J. H., pp. 339-344.

16. Narkis, M., and Chen, E. J. H., "Review of Methods for Characterization of Interfacial Fiber-Matrix Interactions," Polymer Composites, Vol. 9, No. 4, August 1988, pp. 245-251.

17. Kelly, A., and Tyson, W. R., Journal of Mechanics and Physics of Solids, Vol. 10, No. 2, 1963, pp. 199-208.

18. Drzal, L. T., Rich, M. J., and Lloyd, P. F., Journal of Adhesion, 16,1 (1982).

19. Mandell, J. F., Chen, J. H., and McGarry, F. J., "A Microdebonding Test for In Situ Assessment of Fiber/Matrix Bond Strength in Composite Materials," International Journal of Adhesion and Adhesives, IPC Business Press Ltd., 1980, pp. 40-44.

20. Grande, D. H., Mandell, J. F., and Hong, K. C. C., "Fiber-Matrix Bond Strength Studies of Glass, Ceramic and Metal Matrix Composites," Journal of Materials Science, Vol. 12, 1988, pp. 311-328.

21. Lesko, J. J., "Indentation Testing of Composite Materials : A Novel Approach to Measuring Interfacial Characteristics and Engineering Properties," M. S. Thesis, Virginia Polytechnic Institute and State University, 1991.

22. Carman, G. P., Lesko, J. J., Reifsnider, K. L., and Dillard, D. A., " A Cellular Modelling Approach for the Micromechanics Analysis of Composite Indentation," Submitted to Composite Science and Technology, 1991.

23. Verpoest, I., Desaegkr, M., and Keunings, R., "Critical Review of Direct Micromechanical Test Methods for Interfacial Strength Measurements in Composites," Controlled Interphases in Composite Materials, H. Ishida, Ed., Elsevier Sciences Publishing Co., Inc., 1990, pp. 653-666.

24. Tsai, H. C., Arocho, A. M., and Gause, L. W., "Prediction of Fiber-Matrix Interphase Properties and their Influence on Interface Stress, Displacement and Fracture Toughness of Composite Materials," Science of Composite Interfaces, Ed. Brandt et al., Elsevier Science Publishing Co. Inc., 1989, pp. 295-304.

25. Asloun, E. M., Nardin, M., and Shultz, J., "Stress Transfer in Single-Fiber Composites : Effect of Adhesion, Elastic Modulus of Fiber, Matrix, and Polymer Chain Mobility," Journal of Materials Science, Vol. 24, pp. 1835-1844, 1989.

26. Sottos. N. R., Scott, W. R., and McCllough, R. L., " Micro-Interferometry for Measurement of

Thermal Displacements at Fiber/Matrix Interfaces," Experimental Mechanics, Vol. 31, pp. 98-103, 1991.

27. Madhukar, M. S., and Drzal, L. T., "Affect of Fiber-Matrix Adhesion on the Longitudinal Compressive Properties of Graphite/Epoxy Composites," Proceedings of the Fifth Technical Conference of American Society for Composites, 1990, pp. 849-858.

28. Madhukar, M. S. and Drzal, L. T., "Fiber-Matrix Adhesion and its Affects on Composite Mechanical Properties:I. In-Plane and Interlaminar Shear Behaviour of Graphite/Epoxy Composites," Journal of Composite Materials, Vol.25, 1991, pp.932-957.

29. Madhukar, M. S. and Drzal, L. T., "Fiber-Matrix Adhesion and its Affects on Composite Mechanical Properties :II. Longitudinal and Transverse Tensile and Flexure behaviour of Graphite/Epoxy Composites," Journal of Composite Materials, Vol.25, 1991, pp.958-991.

30. Madhukar, M. S. and Drzal, L. T., "Fiber-Matrix Adhesion and its Affects on Composite Mechanical Properties :IV. Mode I and Mode II Fracture Toughness of Graphite/Epoxy Composites," Journal of Composite Materials, Vol.26, 1992, pp.936-968.

31. Lehmann, S., Megerdigian, C., and Papalia, R., "Carbon Fiber/Resin Matrix Interphase : Effect of Carbon Fiber Surface Treatment on Composite Performance," SAMPE Quarterly, April 1985, pp. 7-13.

32. Fitzer, E., and Weiss, R., "Effect of Surface Treatment and Sizing on C-Fibers on the Mechanical Properties of CFR Thermoseting and Thermoplastic Polymers," Carbon, Vol. 25, No. 4, pp. 455-467, 1987.

33. Peters, P. W. M., and Albertsen, H., "The Fiber/Matrix Interphase in CFRP with a Phase-Separating Matrix System," Interfaical Phenomena in Composite Materials, Proc. II International Conference, Ed. I. Verpoest, Sept. 17-19, 1991, pp. 101-104.

34. Albertsen, H., and Peters, P. W. M., "The Influence of Fiber/Matrix Interphace strength on Interlaminar Fracture Toughness on CFRP," Interfaical Phenomena in Composite Materials, Proc. II International Conference, Ed. I. Verpoest, Sept. 17-19, 1991, pp. 247-248.

35. Schwartz, H. S., and Hatrness, J. T., "Effect of Fiber Coatings on Interlaminar Fracture Toughness of Composites," Toughened Composites, ASTM STP 937, Norman J. Johnston, Ed., American Society for Testing and Materials, Philadelphia, 1987, pp. 150-178.

36. Ivens, J., Wevers, M., Verpoest, I., and de Meester, P., "Influence of the Fiber-Matrix Interface on the matrix crack development in Carbon-Epoxy Cross-Ply laminates," in Developments in the Science and Technology of Composite Materials, ECCM 3, Ed., A. R. Bunsell, P. Lamicq, A. Massiah, March 1989, pp. 465-471.

37. Lesko, J. J., et al., " A global local investigation of compressive strength to determine the influence of the fiber/matrix interphase," Compression Response of Composite Structures, ASTM STP, American Society for Testing and Materials, Philadelphia, 1992.

38. Ivens, J., Wevers, M., and Verpoest, I., " An energy based model for the influence of the fiber-

matrix interface strength on the interlaminar fracture toughness of UD-Composite laminates," in Local Mechanics Concepts for Composite Material System, IUTAM Symposium Blacksburg, VA, 1991, J. N. Reddy, and K. L. Reifsnider, Ed., pp. 215-228.

39. Drzal, L. T., Madhukar, M., and Waterbury, M. C., " Surface Chemical and Surface Energetic Alterations of the IM6 Carbon Fiber Surface," Proceedings of the Adhesion Society, 15th Annual Meeting, February 1992, pp. 144-147.

40. Lehmann, S., Robinson, R., and Tae, M. K., " Characterization of Carbon Fiber/Resin Matrix Interphase," Presented at the 31st International SAMPE Symposium, April 7-10, 1986, pp. 291-302.

41. Lee, S., M., " Influence of fiber/matrix interfacial adhesion on composite fracture behavior," Composites Science and Technology, Vol. 43, 1992, pp. 317-327.

42. Lesko, J. J., Subramanian, S., Dillard, D. A., and Reifsnider, K. L., " The Influence of Fiber Sizes Developed Interphases on Interlaminar Fracture Toughness," To be presented at the 39th Intenational SAMPE Conference, April 11-14, 1994, Anaheim, California.

43. Swain, R. E., " The Role of the Fiber/Matrix Interphase in the Fatigue Behaviour of Polymeric Composite Laminates," PhD. Dissertaion, Virginia Polytechnic Institute and State University, 1992.

44. Shih, G. C., and Ebert, L. J., " The Affect of the Fiber/Matrix Interface on the Flexural Fatigue Performance of Unidirectional Fiberglass Composites," Composites Science and Technology, 1987, pp. 137 -161.

45. Vincent, L., Fiore, L., and Fournier, P., "Fatigue Behaviour of GFRP: Some Considerations about Interfaces," ECCM3, 1988, pp. 609-614.

46. Alstadt, V., Lang, R. W., and Neu, A., "The Influence of Resin, Fiber and Interface on Delamination Fatigue Crack Growth of Composites," Durablity of Polymer Based Composite Systems for Stuctural Applications, Eds. A. H. Carden, G. Verchery, 1990, pp. 180-189.

47. Reifsnider, K. L., Henneke, E., G., Stinchcomb, W. W., and Duke, J. C., "Damage Mechanics and NDE of Composite Laminates," in Mechanics of Composite Materials, Recent advances, Z. Hashin and C. T. Heracovich, eds., 1983, pp. 399-420.

48. Jamison, R. D., and Reifsnider, K. L., International Journal of Fatigue, Vol. 4, 1982, pp. 187-195.

49. Jamison, R. D., " Advanced Fatigue Damage Development in Graphite Epoxy Laminates," Dissertation, PhD. Dissertation, Virginia Polytechnic Institute and State University, 1982.

50. Rotem, A., "Stiffness change of a graphite/epoxy laminate under reverse fatigue loading," Journal of Composites Technology and Research, Vol. 11, No. 2, 1989, pp. 225-246.

51. Camponeschi, E. T., Stinchcomb, W. W., "Stiffness reduction as an indicator of damage in graphite/epoxy laminates," Composite Materials: Testing and Design (Sixth Conference), ASTM STP 787, I. M. Daniel, Ed., ASTM, 1982, pp. 225-246.

52. Talreja, R., "Stiffness based fatigue damage characterization, " Fatigue of Composite Materials,

Ch.5, Technomic, 1987.

53. Reifsnider, K. L., and Stinchcomb, W. W., "Stiffness change as a fatigue damage parameter for composite laminates," Advances in Aerospace Structures, Materials and Dynamics, Yuceoglu, U., Seirakowski, R. L., Glasow, D. A., eds., ASME, New York, 1983.

54. Talreja, R., "Damage Characterization," Chapter 3, *Fatigue of Composite Materials*, Ed., K. L. Reifsnider, Composite materials Series, Series Editor, N. J. Pagano.

55. Aboudi, J, "Microfailure Criteria for Coated-Fiber Composites," Journal of Reinforced Plastics and Composites, Vol. 10, March, 1991, pp. 146-157.

56. Allen, D. H., Harris, C., and Nottorf, E., "A thermomechanical constitutive theory for elastic composites and distributed damage," Part 1 and 2, Texas A&M report MM-5023-85-15, 1985.

57. Joshi, S. P., and Frantziskonis, G., "Damage Evolution in Laminated Advanced Composites," Composite Structures, Vol. 17, 1991, pp. 127-139.

58. Reifsnider, K. L. and Stinchcomb, W. W., "A Critical Element Model of the Residual Strength and Life of Fatigue-Loaded Composite Coupons," Composite Materials: Fatigue and Fracture, ASTM STP 907, H. T. Hahn, Ed., ASTM, Philadelphia, 1986, pp. 298-303.

59. Lee, J. W., Daniel, I. M., and Yaniv, G., "Fatigue life prediction of cross-ply composite laminates," Composite Materials: Fatigue and Fracture, 2nd Volume, ASTM STP 1012, P. A. Lagace, ed., 1989, pp.19-28.

60. Wang, A. S. D., Chou, P. C., and Lei, S. C., "A Stochastic Model for the Growth of Matrix Cracks in Composite Laminates," Journal of Composite Materials, Vol. 18, pp. 239-254.

61. Hashin, Z. and Rotem, A., "A fatigue criterion for fiber reinforced materials," J Composites, Vol. 7, pp. 246-256.

62. Reifsnider, K. L. and Gao, Z.,"A micromechanics model for composites under fatigue loading," Int. J of Fatigue, Vol. 13, No.2, 1991, pp. 149-156.

63. Mori, T. and Tanaka, K., "Average stress in matrix and average elastic energy of materials with misfitting inclusions," Acta Metallurgica, Vol. 21, 1973, pp. 571-583.

64. Yeow, Y. T., "The Time-Temperature Behaviour of Graphite/Epoxy Laminates," Ph.D. Dissertation, Virginia Polytechnic Institute and State University, 1978.

65. Dillard, D. A.,"Creep and Creep Rupture of Laminated Graphite/Epoxy Composites," Ph.D. Dissertation, Virginia Polytechnic Institute and State University, March, 1981.

66. Gramoll, K. C., Ph.D. Dissertation, "Thermo-viscoelastic characterization of viscoelastic composite materials," Virginia Polytechnic Institute and State University, 1988.

67. Moore, R. H., "Time dependent matrix cracking in cross-ply Kevlar composites," Master's Thesis, Virginia Polytechnic Institute and State University, 1988.

68. Banerjee, A., Ogale, A. A., and Edie, D. D., "Interfacial characterization of composites by dynamic mechanical analysis," 34 th International SAMPE Symposium, May 1989.

69. Chang, Y. S., and Dillard, D. A., "The Effect of the Interphase/Interface Region on Creep and Creep Rupture of Thermoplastic Composites," CCMS-92-10, May, 1992, Virginia Tech.

70. Leaderman, H., "Elastic and Creep Properties of filamentous materials ans other high polymers," The Textile Foundation, Washington, 1943.

71. Osiroff, R., "Damorheology: Fatigue-Creep interactions in Composite Materials," Ph.D. Dissertation, Virginia Polytechnic Institute and State University, 1990.

72. Schapery, R. A., "Further development of thermodynamic constitutive theory: stress formulation," Perdue Research Foundation, Project 4958, 1969.

73. Evans, R. W., and Wilshire, B., "Power law creep of polycrystalline copper," Creep and Fracture of Enginnering Materials an Structures, Proceedings of the Third Int. Conf., Swansea, April 1987, B. Wilshire and R. W. Evans, eds., The Institute of Metals, London, 1987.

74. Hackett, R. M., and Dozier, J. D., "Viscoelastic/Damage Modeling of Filament-Wound Spherical Pressure Vessels," Journal of Reinforced Plastics and Composites, Vol. 6, April, 1987.

75. Dillard, D. A., Morris, D. H., and Brinson, H. F., "Environmental affects and viscoelastic behaviour of laminated graphite/epoxy composites," Environmental Degradation of Enginnering Materials, Virginia Polytechnic Institute and State University, Sept. 1981, pp. 445-453.

76. Aboudi, J., *Mechanics of Materials : A Unified Micromechanical Approach*, Elsevier Publishers, Amsterdam, 1991.

77. Lesko, J. J., Swain, R. E., Cartwright, J. M., Chin, J. W., Reifsnider, K. L., Dillard, D. A., and Wightman, J. P., "Interphases developed from fiber sizings and their chemical-structural relationship to composite compressive performance," Submitted to the Journal of Adhesion, February, 1993.

78. Dolan, G. L., Wong, R., Wilson, D. W., "Development of Ultrlightweight Materials," Fourth Quarterly Interim Technical Report, Air Force Contract No. F 33615-88-C-5452, May 1989.

79. Hahn, G., Wong, R., Hwang, W.-F., Hartness, T, Drzal, L. T., Robinson, R., and Smith, S., " "Development of Ultrlightweight Materials," Tenth Quarterly Interim Technical Report, Air Force Contract No. F 33615-88-C-5452, Nov. 1990.

80. Stalnaker, D. O., and Stinchcomb, W. W., "Load History-Edge Damage Studies in Two Quasi-Isotropic Graphite Epoxy Laminates," Composite Materials: Testing and Design (Fifth Conference), ASTM STP 674, S. W. Tsai, Ed., ASTM, 1979, pp. 620-641.

81. S. Subramanian, J. S. Elmore, and W. W. Stinchcomb, " The influence of fiber-matrix interphase on the long-term behavior of graphite/epoxy composites," To be presented at the 12th Symposium on Composite Materials : Testing and Design, May 16-17, 1994, Montreal, Quebec, Canada.

82. Talug, A., "Analysis of Stress Fields in Composite Laminates with Interior Cracks," PhD. Dissertation, Virginia Polytechnic Institute and State University, 1978.

83. S. Subramanian, "On the Singularity and Asymptotic Stress Fields Around Cracks Normal to the Interface in Anisotropic Composite Laminates," Project Report for E.S.M 6054, Virginia Tech., 1992.

84. Liu, S., and Nairn, J. A., "The formation and propagation of matrix microcracks in cross-ply laminates during static loading," Journal of Reinforced Plastics and Composites, Vol. 11, Feb 1992, pp. 158-178.

85. Tan, S. C., and Nuismer, R. J., "A theory for progressive matrix cracking in composite laminates," Journal of Composite Materials, Vol. 23, Oct 1989, pp. 1029-1047.

86. Varna, J., and Berglund, L., "Multiple Transverse Cracking and Stiffness Reduction in Cross-Ply Laminates," Journal of Composites Technology and Research, Vol. 13, No.2, Summer 1991, pp. 99-106.

87. Flagg, D. L., and Kural, M. H., "Experimental Determination of the In Situ Transverse Lamina Strength in Graphite/Epoxy Laminates," Journal of Composite Materials, Vol. 16, March 1982, pp. 103-115.

88. Ochiai, S., Peters, P. W. M., Schulte, K., and Osamura, K., "Monte-Carlo simulation of multiple fracture in transverse ply of cross-ply graphite-epoxy laminates," Jounal of Materials Science, Vol. 26, 1991, pp. 5433-5444.

89. Kander, R. G., "A Study of Damage Accumulation in Unidirectional Glass Reinforced Composites via Acoustic Emission Monitoring," Polymer Composites, August 1991, Vol. 12, pp. 237-245.

90. Seigmann, A., and Kander, R. G., "In situ acoustic emission monitoring and mechanical testing in the scanning electron microscope," Journal of Materials Science Letters, 10 (1991), pp. 619-621.

91. Kander, R. G., and Seigmann, A., "Mechanism of Damage and Failure in an Orthotropic Glass/Polypropylene Composite," Polymer Composites, June 1992, Vol. 13, No. 3, pp. 154-168.

92. Ono, K., Jeng, J. S., and Yang, J. M., "Fracture Mechanism Studies of A Carbon Fiber-PEEK Composite by Acoustic Emission," Acoustic Emission : Current Practice and Future Directions, ASTM STP 1077, W. Sachse, J. Roget and K. Yamaguchi, Eds., ASTM, Philadelphia, 1991.

93. Gao, Z., and Reifsnider, K. L., "Tensile Failure of Composites : Influence of Interface amd Matrix Yielding," Journal of Composites Technology and Research, Vol. 14, No. 4, Winter 1992, pp. 201-210.

94. Gao, Z., Reifsnider, K. L., and Carman, G. P., "Strength Prediction and Optimization of Composites with Statistical Flaw Distribution," Journal of Composite Materials, Vol. 26, No. 11, 1992, pp. 1578-1705.

95. Kimoto, M., "Flexural Properties and Dynamic Mechanical Properties of Glass Fiber-Epoxy Composites," Journal of Materials Science, Vol. 25, 1990, pp. 3327-3332.

96. Harlow, D. G., and Phoenix, S. L., "Probability Distribution for Strength and Composite Materials I : Two-Level Bounds," International Journal of Fracture, Vol. 17, 1981, pp.321-336.

97. Reifsnider, K. L., "Some Fundemental aspects of the Fatigue and Fracture of Composite Materials," Proceedings, 14th Annual Conference of Enginnering Mechanics, Lehigh University, Bethleham, PA, 1977, pp. 373-384.

98. Hegdepeth, J. M., and Van Dyke, P., "Local Stress Concentration in Inperfect Filamentary Composite Materials," Journal of Composite Materials, 1968.

99. Harlow, D. G., and Phoenix, S. L., "The Chain-of-Bundles Probability Model for the Strength of Fibrous Materials I : Analysis and Conjectures," Journal of Composite Materials, Vol. 12, April 1978, pp. 195-213.

100. Harlow, D. G., and Phoenix, S. L., "The Chain-of-Bundles Probability Model for the Strength of Fibrous Materials II : A Numerical Study of Convergence," Journal of Composite Materials, Vol. 12, July 1978, pp. 314-334.

101. Fukuda, H., "Statistical Strength of Unidirectional Composites with Random Fiber Spacing," Composite '86 : Recent Advances in Japan and the United States, 1986, pp. 307-314.

102. Zweben C., "Fracture Mechanics and Composite Materials : A Critical Analysis," in Analysis for the Test Methods for High Modulus Fibers and Composites, ASTM STP 521, ASTM, Philadelphia, 1973, pp. 65-97.

103. Barker, R. M., and MacLaughlin, "Stress Concentration Near a Discontinuity in Fibrous Composites," Journal of Composite Materials, 1971.

104. Agarwal, B. D., and Bansal, R. K., "Plastic Analysis of Fiber Interactions in Discontinuous Fiber Composites," Fiber Science and Technology, 1977.

105. Chen, C. H., "Tension of a Composite Bar with Fiber Discontinuities and Soft Inter-Fiber Materials," Fiber Science and Technology, 1973.

106. Weibull, W., "A Statistical Distribution of Wide Application," Journal of Applied Mechanics, September, 1951.

107. Coleman, B. D., "On the Strength of Classical Fibers and Fiber Bundles," Journal of Mechanics and Physics of Solids, Vol. 7, No. 1, 1959, pp. 66-70.

108. Rosen, B. W., "Tensile Failure of Fibrous Composites," AIAA Journal, Vol. 2, No. 11, Nov. 1964, pp. 1985-1991.

109. Hahn, H. T., "Failure Mechanisms," in Failure Analysis and Mechanisms of Mailure of Fibrous Composite Structures, Complied by A. K. Noor and M. J. Shuart, Proc. of a Workshop sponsored by NASA LRC, March 23-25, 1982, pp. 153-171.

110. C. Zweben and Rosen B. W., "A Statistical Theory of Composite Strength with Application to Composite Materials," J. Mech. Phys. Solids, Vol. 18, pp. 189-206.

111. Batdorf, S. B., "Tensile Strength of Unidirectionally Reinforced Composites-I," J. Reinforced Plastics and Composites, Vol. 1, April 1982, pp. 153-164.

112. Batdorf, S. B., "Tensile Strength of Unidirectionally Reinforced Composites-II," J. Reinforced Plastics and Composites, Vol. 1, April 1982, pp. 165-176.

113. Greszcuk, L. B., "Theoretical Studies in the Mechanics of Fiber-Matrix Interface in Composites," Interfaces in Composites, ASTM STP 452, ASTM, Philadelphia, pp. 42-85.

114. Lim, S. G., and Hong, C. S., "Prediction of Transverse Cracking and Stiffness Reduction in Cross-Ply Laminated Composites," Journal of Composite Materials, Vol. 23, July 1989, pp. 695-713.

115. Lee, J.-W., and Daniel, I. M., "Progressive Transverse Cracking of Cross-Ply Composite Laminates," Journal of Composite Materials, Vol. 24, Vov 1990, pp. 1225-1243.

116. Parvizi, A., Garrett, K. W., and Bailey, J. E., "Constrained Cracking in Glass Fiber reinforced Epoxy Cross-Ply Laminates," J. Materials Science, Vol. 13, 1978, pp. 195-201.

117. Flaggs, D. L., "Prediction of Tensile Matrix Failure in Composite Laminates," Journal of Composite Materials, Vol. 19, January 1985, pp. 29-50.

118. Smith, P. A., and Woods, J. R., "Poisson's Ratio as a Damage Parameter in the Static Tensile Loading of Simple Crossply Laminates," Composites Science and Technology, Vol. 38, 1990, pp. 85-93.

119. Zhang, J., Fan, J., and Soutis, C., "Analysis of multiple matrix cracking in $(+\theta_m,90_n)_s$ composite laminates - Part I : In-plane stiffness properties," Composites, Vol. 23, No. 5, Sept 1992, pp. 291-298.

120. Dvorak, G. J., Laws, N., and Hejazi, M., "Analysis ofProgressive Matrix Cracking in Composite Laminates-I. Thermoelastic Properties of a Ply with Cracks," Journal of Composite Materials, Vol. 19, 1985, pp. 216-234.

121. Talreja, R., "Transverse Cracking and Stiffness Reduction in Composite Laminates," Journal of Composite Materials, Vol. 19, 1985, pp. 355-375.

122. Hashin, Z., "Analysis of Cracked Laminates : A Variational Approach," Mechanics of Materials, Vol. 4, 1985, pp. 121-136.

123. Fukunaga, H., Chou, H. T., Peters, P. W. M., and Schulte, K., "Probabilistic Failure Strength Analyses of Graphite/Epoxy Cross-Ply Laminates," Journal of Composite Materials, Vol. 18, 1984, pp. 339-356.

124. Peters, P. W. M., "The Strength Distribution of 90° Plies in 0/90/0 Graphite-Epoxy Laminates," Journal of Composite Materials, Vol. 18, 1984, pp. 545-556.

125. Benveniste, Y., Dvorak, G. J., and Chen, T., "Stress Fields in Composites with Coated Inclusions," Mechanics of Materials, Vol. 7, 1989, pp. 305-317.

VITA

The author was born on 21st August, 1966, in Bangalore, India. He received a Bachelor of Engineering degree in Mechanical Engineering from the College of Engineering, Guindy, Madras, in 1988. He enrolled in the graduate program in the University of Texas at Arlington and worked on his thesis under the supervision of Dr. Wen Chan. He received his Master's degree in Materials Science from the University of Texas at Arlington, in 1990. He has been enrolled in the Ph. D. program in the Engineering Science and Mechanics department at Virginia Polytechnic Institute and State University, Blacksburg, VA, since August, 1990. He has been working in the Materials Response Group, with Dr. W. W. Stinchcomb and Dr. K. L. Reifsnider, while at Virginia Tech.